A RAPID CONSTRUCTION TECHNIQUE FOR BRIDGE ABUTMENTS USING CONTROLLED LOW STRENGTH MATERIALS (CLSM)

by

Vahid Alizadeh

A Dissertation Submitted in

Partial Fulfillment of the

Requirements for the Degree of

Doctor of Philosophy

in Engineering

at

The University of Wisconsin-Milwaukee

August 2014

ABSTRACT
A RAPID CONSTRUCTION TECHNIQUE FOR BRIDGE ABUTMENTS USING CONTROLLED LOW STRENGTH MATERIALS (CLSM)

by

Vahid Alizadeh

The University of Wisconsin-Milwaukee, 2014
Under the Supervision of Professor Sam Helwany

The required time for building bridge abutments is one of the key obstacles facing rapid bridge construction. For typical span bridges, this can be remedied by using Controlled Low Strength Materials (CLSM) as backfill materials placed behind full-height precast concrete panels that are integrated with the CLSM backfill via steel anchors. CLSM bridge abutments can be constructed in a short time as they do not require heavy machinery for excavation, compaction, and piling equipment. The main objective of this study was to examine the behavior of an instrumented laboratory large-scale CLSM bridge abutment with full-height precast concrete panels that was subjected to a monotonically increasing sill (foundation) pressure. The experiment showed that the CLSM bridge abutment, with a relatively short cure time of 7 days, is capable of carrying typical bridge loads with a reasonably large safety margin, and with minimal deformations.

To select a suitable CLSM mixture proportion, several mixtures were developed and tested in the laboratory for engineering properties including flowability, density, compressive strength and stress–strain behavior. The main performance criteria for selection of a potential CLSM mixture were compressive strength to support the bridge loads, excavatability and flowability to fill the entire abutment in one continuous pour. Since it was a critical area of concern in design of the CLSM bridge abutment, the bond strength performance of the CLSM to steel anchors was also investigated. In pullout tests, a CLSM mixture with higher compressive strength resulted in higher bond strength and more brittle slippage. A numerical simulation of pullout tests indicated that the bond strength decreases with increase in bar size and embedment length.

Finite element method (FEM) of analysis was implemented to simulate and explore the performance of CLSM bridge abutments based on bearing pressure capacity, displacements, and the developed axial force in anchors, and to provide an assessment of safety of the design. The accuracy of the finite element results for the response and failure behavior of a CLSM mass was evaluated by a comparison with the experimental results. Good agreement was obtained between the numerical and experimental results. The validated finite element (FE) model was then used for conducting a series of parametric studies to define the effects of CLSM compressive strength, curing age, environment temperature and construction details on response of the abutments. It was also learned that the computed and measured lateral displacements for the facing panels were negligible up to about 70% of the bearing pressure capacity of the abutment when a longitudinal crack developed in the CLSM backfill close to the facing wall.

Table of Contents

INTRODUCTION **1**

1.1 Problem Statement **1**

1.2 Research Objective **3**

1.4 CLSM Bridge Abutment **4**

1.4 Research Methodology **11**

1.5 Outline of the Dissertation **13**

STATE-OF-THE-ART LITERATURE REVIEW **15**

2.1 Controlled Low Strength Material (CLSM) **15**

2.1.1 Historical Background 18

2.1.2 Materials 20

2.1.2.1 Portland Cement 20

2.1.2.2 Fly Ash 21

2.1.2.3 Aggregates 22

2.1.2.4 Water 24

2.1.2.5 Chemical Admixtures 24

2.1.2.6 Other Materials Used in CLSM 25

2.1.3 Mixture Proportions 25

2.1.4 Batching, Mixing, and Transporting 27

2.1.5 Engineering Properties 27

2.1.5.1 Fresh CLSM Properties 29

2.1.5.2 Hardened CLSM Properties 32

2.1.5.3 Durability and Environmental Issues Related to CLSM 37

2.1.3 Specifications, Test Methods, and Practices 41

2.1.6.1 Standard Test Method for Preparation and Testing of CLSM Test Cylinders (ASTM D 4832) 42

2.1.6.2 Standard Practice for Sampling Freshly Mixed CLSM (ASTM D 5971-96)....43

2.1.6.3 Standard Test Method for Unit Weight, Yield, Cement Content and Air Content (Gravimetric) of CLSM (ASTM D 6023)....43

2.1.6.4 Standard Test Method for Ball Drop on CLSM to Determine Suitability for Load Application (ASTM D 6024)....45

2.1.6.5 Standard Test Method for Consistency of CLSM (ASTM D 6103) 45

2.1.6.6 Other Currently Used and Proposed Test Methods....45

2.1.7 Specifications by the State Transportation Agencies....47

2.1.8 Applications....50

2.2 Use of CLSM as a Backfill for Bridge Abutments....52

MATERIAL CHARACTERIZATION TESTS....56

3.1 Materials....58

3.2 Mixture Proportioning....64

3.2.1 Preparation of CLSM Specimens....66

3.2.2 Flowability Tests....69

3.2.3 Unconfined Compressive Strength....69

3.2.4 Material Testing Results....72

3.2.4.1 Effect of Curing Temperature on Compressive Strength....77

3.3 Bond Behavior of Steel Rebar and CLSM....78

3.3.1 Pullout test on Cylindrical Specimens....79

3.3.2 Large-scale Pullout Test....86

3.3.3 Pullout Test on CLSM Abutment....90

3.3.4 Numerical Modeling of Pullout Tests....93

3.3.4.1 Numerical Simulation Methods....95

3.3.4.2 Surface-Based Cohesive Behavior with Damage....98

3.3.4.3 Finite Element Modeling of the Pullout Test....101

3.4 Selection of a CLSM Mixture for the Bridge Abutment 109

LARGE SCALE CLSM BRIDGE ABUTMENT TEST 110

4.1 Introduction 110

4.2 Construction of Large Scale CLSM Bridge Abutment Test Specimen 111

4.2.1 Prefabrication of Concrete Components 114

4.2.2 Construction Sequence 122

4.2.3 Excavation 142

4.3 Experimental Results 144

4.3.1 Displacements 145

4.4.3 Lateral Pressures 149

4.4.4 Strain Gauges 153

NUMERICAL MODELING OF CLSM BRIDGE ABUTMENT AND PARAMETRIC STUDIES 161

5.1 Finite Element Modeling 162

5.1.1 Plastic-Damage Model 163

5.1.2 Identification of Material Parameters 168

5.2 Finite Element Modeling of CLSM Cylinder Tests 176

5.3 Finite Element Modeling of the CLSM Bridge Abutment 179

5.4 Comparison of Numerical and Experimental Results 181

5.5 Parametric Study 191

SUMMARY AND CONCLUSIONS 207

REFRENCES 215

LIST OF FIGURES

Number	Description	Page
1.1	Proposed CLSM integrated bridge system.	3
1.2	Comparison between (a) Conventional bridge abutment and (b) Proposed CLSM bridge abutment.	7
1.3	Construction sequence of CLSM bridge abutment.	10
1.4	Large-scale laboratory test of CLSM bridge abutment.	13
2.1	CLSM Mix.	16
2.2	Excavating CLSM with backhoe.	33
3.1	Design of a CLSM Abutment and Location of Embedded Anchors.	57
3.2	X-Ray Diffraction of the type I portland cement.	61
3.3	X-Ray Diffraction of the class F fly ash.	61
3.4	SEM Images of: a) portland cement; b) fly ash Class F.	63
3.5	Gradation of fine aggregates used in the study	64
3.6	Concrete mixer used for mixing CLSM samples	66
3.7	Cylindrical CLSM samples.	68
3.8	Flow cylinder test.	69
3.9	Compressive strength test setup.	70
3.10	Failure modes of CLSM cylinders after compression test; (a) cone and split failure, (b) shear failure.	71
3.11	Strength development of CLSM mixtures.	73
3.12	Relationship between 28-day compressive strength and w/cm ratio.	74
3.13	Relationship between 28-day compressive strength and cement content at given	74

w/cm.

3.14	Relationship Between the 28-day Compressive Strength and Fly Ash Content.	75
3.15	Stress-Strain Responses of Mixture M7 at 1, 7 and 28 Days.	76
3.16	Effect of curing temperature on compressive strength development of Mixture M7.	78
3.17	Cylindrical specimens for pullout test.	80
3.18	Pullout test setup and associated specimen geometry.	80
3.19	Pullout test setup on cylindrical specimens.	81
3.20	Splitting bond failure.	82
3.21	Schematic bond-slip relationship: (a) pullout failure; (b) splitting failure.	82
3.22	Splitting bond failure and cracks in pullout test using cylindrical specimens.	84
3.23	Results of pullout test using cylindrical specimens for mixture M7.	84
3.24	Results of pullout test using cylindrical specimens for mixture M5.	85
3.25	Development of bond strength in pullout test using cylindrical specimens.	85
3.26	Large-scale pullout test setup, box and location of rebars.	87
3.27	Cylindrical molds placed in the center of the box.	87
3.28	Large-scale pullout testing.	88
3.29	Typical pullout load *vs.* slip response for large-scale pullout tests.	88
3.30	Pullout failure of rebar from CLSM (large-scale pullout test).	89
3.31	Collected samples from inside of the CLSM fill.	89
3.32	Pullout test on CLSM abutment at wing walls.	91
3.33	Pullout load *vs.* slip (pullout test on the abutment).	91
3.34	Pullout failure of rebar in CLSM abutment.	92

3.35	Bond stress-slip behavior in pullout tests.	92
3.36	Idealized force transfer mechanisms.	94
3.37	Bond and splitting stresses between a deformed bar and the surrounding concrete.	94
3.38	Local bond stress-slip laws.	94
3.39	Typical traction-separation response.	99
3.40	Schematic drawing of pullout test on CLSM abutment.	102
3.41	Finite element mesh for pullout test.	102
3.42	Traction-separation behavior for shear bond contact in Abaqus v6.12.	104
3.43	Damage in the CLSM mass due to the contact with the rebar at maximum bond stress.	105
3.44	Comparison of the experimental measurement with numerical results of pullout tests for different bar sizes.	107
3.45	Effect of embedment length on bond strength.	108
4.1	Large scale laboratory test of CLSM bridge abutment.	112
4.2	Inside of CLSM bridge abutment test.	113
4.3	Instrumentation of the laboratory test of CLSM bridge abutment.	113
4.4	Plan view of CLSM bridge abutment and location of the bridge sill.	114
4.5	Lateral loading for the design of concrete panels.	115
4.6	Reinforced concrete panels and corner units.	117
4.7	Tongue and groove connection.	118
4.8	Dywidag thread bar and nut.	118
4.9	Concrete leveling pad modules.	119
4.10	Reinforcement detail of bridge sill.	119

4.11	Prefabrication, (a) panel formworks and rebars, (b) nuts embedded in panels, (c) leveling pad module formworks, (d) corner unit formworks, (e) bridge sill formwork, (f) formworks filled with concrete, (g) formworks remolded.	121
4.12	Construction sequence of CLSM bridge abutment test.	123
4.13	Base preparation, (a) rubber membrane, (b) sand box foundation, (c) soil compaction, (d) leveling pads.	125
4.14	Panels installation; (a)Lifting a panel, (b)Installation of panels, (c)Temporary lateral Supports, (d)Detail of lateral supports at top (left picture) and bottom (right picture).	128
4.15	Interior covers; (a) geotextile filter layer, (b) rubber membrane against the strong-wall of the laboratory.	129
4.16	(a) Anchors Installation, (b) Strain gauges attached to anchors, (c) Pressure Cells.	131
4.17	Continuous batching and pouring CLSM; (a) fly Ash, (b) Sand, (c) Mixer and (d) Pumping and pouring.	134
4.18	(a) Released Water, (b) Drain Pipe, (c) Released water collected in sand box foundation (d) Drainage of water through holes of all panels.	135
4.19	Loading frame assembly; (a) 2× W 24×84 beam, (b) Assembly of loading frame, and lateral bracing.	137
4.20	Bridge sill placement; (a) lifting the sill, (b) leveled surface of the CLSM backfill, (c) placing bridge sill over the backfill.	138
4.21	(left) Location of LVDTs on the sill, (right) wooden frame for LVDTs.	139
4.22	Two steel plates and hydraulic jacks on the bridge sill.	139
4.23	Removing lateral supports.	140

4.24	Large Scale CLSM Bridge Abutment.	141
4.25	Loading the CLSM Abutment with electronic hydraulic pump.	142
4.26	(top) Detachment of the panels, (bottom) excavation of CLSM backfill.	143
4.27	Final undamaged state of the abutment after loading.	144
4.28	Settlement of the bridge sill at corners.	146
4.29	Average settlement of the bridge sill.	147
4.30	Settlement of the foundation soil.	147
4.31	(a) Lateral deflection of the front facing wall, (b) deflection profile of the front panel.	148
4.32	Lateral pressure profile against abutment with CLSM age.	150
4.33	Development of lateral pressure at different heights with CLSM age.	151
4.34	Lateral pressure on the front wall with applied load.	152
4.35	Development of lateral pressure at different heights with the applied bridge load.	153
4.36	Position of steel anchors with the strain gauges at the facing panels.	154
4.37	Strains at top, middle and bottom anchors of left middle panel of front face.	155
4.38	Strains at top, middle and bottom anchors of right middle panel of front face.	156
4.39	Stresses at top, middle and bottom anchors of left middle panel of front face.	157
4.40	Stresses at top, middle and bottom anchors of right middle panel of front face.	158
4.41	Combined bending and axial stresses for an anchor.	159
4.42	Development of axial tension forces in the anchors with the applied bridge load.	160
5.1	Yield surfaces in the deviatoric plane, corresponding to different values of	166

	K_c.	
5.2	Yield surface in plane stress.	166
5.3	Illustration of flow potentials and dilation angle.	168
5.4	Illustration of the definition of (a) cracking and (b) crushing strain used for the definition of strain softening data in tension and compression, respectively.	171
5.5	Idealized Compressive Stress-Strain Relationship of the CLSM.	173
5.6	Material input curves, compressive strain softening and damage evolution curve.	174
5.7	Conical damage (a) at compressive strength, (b) at failure with fixed end conditions, and (c) experimental conical failure.	177
5.8	Shear damage (a) at compressive strength, (b) at failure with one unconstrained end, (c) at failure with capped end conditions, and (d) experimental shear failure.	177
5.9	Comparison of dilation angle ψ and mesh size on numerical results.	178
5.10	Finite element simulation of the CLSM abutment.	180
5.11	Lateral pressures on a facing wall, comparison of experimental results with finite element method.	182
5.12	Bridge sill settlement, comparison of experimental results with finite element method.	184
5.13	Maximum lateral deflection of a front panel, comparison of experimental results with finite element method.	184
5.14	Prediction of the bearing pressure capacity, settlement and maximum lateral deflection.	185

5.15	Predicted damage propagation.	186
5.16	Effect of mesh size of finite element analysis on (top) settlement of the bridge sill, and (bottom) maximum lateral deflection.	187
5.17	Comparison of the measured and computed strain histories at three locations, top, middle, and bottom of a facing panel.	189
5.18	Comparison of the measured and computed axial anchor load at three locations, top, middle, and bottom of a facing panel.	190
5.19	Performance of the bridge abutment with CLSM curing time.	192
5.20	Performance of the bridge abutment with curing temperature.	193
5.21	Early performance of the abutment with different CLSM mixtures.	194
5.22	Late performance of the abutment with different CLSM mixtures.	194
5.23	Comparison of the damage pattern of failure with different strengths of backfill.	195
5.24	Lateral deformations of the concrete panels.	197
5.25	Profile of lateral deformation at the maximum applied pressure with different CLSM strengths.	198
5.26	Profile of lateral deformation of a face panel as a function of the applied pressure.	199
5.27	Development of axial stress in anchors as a function of applied pressure.	200
5.28	Effect of CLSM strength on mobilized axial stress in anchors (at 500 kPa).	201
5.29	Effect of CLSM strength on mobilized axial stress in anchors (at failure).	202
5.30	Plan of mobilized stress in all anchors of the face and wing wall (at failure).	203
5.31	Effect of some design modifications on performance of the CLSM abutment.	205
5.32	Effect of some design modifications on lateral deformation of the CLSM	205

abutment.

5.33 Effect of anchors on damage propagation, (left) without anchors, (right) with anchors. 206

LIST OF TABLES

Number	Description	Page
2.1	CLSM properties typically specified by state DOTs.	28
2.2	Current ASTM standards on CLSM.	41
2.3	States surveyed and their CLSM specification.	48
2.4	Specified acceptance strengths and ages.	49
2.5	Suggested mixture proportions, lb/yd3 (kg/m^3).	49
2.6	Application of CLSM in surveyed states.	51
3.1	Chemical and physical properties of portland cement and fly ash.	62
3.2	CLSM mixture proportions and some fresh properties.	68
3.3	Compressive strength results.	72
3.4	Mixture proportions and characteristics of the investigated CLSMs.	77
5.1	Material parameters of Plastic-Damage Model for 7-days cured CLSM mixture M3.	175

ACKNOWLEDGMENTS

I express my gratitude to my advisor, Professor Sam Helwany, for his continuous guidance, patience, support, and valuable discussions. Professor Helwany provided an excellent atmosphere for research and teaching during these years. His high standards on research and teaching and his commitment towards students made it a privilege to work with him.

I sincerely appreciate my dissertation committee members: Professor Al Ghorbanpoor, Professor Konstantin Sobolev, Dr. Ramme Bruce, and Professor Istvan Lauko for their support, comments and insights. I am also grateful for their time and efforts in evaluating this research work. The laboratory staff, Mr. Rahim Reshadi, is remembered with appreciation for technical assistance during the experiments. I would also like to thank the National Center for Freight & Infrastructure Research & Education (CFIRE) for their financial support.

Finally, special thanks go to my father, for his love and support.

January 25, 2014

Vahid Alizadeh

Chapter 1

INTRODUCTION

1.1 Problem Statement

Bridges as key elements of transportation networks have significant impact on the driving public and surrounding communities. The aging bridge infrastructure with tremendously growing traffic demand has presented an incessantly need to rapid construction/replacement of bridges to accommodate traffic flow and maintaining freight movement with least adverse economic impact.

Most bridges in the U.S. Highway Bridge inventory are inspected at least once every two years following federal guidelines in their bridge inspection and maintenance procedures. According to the latest bridge inspection report in December 2010 by U.S. Department of Transportation (DOT), quarter of bridges in the U.S. is evaluated to be deficient. Of the 604,474 bridges in the United States, 146,633 are deficient, including 69,223 structurally deficient bridges and 77,410 functionally obsolete bridges (FHWA). Even though all deficient bridges are not unsafe for travel, the numbers are revealing the potential number of bridge replacement projects that may happen in forthcoming years. The traveling public is demanding this construction and replacement be done more quickly to reduce congestion and improve safety.

Conventional cast in place bridge construction takes a substantial amount of time as it requires the sequential labor-intensive processes of forming, placing and curing time to complete the foundation, the substructure, the superstructure components, railings, and other accessories. This may cause disruption and inconvenience to the freight movement, traveling public and surrounding communities during the projects.

In meeting the expectations for congestion mitigation, the use of precast concrete components in bridges, including bridge girders, bridge decks, and segmental piers, presents a potential solution, because the components can be fabricated off-site in advance of construction, reducing the amount of time required to complete the bridge and the number of construction tasks that must be completed on-site. In addition to accelerated construction, prefabricated bridge systems can introduce better in plant quality control, so improve quality and durability and reduce life-cycle costs, facilitate construction, allow the use of innovative materials, improve work-zone safety and minimize impact to the environment (Cheng and Capers, 2009).

The concept of prefabricated bridge elements has long been researched as well as applied and put to use in building bridges. Adequate volume of information is currently available for use of such bridge components. Although the superstructure replacement is fast, the overall duration of the construction is controlled by the substructure construction duration since the substructure has to gain strength before the superstructure can be placed; this is a key obstacle facing rapid bridge construction. The construction of bridge abutments and their deep foundations (piles) is very time consuming, thereby delivering any rapid bridge construction method less effective. Therefore, there is an urgent need to

develop and use a novel method of accelerated construction for bridge abutments and foundations.

1.2 Research Objective

One of the major obstacles facing rapid bridge construction for "typical" span type bridges used in railroad and highway situations is the time required to construct bridge abutments and their foundations (shallow or deep). This can be remedied by using the "Controlled low strength materials (CLSM) bridge abutments" comprising prefabricated bridge components along with CLSM bridge abutments (Figure 1.1).

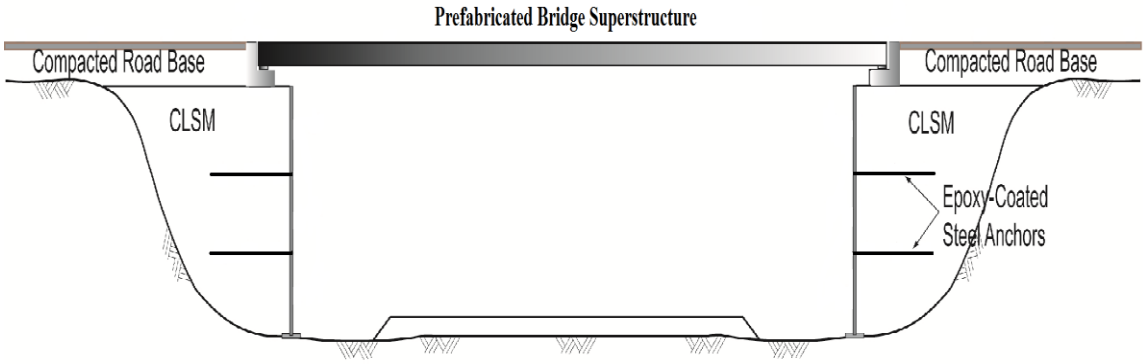

Figure 1.1: Proposed CLSM integrated bridge system.

The CLSM bridge abutment comprises full-height precast concrete panels that are attached to a CLSM backfill via steel anchors. The CLSM bridge abutment provides a load-bearing mechanism for the bridge sill, thus eliminating the need for piling. CLSM bridge abutments can be constructed in a very short time because they do not require

heavy machinery for excavation and compaction, and, most importantly, they do not require the use of piles and piling equipment. It is anticipated that with the CLSM integrated bridge system a complete bridge can be constructed in less than a week compared with a typical construction time of several months for a conventional bridge of the same size. In addition to the speedy construction, the ability to use by-products material, such as fly ash and foundry sand, in CLSM backfill translates into greater economy and the potential for a sustainable design.

It is noteworthy that CLSM has been used by several DOTs as self-leveling backfill behind conventional pile-supported bridge abutments to alleviate the "bump" at the end of the bridge (i.e., approach settlements). In the proposed CLSM abutment, however, the CLSM abutment itself will provide the bearing mechanism for the bridge sill. This unique approach has never been attempted previously, but it has the potential to profoundly reduce the cost and construction time of bridge abutments.

In this research project, the application of the CLSM integrated bridge system in typical span type bridges used in railroad and highway situations will be examined .It is the objective of this research to provide in-depth understanding of the behavior of the proposed CLSM abutments and to show that they are capable of carrying bridge loads with a reasonably large safety margin, and with minimal deformations.

1.4 CLSM Bridge Abutment

Figure 1.2(b) shows a schematic diagram of a typical CLSM bridge abutment with full-height precast concrete panel facing. For contrast, Figure 1.2(a) shows a

schematic diagram of a conventional bridge abutment with pile foundation. As indicated in Figure 1.2(b), the CLSM bridge abutment provides a load-bearing mechanism for the bridge sill, thus eliminating the need for piling. It should to be noted that the CLSM abutment does not require the use of a deep foundation, even if the underlying soil is weak. If the foundation soil is found unacceptable, a flowable fill foundation may be used to provide a stronger platform for the construction. The flowable fill foundation may involve removing about a 3-ft thick layer of the foundation soil and simply replacing it with a flowable fill.

The interlocking full-height concrete panels provide a form that contains the newly poured CLSM backfill until setting. The theory behind CLSM bridge abutments is that the steel rebar anchors make the CLSM mass and the full-height concrete panels behave as a single unit. The concrete facing panels and the reinforced CLSM mass are then treated as one unit and analyzed as a large gravity wall, which must be analyzed for stability in sliding and overturning. In addition, the number of steel anchors required and their spacing must be determined. Finally, the bearing pressure of such a large gravity wall must be checked to ensure that it does not exceed the allowable bearing capacity of the soil.

The internal stability of the CLSM wall must be ensured, as well. Rupture occurs when excessive forces exceed the ultimate tensile strength of the steel rebar anchors. Slippage of reinforcement in the CLSM-reinforcement composite can occur when the interface friction (bond) is insufficient.

The proposed CLSM bridge abutments have great promise in terms of ductility, flexibility, constructability, and costs. One major advantage of CLSM abutments is that they can be constructed rapidly without the need for compaction, piling, and heavy machinery.

It is anticipated that the proposed CLSM abutments with full-height concrete panel facing will have a number of distinct advantages over the conventional reinforced concrete abutments, including:

- Construction of CLSM abutments is rapid and requires only ordinary construction equipment.
- CLSM abutments are more flexible, hence more tolerant to foundation settlement and to seismic loading.
- When properly designed and constructed, CLSM abutments are expected to be remarkably stable. CLSM abutments also have higher ductility (i.e., less likely to experience a sudden catastrophic collapse) than conventional reinforced concrete abutments.
- When properly designed and constructed, CLSM abutments can alleviate the bridge "bumps" that commonly occur at the two ends of a bridge supported by conventional reinforced concrete abutments, especially when they are on piles.
- CLSM abutments do not necessarily require embedment into the foundation soil for stability. This advantage is especially important for speedy construction and when an environmental problem is involved, such as excavation into previously contaminated soil.

- CLSM abutments are expected to be generally less expensive to construct than their conventional counterparts.

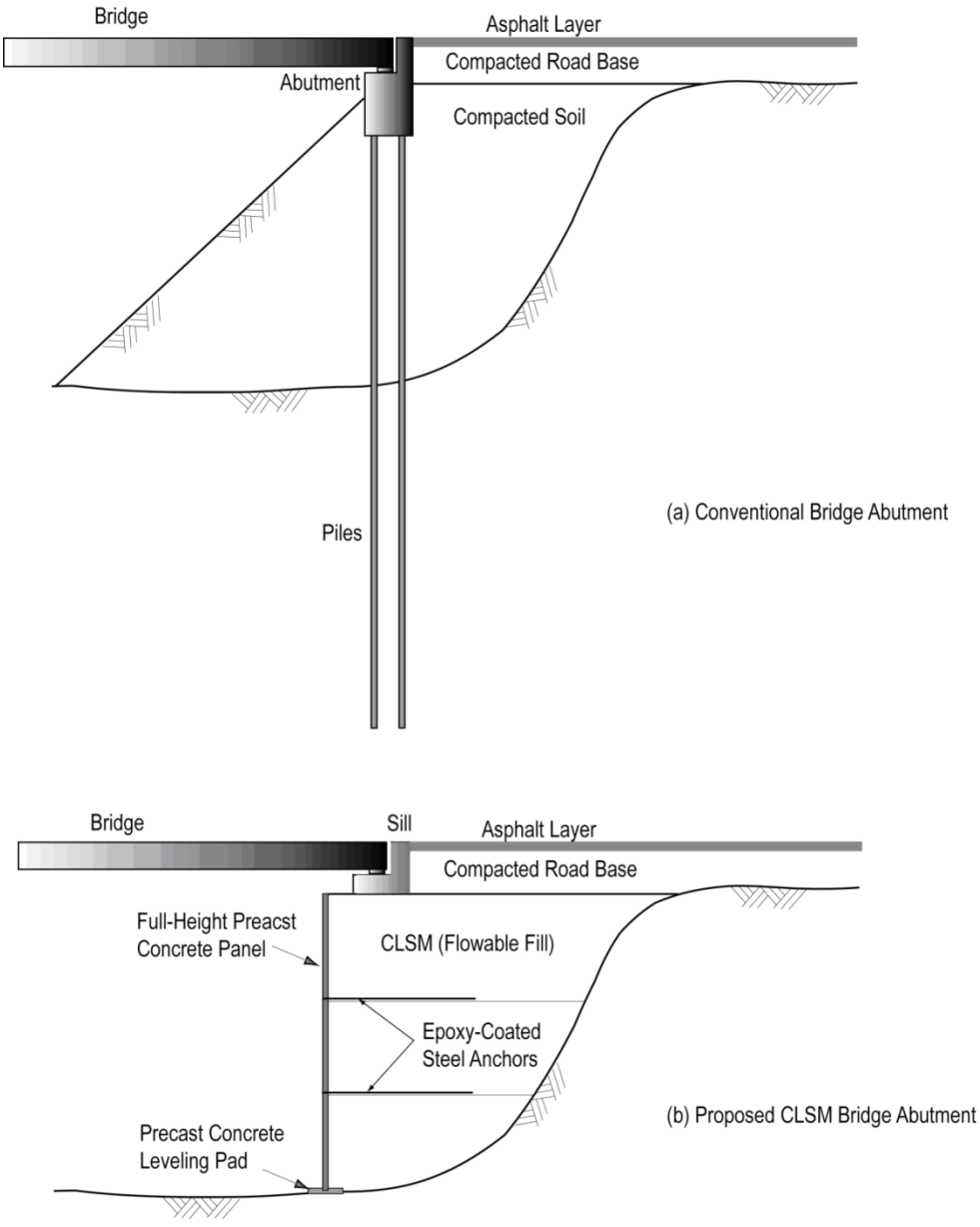

Figure 1.2: Comparison between (a) Conventional bridge abutment and (b) Proposed CLSM bridge abutment.

The construction sequence of a CLSM bridge abutment is very simple and involves the following steps (see Figure 1.3):

Step 1: Level the foundation soil and place a precast concrete leveling pad for the precast concrete panels.

Step 2: Install interlocking full-height precast concrete panels (Example: 18-ft high panels) with temporary lateral supports.

Step 3: Place a 6-ft thick layer of CLSM (flowable fill).

Step 4: Install the first row of half-inch diameter steel rebar anchors (insert through the opening from outside). This can be done even before the flowable fill is set since the guide hole in the concrete panel will keep the anchor in a horizontal position.

Step 5: Place the second 6-ft thick layer of flowable fill.

Step 6: Install the second row of half-inch diameter steel rebar anchors.

Step 7: Place the last 6-ft thick layer of flowable fill.

Step 8: Wait for the flowable fill to set (usually less than 24 hours) then remove lateral supports.

Step 9: Place the precast concrete bridge sill, place the approach fill behind the sill, and place the precast concrete bridge on elastomeric pads (or the equivalent) affixed to the sill.

The bridge does not need to have an approach slab, as road base material can be compacted directly behind the bridge sill to form the approach way and to create a gradual transition from the roadway to the bridge. Asphalt pavement can then be placed on the bridge and approach without a conventional joint system (approach slab) at the

bridge ends. The intent is to allow the bridge and the adjacent road to settle together, providing a smooth, bump-free ride for drivers traveling on and off the bridge.

The CLSM bridge system does not use piles and is more suited for single-span bridges in critical crossings. Simple-span bridges are more tolerant of settlement than multi-span structures, and the CLSM bridge system is designed to compensate for post-construction settlement; the bridge, abutment, and approach are supported on the same foundation system. The bridge is designed for uniform settlement between the sub- and superstructures.

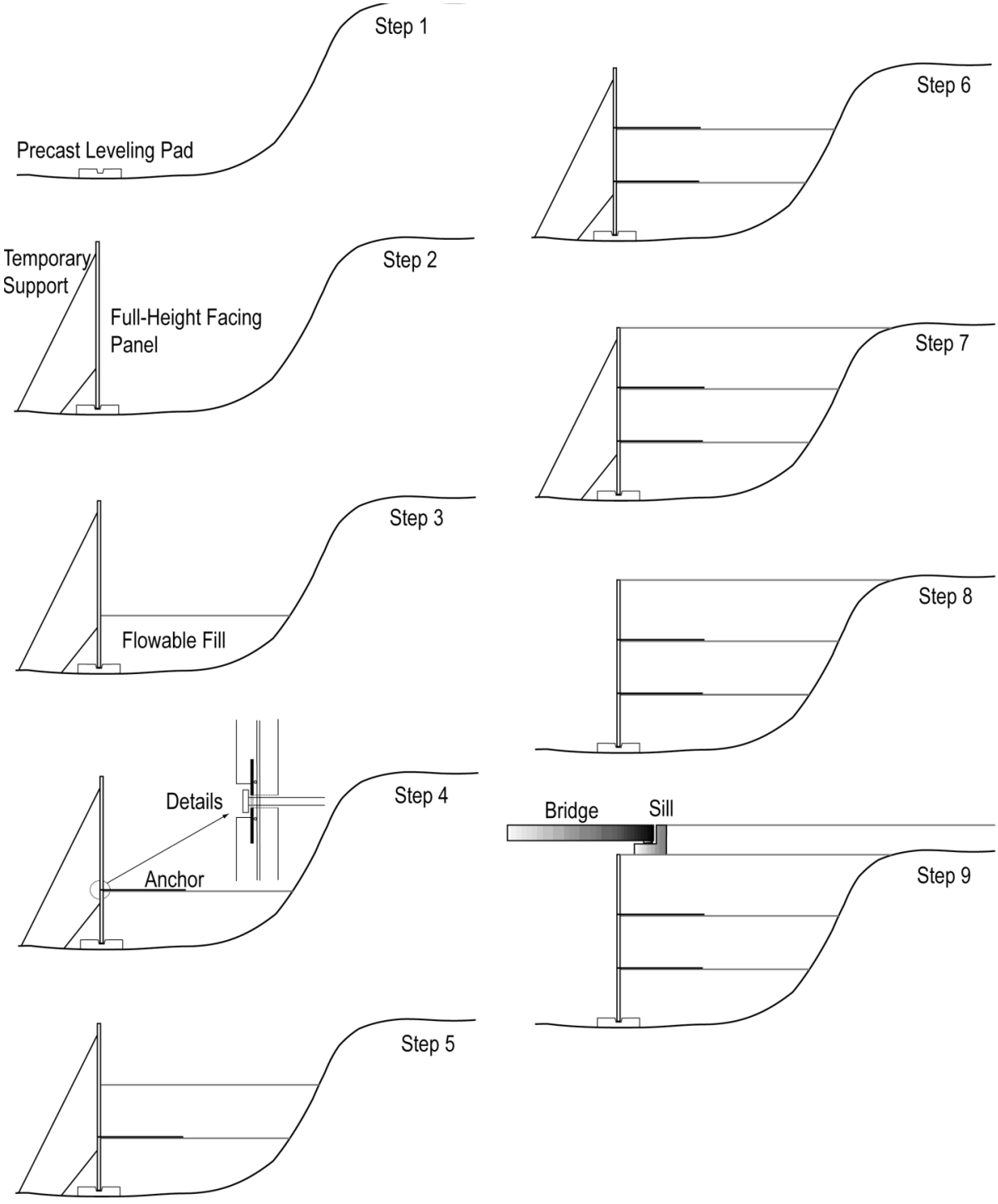

Figure 1.3: Construction Sequence of CLSM Bridge abutment.

1.4 Research Methodology

Several CLSM mixtures were tested for mechanical properties including compressive strength (1 day, 7 days, and 28 days), flow consistency, and pullout strength of rebars embedded in CLSM (Chapter 3). The selection criteria for a final mixture were based on its excavatability as well as its relatively high early strength.

In Chapter 4, the application of the CLSM bridge abutment in typical span type bridges is examined through a full-scale laboratory test to show the effectiveness of the proposed method in terms of construction time (rapidity).

An instrumented CLSM bridge abutment, 2.7 m (8.8 ft) x 2.7 m (8.8 ft) in plan, and 2.75 m (9 ft) in height, with full-height precast concrete panels was constructed to investigate the performance of the abutment due to application of a monotonically increasing sill pressure (Figure 1.4). Full-height precast concrete panels were attached to the CLSM backfill by steel anchors. The objectives of the test were: (1) to determine the constructability of the proposed CLSM bridge abutment, and (2) to determine the behavior of CLSM bridge abutments, in terms of load carrying capacity and deformations, after 7 days of CLSM setting time. The latter objective is of great interest since it will provide evidence about the behavior of the CLSM abutment shortly after the CLSM was poured--a critical issue with respect to rapid construction of the abutment. In the laboratory test performed in this research, foundation loading was applied on the seventh day after placing the CLSM fill; shorter waiting times are also possible.

The CLSM bridge abutment and the concrete sill were instrumented to measure their behavior during construction and upon application of bridge loads. Instrumentation

included load cells, pressure cells, strain gauges, LVDTs and high-resolution digital video cameras. Of particular interest was the displacement of the sill and the lateral pressure and displacement of the facing wall. Understanding that how much lateral pressure is applied during placement of fresh CLSM and after its setting is a key to design the precast concrete panels and their temporary lateral supports.

In chapter 5, the finite element method (FEM) of analysis was implemented to simulate and explore the performance of CLSM bridge abutments based on bearing pressure capacity, displacements, and the developed axial force in anchors, and to provide an assessment of safety of the design. Material properties obtained from the experimental testing on CLSM mixtures was used as a material input for the finite element analyses. The accuracy of the finite element results for the response and failure behavior of a CLSM mass was evaluated by a comparison with the experimental results. The experimental program included both standard compressive strength testing on CLSM cylinders (from chapter 3) and the laboratory large-scale testing on a CLSM bridge abutment (from chapter4). The validated finite element (FE) model was then used for conducting a series of parametric studies to define the effects of CLSM compressive strength, curing age, environment temperature and construction details on response of the abutments.

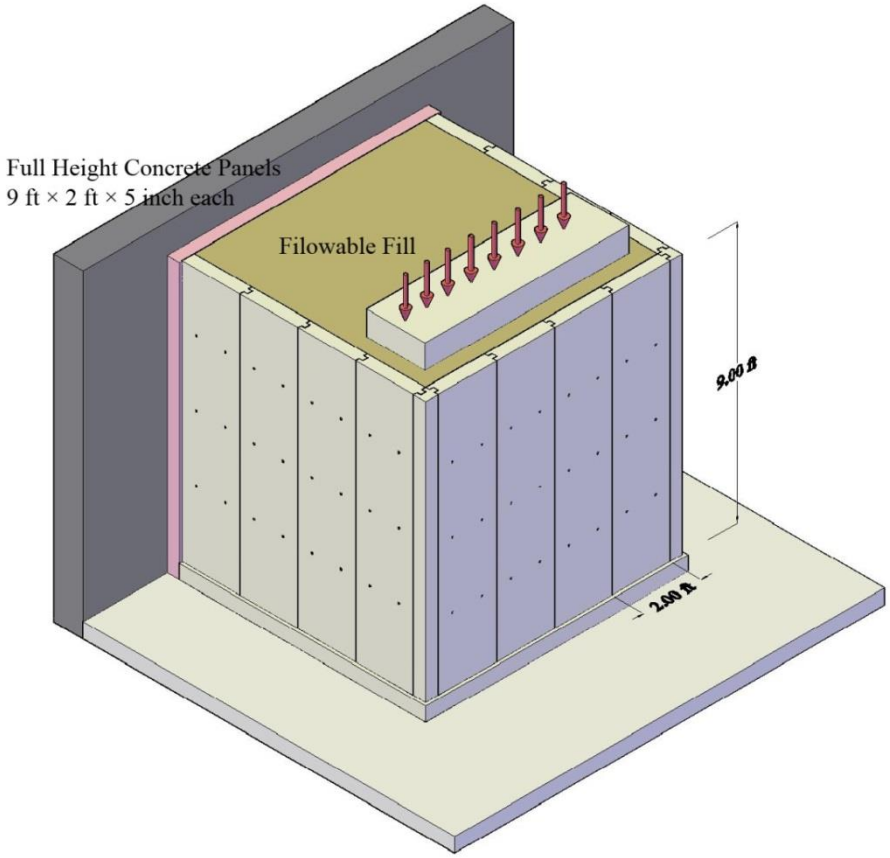

Figure 1.4: Large-scale laboratory test of CLSM bridge abutment (1ft = 0.3048 m).

1.5 Outline of the Dissertation

This dissertation is comprised of six chapters. A brief summary of each chapter is provided below:

Chapter 2 summarizes the state-of-the-art and current practice related to CLSM. Typical applications, advantages, and challenges of CLSM are also provided. Fresh and hardened properties, test methods, constituent materials and CLSM specifications were discussed in detail. Topics such as use of CLSM as a backfill for bridge abutments were also discussed.

Chapter 3 describes design of an optimized CLSM mixture that was used as a structural fill for construction of the bridge abutment. Experimental pullout tests and numerical simulations were performed to evaluate the bond performance of the CLSM and steel anchors.

Chapter 4 presents the construction procedure and experimental results of a large-scale laboratory test on a CLSM abutment that was subjected to a monotonically increasing sill pressure.

Chapter 5 discusses a finite element study to investigate the performance of CLSM bridge abutments. The validated finite element modeling was then used for conducting a series of parametric studies to better understand the performance of the CLSM abutments.

Chapter 6 contains a brief summary of the dissertation and lists the important findings and conclusions.

Chapter 2:

STATE-OF-THE-ART LITERATURE REVIEW

2.1 Controlled Low Strength Material (CLSM)

Controlled low strength material (CLSM) is a form of construction material which has been introduced in the construction industry as a more cost and time efficient substitute of compacted fills and its use has grown considerably in recent years. CLSM, also known as flowable fill, is defined by the ACI Committee 229 as self-compacting cementitious material that is in a flowable state at the time of placement and has a specified compressive strength of 8.3 MPa or less at 28 days, but is defined as excavatable if the compressive strength is 2.1 MPa or less at 28 days. CLSM is a mixture of aggregate, cementitious material, fly ash, water and sometimes chemical admixtures that hardens into a material with a higher strength than the soil. CLSM can be used as a replacement for compacted backfill and typically has strengths of 0.3 MPa to 0.5 MPa for most applications (ASTM D 6103). ACI-229 (1999) reports that the wet density of normal CLSM ranges between 1840 and 2320 kg/m^3, but the dry density is considerably less than the wet density due to water loss. Figure 2.1 shows a CLSM mix (ACI 229R, 1999).

Figure 2.1: CLSM Mix.

CLSM is a rapid fill material with several inherent advantages which allows fast return to traffic flow. A number of these advantages over conventional earthfill materials that require controlled compaction in layers (Dockter, 1998) include the following:

- ease of mixing and placement,
- ability to flow into hard-to-reach places,
- self-leveling characteristics of the fill,
- rapid curing,
- incompressibility after curing,
- excavatability.

Moreover, environment-friendly utilization of by-product materials such as fly ash and foundry sand within its mix, thereby reducing the demands on landfills, where these materials might otherwise be deposited (Trejo et al., 2004, and Najafi and Tia 2004).

Najafi and Tia (2004) noted that when flowable fill is used the need for compaction is eliminated. This reduces the equipment needs, labor costs, and associated inspections.

Although CLSM mixtures provide numerous advantages, there are also technical challenges that have served as obstacles to widespread CLSM use as its benefits might deserve. A major challenge in implementing the use of CLSM is the fact that CLSM is a cementitious material that behaves more like a compacted soil. Therefore, much of the available knowledge and literature on its applications and also the need for further researching, engineering, and promoting the use of this material, have fallen between concrete materials engineering and geotechnical engineering and it is often not given the level of attention it deserves by either group (Javed et al., 2002).

Some disadvantages of CLSM that have served as obstacles to extensive use of CLSM, include (Najafi and Tia 2004, Newman et al. 1993, and Schmitz et al. 2004):

- Requirement of forms,
- Segregation and bleeding,
- Lateral pressure during its fluid state,
- Shrinkage,
- Potential leaching of constituent materials,
- Durability of CLSM subjected to freezing and thawing cycles, and
- Higher-strength mixtures may not allow excavation.

A trial mix is recommended due to the sensitivity of compressive strength if this material is expected to be excavated in the future. Excessive long-term strength gain makes it difficult to excavate CLSM at later stages. ACI 229R (1999) noted that blockage of pumping equipment can result if there is segregation of particles, high fines content, or improper mixing. Also, the final grade level after placement will likely be lower than

during placement because of the reduction in volume of the material as water is released. ACI 229R (1999) has reported that settlement equal to 3 to 6 mm (1/8 to 1/4 in.) per foot of depth is typical and that designers need to consider subsidence in their quantities and in plan preparation. Halmen et al. (2005) believes that a major challenge in implementing the use of CLSM is the lack of knowledge on the corrosion performance of metallic pipe materials embedded in CLSM.

2.1.1 Historical Background

Advancement of plastic soil-cement, with the main improvements of flowability and quality control has led to the development of CLSM (Folliard et al. 2008). The first use of CLSM in the US was reported in 1964 for the bedding of a 515-km long pipeline in the Canadian River Aqueduct Project in north-western Texas (Adaska 1997). Since then, CLSM has been used for many applications.

In the early 70's, CLSM was developed in a contractual agreement between two companies, a power plant interested in finding more use for its fly ash and a cement company looking for extended use of their ready mixed concrete trucks. The primary objective was to find a substitute for conventional backfill materials using fly ash. Conventional backfilling is involved difficult and time consuming compaction of granular materials in thin layers to attain a specified compaction level. Improper compaction of backfill materials is a main reason of excessive settlement problems. In order to re-excavate the CLSM as easily as conventional backfill, it had to be Low strength. The two companies named their low-strength material, K-Krete® and patented

their procedures. By 1974 K-Krete Inc. was nation-wide and in 1977 it was sold (Hitch 1998). Through the 70's, similar products was produced by other companies but there was very little control of these products.

In the early 80's, in order to standardize the technologies and testing procedures for flowable fills some efforts were made. Flowable fills do not fit in perfectly with concrete testing standards and with soil testing standards either (Simmons 2002).

Several terms have been used over the past 40 years to describe what is currently recognized as CLSM, including flowable fill, unshrinkable fill, controlled density fill, flowable mortar, plastic soil-cement, soil-cement slurry, and K-Krete® (Folliard et al. 2008).

In 1984, The American Concrete Institute (ACI) founded Committee 229 to establish national standards to control these mixtures, report on CLSM applications, developments, material properties, mix proportioning, and construction and quality control procedures (Brewer 1990, 1994). The ACI-approved term "controlled low-strength material or CLSM" was chosen by the committee because it was more general, covering more types of fill materials. The American Concrete Institute has helped to standardize the use of CLSM and since the foundation of committee 229 many new ASTM standards have been written that only control CLSM (Simmons 2002). Nowadays, CLSM has been used all over the United States for a broad range of applications, using a variety of different materials (Folliard et al. 2008).

2.1.2 Materials

CLSM mixtures usually consist of water, Portland cement, fly ash or other similar byproducts, aggregates and chemical admixtures. Use of the standardized materials set by ASTM or other standard requirements is not necessary. The ability to use locally available materials including byproduct materials is a significant benefit of CLSM. Selection of materials should be based on availability, cost, specific application, and necessary characteristics of mixture, such as strength, flowability, excavatability, and density (ACI 229R, 1999). Use of by-products such as fly ash and foundry sand will be critical to the continued growth of CLSM usage due to the relatively high material cost of CLSM compared to other compacted fill materials (Folliard at al. 2008). Special low density CLSM (LD-CLSM) mixtures consist of Portland cement, water and preformed foam (ACI 229R, 1999).

2.1.2.1 Portland Cement

Cement is the main component that contributes to the strength and cohesion for CLSM mixtures. Although any type of Portland cement can be used in CLSM, for most applications, ASTM C 150 Type I or Type II is the most commonly used. Type III Portland cement has been successfully used in CLSM to achieve higher early strengths and to reduce subsidence.

2.1.2.2 Fly Ash

Fly ash is one of the by-products generated from the coal combustion in electric power generating plants. The use of fly ash in CLSM provides for excellent flowability and helps to minimize segregation, as well as increases the strength of CLSM. In many cases, fly ash also reduces the cost of the CLSM mixture, as it is typically less costly than Portland cement (Horiguchi et al. 2001). Compared with mixtures with high aggregate contents, high fly ash content mixtures result in lower-density CLSM (ACI 229R, 1999).

Although fly ash has become an important construction material and is used mostly in Portland cement concrete, approximately 70 to 75 percent of fly ash generated annually is still disposed in landfill. Much of this fly ash does not meet the specification for use in Portland cement concrete, due to high content of unburned carbon, as measured by the loss on ignition (LOI) test (Trejo at al. 2004). However, CLSM has no problem with the higher unburned carbon in the fly ash and it has been demonstrated that CLSM can be successfully produced using a wide variety of fly ash types and sources.

Therefore, CLSM can present a good solution to the environmental issues caused by fly ash landfill. Fly ashes used in CLSM mixtures do not need to conform to either Class F or C as described in ASTM C 618 (ACI 229R, 1999). Class F exhibits pozzolanic reactivity but rarely shows any self-cementitious behavior, while, Class C fly ash exhibits both pozzolanic and self-cementitious behavior. Higher amount of Fly ash is used in CLSM than in conventional concrete mixtures. Half the binder in CLSM is typically fly ash, and it is used as the only binder (without Portland cement) for rapid-setting CLSM (Folliard et al. 2008).

2.1.2.3 Aggregates

Aggregates are often the main part of CLSM mixtures. The type, grading, and shape of aggregates can affect the physical properties of CLSM, such as flowability and compressive strength (ACI 229R, 1999). Various aggregate types have been used successfully in CLSM.

Concrete Sand:

A wide range of fine aggregates may be used successfully in CLSM, but conventional concrete sand complying with ASTM C 33 are generally used because ready-mixed concrete plants as the main producers of CLSM have these materials in stock. Granular excavation materials that do not meet ASTM C 33 requirements (e.g., gradation) are a potential source of CLSM materials, and should be considered, provided that the specified flowability and constructability requirements are satisfied (Folliard et al. 2008).

Foundry Sand:

Foundry sand is a by-product of the metal-casting industry, it has been studied and used effectively in CLSM and its use has increased in recent years (Bhat and Lovell 1996). Foundry sand is becoming a more feasible candidate for use in CLSM because of its lower cost, increasing availability, and satisfactory performance (Trejo at al. 2004). It is estimated that a typical foundry generates about one ton of waste sand for every ton of metal castings produced and shipped (Kennedy and Linne 1987).

Environmental impact caused by leaching of heavy metals content is an issue of concern with using foundry sand in CLSM. Because of the concerns about the heavy metals present in the nonferrous foundry sands, ferrous foundry sands are more commonly used in CLSM (Trejo et al. 2004).

The Federal Highway Administration (FHWA) has issued a report, "User Guidelines for Waste and By-Product Materials in Pavement Construction," which covers in detail the use of foundry sand (and fly ash) in CLSM and provides guidelines for its proper usage (FHWA 1997). The U.S. Environmental Protection Agency (EPA) has also accepted foundry sand, along with fly ash, as suitable materials for CLSM (EPA 1998).

Bottom Ash:

Bottom ash is another by-product material of coal combustion. Bottom ash is formed by large non-combustible particles that cannot be carried by the hot gases. These particles are put into crusher to reduce the particle size to approximately 75 μm to 25 mm (Trejo et al. 2004). Bottom ash is used in CLSM as the fine aggregates because its size is similar to fine aggregates and it has relatively no cementitious properties of fly ash

Under the microscope, bottom ash particles are typically porous and angular in shape. Water will be absorbed and retained on the porous surface of bottom ash, while excessive water will be drained off (Kasemchaisiri and Tangtermsirikul 2006) which may cause the free water in CLSM to be excessive. This will actually cause bleeding condition in CLSM.

Aggregates used in CLSM have to fulfill either one of the following specification:

- ASTM C 33 specification aggregates within specified gradations;
- Pea gravel with sand;
- 19mm minus aggregate with sand;
- Native sandy soils, with more than 10% passing a 75μm sieve;
- Quarry waste products, generally 10mm minus aggregates (ACI 229R, 1999).

2.1.2.4 Water

According to ACI Committee 229, water that is suitable for concrete will work well for CLSM mixtures. More information on water quality requirements can be obtained from ASTM C 94 standard.

2.1.2.5 Chemical Admixtures

Air-entraining agents (AEAs) and foaming agents are valuable chemical admixture for the manufacture of CLSM. These AEAs and foaming agents are formulated specifically for use in CLSM to obtain higher air contents than conventional concrete.

The inclusion of air in CLSM can help provide improved workability, reduced shrinkage, minimal segregation and bleeding, lower density, control of ultimate strength development, enhanced thermal insulation, improved frost resistance, and lower material cost. Water content can be reduced as much as 50% when using air-entraining admixtures (ACI 229R, 1999).

Set accelerators have been used to a lesser extent to design CLSM mixtures with higher early strength and to minimize subsidence of CLSM. Other chemical admixtures can be used in CLSM to obtain specific target properties (Folliard et al. 2008).

2.1.2.6 Other Materials Used in CLSM

One advantage of CLSM technology is its capacity to include nonstandard materials, which can be available and more economical. However, these materials must be tested prior to use to verify their suitability in CLSM mixtures (ACI 229R, 1999).

Although fly ash is the most commonly used cementitious material in CLSM, other materials such as slag, metakaolin, silica fume, and rice husk ash have been used (Folliard et al. 2008).In addition to the aggregate materials previously described, there are other materials used in CLSM as aggregates such as glass cullet, Phosphogypsum and reclaimed crushed concrete.

Use of Cement kiln dust (CKD), which is a powder by-product of Portland cement manufacturing in rotary kilns, as the replacement for cement in CLSM was examined by Pierce et al. (2003). Various contents of CKD were found to produce excavatable CLSM mixtures.

2.1.3 Mixture Proportions

According to the review of literature, currently no standard mixture proportioning method for CLSM has been widely adopted. Considerable research has been done on factors affecting proportioning (Bhat and Lovell 1996), but there is no single, unified

method such as ACI 211 for conventional concrete (Folliard et al. 2008). Many studies show the proportioning of CLSM is actually based on past experience and the availability of local materials.

It is often a trial-and-error process used for Proportioning of CLSM mixtures until mixtures with appropriate properties are achieved. Trial mixtures have to be evaluated to decide how well they meet certain goals for fluidity with minimal segregation, acceptable setting times, adequate strength gain and excavatability. Adjustments are then made to achieve the desired properties (ACI 229R, 1999).

ACI Committee 229 summarizes number of mixture proportions that have been used by state DOTs and others and notes that this information is provided as a guide and should not be used for design purposes without first testing with locally available materials because requirements and available materials can vary significantly from project to project (ACI 229R, 1999). It can be concluded that cement contents commonly range from 30 to 120 kg/m^3, depending on strength and hardening-time requirements. Class F fly ash contents range from none to as high as 1200 kg/m^3 where fly ash serves as the aggregate filler. Class C fly ash is used in quantities of up to 210 kg/m^3. The majority of specifications call for the use of fine aggregate and its quantity varies with the quantity required to fill the volume of the CLSM after considering cement, fly ash, water, and air contents.. Coarse aggregate is generally not used in CLSM mixtures as often as fine aggregates. When used, however, the coarse aggregate content is approximately equal to the fine aggregate content. Water contents typically range from 193 to 344 kg/m^3 for

most CLSM mixtures containing aggregate. Water contents will be higher with mixtures using finer aggregates (ACI 229R, 1999).

2.1.4 Batching, Mixing, and Transporting

CLSM is typically batched, mixed, and transported in similar fashions as concrete. It is mostly batched at ready mixed plants and mixed in truck mixers. A survey performed in 1995 found that ninety percent of the 3000 ready mixed concrete producers in the United States produce some type of CLSM (EPA 1998).

CLSM can be delivered in ready-mix concrete truck mixers and placed in a flowable condition directly into the void to be filled, simply by chutes, conveyors, buckets, or pumps depending upon the application and its accessibility. For efficient pumping, some granular material is needed in the mixture (ACI 229R, 1999).

Some CLSM mixtures are produced using volumetric, mobile-type mixers. Rapid-setting CLSM mixtures with fly ash as the only binder are almost always produced on site using volumetric mixers because of the short handling time of such mixtures before setting (Folliard et al. 2008).

2.1.5 Engineering Properties

CLSM has some of the same ingredients concrete has, and is placed from equipment in a fashion similar to that of concrete. In-service CLSM, however, behaves more like a compacted soil.

When a CLSM mixture is designed, a variety of engineering parameters needs to be evaluated before, during, and after placement in the field. This section provides information on the properties of CLSM that most affect its performance in key applications. According to the 1998 survey of current practice by Folliard et al. (1999), CLSM properties and tests typically found in state DOT specifications are summarized in Table 2.1.

Table 2.1: CLSM properties typically specified by state DOTs (Folliard et al. 1999).

Property	Number of States Testing	Common Test Method(s)
Flow	18	ASTM D 6103 and ASTM C 143
Compressive strength	17	AASHTO T 22 and ASTM D 4832
Unit weight	14	AASHTO T 121
Air content	10	AASHTO T 152
Set time	7	ASTM C 403
Durability	2	pH and resistivity
Shrinkage	1	Visual
Geotechnical	1	Direct shear
Temperature	1	Modified ASTM C 1064
Chlorides/sulfates	1	Determination of ion contents
Permeability	0	None

2.1.5.1 Fresh CLSM Properties

Flowability:

One of the most important properties of CLSM is its ability to be self-leveling; to flow into and easily fill a void, without the need for conventional placing and compacting equipment which considerably reduce labor and enhance construction speed. Because the improved flow properties of CLSM are critical to the placement and performance, flowability is measured consistently.

ASTM D 6103, "Flow Consistency of Controlled Low Strength Material," as the main method of flowability measurement, includes the use of a 75 mm diameter × 150 mm long, open-ended cylinder, which is lifted, allowing the CLSM to slump and increase in diameter. The final diameter is typically used to separate between various degrees of flowability. Good flowability is achieved where there is no noticeable segregation and the diameter of CLSM material spread is 200 mm or higher.

Another method of expressing flowability is the measurement of the efflux time of CLSM as it flows through a standard flow cone apparatus in accordance with ASTM C 939, "Flow of Grout for Preplaced-Aggregate Concrete".

Segregation and Bleeding:

Separation of constituents in the CLSM mixture and bleeding can occur at high levels of flowability, particularly with very high water contents. Proportioning mixtures with sufficient fine materials, such as fly ash is helpful to provide suitable cohesiveness and reduce the potential for segregation and excessive bleeding. Even though, there are

no commonly used methods available to evaluate the segregation of CLSM, visual observations during mixing and placing provide a good, practical indicator.

According to ACI Committee 229, acceptable performance of CLSM has been obtained with Class F fly ash contents as high as 415 kg/m^3 in combination with cement, sand, and water. CLSM mixtures which have been designed using only fly ash as filler material, without sand or gravel, require much higher water content, but produce no noticeable segregation.

Hardening Time:

Hardening time is the approximate period of time required for CLSM to attain sufficient strength to support the weight of a person (ACI 229R, 1999). This time is influenced by amount and rate of bleed water released and other parameters, including mixture proportions, climatic conditions, and the surrounding environment, especially drainage conditions. Measuring the early age compressive strength of CLSM is not practical; hence a penetration-resistance test according to ASTM C 403 may be used as a measure of the hardening time and bearing strength. The hardening time can be as short as 1 hour, but generally takes 3 to 5 hours (Smith 1991). Another beneficial test method is ASTM D 6024, which determines the ability of CLSM for load application by repeatedly dropping metal weight onto in-place material (Hitch 1998).

Subsidence:

Subsidence is the reduction in initial in-place volume of CLSM caused by the displacement of water and release of entrapped air as a result of consolidation. Excessive

water is released to the surface as bleed water or through absorption into the surrounding soil.

CLSM will not experience settlement after hardening occurs. Subsidence and settlement are typically experienced during the initial 2-4 hours after placement. The actual amount of settlement that occurs depends on the materials and mixture proportions used, as well as placement heights, the environmental conditions and permeability of surrounding soil. ACI 229R (1999) has reported that settlement equal to 3 to 6 mm (1/8 to 1/4 in.) per ft of depth is typical and is generally found with mixtures of high water content. In order to limit the subsidence, utilizing sufficient fines such as fly ash, accelerating admixtures or high early-strength cement has been reported to be effective by reducing the tendency for subsidence or decreasing the susceptibility duration of CLSM (Folliard et al. 2008).

Pumping

CLSM mixtures may be proportioned to allow transport by conventional concrete pumping equipment without segregating or excessive bleeding. To decrease segregation and improve pumpability, the mixtures must be proportioned with sufficient fine materials, such as fly ash, to provide adequate void filling. High pump pressure may cause a loss in air content which increases the density and reduces pumpability.

2.1.5.2 Hardened CLSM Properties

Compressive Strength:

The ability of a CLSM backfill to support foundations and pavements, and resist lateral forces without failures or undergoing excessive deformation or settlement is related to its mechanical strength. The unconfined compression strength test is typically used to monitor strength development in CLSM mixtures. The compressive strength of CLSM is the most common hardened property found in state DOT specifications (Table 2.1) and probably the most important criterion to control in developing the mixture design.

Unlike many granular compacted backfill materials, CLSM develops mechanical strength with time. Compressive strengths must be retained at a low level for projects where later excavation is anticipated or specified. The extent of the strength development in the long term must be controlled by proper selection and proportioning of the constituent materials.

ASTM D 4832, "Preparation and Testing of Controlled Low-Strength Material (CLSM) Test Cylinders" is the most common method for evaluating CLSM strength. The relatively low strength of CLSM is the most serious potential problem of compression test methods for CLSM. This creates difficulties in stripping CLSM test specimens and in testing cylinders, where large-capacity concrete compression machines have poor accuracy in the required low load range (Folliard et al. 2008).

Excavatability:

Material properly which relates to the ease at which the material may be removed. Easy removal of CLSM from trenches is critical when utilities fail or require repair. According to ACI Committee 229, CLSM with a compressive strength of 0.3 MPa or less can be excavated manually and mechanical equipment, such as backhoes, are used for compressive strengths of 0.7 to 1.4 MPa (Figure 2.2). Undesired long-term strength gain may prevent the removal of CLSM using conventional means of shovels or backhoes.

The composition of the mixture influence excavatability; CLSM with coarse aggregate may be difficult to excavate even at low strengths while mixtures using fine sand or only fly ash as the aggregate filler have been removed with a backhoe at higher strengths.

Figure 2.2: Excavating CLSM with backhoe (ACI 229R, 1999).

Density:

According to ACI Committee 229, Wet density of normal CLSM in place is greater than most compacted materials and ranges between 1840 to 2320 kg/m^3. CLSM mixtures proportioned using lightweight aggregates, high entrained-air contents, and foam, have lower unit weights. CLSM with only fly ash, cement, and water should have a density between 1440 to 1600 kg/m^3. Dry density of CLSM is substantially less than the wet density due to water loss.

Permeability:

An important hydraulic property of a backfill material is permeability. The permeability affects the rate of seepage of water through a backfill material. The permeability of a soil is typically measured by Darcy's law (laminar flow) where the flow of water through a soil is:

$$Q = kiA$$

Where: Q = Water flow

k = Coefficient of Conductivity (permeability coefficient)

i = Hydraulic gradient, head or water pressure divided by length of flow path

A = Cross sectional area Perpendicular to flow path

A uniformly, well graded coarse sand has a relatively high permeability with a coefficient of permeability of approximately 4.0 x 10^{-1} cm/sec. On the other hand, clay has relatively low permeability with a coefficient of water conductivity of 1.0 x 10^{-7} cm/sec.

The permeability of CLSM to both liquids and gases has a significant impact on performance of CLSM in various applications. The permeability of CLSM affects several important properties, including drainage characteristics, durability, and leaching potential. CLSM may be designed to be as permeable as uniform coarse sand or as dense as clay. An advantage that CLSM has, compared to conventional concrete, is that actual water permeability tests can be conducted. Typical values for CLSM are in the range of 10^{-4} to 10^{-5} cm/s, but higher strength mixtures with higher fines-content may reduce the permeability to as low as 10^{-7} cm/s. Permeability is increased as cementitious materials are reduced and aggregate contents are increased (ACI 229R, 1999).

Shear Strength:

Since engineered applications of CLSM as a substitute to conventional compacted fill is growing, it is getting more important to measure CLSM properties in terms of geotechnical engineering parameters by either direct measurement or by developing correlations between geotechnical and concrete test results. The shear properties of CLSM are specially important and can be evaluated using both a direct shear test (ASTM D 3080) and a triaxial shear–consolidated drained test (Folliard et al. 2008).

Some studies have focused on the shear properties of CLSM (Bhat and Lovell, 1996, Dolen and Benavidez, 1998, and Hoopes 1998). The shear properties of CLSM often exceed typical compacted fill shear strengths, especially at later ages as hydration proceeds (Hoopes 1998). CLSM showed an internal friction angle ranging from 20 to 30 degrees (FHWA 1997). The shear modulus, which is the ratio of unit shearing stress to

unit shearing strain, of normal density CLSM is typically in the range of 3400 to7900 ksf (ACI 229R, 1999).

California Bearing Ratio:

California bearing ratio (CBR) testing is used to determine the strength of subbase and subgrade materials. CLSM can be designed to significantly increase the bearing capacity of a subbase or base for pavements. The bearing capacity of CLSM may be measured as California bearing ratio (CBR) with the soil test method, AASHTO T 193, "Standard Method of Test for the California Bearing Ratio".

Consolidation:

ASTM Test Method D 2435, "One-Dimensional Consolidation Properties of Soil", can be used for consolidation properties of CLSM. This method assists to estimate both the rate and total amount of differential and total settlement for CLSM used in various applications. In addition, consolidation data are used to derive bedding factors and soil stiffness values needed for pipe bedding design (Hoopes 1998).

Shrinkage:

Compared to concrete, CLSM typically has a very high water-cement ratio and water content, factors that cause excessive drying shrinkage in concrete. However, the limited studies that have focused on CLSM shrinkage have not found it to be a significant factor. Hardened CLSM may exhibit shrinkage cracks; however, they do not affect the structural integrity of the material for most applications (Folliard et al. 2008).

Typical linear shrinkages in the range of 0.02 to 0.05 percent have been reported by ACI Committee 229 (1999). Because of the low strength and fragile nature of CLSM specimens, the standard concrete method to measure shrinkage, AASHTO T160 may not be appropriate.

Thermal Insulation/Conductivity:

Low density, air-entrained CLSM with its enhanced insulating properties is particularly well suited for pipe backfill to prevent heat loss from the pipe. Foamed or cellular CLSM mixtures have low densities and exhibit good insulating properties (ACI 229R, 1999). Thermal needle test method, ASTM D 5334, may be applied to CLSM to measure the thermal and insulating properties of CLSM.

High density low porosity CLSM should be used where high thermal conductivity is desired such as backfill around underground power cables. As the moisture content and dry density increases, so does the CLSM's thermal conductivity (Ramme at al. 1995).

2.1.5.3 Durability and Environmental Issues Related to CLSM

Freezing and Thawing Resistance:

It is a measure of the ability of a material to withstand climatic changes overtime without loss of strength. Where freezing and thawing resistance of CLSM is concerned, some issues must be considered. CLSM is susceptible to both internal hydraulic pressure and frost heave, when exposed to freezing and thawing cycles. Besides, test methods that

have been developed for conventional concrete have been found to be too severe for testing CLSM (Folliard et al. 2008).

Nantung (1993) reported that AASHTO T 161, the most common method used for concrete, was far too severe for testing CLSM and proposed some modifications to the method. Gress (1996) found that CLSM can survive freezing and thawing damage, but proposed that the top 50 to 150 mm of CLSM trenches be removed after set and backfilled with a frost heave–compatible base material to ensure uniform heaving of pavement and trench. ASTM D 560, "Freezing and Thawing of Compacted Soil- Cement Mixtures," is much less severe and may be a more practical test method for CLSM (Janardhanam et al. 1992).

Corrosion:

Corrosion deterioration of metallic pipe materials embedded in CLSM has not yet reported as a serious problem in field applications. But, because of the long-term nature of corrosion and other durability problems, it could prove to be an important aspect of CLSM durability (Folliard et al. 2008). Test methods developed to evaluate the potential for corrosion of metals in soil backfills can be used to evaluate the corrosivity of CLSM, even though existing guidelines on corrosion potential of soils do not consider the unique characteristics of a cementitious material such as CLSM and may not reliably predict the performance of CLSM. These methods often indicate that CLSM could be detrimental to the corrosion performance of metallic pipes.

Electrical resistivity tests to compare corrosion potential of natural soils on corrugated metal culvert pipes, California Test 643, can be performed in the same manner

on CLSM. The moisture content of the sample is an important parameter for the resistivity of a sample and the samples should be tested at their expected long term field moisture content (Ramme and Naik 1997). The most important properties that have effect on corrosivity of CLSM include permeability, pH, resistivity, buffering capacity, presence of chlorides, and exposure conditions (i.e., type and nature of native soil, etc.). The permeability of CLSM to water and oxygen, required for the corrosion process to occur, and migration rate of chloride which can significantly increase localized corrosion are critical (Folliard et al. 2008).

The most important properties that have effect on corrosivity of CLSM include permeability, pH, resistivity, buffering capacity, presence of chlorides, and exposure conditions (i.e., type and nature of native soil, etc.). The permeability of CLSM to water and oxygen, required for the corrosion process to occur, and migration rate of chloride which can significantly increase localized corrosion are critical (Folliard et al. 2008). The Ductile Iron Pipe Research Association has one of the most common methods used to determine the corrosivity of backfill materials around ductile iron pipes. The evaluation procedure assigns points for various soil backfill characteristics: soil resistivity, pH, oxidation-reduction potential, sulfides and moisture. For a given sample, if the sum of the points from all characteristics is more than 10, the soil is assumed to be corrosive (Hill and Sommers 1997, Straud 1989). The corrosion potential of CLSM flowable fly ash slurry produced with fly ash derived from some of Wisconsin Electric's power plants has been shown to be considerably less than corrosion potential of typical soils used for trench backfill and so is not considered corrosive (Ramme at al. 1995).

NCHRP web-only document 116 is a comprehensive study about corrosivity of CLSM (Folliard et al. 2006). The study evaluated the corrosion of ductile iron and galvanized steel embedded in CLSM through mass loss measurements of metallic coupons which is one of the more reliable techniques even though it is a time consuming corrosion testing method.

Leaching and Environmental Impact:

The potential leaching of constituent materials and elements is considered as obstacle to widespread CLSM use. Since the use of by-product materials, such as fly ash and foundry sand which may contain heavy metals, is more common and also because of its higher permeability, leaching and subsequent environmental impact is more critical for CLSM applications, compared to conventional concrete. Because CLSM is a relatively new technology and leaching is a rather slow process, adequate long-term field data and observations are not available for evaluation of CLSM leaching effects (Trejo et al. 2004).

Research at Purdue University, on the effects of foundry sands on CLSM leachate and environmental impact, found that only one of eleven mixtures showed unusually high concentrations of heavy metals in the expressed pore solution (Bhat and Lovell 1996). Naik et al. (1998) found relatively high concentrations of total dissolved solids in leachate extracted from CLSM containing clean coal ash.

2.1.3 Specifications, Test Methods, and Practices

In order to control the use of CLSM, many states have developed their own specifications (in some cases, provisional) which is differ from state to state. Moreover, a variety of different test methods are currently being used to define the same properties. This lack of consistency, both on specifications and testing methods, has also been an obstacle for the propagation of CLSM applications (Javed et al. 2002).

The Environmental Protection Agency (EPA) recommends that procuring agencies use ACI 229R (1999) and the ASTM standards listed in Table 2-2 when purchasing flowable fill or contracting for construction that involves backfilling or other fill applications. More than 20 states in the US have specifications for flowable fill containing coal fly ash. They include California, Colorado, Delaware, Florida, Georgia, Illinois, Indiana, Kansas, Kentucky, Maryland, Massachusetts, Michigan, Minnesota, Nebraska, New Hampshire, New Mexico, North Carolina, Ohio, Texas, Washington, West Virginia, and Wisconsin.

Table 2.2: Current ASTM standards on CLSM.

ASTM Specification Number	Title
D 4832-02	Standard Test Method for Preparation and Testing of Controlled Low Strength Material (CLSM) Test Cylinders

D 5971-01	Standard Practice for Sampling Freshly Mixed Controlled Low Strength Material
D 6023-02	Standard Test Method for Unit Weight, Yield, Cement Content and Air Content (Gravimetric) of Controlled Low Strength Material (CLSM)
D 6024-02	Standard Test Method for Ball Drop on Controlled Low Strength Material (CLSM) to Determine Suitability for Load Application
D 6103-97	Standard Test Method for Flow Consistency of Controlled Low Strength Material

2.1.6.1 Standard Test Method for Preparation and Testing of CLSM Test Cylinders (ASTM D 4832)

Cylinders of CLSM are tested to determine the compressive strength of the material. The cylinders are prepared by pouring a representative sample into molds, curing them, removing the cylinders from the molds, and capping the cylinders for compression testing. The cylinders are then tested by machine to obtain compressive strengths by applying a load until the specimen fails. Duplicate cylinders are required (Howard and Hitch, 1998).

The compressive strength of a specimen is calculated as follows:

$$f_c = \frac{P}{A}$$

Where f_c = compressive strength in pounds per square inch (MPa);

P = maximum failure load attained during testing in pounds (KN); and

A = load area of specimen in square inches (mm^2).

This test is one of a series of quality control tests that can be performed on CLSM during construction to monitor compliance with specification requirements.

2.1.6.2 Standard Practice for Sampling Freshly Mixed CLSM (ASTM D 5971-96)

This practice explains the procedure for obtaining a representative sample of the freshly mixed CLSM as delivered to the project site for control and properties tests and includes sampling from revolving-drum truck mixers and from agitating equipment used to transport central-mixed CLSM. The minimum sample of CLSM for compressive strength test must be 0.0142 m^3 (0.5 ft^3) and for other tests, the composite sample size shall be large enough to perform so as to ensure that a representative sample of the batch is taken (Howard and Hitch, 1998).

2.1.6.3 Standard Test Method for Unit Weight, Yield, Cement Content and Air Content (Gravimetric) of CLSM (ASTM D 6023)

The unit weight of the freshly mixed CLSM is determined by filling a measure with CLSM, determining the mass, calculating the volume of the measure, then dividing the mass by the volume. The yield, cement content, and air content of the CLSM are

calculated based on the masses and volumes of the batch components (Howard and Hitch 1998).

a) Yield:

$$Y = \frac{W_1}{W}$$

Where Y = volume of CLSM produced per batch in cubic feet (m^3);

W = density of CLSM in pounds per cubic foot (kg/m^3); and

W_1 = total mass of all materials batched, kg.

b) Cement content:

$$N = \frac{N_1}{Y}$$

Where N = actual cement content in pounds per cubic yard (kg/m^3);

N_t = mass of cement in the batch, kg; and

Y = volume of CLSM produced per batch in cubic yards (m^3).

c) Air content:

$$A = \frac{T - W}{T} \times 100$$

Where A = air content (percent of voids) in the CLSM;

T = theoretical density of the CLSM computed on an air free basis, kg/m^3;

And W = density of CLSM, kg/m^3.

2.1.6.4 Standard Test Method for Ball Drop on CLSM to Determine Suitability for Load Application (ASTM D 6024)

This test method is used mainly as a field test to determine the ability of the CLSM to withstand loading prior to adding a temporary or permanent wearing surface. A standard cylindrical weight is dropped five times from a specific height onto the surface of in-place CLSM. The diameter of the resulting indentation is measured and compared to established criteria. The indentation is inspected for any free water brought to the surface from the impact (Howard and Hitch, 1998).

2.1.6.5 Standard Test Method for Consistency of CLSM (ASTM D 6103)

This test method determines the flow consistency of fresh CLSM mixtures for use as backfill or structural fill. It applies to flowable CLSM with a maximum particle size of 19.0 mm (3/4 in.) or less, or to the portion of CLSM that passes a 19.0-mm sieve. An open-ended cylinder is placed on a flat, level surface and filled with fresh CLSM. The cylinder is raised quickly so the CLSM will flow into a patty. The average diameter of the patty is determined and compared to established criteria (Howard and Hitch, 1998).

2.1.6.6 Other Currently Used and Proposed Test Methods

In order to ensure quality control and ease of placement it is required to specify minimum level of flowability or consistency and a specified method of measuring it.

Flowability can be measured by one of several different methods, including slump (ASTM C 143) and flow cone tests (ASTM C 939). A slump range of 6 to 10 in which corresponds to a flow time of 30 to 60 seconds through a standard flow cone would be the practical design parameters. Another method to specify CLSM consistency is very similar to the ASTM standard test specification, "Flow Table for Use in Tests of Hydraulic Cement" (C 230), for determining the flow of mortar mixtures (Dockter 1998).

Permeability of the CLSM mixtures has been measured as the same as for soils testing using the constant head or falling head principles, ASTM D 5084 (Dockter 1998). The aggregate gradation has been determined by ASTM C136-01, "Standard Test Method for Sieve Analysis of Fine and Coarse Aggregates" and ASTM C117, "Standard Test Method for Materials Finer than 75 μm (No. 200) Sieve in Mineral Aggregates by Washing." (Javed et al. 2002). A new ASTM standard, "Standard Practice for Installing Buried Pipe Using Flowable Fill" has been proposed, which describes how to use flowable fill for installing buried pipe. ASTM Committee C 3 on Clay Pipe has already initiated mentioning the use of flowable fill in the Standard C 12 that covers installation of clay pipe (Howard 1998).

A summarized overview of the test standards and provisional test methods currently in use is as follows (Dockter 1998):

Provisional methods of testing:

1. AASHTO Designation: X7 (2001)–"Evaluating the Corrosion Performance of Samples Embedded in Controlled Low Strength Material (CLSM) via Mass Loss Testing."

2. AASHTO Designation: X8 (2001)–"Determining the Potential for Segregation in Controlled Low Strength Material (CLSM) Mixtures."
3. AASHTO Designation: X9 (2001)–"Evaluating the Subsidence of Controlled Low Strength Materials (CLSM)."

Other ASTM test methods used in CLSM technology:

1. ASTM C231-97–"Standard Test Method for Air Content of Freshly Mixed Concrete by the Pressure Method."
2. ASTM C403/C 403M-99–"Standard Test Method for Time of Setting of Concrete Mixtures by Penetration Resistance."
3. ASTM D560-96–"Standard Test Methods for Freezing and Thawing Compacted Soil-Cement Mixtures."
4. ASTM D5084-90 (Reapproved 1997)–"Standard Test Method for Measurement of Hydraulic Conductivity of Saturated Porous Materials Using a Flexible Wall Permeameter."
5. ASTM G51-95 (Reapproved 2000)–"Standard Test Method for Measuring pH of Soil for Use in Corrosion Testing."

2.1.7 Specifications by the State Transportation Agencies

Riggs and Keck (1998) carried out a survey of how CLSM is specified in six southeastern states of US. As shown in Table 2.3, it is apparent that all of the

specifications were issued after 1990, and so the use of CLSM is relatively new to standard transportation road construction.

Table 2.3: States surveyed and their CLSM specification.

State	Specification and Title of Section	Issue Date
Alabama	Section 260, Low Strength Cement Mortar	1996
Florida	Section 121, Flowable Fill" (revised 1996)	1997
Georgia	Section 600, Controlled Low Strength Flowable Fill	1995
N. Carolina	Controlled Low Strength Material Specification	1996
S. Carolina	Specification 11, Specification for Flowable Fill	1992
Virginia	Special Provisions for Flowable Backfill	1991

Table 2.4 compares specified acceptance compressive strengths and ages. The general acceptance age is 28 days with 2 states having 56-day requirements. As a result of the high levels of pozzolans in many CLSM mixtures, there can be significant strength increases after 28 days. Several states have both excavatable and nonexcavatable mixtures. If the CLSM will be removed at a later date, its strength must be limited to less than 2.1 MPa, which can be assured only if later age strengths are evaluated (Riggs and Keck, 1998). According to the survey, all states except Virginia have recommended mixture proportions (Table 2.5).

Table 2.4: Specified acceptance strengths and ages.

State	Age, days	Strength, psi (MPa)
Alabama	28	80 (0.55); 200(1.4); 1000 (6.9); 1100 (7.6);175 (1.2)
Florida	28	100 (0.7) (maximum); 125 (0.9)
Georgia	28	100 (0.7) (maximum); 125 (0.9)
N. Carolina	28;56	125 (0.9); 150 (1.0) (maximum)
S. Carolina	28;56	80 (0.55); 125 (0.86)
Virginia	28	30 – 200 (0.2 – 1.4)

Table 2.5: Suggested mixture proportions, lb/yd^3 (kg/m^3).

State	Cement	Pozzolan	Fine Aggregate	Water	Air Range
Alabama	61 (36)	331 (196)	2859 (1696)	509 (302)	Not given
	185 (110)	0	2637 (1586)	500 (297)	″
	195 (116)	572 (339)	2637 (1586)	488 (290)	″
	195 (116)	572 (339)	2673 (1586)	488 (290)	″
	517 (307)	0	413 (245)	341 (202)	″
Florida	75-100 (44-89)	0	(a)	(a) (b)	5-35
	75-150 (44-89)	150-600 (89-356)	(a)	(a) (b)	15-35
Georgia	75-100 (44-89)	0	(a)	(a) (b)	15-35
	75-150 (44-89)	150-600 (89-356)	(a)	(a) (b)	5-15
N. Carolina	40-100 (24-59)	(a)	(a)	(a) (b)	0-35
	100-150 (59-89)	(a)	(a)	(a) (b)	0-35
S. Carolina	50 (30)	600 (356)	2500 (1483)	458 (272)	none (c)
	50 (30)	600 (356)	2500 (1483)	541 (321)	none (c)
Virginia	Contractor must submit his own mixture (“mix design”)				

2.1.8 Applications

Flowable fill is a multipurpose construction material that has been used in a wide variety of applications that are well documented in the literature. The primary application of CLSM is as a backfill in place of compacted soil. Among the many applications of CLSM, the following are the main (ACI 229R, 1999, and NRMCA 1989):

- Backfill for sewer trenches, conduit trenches, utility trenches, building excavations, bridge abutments and retaining walls
- Structural fill for foundation footings, sub footings, floor slab bases, road bases, subbases, subgrades, and utility bedding
- Void-filling for underground storage tanks, abandoned sewers, abandoned utility, voids under pavement, basements or other underground structures
- Bridge approaches; either as a subbase for the bridge approach slab or as backfill with other elements.

Utility bedding applications involve the use of CLSM as a bedding material for pipes, electrical and other types of utilities, and conduits. Because it resists erosion better than many other fill materials, CLSM can be used for erosion control in embankments and slopes, and to fill voids under culverts, pavements, sidewalks, bridges and other structures where natural soil or noncohesive granular fill has eroded away (ACI 229R, 1999). It was also indicated that appropriate CLSM mixtures can be designed as anti-corrosion fill, thermal and isolation fill (Brewer 1994). The use of CLSM for

encapsulation of contaminated soil was also documented in the literature (Melton et al. 2005).

According to the survey by Riggs and Keck (1998) (Table 2.6), CLSM mostly has been used in lieu of compacted soil, however, some of states have expanded the list to include many applications. Also a survey performed by Folliard et al. (1999) among state agencies found that CLSM was used for bedding applications for granite curbs and as lightweight fill to cover swamp areas. CLSM is used in nuclear facilities for conventional applications because it decreases personnel exposure to radiation (ACI 229R, 1999). In addition to the applications previously discussed, new applications of CLSM are expected to surface as the construction community gets more familiar with this material.

Table 2.6: Application of CLSM in surveyed states.

State	**Applications**
Alabama	Backfill for drainage structures and utility cuts
Florida	Bedding; encasements; closures for tanks, pipes; trench backfill
Georgia	Bedding; encasements; closures for tanks, pipes; trench and abutment backfill
N. Carolina	Filling underground storage pipes and pipe culverts; backfilling culverts, bridges (where culverts or pipes are installed under a bridge), retaining walls, roadway trenches
S. Carolina	Backfilling under foundations, abandoned pipelines, culverts, tanks, utility trenches, catch basins, drop inlets, vertical taps, bridge abutments
Virginia	In lieu of compacted soil or aggregate backfill

2.2 Use of CLSM as a Backfill for Bridge Abutments

CLSM is used in bridge approaches, either as a sub-base for the bridge approach slab or as backfill. There are several essential advantages of using CLSM as backfill in lieu of compacted soil and granular backfills. In 1991, Smith published a list of 15 main advantages of CLSM. The list was later adopted by the ACI 229 committee and included in their report on CLSM. These advantages are listed below:

1. Ready available: Using locally available materials, ready mixed concrete suppliers can produce CLSM to meet most project specifications.
2. Easy to deliver: Truck mixers can deliver specified quantities of CLSM to the jobsite whenever the material is needed.
3. Easy to place: Depending on the type and location of void to be filled, CLSM can be placed by chute, conveyor, pump, or bucket. Because CLSM is self-leveling, it needs little or no spreading or compacting. This speeds construction and reduces labor requirements.
4. Versatility: Flowable fill mix designs can be adjusted to meet specific fill requirements, thus making the fill more customized and efficient.
5. Strength and durability: Flowable fill is stronger and more durable than compacted soil or granular fill.
6. Excavatability: CLSM having compressive strengths from 0.34 to 0.69 MPa (50 to 100 psi) can be easily excavated with conventional digging equipment yet is strong enough for most backfilling needs.

7. Requires less inspection: During placement, soil backfill must be tested after each lift for sufficient compaction. CLSM self-compacts consistently and does not need this extensive field testing.
8. Allows fast return to traffic: Because many CLSM mixtures can be placed quickly and support traffic loads within several hours, downtime for pavement repairs is minimal.
9. Lower settlement: Flowable fill does not form voids during placement nor settle or rut under loading. It hardens to a degree that prevents any future settlement of the backfill.
10. Reduces excavating costs: CLSM allows narrower trenches because it eliminates having to widen trenches to accommodate compaction equipment.
11. Improves worker safety: Since it reduces exposure to possible cave-ins, flowable fill provides a safer environment for workers.
12. Allows all weather construction: CLSM will displace standing water left in a trench from rain or melting snow, reducing the need for dewatering pumps. To place CLSM in cold weather, materials can be heated using the same methods for heating ready mixed concrete.
13. Reduces equipment needs: Unlike soil or granular backfill, CLSM can be placed without loaders, rollers, or tampers.
14. Requires no storage: It makes storage unnecessary because ready-mix trucks deliver flowable fill to the jobsite in the quantities needed.

15. Makes use of a byproduct: Flowable fill containing fly ash benefits the environment by making use of this industrial waste by-product.

The extra cost for the material, compared to compacted backfill, is offset by the fact that it eliminates the costs for compaction and labor, reduces the manpower required for close inspection of the backfill operation, requires less trench width, and reduces the time period and costs of public protection measures.

As it is mentioned before, CLSM answers the need for a fill that allows prompt return to traffic flow. Faster construction due to ease of placement and fast curing presents the CLSM a potential alternative fill when rapid construction is requisite.

CLSM has been used by several DOTs as self-leveling backfill behind conventional pile-supported bridge abutments to alleviate the "bump" at the end of the bridge (i.e., approach settlements) and generally, its performance has been good. A survey by Trejo et al. (2004) indicated that 42 out of 44 state DOTs have specifications for CLSM. A study of 177 bridges in Oklahoma compared different backfills behind conventional bridge abutments (Snethen and Benson, 1998; and Snethen et al., 1997), and the results of the CLSM approaches showed very little movement prior to placement of the pavement. In addition, a WisDOT study (Wilson 1999) found that rideability over approaches with CLSM was better than approaches with granular backfill (both fills were used behind conventional pile-supported abutments).

Regarding the lateral earth pressures against the abutment, Schmitz et al. (2004) concluded that the lateral earth pressure after curing is negligible, but during placement of CLSM, the structure must be designed to temporarily support fluid pressures. Snethen

et al. (1997) found that the lateral earth pressure was higher in the center layer of the flowable fill at curing due to the speed of hydration and the length of the drainage path. At the center, water could not dissipate or evaporate as fast as points near the surface.

Chapter 3:

MATERIAL CHARACTERIZATION TESTS

Controlled low strength materials (CLSM) as flowable and self-compacting construction materials with potential advantages, have been used in a wide variety of applications. This chapter describes detail information about material specification tests conducted to design an optimum CLSM mixture that was used as a structural fill for construction of a bridge abutment.

CLSM is a multipurpose construction material that has been used in a wide variety of applications that are well documented in the literature. Among the many applications of CLSM, the following are the most important (ACI 229R, 1999): backfill for building excavations, utility trench, and retaining walls; structural fill for footings, road bases and utility bedding; and void-filling for underground structures. It has recently been implemented in bridge approaches to minimize the bump at the end of the bridge. This study looks at the new application of CLSM in rapid construction of bridge abutments. As illustrated in Figure 3.1, CLSM as a structural fill can be placed behind full-height precast concrete panels that are attached to the CLSM backfill via steel anchors.

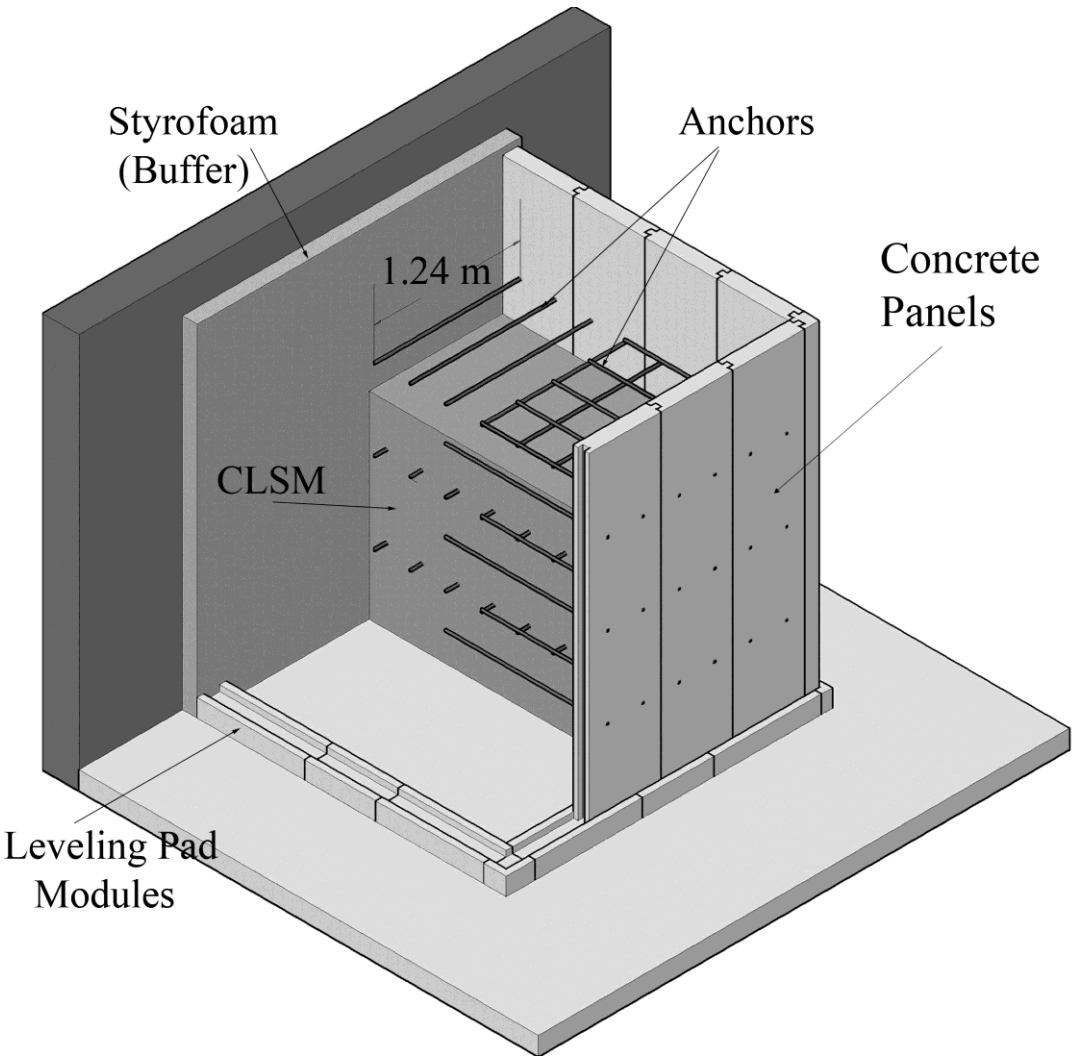

Figure 3.1: Design of a CLSM abutment and location of embedded anchors.

Required engineering and performance properties of CLSM vary depending upon application. For example, it might be desirable for utility trench backfill material to be excavatable and permeable to ground water. For the CLSM abutment application in this study, the main performance properties for selection of a potential CLSM mixture were compressive strength to support the bridge loads, excavatability and flowability to fill the

entire abutment in one continuous pour by pumping. Density and stress–strain behavior were also required for the finite element analysis.

Several CLSM mixtures were developed and tested in the laboratory for the required engineering properties including flowability, density, unconfined compressive strength and stress–strain behavior. The constituent materials in CLSM, mixture proportions and testing methods used in this study are also presented. Material properties obtained from the laboratory tests would be used for future finite element analysis of the proposed test.

Moreover, the bond between steel rebar and CLSM matrix has an essential role in the structural stability of the abutment. The existence of this bond is a basic condition for these materials to work together as a kind of composite material by transferring load between the rebar and surrounding CLSM. Since bond strength of CLSM to steel anchors was a critical area of concern in structural stability the CLSM abutment, the bond performance was also investigated. Experimental pullout tests and numerical simulations were also performed to evaluate the bond performance of the CLSM and steel anchors.

3.1 Materials

CLSM is a mixture of soil or aggregate, cementitious material, fly ash, water and sometimes chemical admixtures that hardens into a material with a higher strength than the soil. Selection of materials for CLSM should be based on availability, cost, specific application and the necessary characteristics of the mixture including flowability, strength, excavatability, density, etc (ACI 229R, 1999). Selected materials for CLSM

mixes in this study included type I portland cement, class F fly ash, fine aggregates and water. Even though materials used in CLSM mixtures may meet ASTM or other standard requirements, the use of standardized materials is not always required.

Cement, a key ingredient in flowable fill, when mixed with water forms a paste that coats each particle of aggregates. Through a chemical reaction called hydration, the cement paste hardens and gains strength. The hardened cement paste is what binds all the other ingredients together to form CLSM. Commercial type I portland cement used in this research was manufactured by Lafarge Cement and it met the chemical and physical requirements of the ASTM C150 specifications, "Standard Specification for Portland Cement". The portland cement had the following compound composition: C_3S - 55%, C_2S - 17.6%, C_3A - 8.0%, C_4AF - 8.2% and contained 3.4% of limestone filler. The mineralogical composition of the portland cement was confirmed by X-ray diffraction (XRD), Figure 3.2.

Fly ash is a cementing agent that increases long-term strength, and also improves workability by improving flowability. Fly ash is a by-product of the coal combustion in electric power generating plants. Locally available class F fly ash for this research was from We Energies, the Elm Road Generating Station, Wisconsin, located along the shore of Lake Michigan near the existing Oak Creek Power Plant (OCPP). Some chemical and physical properties of the used portland cement and fly ash are shown in Table 3.1. Properties of the fly ash are compared with the requirements of ASTM C 618, "Standard Specification for Coal Fly Ash and Raw or Calcined Natural Pozzolan for Use in

Concrete". The fly ash is represented by a significant portion of amorphous phase, but also by quartz and mullite as demonstrated by XRD, Figure 3.3.

The morphology of OPC and fly ash type F were analyzed using scanning electron microscope (SEM), Figure 3.4. Angular particles with sizes from 0.2 to 35 μm were found in ordinary portland cement. Spherical particles with sizes from 0.3 to 15 μm were found in fly ash Class F. The presence of spherical particles in fly ash is important for design of cement based materials with improved rheological properties (Sobolev, 1999).

Quartz sand was used as fine aggregates. The most important property of an aggregate is gradation because it affects almost all important properties of the produced mixture (such as workability, pumpability, etc). Aggregate gradation is the distribution of particle sizes expressed as a percent of the total weight. This sand had been stored in the laboratory prior to use and it was at a room temperature and with a moisture content of 1.16%. The particle size distribution of the sand is shown in Figure 3.5, along with the upper limit (UL) and lower limit (LL) of ASTM C 33 that classify the fine aggregates for use in concrete. Sand had a specific gravity of 2.65 and water absorption of 0.5%.

Potable tap water at the temperature of 23 ºC (75 ºF) was used as a mixing water for production of the flowable fill mixtures.

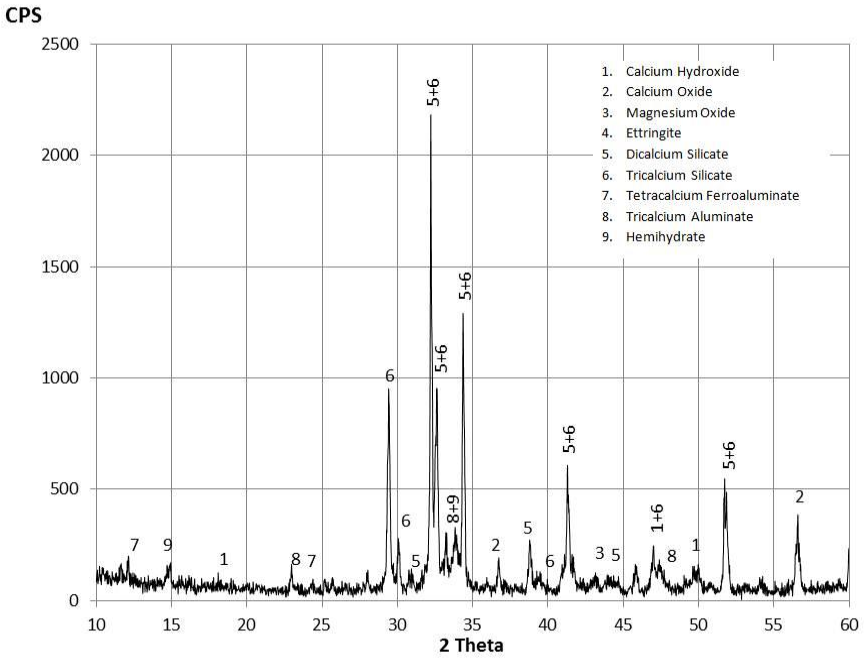

Figure 3.2: X-Ray diffraction of the type I portland cement.

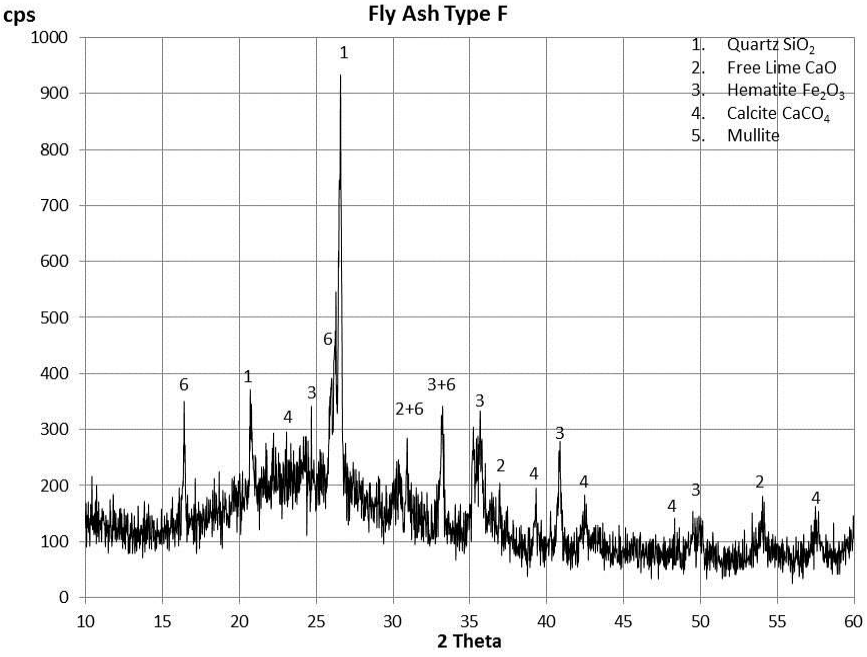

Figure 3.3: X-Ray diffraction of the class F fly ash.

Table 3.1: Chemical and physical properties of portland cement and fly ash type F.

Property	Cement	ASTM C150	Fly Ash	ASTM C618
Chemical properties				
Silicon dioxide, SiO_2, %	20.6		49.9	
Aluminum oxide, Al_2O_3, %	4.7		24.0	70 min
Iron oxide, Fe_2O_3, %	2.7		14.4	
Calcium oxide, CaO, %	63.9		3.23	
Magnesium oxide, MgO, %	2.3	6.0 max	0.98	
Sodium oxide, Na_2O, %	0.55	0.6 max		
Sulfur trioxide, SO_3, %	2.4	3.0 max	0.88	5.0 max
Loss on ignition (LOI), %	2.1	3.0 max	3.50	6.0 max
Insoluble residue, %	0.36	0.75 max		
Physical properties				
Moisture content, %			0.11	3.0 max
Blaine fineness, m^2/kg	380	260 min		
Autoclave expansion, %	0.02	0.8 max	0.08	0.8 max
Compressive strength, MPa				
3-day	21.7	12.0 min		
7-day	27.6	19.0 min		
28-day	37.9	28.0 min		
Time of setting, minutes				
Initial	110	45 min		
Final	225	375 max		
Heat of hydration at 7 days, kJ/kg	411			
Pozzolanic activity index with-portland cement, 28 days, %			93	75 min
Percent retained on #325 sieve	4.6		25.7	34 max
Specific gravity	3.15		2.30	

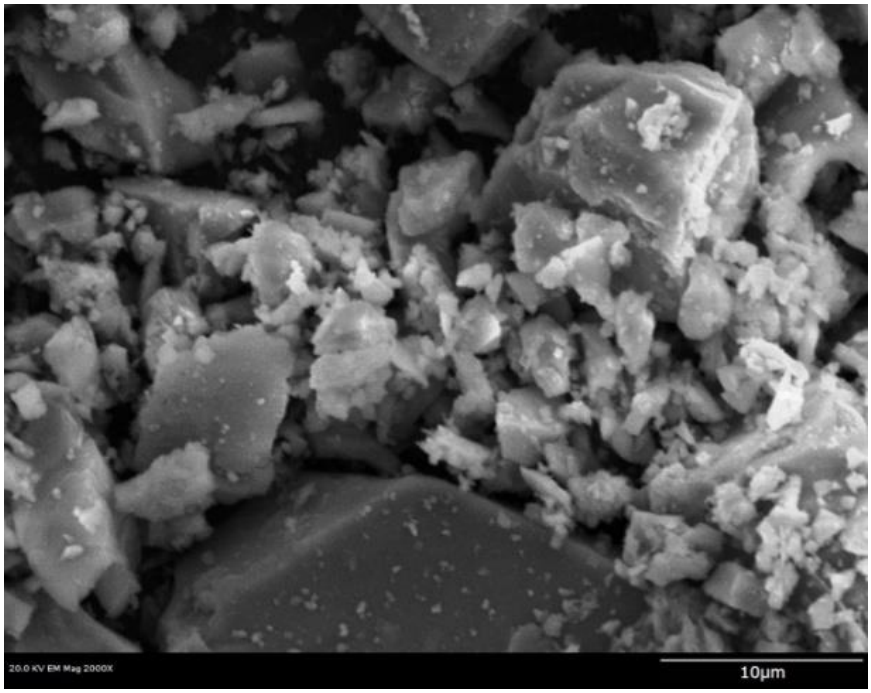

(a)

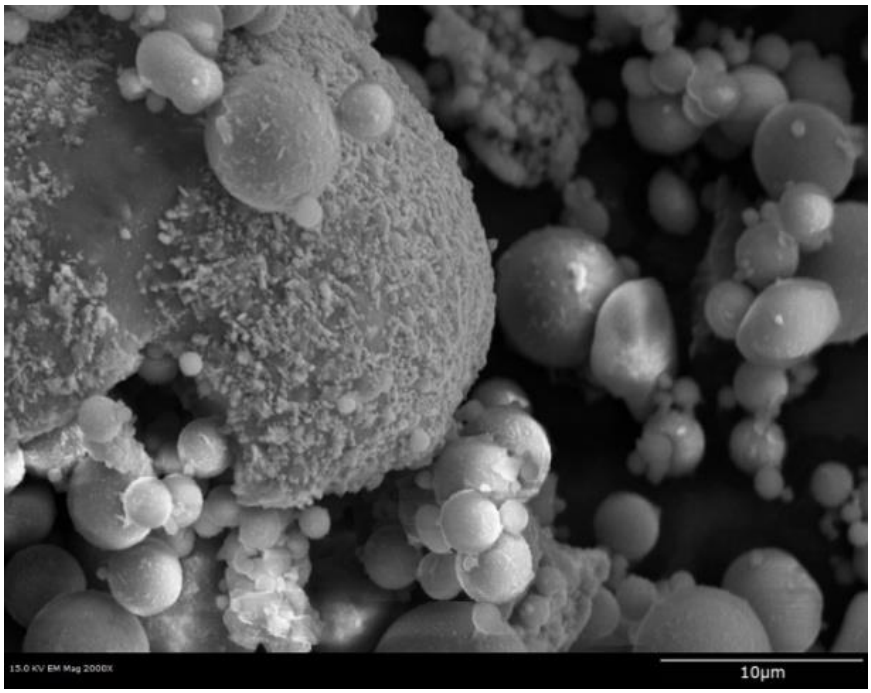

(b)

Figure 3.4: SEM images of: a) portland cement; b) fly ash class F (2000x magnification).

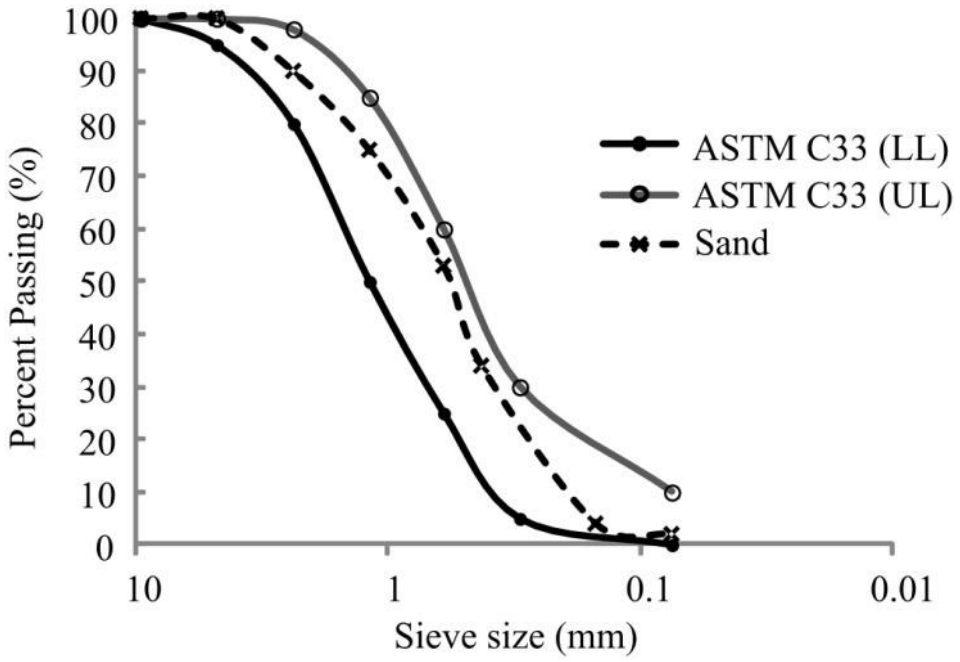

Figure 3.5: Gradation of fine aggregates used in the study.

3.2 Mixture Proportioning

CLSM mixtures are usually designed based on development of compressive strength. To design a CLSM mix, it is not just required to meet the minimal strengths to maintain structural support, but also the ultimate strength must be controlled to allow for future excavation (Lovencin et al., 2006). Due to the sensitivity of compressive strength and other properties, trial and error process has been recommended for proportioning of flowable fill mixtures (FHWA, 1997). When a CLSM mixture is designed, a number of engineering parameters must be evaluated prior to, during, and after placement (Javed et al., 2002). Depending on the specific application in this project, the following criteria

were set for CLSM mixture: flowability, setting time, strength development, and bond behavior between steel rebar and CLSM.

Trial mixtures were evaluated and then adjusted to achieve the target properties, flowability and strength (ACI 229R, 1999). In this study, several CLSM mixes were tested for compressive strength and flow consistency. In order to evaluate and select a potential CLSM mixture for the specified structural fill application, the following criteria were considered:

1. Preliminary finite elements analysis of the CLSM abutment showed that a backfill with a minimum compressive strength of 0.21 MPa provides sufficient load-carrying capacity for typical span type bridges. This is actually equivalent to the bearing capacity of a well-compacted soil. Therefore, the selection criteria favored the mixture with relatively high early strength (minimum of 0.21 MPa in 1 to 3 days) with respect to rapid construction of the abutments and with 28-day strength not exceeding 8.3 MPa. Besides, for the laboratory construction it was required to develop some mixture proportions with lower ultimate strength to assure excavatability (with 28-day strength not exceeding 1.4 MPa).
2. According to the ACI 229R (1999), high flowable material must have a flow of at least 200 mm using the ASTM D 6103 method. A flow of 300 mm or more was desired for this project to prevent blockage of pumping equipment.

3.2.1 Preparation of CLSM Specimens

The test cylinder molds were always properly cleaned and greased with mineral oil before mixing of CLSM proportions. The oil was used to help prevent the molded sample from sticking to the molds, after casting the flowable fill sample. This practice was needed in order to reuse the molds after casting. Also before the start of each mix, all constituent materials (i.e., fine aggregate, cement, fly ash) were carefully weighted and placed into buckets with sealed lids.

The batching sequence was to place half of aggregates into the drum mixer (Figure 3.6) and mix for ½ minute to ensure the uniformity, and then most of the water was added. After about 1 min, cement and fly ash and after that the remaining of aggregates was added to the mixture. After placement of all materials, the mixer was kept rotating for three minutes, then the remaining water was added. After this, the mixing was resumed for 2½ additional minutes until the produced slurry turned into a homogeneous phase.

Figure 3.6: Concrete mixer used for mixing CLSM samples.

Immediately after mixing, flowable fill was poured into a large container ready to cast the prepared specimen molds. Prior to pouring into specimen molds, a sample of the fresh mixture was tested to measure plastic properties including unit weight (ASTM D 6023) and flowability (ASTM D 6103). Each specimen was properly labeled for identification and testing purposes.

Because of the self-leveling characteristics of CLSM, casting the cylinder molds did not require densification as is normally needed for concrete samples. After specimens were cast, they were covered by plastic film and cured in the lab at a room temperature of 23 ºC (75 ºF). Specimens were kept in the molds until the testing age.

Finally, a total of 12 CLSM mixtures with different levels of cement content, fly ash dosage and water to cementitious materials (w/cm) ratio were produced. Table 3.2 shows the different CLSM mixture proportions produced in this research study and measured flowability and unit weight of each mixture (plastic properties). The specimens were cast in 100 × 200 mm cylindrical molds (Figure 3.7) and cured for varying periods, 1-day, 7-day and 28-day, before the compressive strength tests.

Table 3.2: CLSM mixture proportions and some fresh properties.

Mixture	Mixture proportions, kg/m^3 (lb/yd^3)					w/cm	Density, kg/m^3, (lb/ft^3)	Flow, mm (in.)
	Cement	Fly ash	Sand	Water	Plasticizer			
M1	79 (133)	20 (33)	1458 (2458)	452 (762)	-	4.60	2009 (125.4)	241 (9.5)
M2	76 (129)	497 (838)	1338 (2255)	287 (483)	1.6 (2.7)	0.50	2198 (137.2)	330 (13)
M3	50 (85)	270 (455)	1569 (2644)	245 (413)	-	0.76	2134 (133.2)	210 (8.25)
M4	58 (98)	331 (558)	1557 (2625)	234 (394)	1 (1.6)	0.60	2180 (136.1)	191 (7.5)
M5	95 (161)	572 (965)	1240 (2091)	267 (450)	1.9 (3.2)	0.40	2175 (135.8)	305 (12)
M6	56 (95)	319 (538)	1501 (2529)	263 (443)	1.1 (1.9)	0.70	2139 (133.5)	267 (10.5)
M7	45 (77)	258 (434)	1516 (2555)	303 (511)	-	1.00	2122 (132.5)	356 (14)
M8	123 (208)	31 (52)	1215 (2047)	706 (1189)	-	4.58	2074 (129.5)	140 (5.5)
M9	57 (96)	323 (545)	1521 (2564)	266 (449)	1 (1.6)	0.70	2167 (135.3)	330 (13)
M10	87 (146)	299 (504)	1545 (2603)	251 (423)	1 (1.6)	0.65	2182 (136.2)	229 (9)
M11	172 (290)	576 (971)	1122 (1891)	299 (504)	2.3 (3.8)	0.40	2169 (135.4)	222 (8.75)
M12	50 (84)	260 (439)	1514 (2552)	303 (510)	-	0.99	2127 (132.8)	432 (17)

Figure 3.7: Cylindrical CLSM samples.

3.2.2 Flowability Tests

Flowability tests had to be conducted to assure the ability of CLSM to fill the whole abutment in one lift and to prevent blockage of pumping equipment. Flowability of mixtures was measured by flow cylinder test as shown in Figure 3.8, according to the "Standard Test Method for Flow Consistency of CLSM" (ASTM D 6103) and the target flow value was set to be 300 mm. The measured flowability of mixtures is shown in the Table 3.2.

Figure 3.8: Flow cylinder test.

3.2.3 Unconfined Compressive Strength

Compressive strength is the main parameter used to design a CLSM mixture. Cylindrical specimens were tested to determine the compressive strength of the material. As described before, the cylinders were prepared by pouring a representative sample into

molds, and after a curing period they were removed from the plastic molds for compressive testing. Removing a specimen from a mold involved careful handling due to the low strength of the material (as compared to hardened concrete cylinders). The cylinders were then tested to obtain the compressive strengths (ASTM D 4832). Three 100 × 200 mm cylindrical specimens from each batch were tested at 1, 7 and 28 days except when the testing was obstructed by cylinder damage from demolding. Load-controlled unconfined compressive strength test was employed using a relatively low-load capacity computerized testing machine at a constant rate such that a cylinder would fail in not less than 2 min. The typical setup for the compressive strength testing is shown in Figure 3.9.

Figure 3.9: Compressive strength test setup.

The compressive strength of the test specimen is calculated by dividing the maximum load attained from the test by the cross-sectional area of the specimen. Two more typical compressive failure modes of samples are shown in Figure 3.10. According to ASTM C 39-03, Figure 3.10a shows cone and split failure mode and Figure 3.10b shows shear failure mode.

(a) (b)

Figure 3.10: Failure modes of CLSM cylinders after compression test; (a) cone and split failure, (b) shear failure.

3.2.4 Material Testing Results

The compressive strength results for 1, 3 and 28 days age along with the coefficients of variation of data are shown in Tables 3.3. Figure 3.11 demonstrates the development of compressive strength with curing age for six mixtures and corresponding water to cementitious material (w/cm) and fly ash to cementitious material (FA/cm) ratios. The 28-day compressive strength of these mixtures was ranged from a low strength of 0.85 MPa to a relatively high strength of 8.2 MPa.

Table 3.3: Compressive strength results.

Mixture	1-day Strength (MPa)	C.O.V. (%)	7-day Strength (MPa)	C.O.V. (%)	28-day Strength (MPa)	C.O.V. (%)
M1	NR		0.16	25.43	0.38	5.18
M2	0.19	4.35	1.97	1.02	4.39	15.72
M3	0.16	4.70	0.21	25.00	0.4	9.14
M4	0.30	1.62	1.41	5.22	2.87	9.36
M5	0.42	1.16	3.68	5.71	8.20	2.10
M6	0.13	2.73	1.02	4.19	2.14	6.21
M7	0.08	5.45	0.38	3.27	0.85	10.81
M8	NR		0.24	10.29	0.59	8.60
M9	0.16	5.53	0.94	5.88	1.88	1.14
M10	0.44	3.31	1.92	2.19	3.90	8.25
M11	0.29	6.38	6.46	3.34	9.11	9.61
M12	0.10	9.27	0.56	12.59	1.48	7.57

Note: NR (Not recorded), C.O.V. (Coefficient of variation).

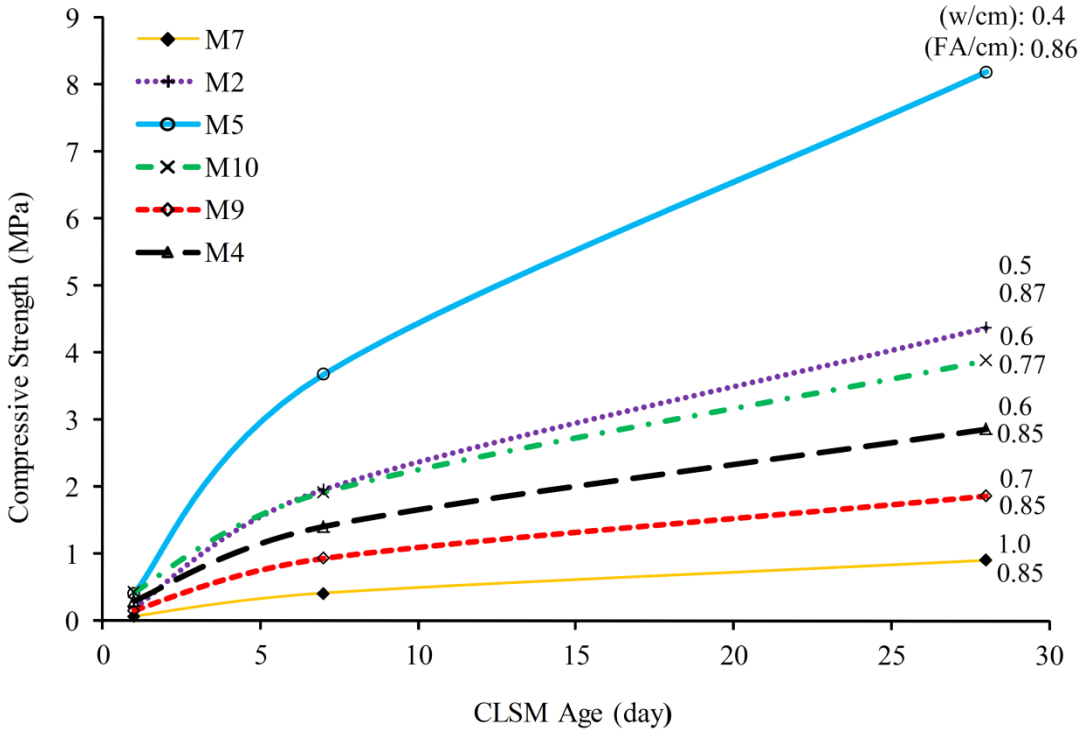

Figure 3.11: Strength development of CLSM mixtures.

Strength is the main parameter to design a concrete and a flowable fill mixture. Figure 3.12 proves that the ratio of water to cementitious material (cement and fly ash) is an important factor affecting the strength of a flowable fill (similar to concrete). The plot illustrates that as the water to cementitious material ratio (w/cm) increases, strength of CLSM decreases. The cement content is another important factor affecting the compressive strength. Figure 3.13 indicates that CLSM mixtures with the same levels of water to cementitious material ratio gain higher strength when cement content is increased. Strength of CLSM is also improved by adding fly ash to a mixture (Figure 3.14). The calcium oxide (CaO) content in fly ash is a cementing agent and believed to be an important variable that improves long-term strength. In addition to strength, visual

observation revealed that the mixtures containing higher fly ash content had less bleeding and segregation.

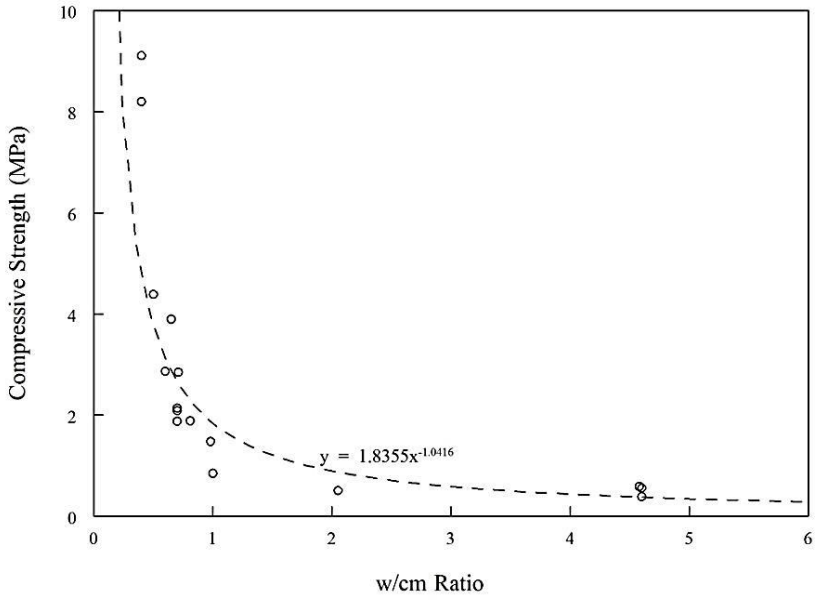

Figure 3.12: Relationship between 28-day compressive strength and w/cm ratio.

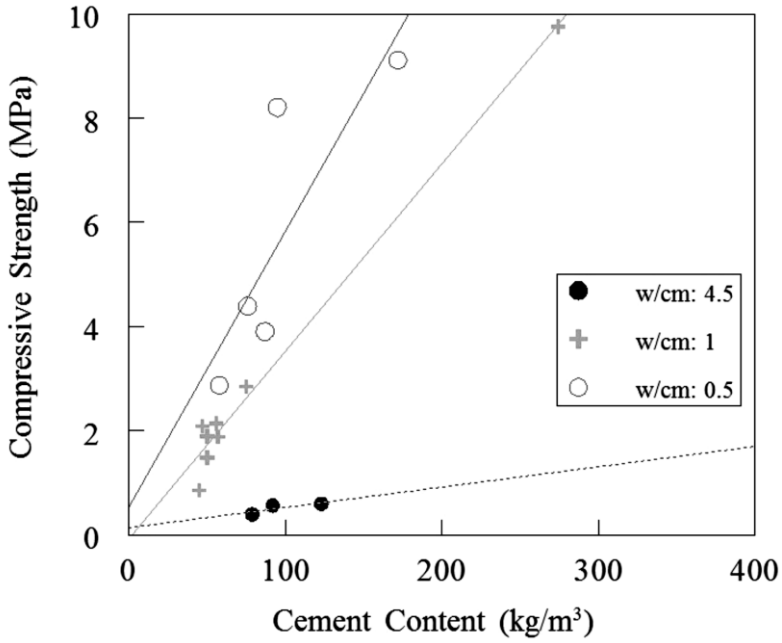

Figure 3.13: Relationship between 28-day compressive strength and cement content.

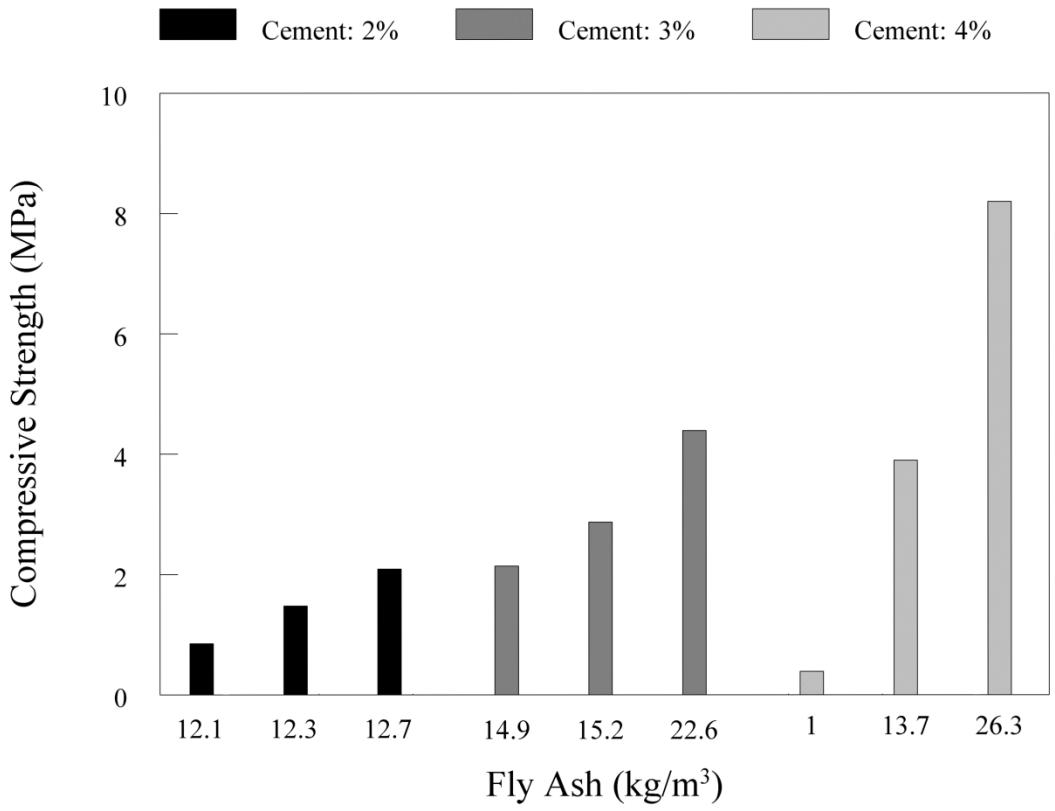

Figure 3.14: Relationship between the 28-day compressive strength and fly ash content.

In addition to the compressive strength, the stress-strain response of all cylinders was obtained. All tested mixtures had a changing stress-strain response with the curing time. At early ages, CLSMs showed more ductile response like soil samples, but with age, CLSM behaved more like concrete with higher strength and lower ductility. This behavior is illustrated in Figure 3.15 for mixture M7. Stress-strain behavior and the resulting elastic modules of the mixtures were used for follow-up numerical modeling.

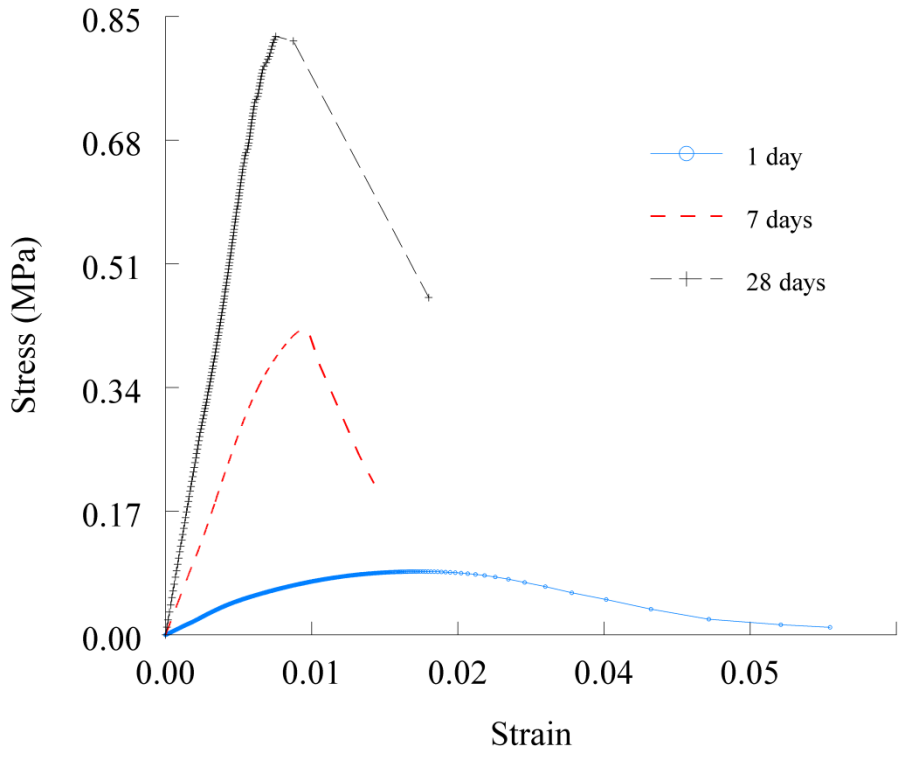

Figure 3.15: Stress-strain responses of mixture M7 at 1, 7 and 28 days.

Table 3.4 shows different CLSM mixture proportions tested in this research study as well as density, flowability and compressive strength results. This can be used as an initial guide for the selection of raw materials and their proportions to use as a structural fill for the proposed CLSM abutment based on minimum strength requirements and flowability. However, since requirements and locally available materials can vary considerably from project to project, adjustments can be made to achieve the desired properties. For example, sustainability or speedy construction might be emphasized by producing a CLSM using only by-product materials or using accelerating admixtures, respectively.

Table 3.4: Mixture proportions and characteristics of the investigated CLSMs.

Mixture	Mixture proportions, kg/m^3 (lb/yd^3)					w/cm	Density, kg/m^3, (lb/ft^3)	Flow, mm (in.)	Compressive Strength, MPa (psi)		
	Cement	Fly ash	Sand	Water	Plasticizer				**1**-day	**7**-day	**28**-day
M1	79 (133)	20 (33)	1458 (2458)	452 (762)	-	4.60	2009 (125.4)	241 (9.5)	-	0.16±0.04 (23.2±5.9)	0.38±0.02 (56±2.9)
M2	76 (129)	497 (838)	1338 (2255)	287 (483)	1.6 (2.7)	0.50	2198 (137.2)	330 (13)	0.19±0.01 (27.6±1.2)	1.97±0.02 (285±2.9)	4.39±0.69 (636±100)
M3	50 (85)	270 (455)	1569 (2644)	245 (413)	-	0.76	2134 (133.2)	210 (8.25)	0.16±0.06 (22.7±8.7)	0.21±0.05 (30±7.5)	0.4±0.04 (58±5.3)
M4	58 (98)	331 (558)	1557 (2625)	234 (394)	1 (1.6)	0.60	2180 (136.1)	191 (7.5)	0.30±0.00 (43.3±0.7)	1.41±0.07 (205±10.7)	2.87±0.27 (416.6±39)
M5	95 (161)	572 (965)	1240 (2091)	267 (450)	1.9 (3.2)	0.40	2175 (135.8)	305 (12)	0.42±0.00 (60.5±0.7)	3.68±0.21 (534±30.5)	8.20±0.18 (1190±25)
M6	56 (95)	319 (538)	1501 (2529)	263 (443)	1.1 (1.9)	0.70	2139 (133.5)	267 (10.5)	0.13±0.00 (18.3±0.5)	1.02±0.04 (148±6.2)	2.14±0.13 (311±19.3)
M7	45 (77)	258 (434)	1516 (2555)	303 (511)	-	1.00	2122 (132.5)	356 (14)	0.08±0.00 (11±0.6)	0.38±0.01 (55±1.8)	0.85±0.09 (124±13.4)
M8	123 (208)	31 (52)	1215 (2047)	706 (1189)	-	4.58	2074 (129.5)	140 (5.5)	-	0.24±0.02 (35±3.6)	0.59±0.05 (86±7.4)
M9	57 (96)	323 (545)	1521 (2564)	266 (449)	1 (1.6)	0.70	2167 (135.3)	330 (13)	0.16±0.01 (23.5±1.3)	0.94±0.06 (136±8)	1.88±0.02 (272±3.1)
M10	87 (146)	299 (504)	1545 (2603)	251 (423)	1 (1.6)	0.65	2182 (136.2)	229 (9)	0.44±0.01 (63.4±2.1)	1.92±0.04 (279±6.1)	3.90±0.32 (565±46.6)
M11	172 (290)	576 (971)	1122 (1891)	299 (504)	2.3 (3.8)	0.40	2169 (135.4)	222 (8.75)	0.29±0.02 (42.3±2.7)	6.46±0.22 (937±31.3)	9.11±0.88 (1322±127)
M12	50 (84)	260 (439)	1514 (2552)	303 (510)	-	0.99	2127 (132.8)	432 (17)	0.10±0.01 (15.1±1.4)	0.56±0.07 (81±10.2)	1.48±0.11 (214±16.2)

3.2.4.1 Effect of Curing Temperature on Compressive Strength

The curing temperature is an important factor that affects the strength gain of CLSM mixtures (Folliard et al. 2008). This influence was studied with three batches of mixture (M7) cured for 90 days at 40°F, 73°F and 100°F. Effect of curing temperature on compressive strength development is presented in Figure 3.16. Higher curing temperatures promote an early strength in CLSM, but lower the rate of later-age strength

gain. It can be observed that 90-day compressive strength of a CLSM material cured at a temperature of 40°F is about 60% lower than that cured at a room temperature (73°F). When cured at higher temperature of 100°F, the same material can gain up to 80% higher strength vs. reference cured at a room temperature (73°F). Figure 3.16 also demonstrates that the long-term strength development (28-day to 90-day) for the mixture M7 at room temperature is less than 25%.

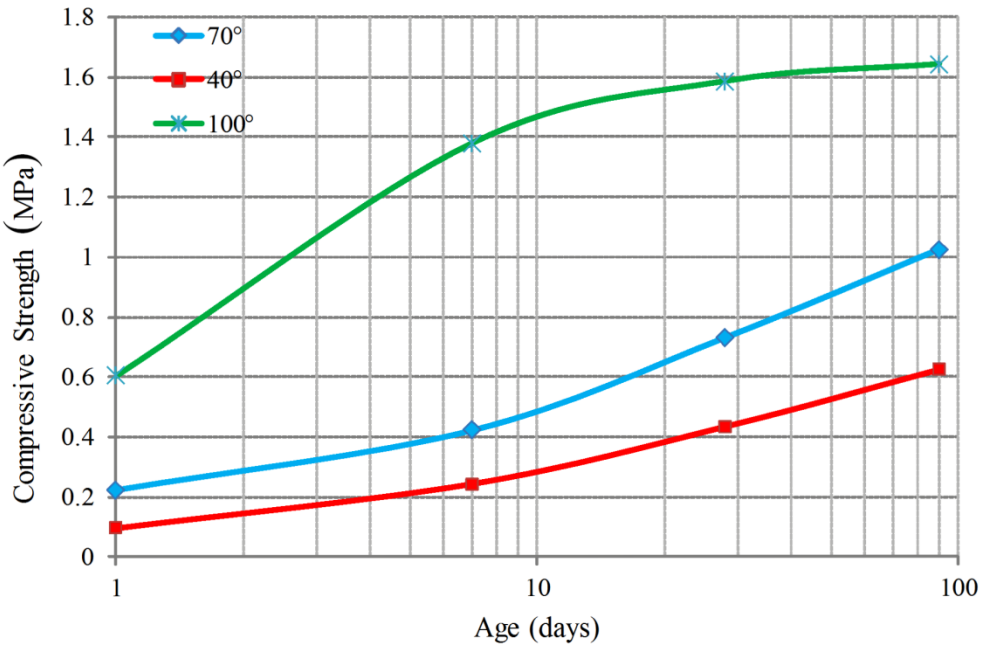

Figure 3.16: Effect of curing temperature on compressive strength development of Mixture M7.

3.3 Bond Behavior of Steel Rebar and CLSM

In the proposed abutment design, the concrete panels were anchored to the CLSM backfill by steel rebars to aid the whole structure to act as a monolith (Figure 3.1). Therefore, the bond between steel rebar and CLSM matrix has an essential role in the

structural stability of the abutment. The existence of this bond is the basic condition for these materials to work together as a kind of composite material by transferring load between the rebar and the surrounding CLSM.

CLSM is much lower in strength than concrete and so its bond performance to steel rebars was identified as a critical area of concern in design of the CLSM abutment. Due to the importance of the bonding strength, different pullout test setups were implemented and compared.

3.3.1 Pullout test on Cylindrical Specimens

Two mixtures with different strengths, M5 and M7, were selected for this test. Mixture M5 has a high compressive strength equal to 8.2 MPa to make a strong backfill and could be used if excavation is not intended. Mixture M7 has the average strength of 0.85 MPa which is within the range of excavatable CLSM.

The first pullout test setup was carried out on 100 × 200 mm cylindrical samples with a 12.7 mm diameter bar centrally embedded in a CLSM mixture, for an embedment length of 200 mm and cured for 1, 7 and 28 days, see Figure 3.17. In order to measure the pullout resistance, a special frame was attached to the universal testing machine. Figure 3.18 shows the schematic drawing of the pullout test setup and specimen. A thin circular rubber disk was used at the top of the specimen to aid uniform distribution of the load. For each curing period, three pullout specimens for each mixture were made. Figure 3.19 shows the pullout test setup and a cylindrical specimen during the test.

Figure 3.17: Cylindrical specimens for pullout test.

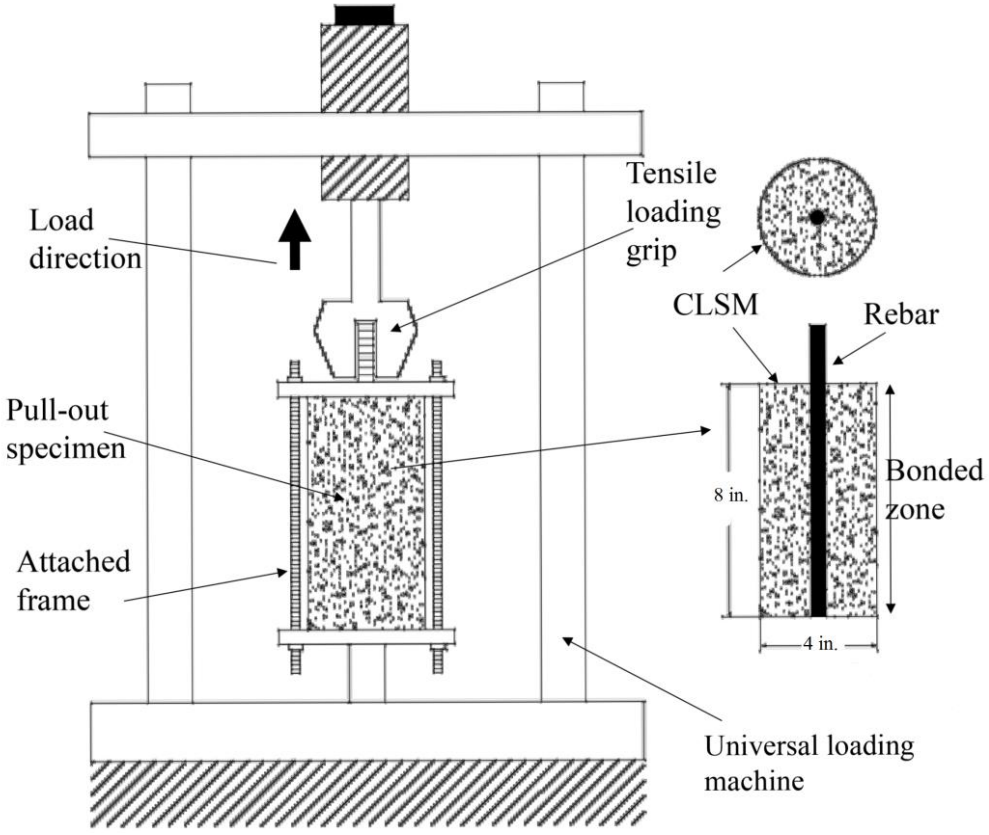

Figure 3.18: Pullout test setup and associated specimen geometry.

Figure 3.19: Pullout test setup on cylindrical specimens.

Two main types of bond failures are commonly recognized; splitting and pullout failure. If the cover on the bars is relatively small, because of the splitting stress, longitudinal splitting cracks will form and radiate outward in the concrete, see Figure 3.20 (Lundgren 1999). This type of failure is called splitting failure. When the concrete surrounding the reinforcement bar is well-confined (enough cover exists), meaning that it can withstand the normal splitting stresses, and the reinforcement does not start yielding, a pullout failure is obtained. In pullout failure, the concrete between the bar ribs is sheared from the surrounding concrete. Schematic bond-slip relationships for splitting and pullout failure are shown in Figure 3.21 (Lundgren 1999).

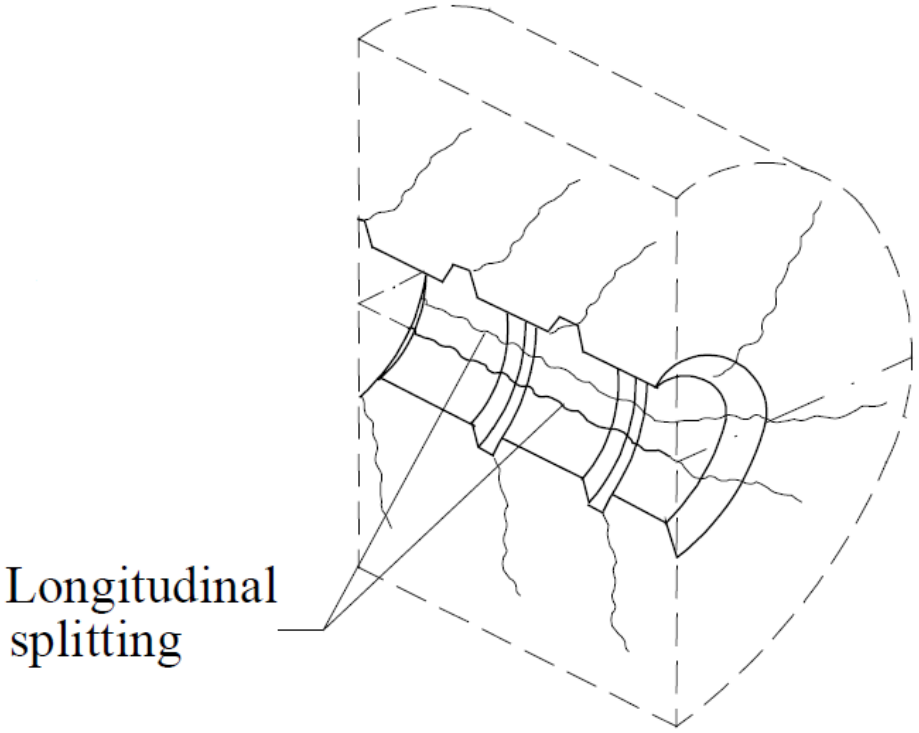

Figure 3.20: Splitting bond failure (Lundgren 1999).

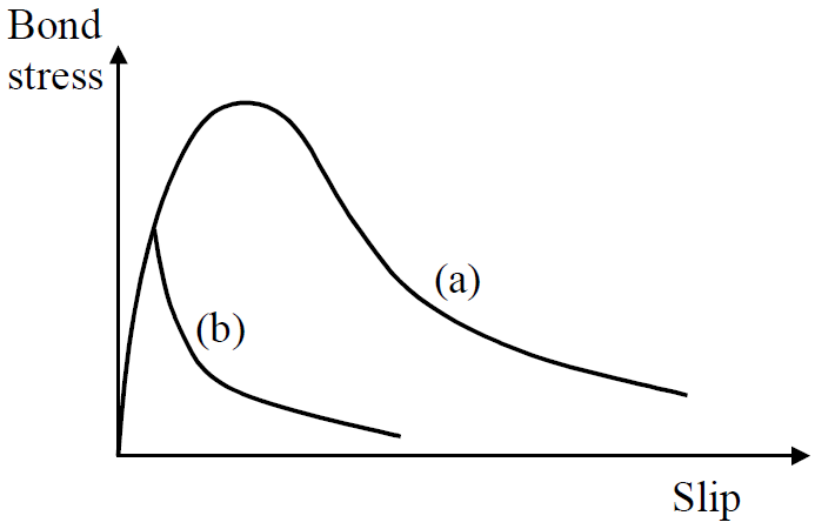

Figure 3.21: Schematic bond-slip relationship: (a) pullout failure; (b) splitting failure (Lundgren 1999).

In this test because cover on the bar was relatively small, longitudinal splitting cracks formed and bond failure resulted from splitting of the CLSM surrounding the bar rather than bar pullout, see Figure 3.22. Pullout load versus slip of the rebar in both mixtures is illustrated in Figure 3.23 and 3.24. In order to achieve a better assessment, the bond stress evaluation was made by using the following equation:

$$\tau = \frac{F}{\pi . \emptyset . l_d}$$

Where, F is the pullout load, ϕ is the steel bar diameter and l_d is the embedment length.

Development of bond strength as average bond strength versus slip of the rebar for both mixtures at each curing age is compared in Figure 3.25. The more it cures, the stronger a CLSM mixture becomes and the bond performance improves. In other words, higher splitting bond strength and more slip can be expected for CLSM with higher compressive strength.

When CLSM surrounding the reinforcement bar is well-confined (enough cover exists), and the reinforcement does not start yielding, a pullout failure is obtained. This presented the need for an updated pullout test in order to implement the CLSM specimens with a larger cover to withstand the splitting stresses.

Figure 3.22: Splitting bond failure and cracks in pullout test using cylindrical specimens.

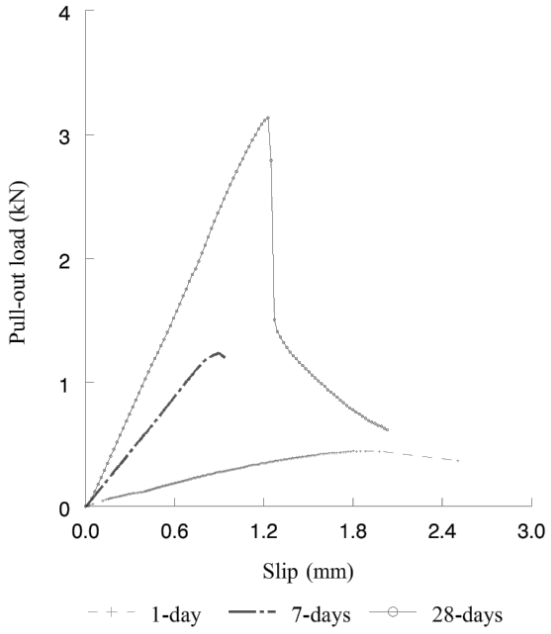

Figure 3.23: Results of pullout test using cylindrical specimens for mixture M7.

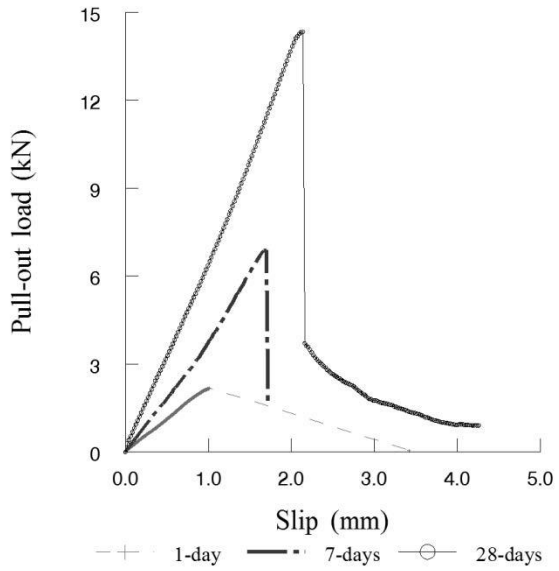

Figure 3.24: Results of pullout test using cylindrical specimens for mixture M5.

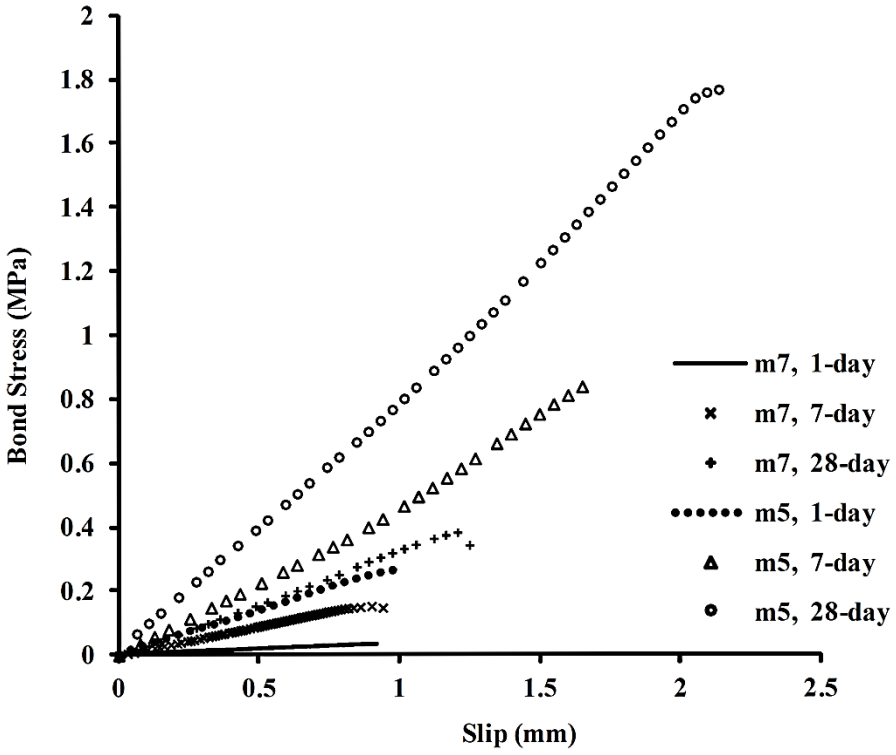

Figure 3.25: Development of bond strength in pullout test using cylindrical specimens.

3.3.2 Large-scale Pullout Test

The bond strength was further investigated in a large-scale testing setup. A wooden box of 0.61 m × 0.61 m × 0.91 m (2 ft × 2 ft × 3 ft) was made and divided into four equal partitions. Four ribbed rebars, 12.7 mm diameter with the embedment length of 0.91 m, were placed and secured in the center of each partition, Figure 3.26. The box was filled with CLSM mixture M7 while some cylindrical molds 100 × 200 mm were placed in the center of the box (Figure 3.27); these were used to produce the test specimens for compression test. It was intended to compare the strength of the material inside the mass backfill with the obtained compressive strength of the mixture.

For pullout test, a simple frame was made over the box to set up the loading device and instrumentations, Figure 3.26. A hydraulic jack was used for the loading. After 7 days curing, the tension load was applied gradually to each rebar and the slip was measured, Figure 3.28. Figure 3.29 illustrates the typical outcome of the tests. The average pullout load for slip failure of the rebars was 21.4 kN at the coefficient of variation of 6.28%. Figure 3.30 shows the pullout failure of a rebar. After the pullout tests, the cylinders embedded inside the box were retrieved, Figure 3.31, to measure their compressive strength and estimate the properties of CLSM in real-size applications. The average compressive strength of the samples at 7 days was about 0.52 MPa which is higher than the strength found through standard CLSM sampling for compression test. This might be due to the temperature, drainage and insulated conditions inside of the massive block of fill.

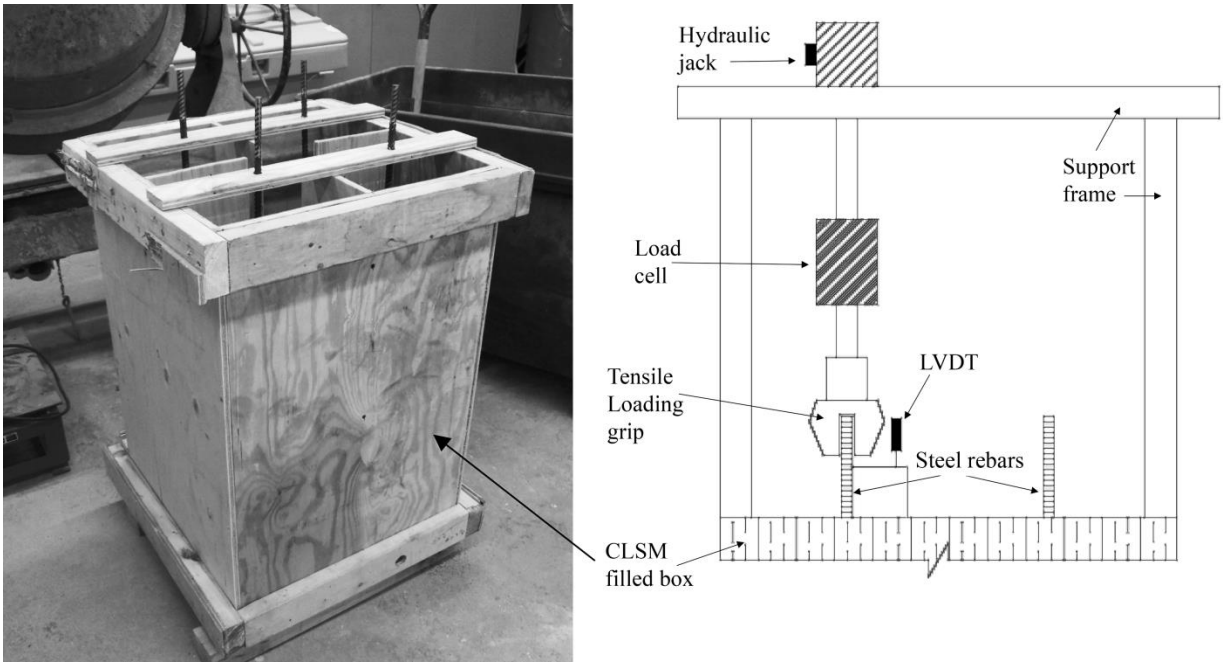

Figure 3.26: Large-scale pullout test setup, box and location of rebars.

Figure 3.27: Cylindrical molds placed in the center of the box.

Figure 3.28: Large-scale pullout testing.

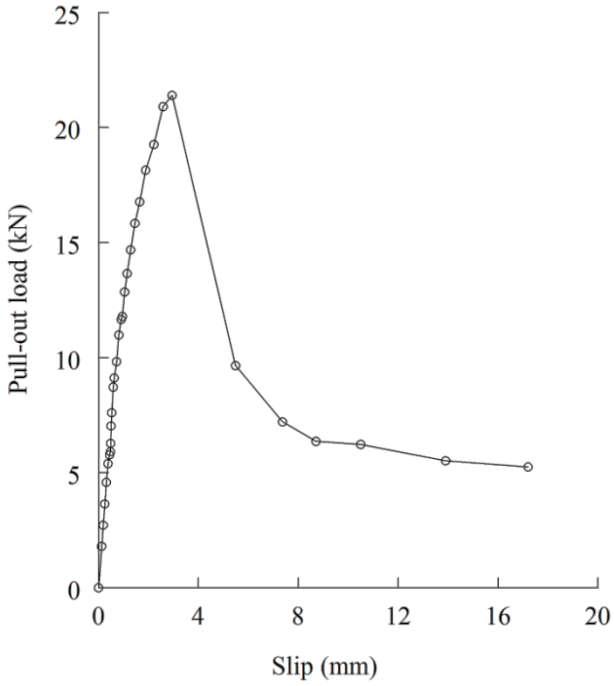

Figure 3.29: Typical pullout load *vs.* slip response for large-scale pullout tests.

Figure 3.30: Pullout failure of rebar from CLSM (large-scale pullout test).

Figure 3.31: Collected samples from inside of the CLSM fill.

3.3.3 Pullout Test on CLSM Abutment

In order to confirm the results of the pullout tests, it was decided to perform a pullout test using the large-scale laboratory CLSM bridge abutment specimen which was constructed to study the performance of the abutment under a bridge loading, see Figure 3.32. Two 12.7 mm diameter steel rebars were placed inside the CLSM abutment at wing walls through drilled holes in the concrete panels to ensure the embedment length of 1.24 m. These anchors were long enough to extend beyond the concrete face to allow the attachment of required testing equipment for the pullout test.

Seven days after placement of an excavatable CLSM mixture, M3, with 7-day compressive strength of 0.21 MPa, a hydraulic jack loading device, a load cell and a Linear Variable Differential Transformer (LVDT) were attached to the rebar (Figure 3.32) and the tension load was monotonically increased until the rupture occurred (this test was done before applying the bridge load to the large-scale CLSM abutment specimen). Pullout load versus slip of the steel anchor is illustrated in Figure 3.33. Average of the ultimate pullout force in this test was about 22 kN. Figure 3.34 shows the pullout failure of a steel anchor in this test.

Average bond strength versus slip of the rebar for both pullout tests, large-scale and pullout test on the CLSM abutment, is compared in Figure 3.35. From these results it can be concluded that the square root of compressive strength (in MPa) provides a good representation of the contribution of the CLSM strength to bond strength. For example, average bond strength of mixture M7 is 0.6 MPa which is approximately equal to the

square root of its compressive strength. It must be also noted that, due to the high confining pressure in this test, a high residual bond stress is developed.

Figure 3.32: Pullout test on CLSM abutment at wing walls.

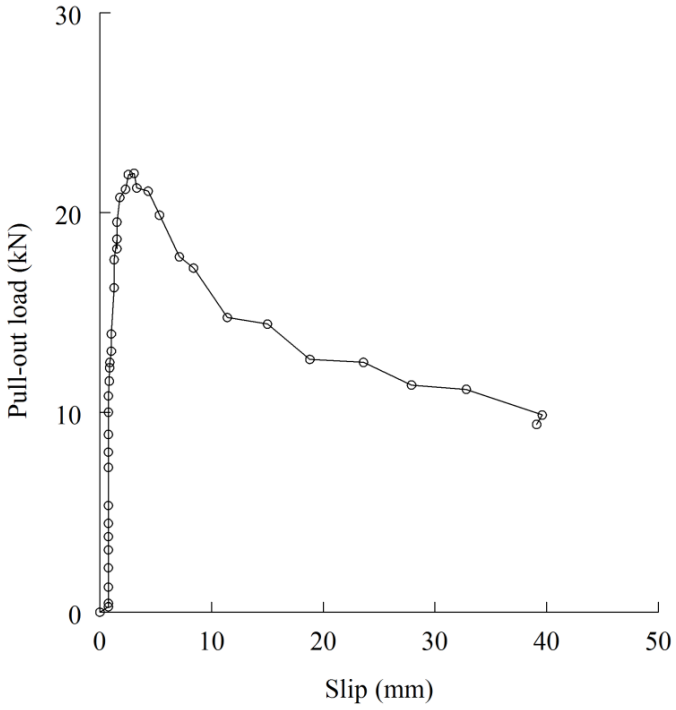

Figure 3.33: Pullout load *vs.* slip (pullout test on the abutment).

Figure 3.34: Pullout failure of rebar in CLSM abutment.

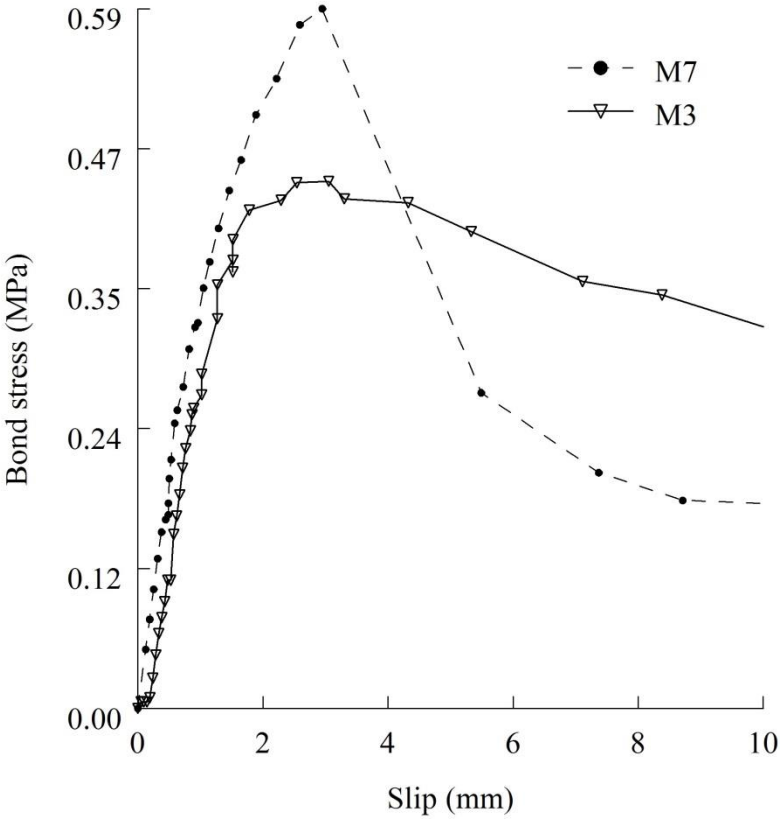

Figure 3.35: Bond stress-slip behavior in pullout tests.

3.3.4 Numerical Modeling of Pullout Tests

Based only on the experimental results, it is difficult to assess the influences of geometrical parameters on the bond behavior. Hence, to better evaluate the bond of steel rebars and CLSM and assess the influence of geometrical parameters, a 3D finite element discrete model was employed to simulate the pullout tests. This section describes an attempt to accurately model the bond-slip relationship between CLSM and rebar using the finite element (FE) analysis software, Abaqus v6.12. The accuracy of this model is later assessed by comparison of the numerical results with the experimental data from conducted pullout tests.

According to the literature review of steel-concrete bond in the reinforced concrete structures, the surficial interaction is considered to be a result of three different mechanisms: friction, chemical adhesion and mechanical interaction between the ribs of the reinforcement bars and the concrete, see Figure 3.36 (ACI 408.2R, 1992). The main component of the bond is the inclined forces resulting from the bearing action of the ribs. This inclined stress is often divided into a longitudinal component, denoted the bond stress, and a radial component, denoted normal stress or splitting stress, Figure 3.37 (Magnusson 1997).

Researchers have conducted numerous studies to characterize the constitutive bond-slip relationship. In the state-of-the-art report "Bond of reinforcement in concrete" from CEB-FIP (The International Federation for Structural Concrete), the authors agree that the interaction between the concrete and the rebar subjected to a pullout force is characterized by four different stages, as represented in Figure 3.38.

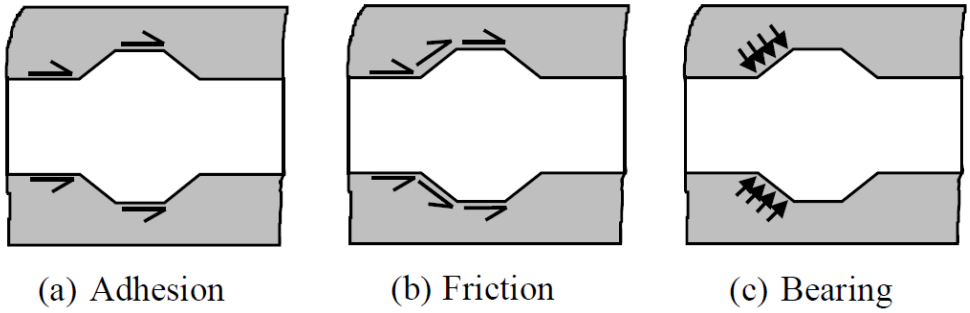

Figure 3.36: Idealized force transfer mechanisms (ACI 408.2R, 1992).

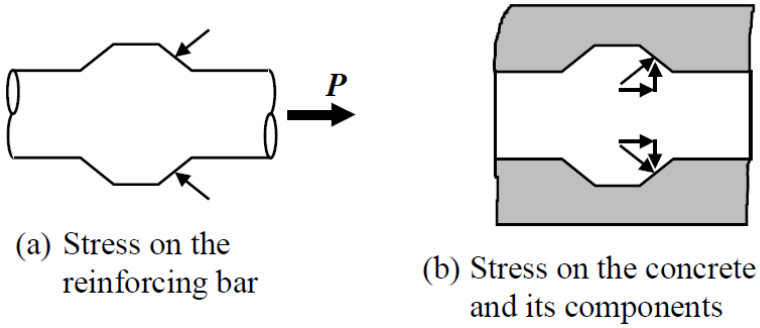

Figure 3.37: Bond and splitting stresses between a deformed bar and the surrounding concrete (Magnusson 1997).

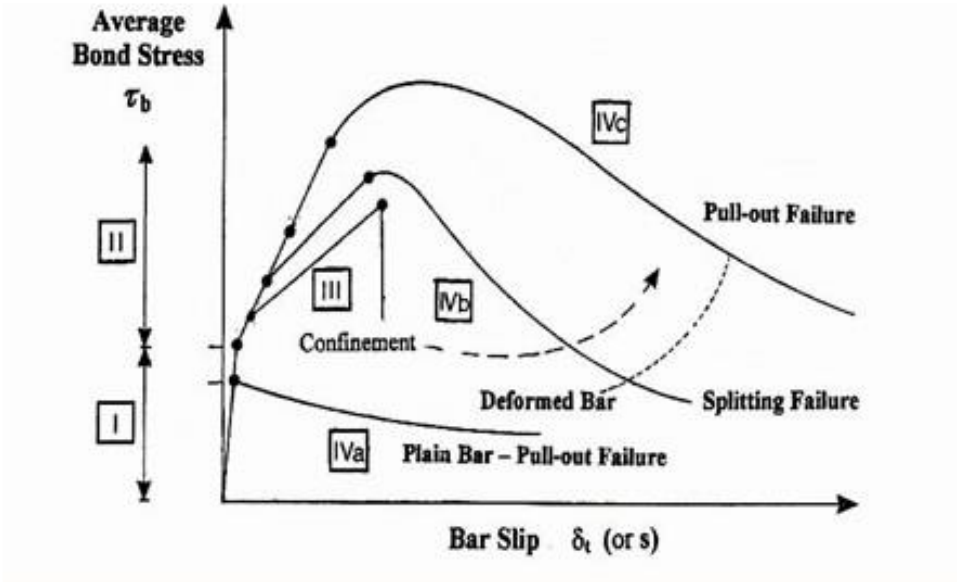

Figure 3.38: Local bond stress-slip laws (CEB-FIP 2000).

In Figure 3.38, in Stage I the concrete is uncracked. For the low bond stress levels present in Stage I, bond efficiency is assured mostly by chemical adhesion, and there is little rebar slip, but highly localized stresses arise close to lug tips (CEB-FIP 2000). Stage II is the stage in which first cracking occurs. For the higher bond stresses present in Stage II, the chemical adhesion breaks down; in deformed bars, the lugs induce large bearing stresses and transverse micro cracks originate at the tips of the lugs, allowing the bar to slip (CEB-FIP 2000). The progression through the relationship for regular reinforced concrete (i.e., including deformed bars) will be from Stage I to Stage II, then either to Stage III, or Stage IVb, or Stage IVc, depending on the confinement level and amount of transverse reinforcement present. Stage IVa, as indicated in the figure, is a special case for plain bars (i.e., without deformations).

3.3.4.1 Numerical Simulation Methods

In finite element modeling of reinforced structures, there are three different methods which are widely used in the literature to simulate the reinforcement including discrete, distributed and embedded models.

The discrete modeling of reinforcement is the first approach used in the finite element analysis of reinforced concrete structures. In this modeling technique, concrete and the reinforcement are two totally independent parts and separate and distinct elements are used to represent them. A significant advantage of discrete representation is that it can account for relative displacement of the reinforcement with respect to the surrounding material. This model is the only model of the three which can consider the

bond slip mechanism directly, so it is very useful in more accurate simulations, despite the fact that the modeling process for this technique is the most complex. Moreover, it is more convenient to simulate irregular reinforcement in the discrete model, because the concrete and steel are separate entities.

When using the embedded modeling technique, the rebar is built into the concrete element such that its displacements are consistent with neighboring concrete elements. Perfect bond is assumed in this modeling technique, so that the two materials are assumed to work together completely as one unit (Khalfallah and Ouchenane, 2007). In Abaqus, finite element software, an embedded element is used to specify that an element or group of elements is embedded in another "host" element or group of elements with perfect bond condition, because the degree of freedom of the embedded element (reinforcement) nodes are all eliminated and forced to be the same as the host element (concrete) nodes.

In the distributed modeling approach, the reinforcement is assumed to be smeared into every element of the concrete. Compared to the embedded model, in which the contribution of the concrete and steel is calculated independently, for the distributed modeling technique, the rebar is transferred to an equivalent amount of concrete and the reinforced structure is considered as a homogeneous material in this model. Perfect bond is again assumed for this technique. The distributed model is frequently used in practical structural design and analysis, based on its simplicity of implementation. However, the internal force of the reinforcement is not available to be quantified in this model since the

steel has been smeared. The embedded modeling technique falls between the distributed and discrete model in terms of complexity and ease of implementation.

Based on the different FE models of concrete, there are various corresponding methods to represent the bond behavior. In a discrete concrete model, the bond may be considered as a contact problem between two different materials and some dedicated elements have been developed to simulate this contact in the commercial FE software. In Abaqus software, there are various methods for simulating the interaction of contacting surfaces, such as friction model, surface –based cohesive behavior model, constraints and connector elements.

In the distributed concrete model, bond phenomena can be represented by a special property of the material, rather than by a connection, since the reinforcement is smeared into the concrete in the distributed model. In Abaqus software, bond-slip is implicitly approximated by introducing some tension stiffening into the concrete model to simulate load transfer through the rebar (Abaqus 2012).

In the literature review summarized by Darwin and Graham (1993), because of the limitation of the computer technology, it was very popular to assume that bond slip performance between concrete and steel was a perfect bond. Today, with advanced finite element software like Abaqus, one can afford to build a three-dimensional discrete model of concrete which can simulate a more complex bond slip effect.

For the present study, a 3D finite element discrete model in Abaqus was developed and to simulate the bonding of steel and CLSM, a surface-based cohesive contact behavior with damage was employed. The cohesive contact model technique is

selected since it is considered one of most efficient and simple methodologies to represent interfacial deterioration.

3.3.4.2 Surface-Based Cohesive Behavior with Damage

Surface-based cohesive behavior is surface interaction property which allows the specification of generalized traction-separation behavior for surfaces. The available traction-separation model in Abaqus assumes an initial linear elastic behavior followed by the initiation and evolution of damage. The slope of the constitutive equation before damage initiation, *K*, is refereed as the interface stiffness. The elastic behavior is written in terms of an elastic constitutive matrix that relates the normal and shear stresses to the normal and shear separations across the interface.

The nominal traction stress vector, *t*, consists of three components: t_n, t_s, and t_t, which represent the normal and the two shear tractions, respectively. The corresponding separations are denoted by δ_n, δ_s, and δ_t. Then, the traction-separation law can then be written as (Abaqus 2012):

$$t = \begin{Bmatrix} t_n \\ t_s \\ t_t \end{Bmatrix} = \begin{bmatrix} K_{nn} & K_{ns} & K_{nt} \\ K_{ns} & K_{ss} & K_{st} \\ K_{nt} & K_{st} & K_{tt} \end{bmatrix} \begin{Bmatrix} \delta_n \\ \delta_s \\ \delta_t \end{Bmatrix} = K\delta$$

The elasticity matrix *K* provides fully coupled behavior between all components of the traction vector and separation vector.

Damage modeling allows simulating the degradation and failure of the bond between two cohesive surfaces. Modeling of this contact damage consists of two ingredients: a damage initiation criterion and a damage evolution law. The initial

response of surface-based cohesive behavior is assumed to be linear as discussed above. However, once a damage initiation criterion is met, damage can occur according to a user-defined damage evolution law. Figure 3.39 shows a typical traction-separation response with a failure (damage) mechanism.

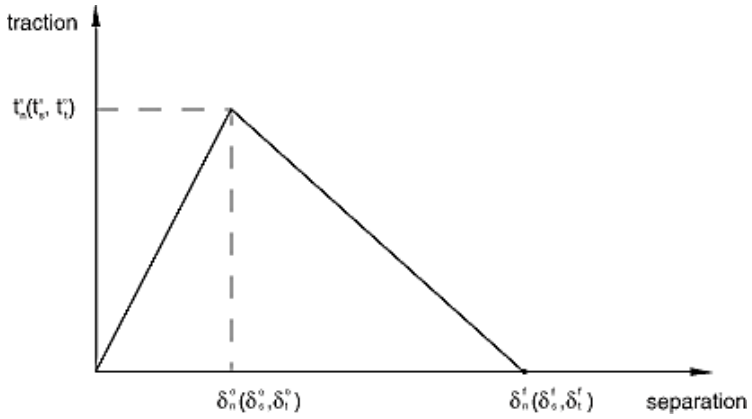

Figure 3.39: Typical traction-separation response.

Damage initiation refers to the beginning of degradation of the cohesive response at a contact surface. The process of degradation begins when the contact stresses and/or contact separations satisfy certain damage initiation criteria that are specified. Several damage initiation criteria are available and are discussed below (Abaqus 2012).

Maximum stress criterion; Damage is assumed to initiate when the maximum contact stress ratio (as defined in the expression below) reaches a value of one. This criterion can be represented as:

$$max\left\{\frac{\langle t_n \rangle}{t_n^0}, \frac{t_s}{t_s^0}, \frac{t_t}{t_t^0}\right\} = 1$$

Where t_n^0 , t_s^0 , and t_t^0 represent the peak values of the contact traction, when the traction is either purely along the contact normal or purely in the first or the second shear direction, respectively.

Maximum separation criterion; Damage is assumed to initiate when the maximum separation ratio (as defined in the expression below) reaches a value of one. This criterion can be represented as:

$$max\left\{\frac{\langle\delta_n\rangle}{\delta_n^0}, \frac{\delta_s}{\delta_s^0}, \frac{\delta_t}{\delta_t^0}\right\} = 1$$

Where δ_n^0 , δ_s^0 , and δ_t^0 represent the peak values of the contact separation, when the separation is either purely along the contact normal or purely in the first or the second shear direction, respectively.

Quadratic separation criterion; Damage is assumed to initiate when a quadratic interaction function involving the separation ratios (as defined in the expression below) reaches a value of one. This criterion can be represented as:

$$\left\{\frac{\langle\delta_n\rangle}{\delta_n^0}\right\}^2 + \left\{\frac{\delta_s}{\delta_s^0}\right\}^2 + \left\{\frac{\delta_t}{\delta_t^0}\right\}^2 = 1$$

The damage evolution law describes the progressive degradation of the interface stiffness once the corresponding initiation criterion is reached. A scalar damage variable, *D*, is employed and represents the overall damage at the contact. The damage variable initially has a value of zero and monotonically evolves from 0 to 1 upon further loading after the initiation of damage. The contact stress components affected by the damage are expressed as follows (Abaqus 2012):

$$t_n = \begin{cases} (1-D)\bar{t}_n, & \bar{t}_n \geq 0 \\ \bar{t}_n, & otherwise\ (no\ damage) \end{cases}$$

$$t_s = (1-D)\bar{t}_s$$

$$t_t = (1-D)\bar{t}_t$$

Where $\bar{t}_n$, $\bar{t}_s$, and $\bar{t}_t$ are the contact stress components predicted by the elastic traction-separation behavior for the current separations without damage.

3.3.4.3 Finite Element Modeling of the Pullout Test

A 3D finite element (FE) discrete model was employed to simulate the pullout tests and assess the influence of geometrical parameters on bond strength. The commercial FE analysis software, Abaqus v6.12 is used for the analysis. Geometry and boundary conditions used in FE simulation are consistent with the pullout test on CLSM abutment which was described before. Figure 3.40 shows the schematic drawing of the conducted pullout test. As mentioned, a 12.7 mm diameter steel rebar is embedded in the CLSM mass with the embedment length of 1.24 m.

Both the CLSM matrix and steel rebar were modeled by 8-node linear brick with reduced integration elements (C3D8R). Very fine mesh was used in the vicinity of the interaction and is coarsened towards the outer surface boundary in order to reduce the computational time. A portion of the mesh adopted for the zone of steel bar-CLSM interaction is shown in Figure 3.41.

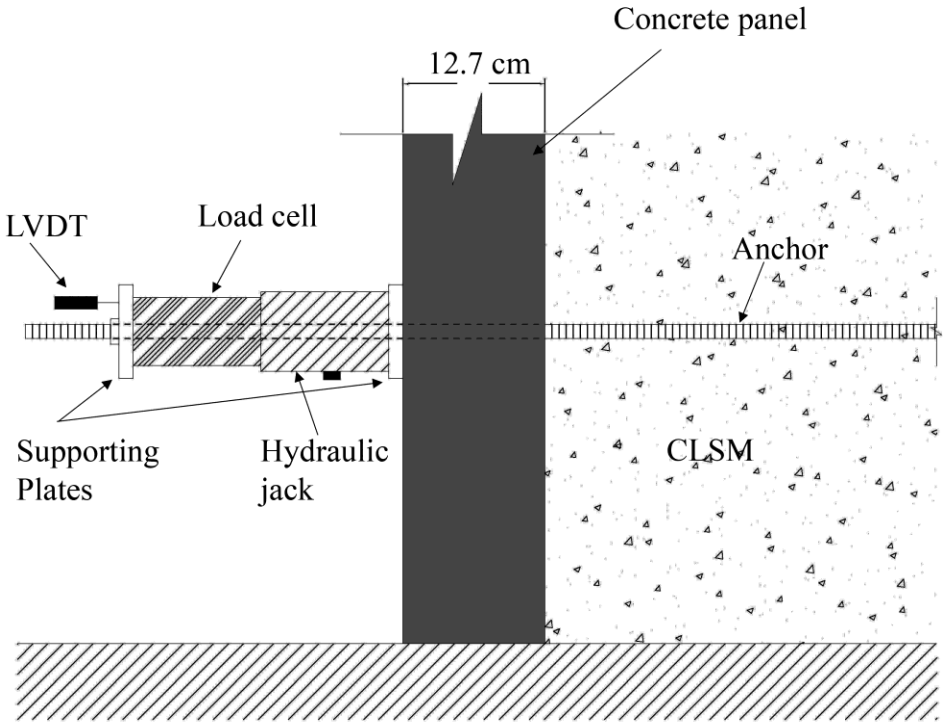

Figure 3.40: Schematic drawing of pullout test on CLSM abutment.

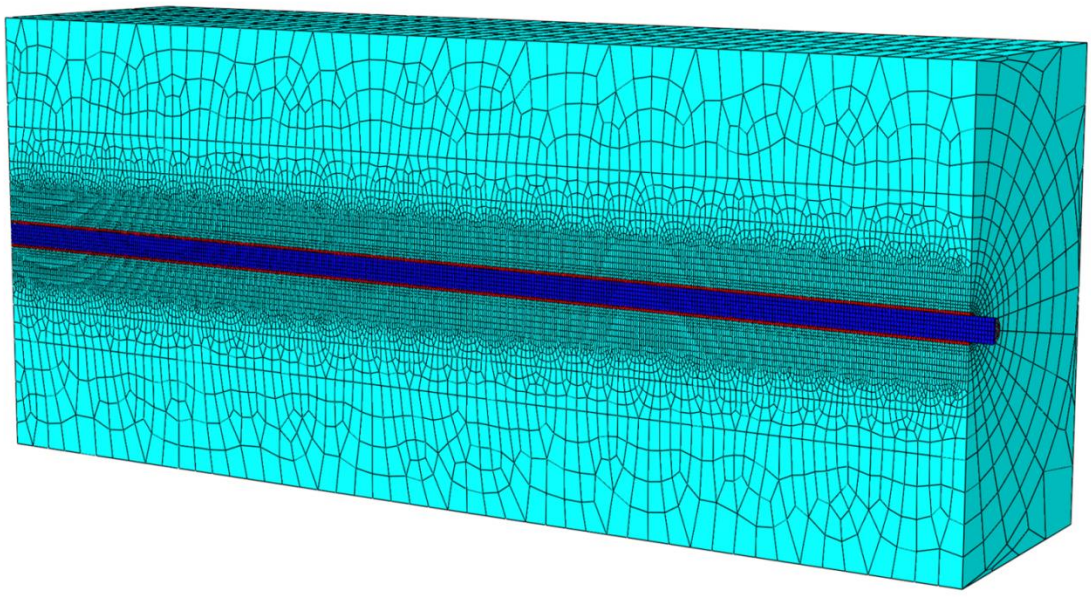

Figure 3.41: Finite element mesh for pullout test.

The material properties used in the finite element analyses are based on the compressive strength testing on CLSM cylindrical specimens. The inelastic behavior of CLSM with compressive strength of 0.21 MPa (mixture M3) was modeled using the concept of isotropic damaged elasticity in combination with isotropic tensile and compressive plasticity in the Concrete Damaged Plasticity model available in Abaqus (Abaqus, 2012; Lee and Fenves, 1998; Lubliner 1989). From the stress-strain curve, Young's modulus of 23 MPa and yield stress of 0.15 MPa were determined and Poisson's ratio was assumed to be 0.19. Four parameters are required to define the yield surface and flow potential function in this model. The dilation angle was taken as 35° while the other parameters, eccentricity, equibiaxial to uniaxial compressive stress ratio, and ratio of the second stress invariant on the tensile to compressive meridian were set to 0.1, 1.16, and 0.67, respectively, as recommended (Abaqus 2012). Compressive behavior of the CLSM provided to the model by tabular data which specifies compressive stress and damage at their corresponding values of inelastic strain from the softening zone of the stress-strain curve (based on experimental results of the unconfined compressive tests in section 3.2.3). Tensile behavior of the CLSM was estimated from uniaxial compressive strength and defined with a linear strain softening.

The surface-based cohesive contact behavior with damage, as was mentioned earlier and illustrated in Figure 3.42, was used to simulate the bonding of steel and CLSM. For the pullout test, purely shear cohesive contact (along the direction of the pullout load) is considered. Based on the experimental bond strength-slip response for mixture M3, interface shear stiffness and shear strength were determined as 0.35 N/mm^3

and 0.45 MPa, respectively. For the softening branch, an exponential damage evolution law shown in Figure 3.42 is employed.

Frictional resistance was not considered in the model assuming that its effect was implicitly present in the horizontal shear property of the cohesive contact due to the fact that it was derived directly from a pullout test. The normal interaction was modeled using the Hard Contact option (Abaqus, 2012) which minimizes penetration of the steel elements into the surrounding CLSM at the contact interface.

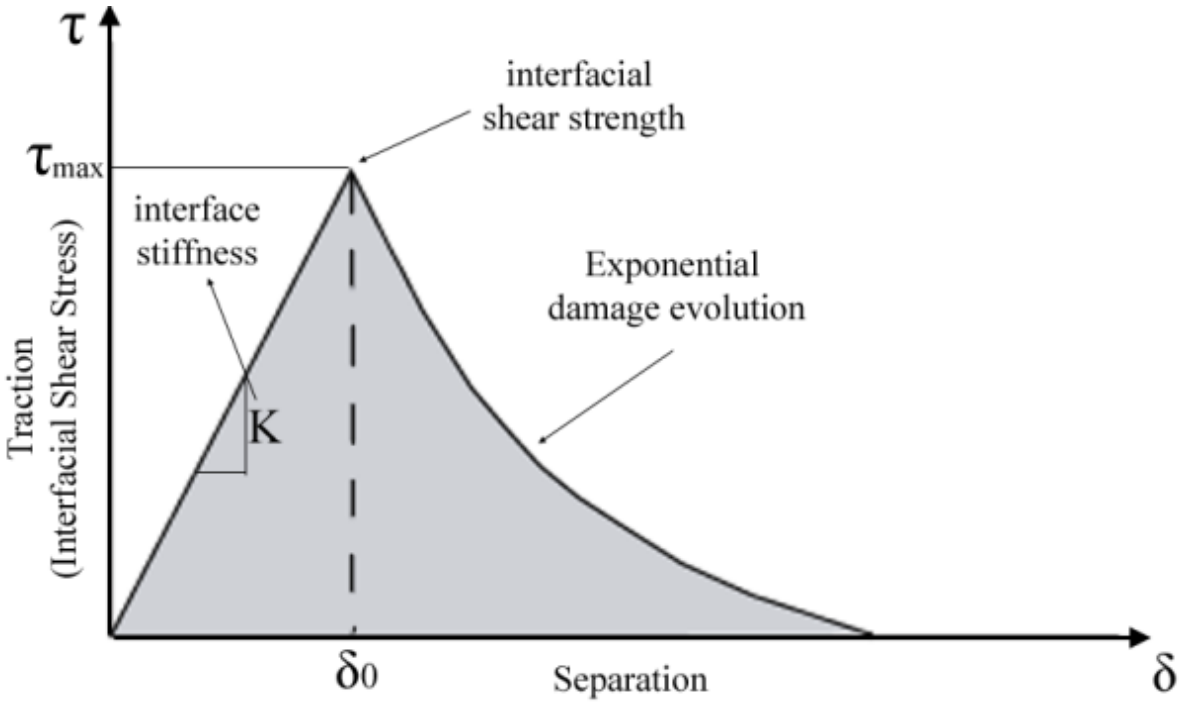

Figure 3.42: Traction-separation behavior for shear bond contact in Abaqus v6.12.

In a displacement control mode a prescribed displacement imposed at the free end of the rebar, applied in the pullout direction, which generated a force used to pull the

rebar for a certain distance. The load was applied in small increments to overcome numerical instability difficulties that can occur when a large load is applied suddenly. To accurately simulate the effect of bearing on the abutment in the pullout test, a fixed boundary condition was also assigned at the front face to fix the CLSM mass.

Quasi-static response was obtained using Abaqus/Explicit module software. The explicit dynamic solution procedure was chosen because it is most accurate in applications where brittle behavior dominates (Abaqus, 2012).

As a result of the simulation, damage of the surrounding CLSM matrix due to the contact interaction with the steel rebar at maximum bond stress is presented in Figure 3.43. Damage in the matrix during pullout process is not distributed uniformly through the whole length of the matrix, but tends to be localized at some regions.

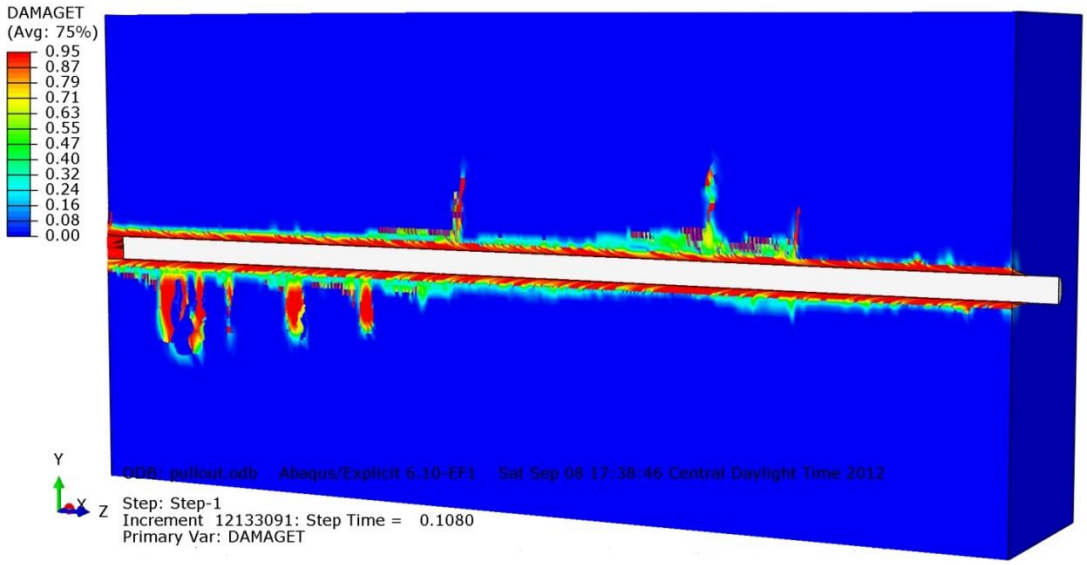

Figure 3.43: Damage in the CLSM mass due to the contact with the rebar at maximum bond stress.

Accuracy of the simulation was assessed by comparison with the measurements obtained in the pullout test. As shown in Figure 3.44, the numerical result is in good agreement with the experiment and therefore the adapted cohesive bond model can effectively simulate the bond behavior of CLSM and steel and reproduce the pullout force.

In order to determine the effects of bar size on the bond strength, results of numerical pullout tests for bar sizes ranging from No. 4 to No. 10 (bar diameters ranging from 12.7 mm to 32 mm) with an embedment length of 1.24 m are compared in Figure 3.44. Numerical results indicate that the bond capacity decreases slightly with increasing bar size because the rebar has less CLSM cover due to the larger diameter. The bond capacity of the model with No. 10 bar is 83 percent of that of the model with No. 4 bar.

Effect of the rebar embedment length on the pullout resistance for a given bar size was also investigated. For the simulation, three different embedded bar length models, 0.51, 0.76, 1.24 and 1.52 m, were considered. As can be seen in Figure 3.45, with increase in embedment length the average bond strength decreases. Although, because of the improvement of bond-slip response, the total energy required for the pullout failure (area under the bond-slip curve) and, in turn, the total pullout force increases at a rate that is less than the increase in embedment length (ACI 408R-03). It is thought that the decrease in bond with increase in embedment length is due to a non-linear stress distribution along the embedment length of the rebar (Larralde et al., 1994). The majority of the bond stress is taken by the CLSM surface near the loaded end of the rebar.

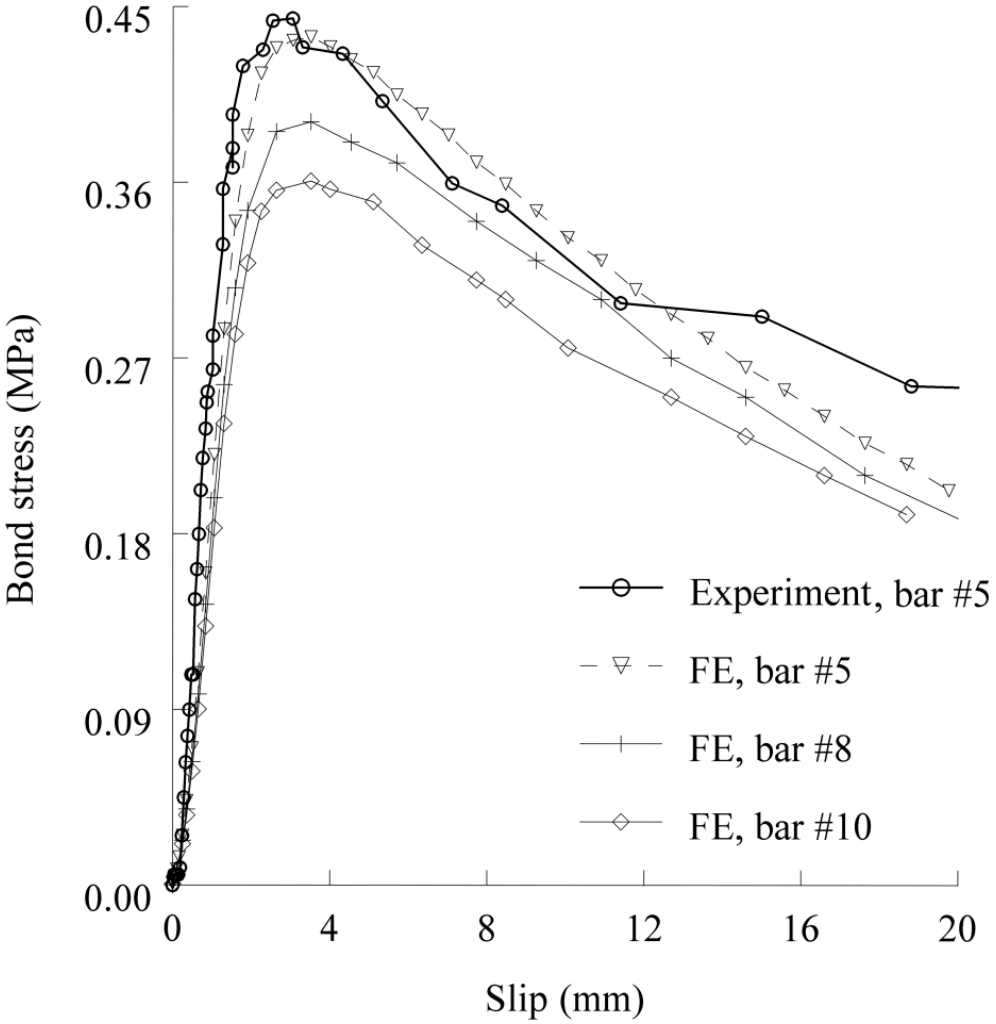

Figure 3.44: Comparison of the experimental measurement with numerical results of pullout tests for different bar sizes.

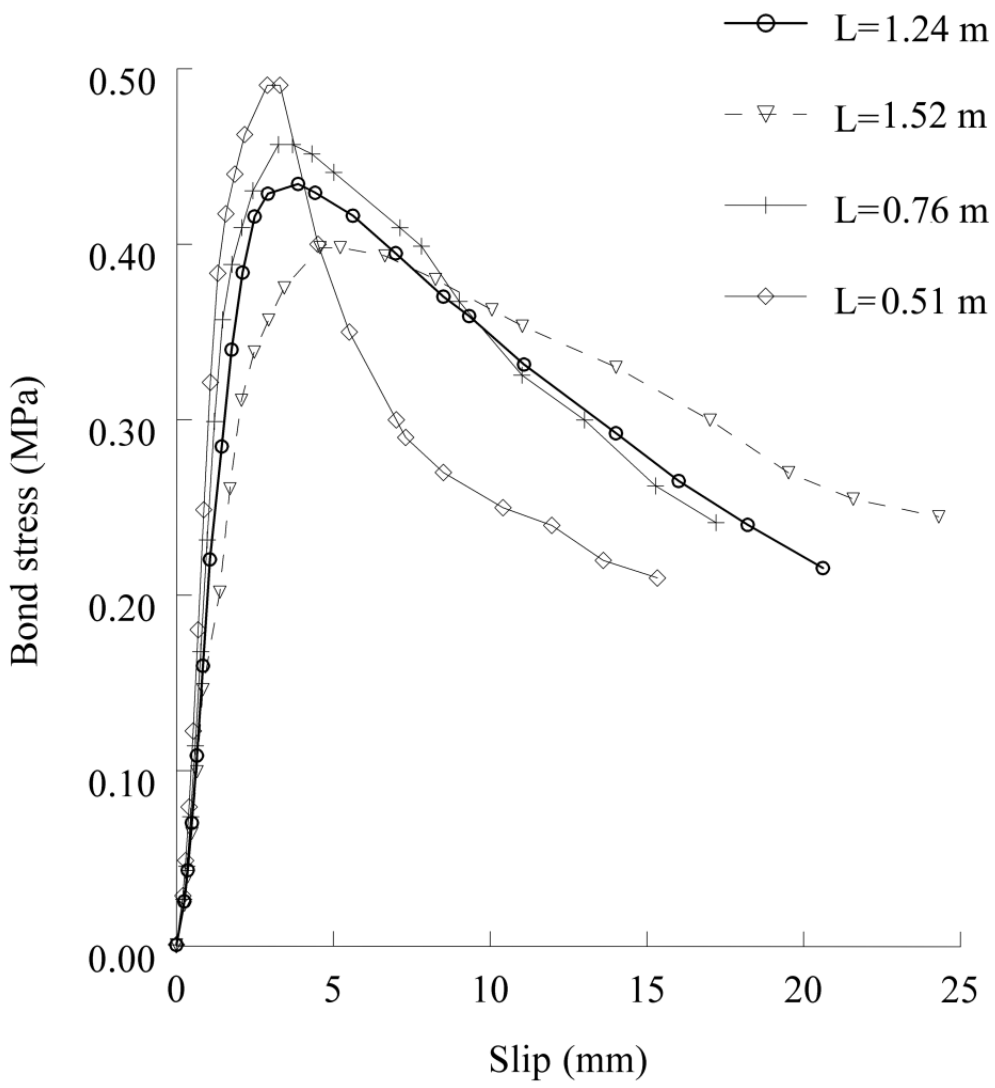

Figure 3.45: Effect of embedment length on bond strength.

3.4 Selection of a CLSM Mixture for the Bridge Abutment

For laboratory construction in this study, mixture M7 in Table 3.4, with acceptable early strength and with 28-day strength not exceeding 1.4 MPa for excavatability and with a flow of 350 mm to prevent blockage of pumping equipment was recommended. This mixture gains early strength of about 0.21 MPa in 3 days but to assure the safety in the laboratory, 7-day strength of 0.38 MPa was considered.

For maintaining laboratory safety during the testing of CLSM abutment, strain gauges were used to monitor the development of tensile forces in steel anchors with the application of bridge load. The maximum axial force in steel rebars during the test was less than 50% of the ultimate pullout force of 22 kN measured in the pullout tests.

Chapter 4

LARGE SCALE CLSM BRIDGE ABUTMENT TEST

4.1 Introduction

Aging bridges with growing traffic demands present an increasing need for rapid construction/replacement of bridges to accommodate traffic flow and maintain freight movement with the least adverse economic impact. To mitigate the traffic congestion problems, it has been shown that the use of precast concrete components in bridges, including bridge girders, bridge decks, and segmental piers, could be a good solution. Normally, most of the bridge construction duration is controlled by the construction of the substructure that typically consists of reinforced concrete abutments and piers with pile foundations. As such, utilizing rapid construction of only the bridge superstructure can only result in minor time saving. Hence, there is a vital need for developing and utilizing a novel method of accelerated construction for bridge substructures including bridge abutments.

Effective rapid bridge construction may be achieved by using Controlled Low Strength Materials (CLSM) as backfill materials placed behind full-height precast concrete panels that are integrated with the CLSM backfill via steel anchors.

In this chapter, the application of a CLSM bridge abutment in normal-span bridges is examined through a full-scale laboratory test. The objectives of the test were: (1) to determine the constructability of the proposed CLSM bridge abutment, and (2) to determine the behavior of CLSM bridge abutments, in terms of load carrying capacity and deformations, after 7 days of CLSM setting time. The latter objective is of great interest since it will provide evidence about the behavior of the CLSM abutment shortly after the CLSM was poured--a critical issue with respect to rapid construction of the abutment.

4.2 Construction of Large Scale CLSM Bridge Abutment Test Specimen

An instrumented CLSM bridge abutment, 2.7 m (8.8 ft) x 2.7 m (8.8 ft) in plan, and 2.75 m (9 ft) in height, with full-height prefabricated concrete panels was constructed to investigate the performance of the abutment due to application of a monotonically increasing sill pressure, see Figure 4.1. Full-height precast concrete panels were attached to the CLSM backfill via steel anchors (Figure 4.2).

The CLSM bridge abutment and the concrete sill were instrumented, as shown in Figures 4.1 and 4.3, to measure their behavior during construction and upon application of bridge loads. Instrumentation included load cells, pressure cells, strain gauges, LVDTs and high-resolution digital video cameras. Of particular interest was the displacement of the sill and the facing wall to determine the performance of CLSM bridge abutments, in

terms of load carrying capacity and deformations after 7 days of CLSM setting time and the lateral pressures; Understanding that how much lateral pressure is applied during placement of fresh CLSM and after its setting is a key to design the precast concrete panels and their temporary lateral supports. Strain gauges were used to monitor strain development in rebars during loading.

Also, because of the three-dimensional behavior of the abutment, the wing walls were also instrumented to measure their lateral displacements. In addition, one LVDT was installed on the base leveling pad at the front facing wall to measure the settlement of the 15-cm (6 in.) thick foundation soil.

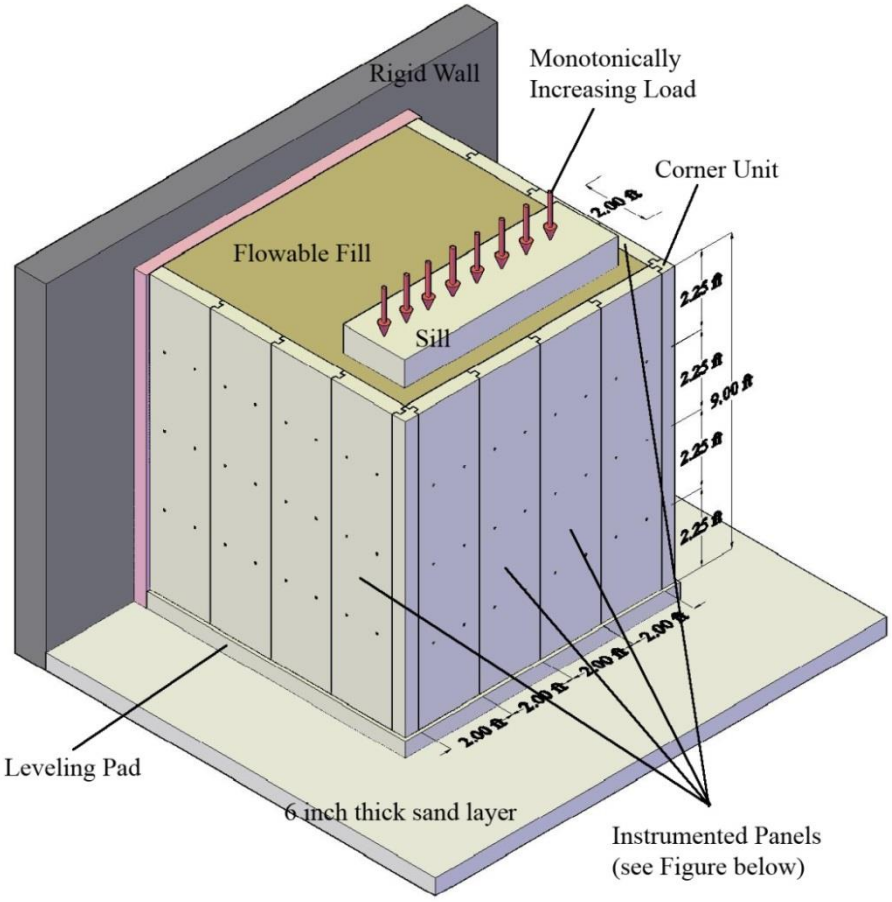

Figure 4.1: Large scale laboratory test of CLSM bridge abutment.

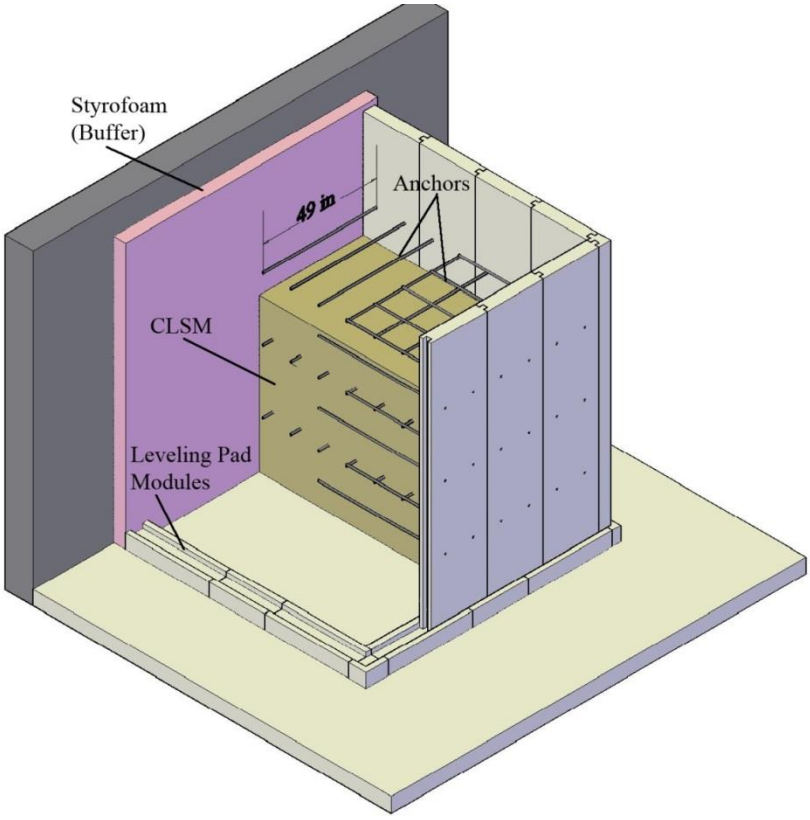

Figure 4.2: Inside of CLSM bridge abutment test.

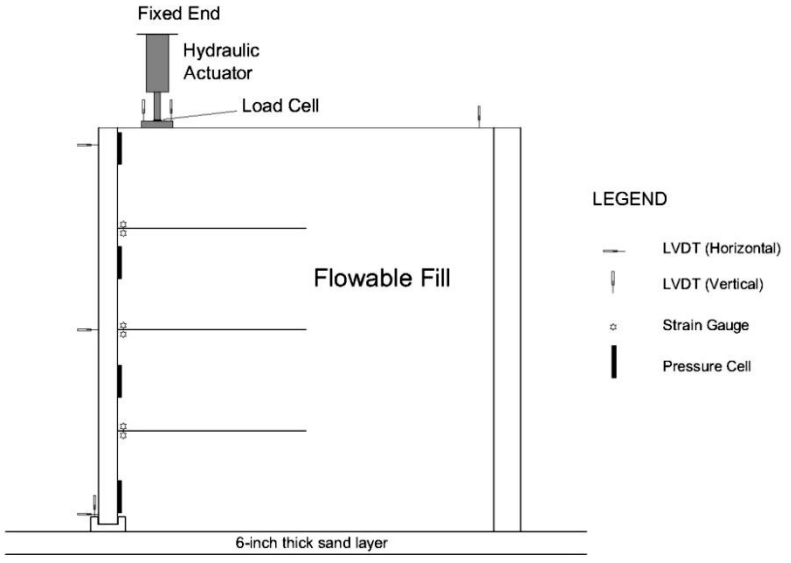

Figure 4.3: Instrumentation of the laboratory test of CLSM bridge abutment.

4.2.1 Prefabrication of Concrete Components

Considerations were made for both the size and position of the concrete panels surrounding the CLSM. It was decided to utilize the existing rigid wall already in place in the structural laboratory of UW-Milwaukee. This allowed for a three-sided cube to be constructed, thus saving time and materials. Figure 4.4 shows the CLSM bridge abutment plan and location of the bridge sill.

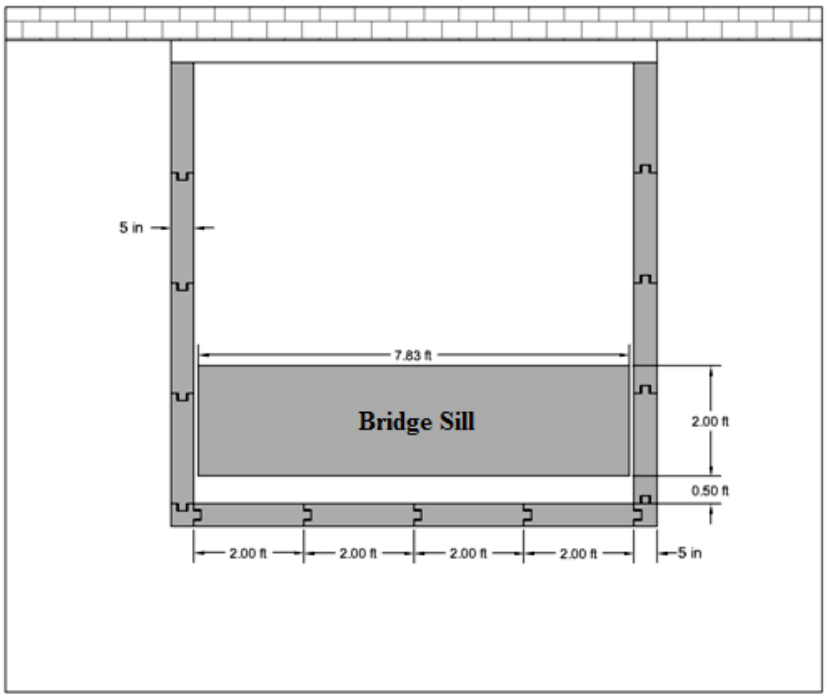

Figure 4.4: Plan view of CLSM bridge abutment and location of the bridge sill.

A height of 2.75 m was decided upon with the understanding that it would be sufficient enough to imitate large scale actual applications while still being a manageable size for a lab environment. Reinforced concrete panels and the corner units were designed according to structural analysis and an initial 3-D finite element of the CLSM abutment

for an estimation of stresses. Lateral loading due to fluid pressure of CLSM backfill with unit weight of 2165 kg/m^3 (135 psf) and bridge pressure of 206.8 kPa (30 psi = 4.32 ksf) was used for the design of concrete panels as illustrated in Figure 4.5.

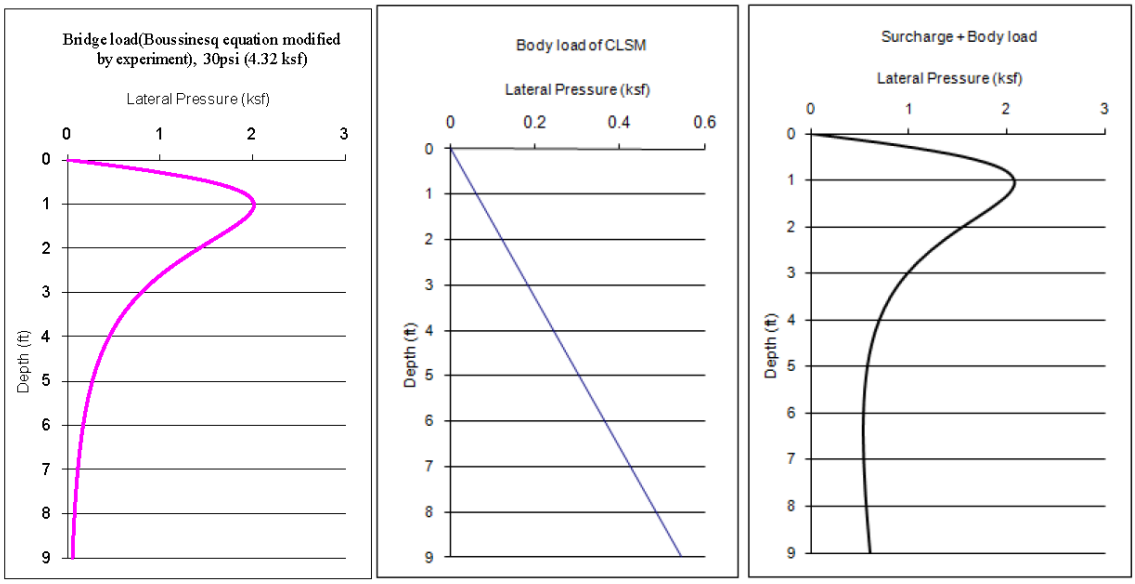

Figure 4.5: Lateral loading for the design of concrete panels (1 ksf = 47.880 kPa)

Figure 4.6 shows design details of reinforced concrete panels and corner units with tongue-and-groove connection type, which were designed to withstand the fluid pressure of the CLSM material and the lateral pressure due to the bridge load. Each panel had six 19 mm diameter openings, as indicated in Figure 4.6, to accommodate the installation of threaded steel bar anchors, 12.7 mm diameter, prior to the placement of the CLSM material. Matching nuts were cast in the panels at the position of the openings. The system is designed in a way that the anchors can be installed from outside the abutment during the gradual pouring of CLSM.

As illustrated in Figures 4.6 and 4.7, tongue-and- groove connection type was as follow; groove width: 57 mm ($2^1/_8$ in.), tongue width: 45 mm ($1^3/_4$ in.). This allowed for some variability in the panel construction largely due to the flexible and warping nature of wood formwork. Both the tongue and groove had a depth of 41 mm (1.5 in.). Dywidag thread bars and nuts were used instead of regular rebars to make the installation of anchors even easier (Figure 4.8).

Concrete leveling pad modules was designed and fabricated as a means for ensuring proper vertical placement of the finished concrete panels in 0.9 m (3 ft) and 0.61 m (2 ft) length modules (Figure 4.9). Also a 30 cm (1 ft) thick, heavy reinforced concrete bridge sill was designed and constructed (Figure 4.10). According to the designs, formworks were assembled, rebars installed, concrete casted and when it cured formworks were remolded as shown in Figure 4.11. Twelve reinforced concrete facing panels and two corner units with groove or tongue parts for connection, leveling pad modules and bridge sill were fabricated.

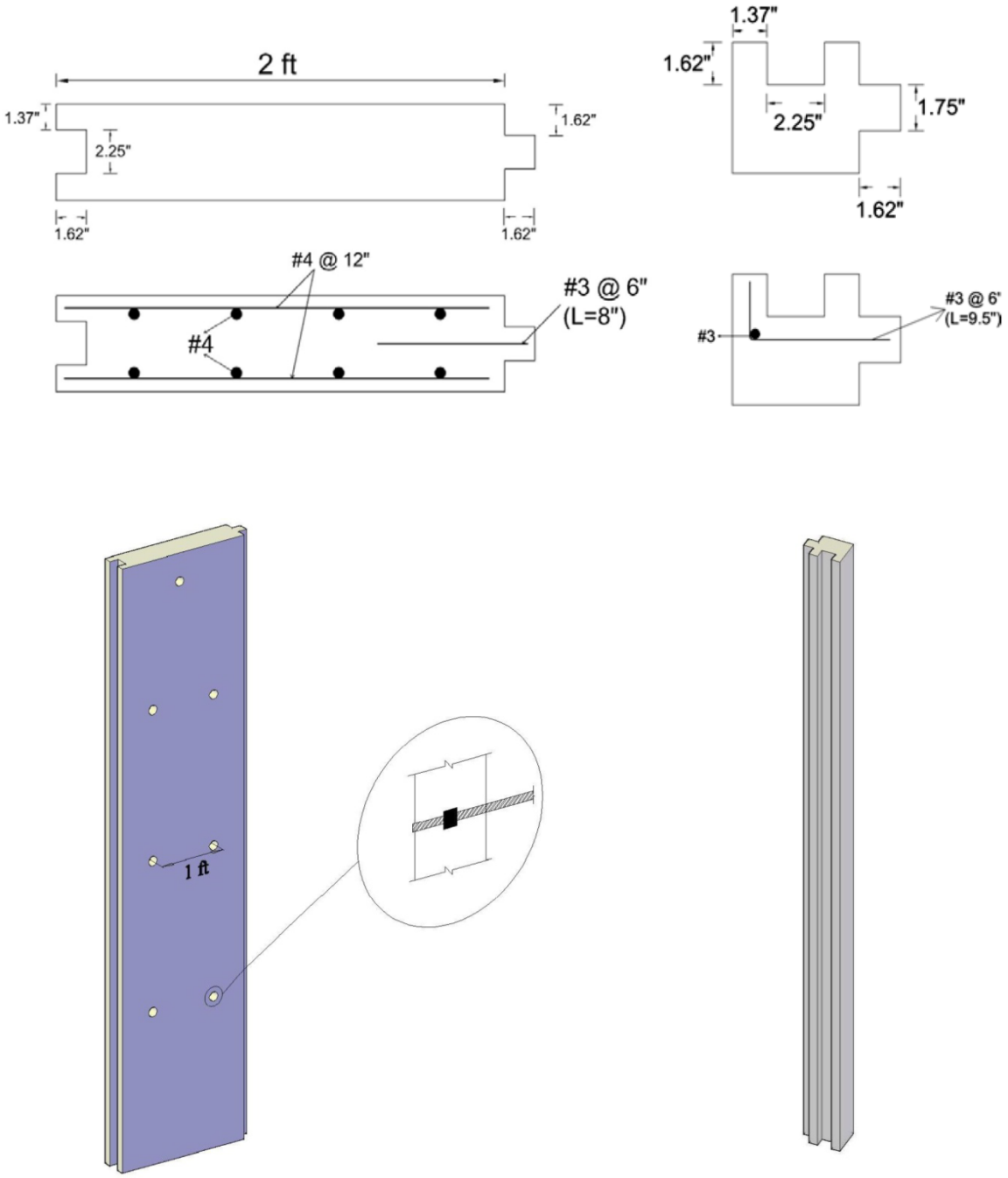

Figure 4.6: Reinforced concrete panels and corner units.

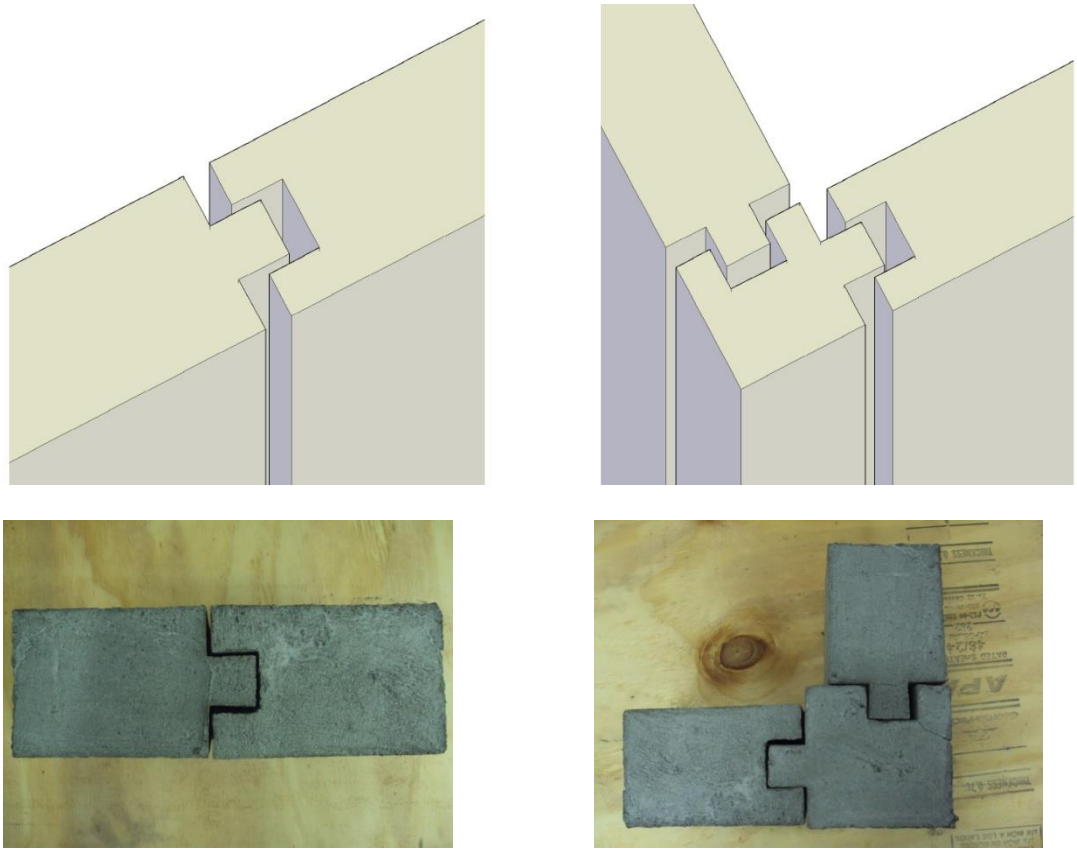

Figure 4.7: Tongue and groove connection.

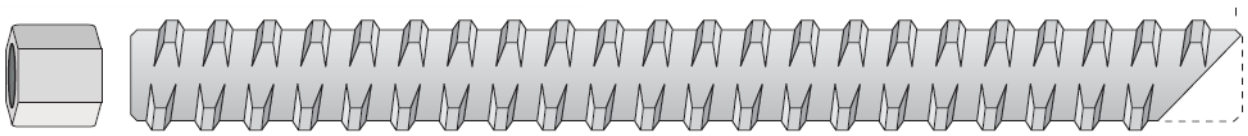

Figure 4.8: Dywidag thread bar and nut.

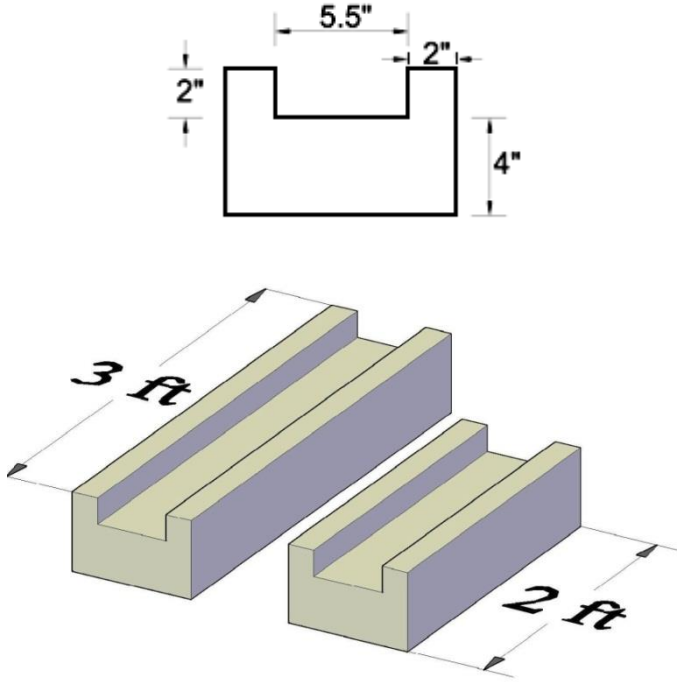

Figure 4.9: Concrete leveling pad modules.

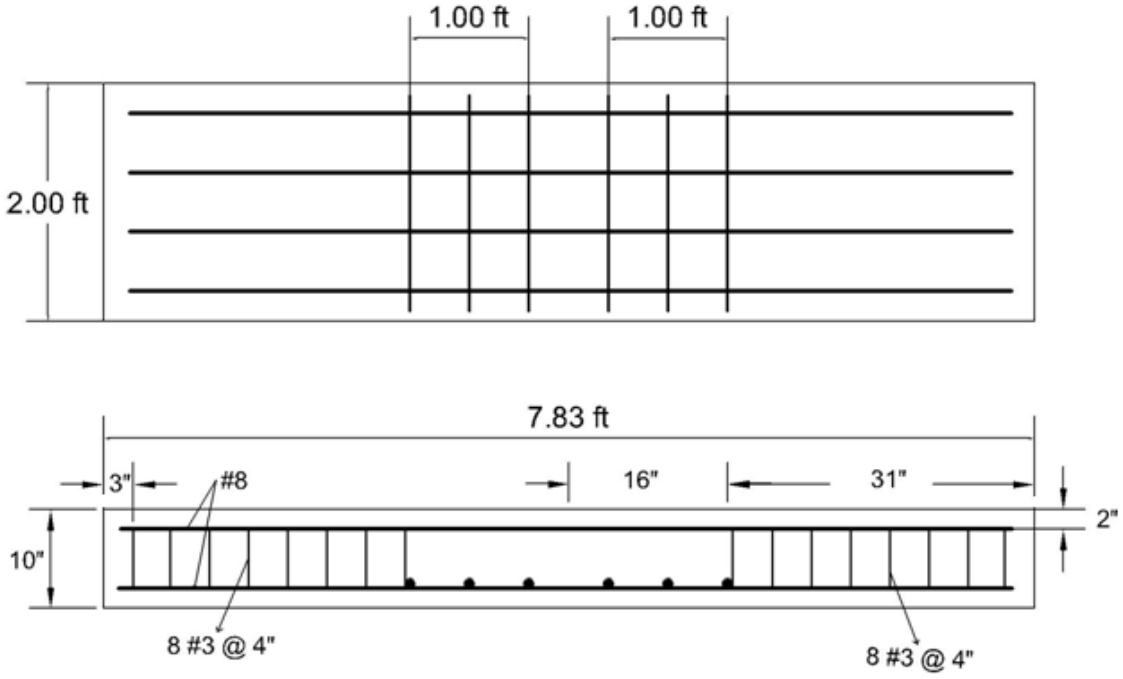

Figure 4.10: Reinforcement detail of bridge sill.

(a)

(b)

(c)

(d)

(e)

(f)

(g)

Figure 4.11: Prefabrication, (a) panel formworks and rebars, (b) nuts embedded in panels, (c) leveling pad module formworks, (d) corner unit formworks, (e) bridge sill formwork, (f) formworks filled with concrete, (g) formworks remolded.

4.2.2 Construction Sequence

Construction sequence of the CLSM Bridge Abutment for the large-scale testing is illustrated in Figure 4.12 and was as follows (in the structural laboratory of UW-Milwaukee):

Step 1; Base Preparation:

To preserve the lab floor and best imitate a field-test environment, a compacted soil foundation was constructed as shown in Figure 4.12. A “sandbox” style foundation was formed with a 30 cm, (12 in.) apron surrounding the whole structure. A 15-cm (6-in.) thick layer of compacted soil was placed on the laboratory’s strong floor to serve as the base for the CLSM abutment. A layer of geomembrane was installed prior to the installation of the soil layer to ensure a water-tight testing environment. A water drainage system was then developed to collect the drained water from the fresh poured CLSM backfill. After the soil was placed and sufficiently compacted, the precast concrete leveling pad modules locations were marked out and placed accordingly. These modules were placed over the compacted soil prior to panel installation.

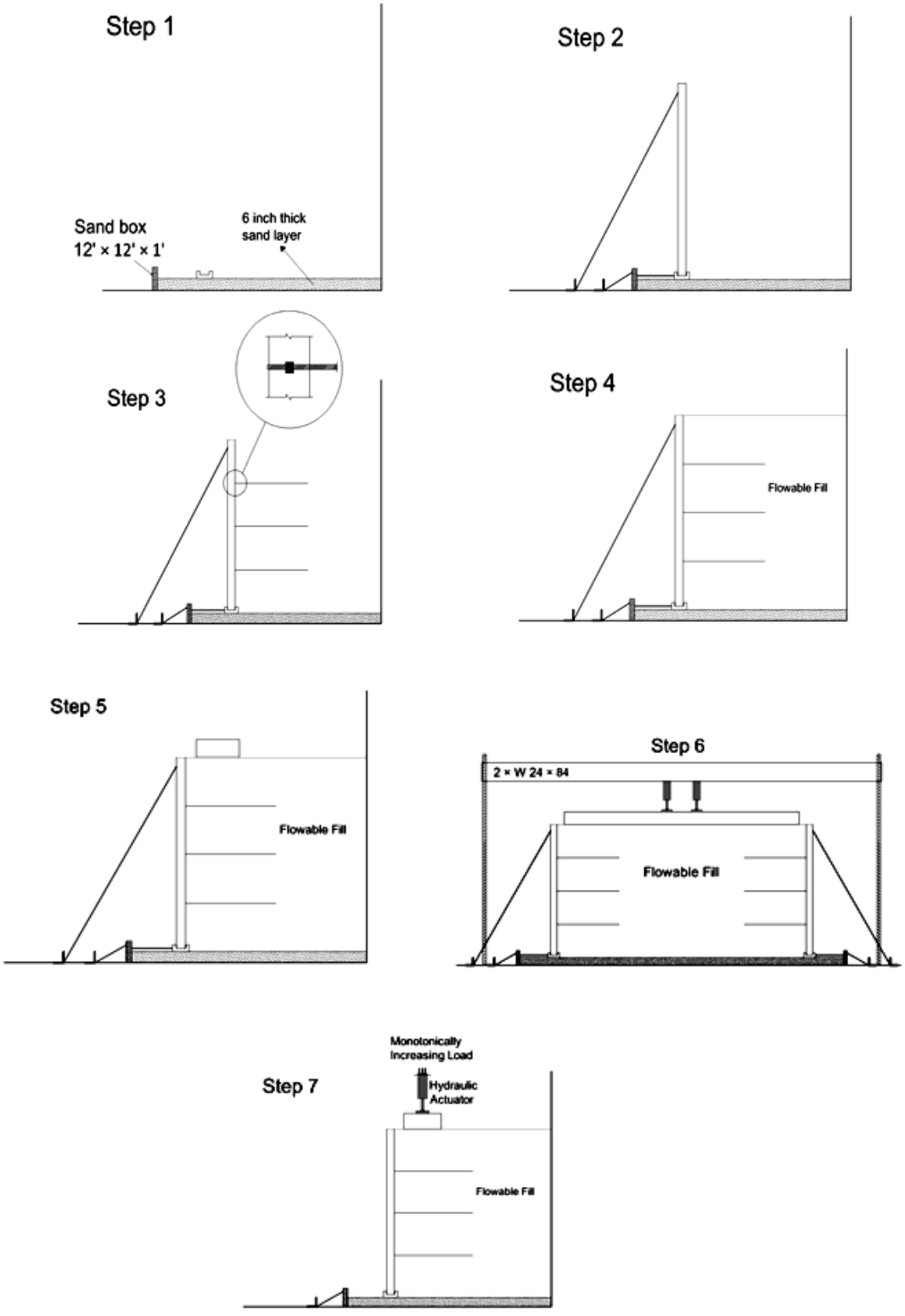

Figure 4.12: Construction sequence of CLSM bridge abutment test.

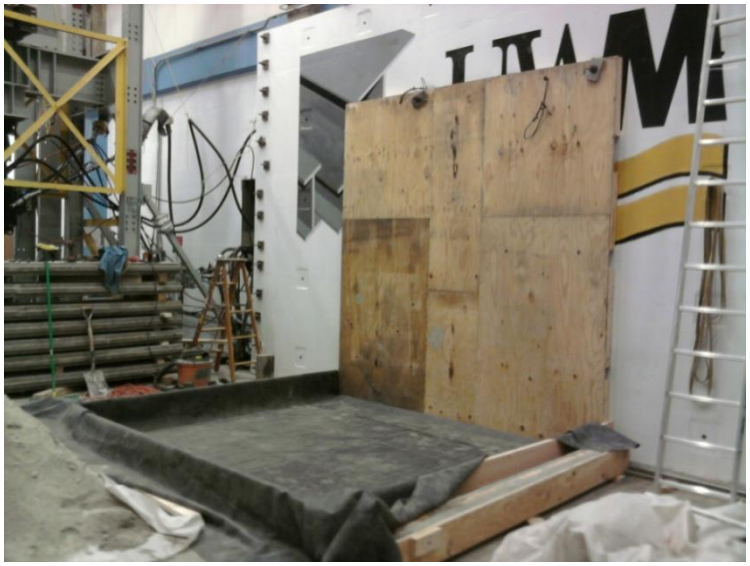

(a)

(b)

(c)

(d)

Figure 4.13: Base preparation, (a) rubber membrane, (b) sand box foundation, (c) soil compaction, (d) leveling pads.

Step 2; Panels Installation:

Each panel was assembled and connected to one-another using the laboratory's overhead crane to make the abutment box, see Figure 4.14a and b. Then the designed temporary bracing system was set up to support the panels laterally to ensure a safe working environment. Two sets of diagonal supports were used to secure the top and bottom of the panels temporarily (Figure 4.14c and d).

After all the concrete panels were installed, a geotextile layer (Typar 3301), as in Figure 4.15a, was installed as a filter in one-piece cover for the interior side of the abutment to let the water drain and keep the fine grained materials of the backfill. Another rubber membrane against the strong-wall of laboratory was also installed, glued both to the inside corners of the panels as well as to the previously installed membrane on the floor to make barrier against possible excessive leaking of CLSM mixture (Figure 4.15b).

Step 3; Anchors Installation:

As shown in Figure 4.16a, steel anchors were threaded through the nuts in the panels from the outside of the abutment. Strain gauges were attached to the anchors, at the top and bottom of one end, adjacent to the facing panels (Figure 4.16b). Length of all anchors was 1.24 m (4.5 ft) (50% of the panel height). This length was deemed necessary based on static design considerations. The test would provide insight into the behavior of the CLSM bridge abutment when loaded to failure. If the above design is deemed inadequate based on experimental results, the design could be refined based on the

follow-up advanced 3D finite element analysis. Pressure cells were also mounted on the inner side of the front wall to monitor the developed lateral pressures (Figure 4.16c).

(a)

(b)

(c)

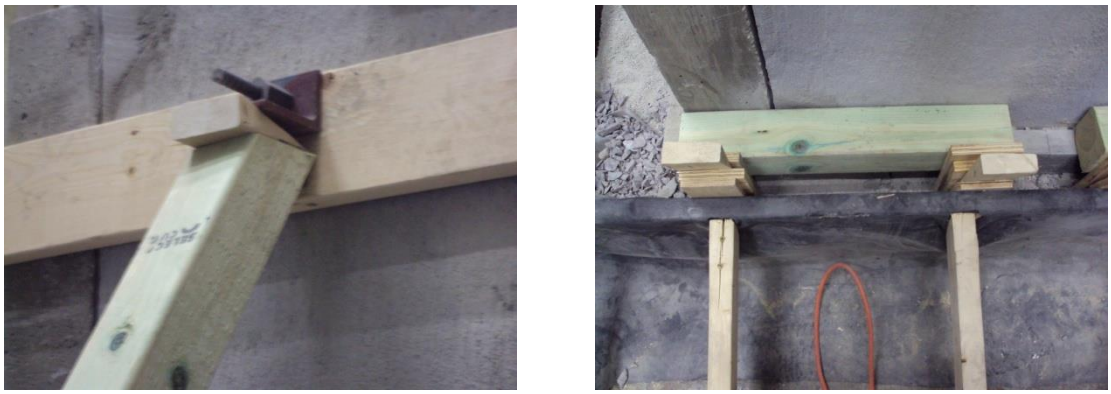

(d)

Figure 4.14: Panels installation; (a)Lifting a panel, (b)Installation of panels, (c)Temporary lateral Supports, (d)Detail of lateral supports at top (left picture) and bottom (right picture).

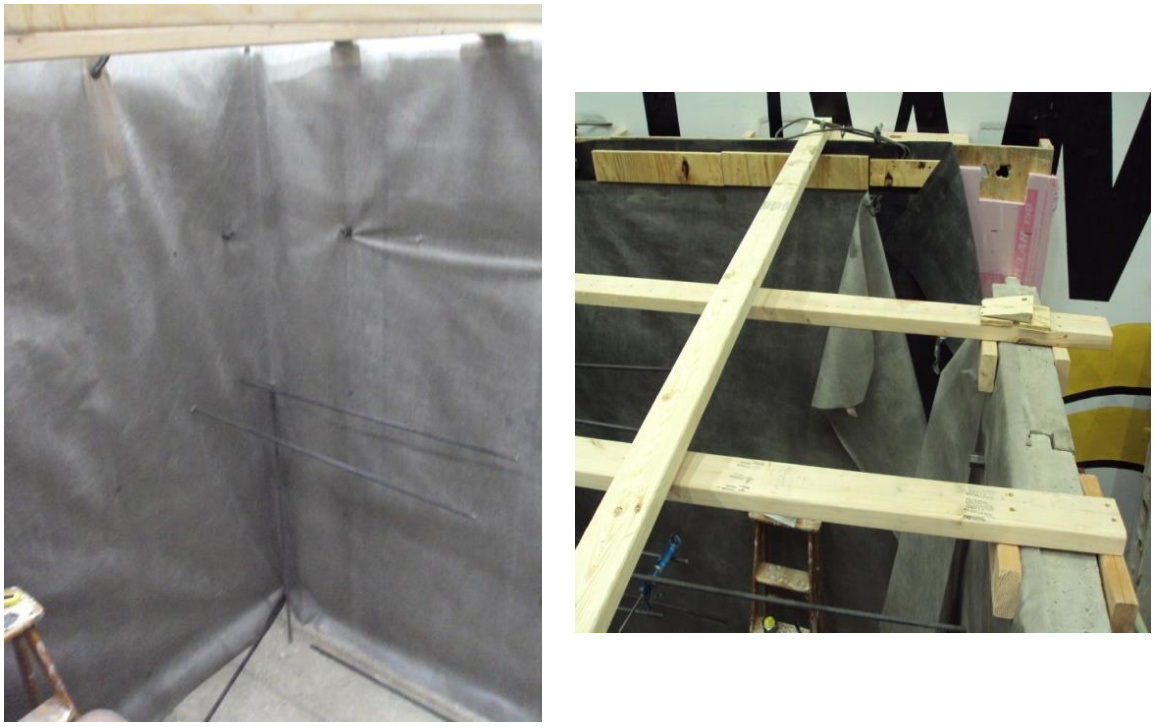

(a) (b)

Figure 4.15: Interior covers; (a) geotextile filter layer, (b) rubber membrane against the strong-wall of the laboratory.

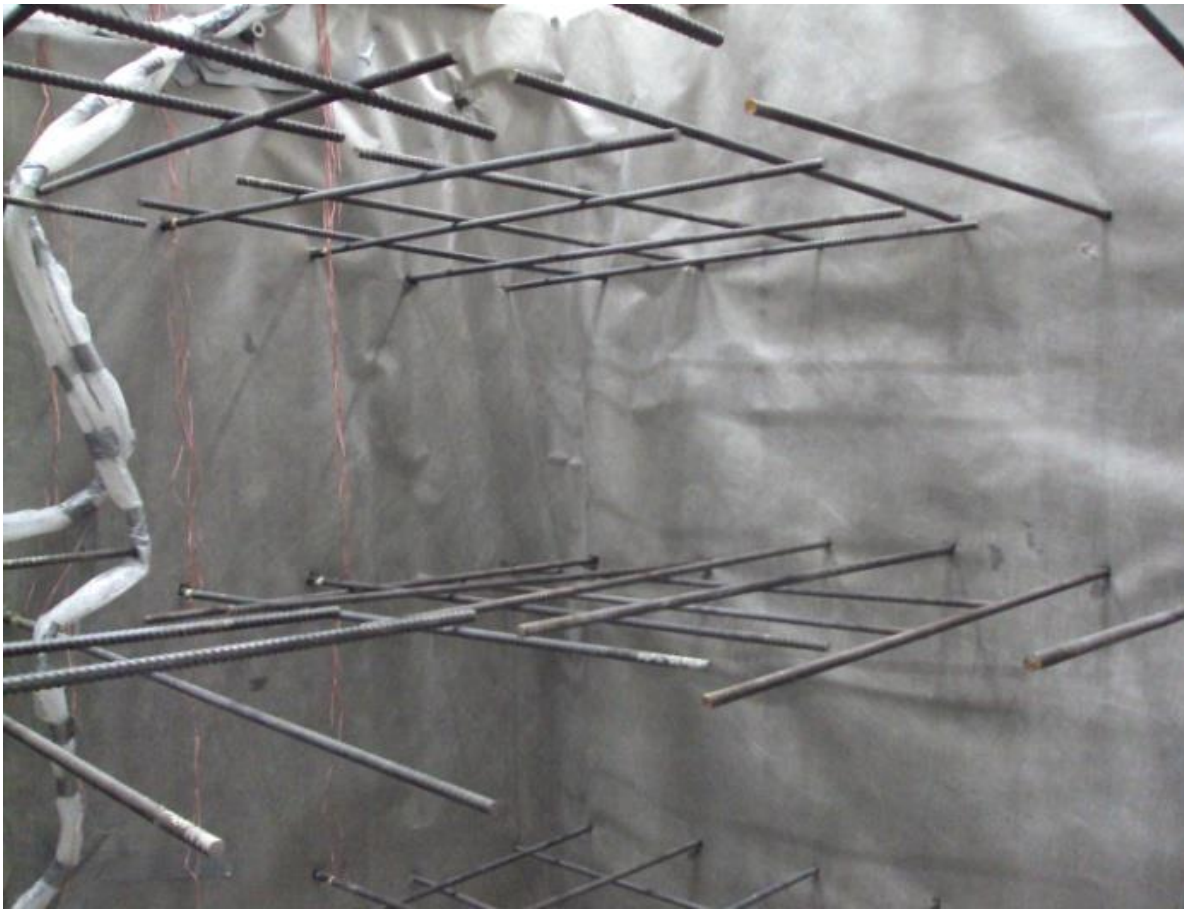

(a)

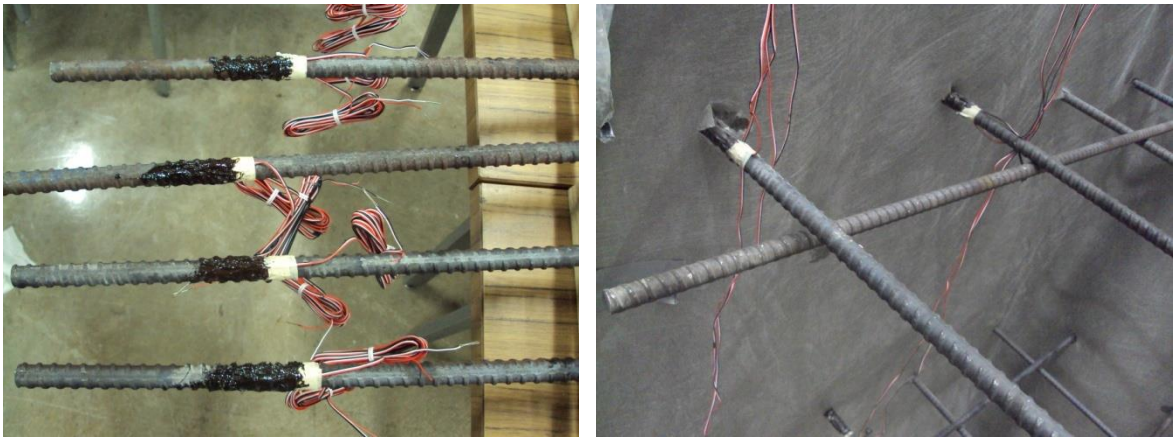

(b)

(c)

Figure 4.16: (a) Anchors Installation, (b) Strain gauges attached to anchors, (c) Pressure Cells.

Step 4; CLSM Placement:

The entire abutment was backfilled in one continuous pour by pumping of the CLSM material. Figure 4.17 shows the continuous batching process and pouring of CLSM. Samples were collected during the placement of the CLSM material to compare the strength with that from the designed mix. Unconfined compression strengths of the samples were 0.2 MPa and 0.4 MPa at 7 days and 28 days, respectively. Flowability of the mixture was controlled frequently in order to be kept around 350 mm according to the Standard Test Method for Flow Consistency of CLSM (ASTM D 6103). The excess water of the placed CLSM was released through anchor openings of the panels (Figure 4.18). It was scheduled to wait seven days for flowable fill to set before removing lateral supports and loading.

(a)

(b) (c)

(d)

Figure 4.17: Continuous batching and pouring CLSM; (a) Fly Ash, (b) Sand, (c) Mixer and (d) Pumping and pouring.

(a)

(b)

(c)

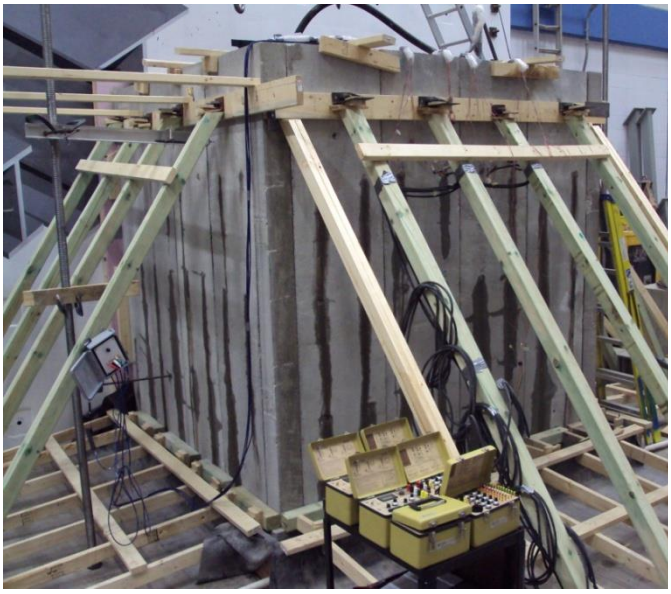

(d)

Figure 4.18: (a) Released Water, (b) Drain Pipe, (c) Released water collected in sand box foundation (d) Drainage of water through holes of all panels.

Step 6; Loading Frame:

A loading frame was assembled using steel columns and beams and braced to the laboratory's wall. Two hydraulic jacks were mounted under the frame to allow application of load to the bridge sill, see Figure 4.19. The loading frame was designed for 1335 kN load. The beam section was made up of two W sections of 24×84, welded together.

Step 5; Bridge Sill Placement:

After six days from the time of the placement of the CLSM material, the precast concrete bridge sill was installed on top of the CLSM abutment as shown in Figure 4.20. The sill was 0.61 m (2 ft) wide, 2.4 m (7.83 ft) long, with its centerline aligned with the centerline of the abutment. The sill clear distance, measured from the back face of the front wall to the front edge of the sill, was 13 cm (0.5 ft). The left and right edges of the sill were 2.54 cm (1 in.) away from the back face of the wing walls (Figure 4.4).

LVDTs were mounted on the four corners of the sill to measure its settlement, and also on the front face and wing walls to measure their lateral displacements (Figure 4.21). As in Figure 4.21, wooden frame was used as a reference base against which all LVDTs were mounted. Positions of the LVDTs are shown in Figure 4.3. Two steel plates were placed on the concrete sill as loading pads at the loading positions. As pictured in Figure 4.22, hydraulic jacks were mounted under the beam of the strong frame and seated on the loading pads.

(a)

(b)

Figure 4.19: Loading frame assembly; (a) 2× W 24×84 beam, (b) Assembly of loading frame, and lateral bracing.

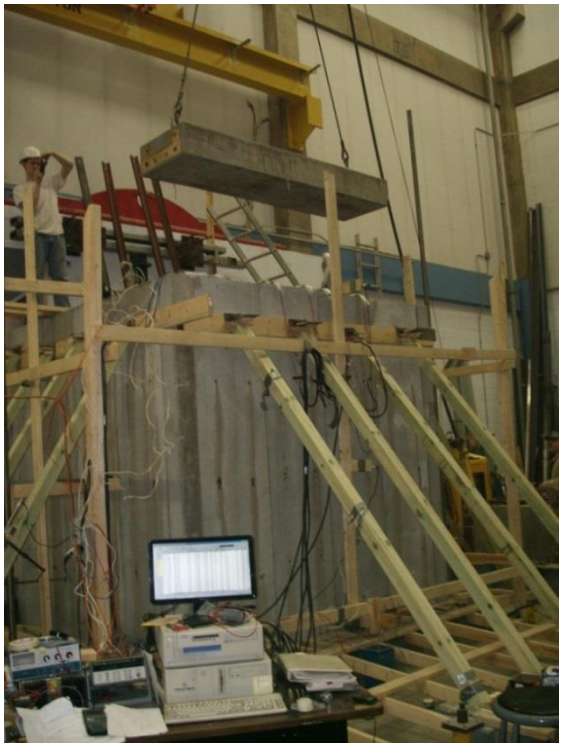

(a)

(b)

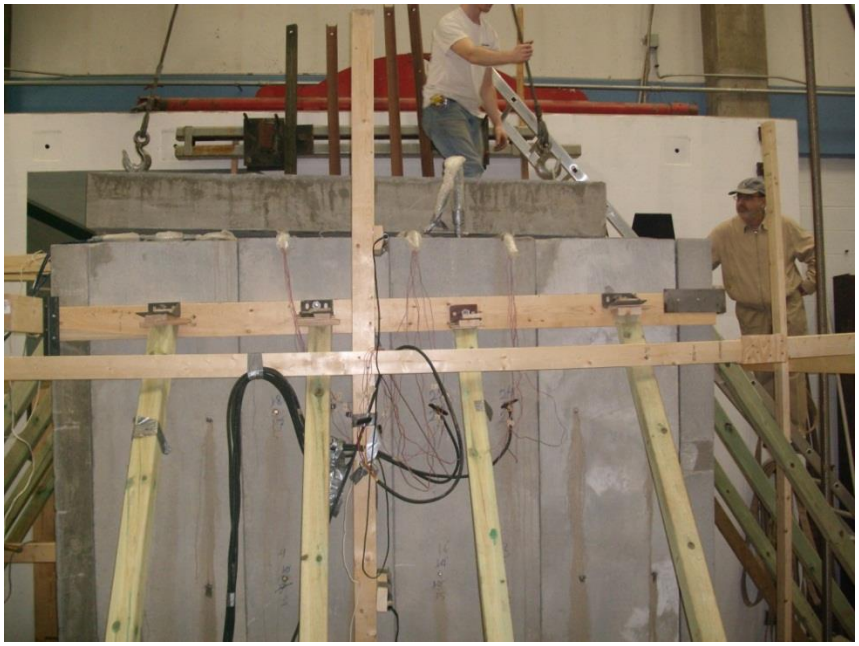

(c)

Figure 4.20: Bridge sill placement; (a) lifting the sill, (b) leveled surface of the CLSM backfill, (c) placing bridge sill over the backfill.

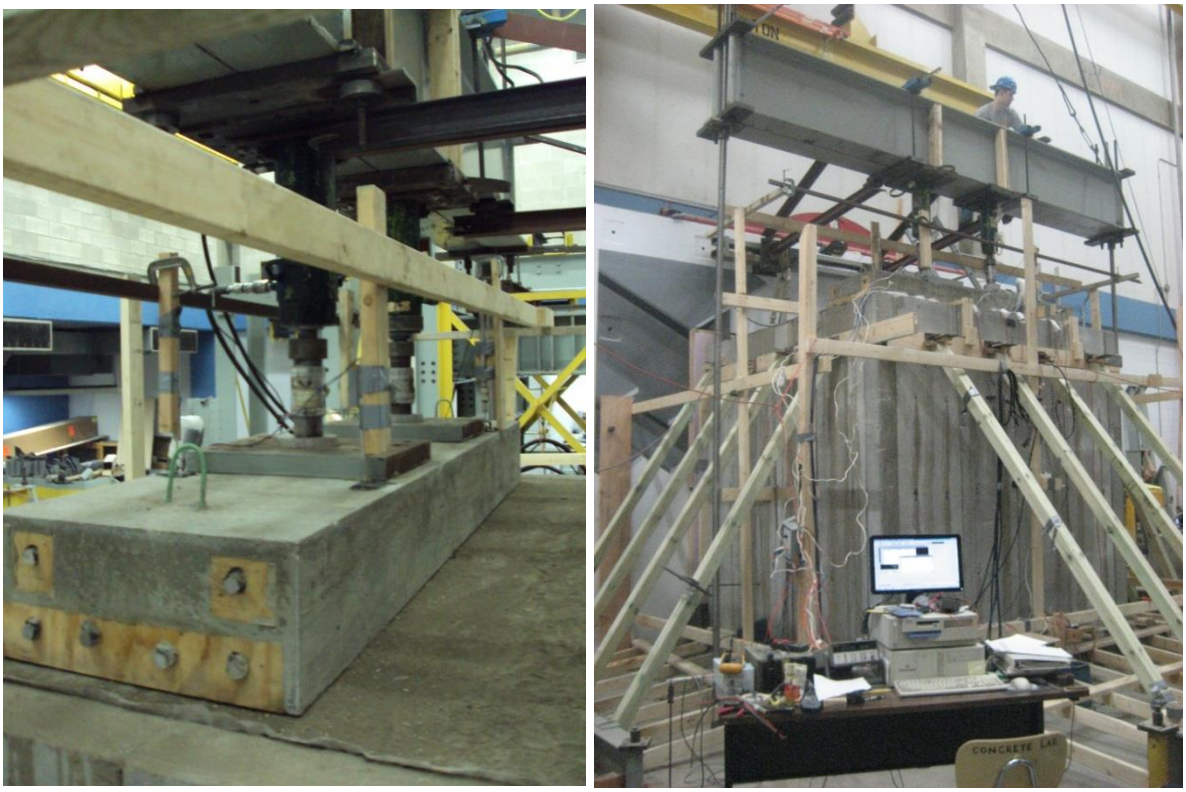

Figure 4.21: (left) Location of LVDTs on the sill, (right) wooden frame for LVDTs.

Figure 4.22: Two steel plates and hydraulic jacks on the bridge sill.

Step 7; Application of Load:

Seven days after placement of the CLSM material, the lateral supports were removed from the abutment panels (Figure 4.23). Figure 4.24 shows the CLSM abutment just prior to the loading test. Static loads were applied to the bridge sill in steps using electronic hydraulic pump (Figure 4.25) and hydraulic jacks. All measurements including applied loads, lateral pressures on panels, displacements and strains were recorded using a data acquisition system. Dial displacement gauges were recorded manually.

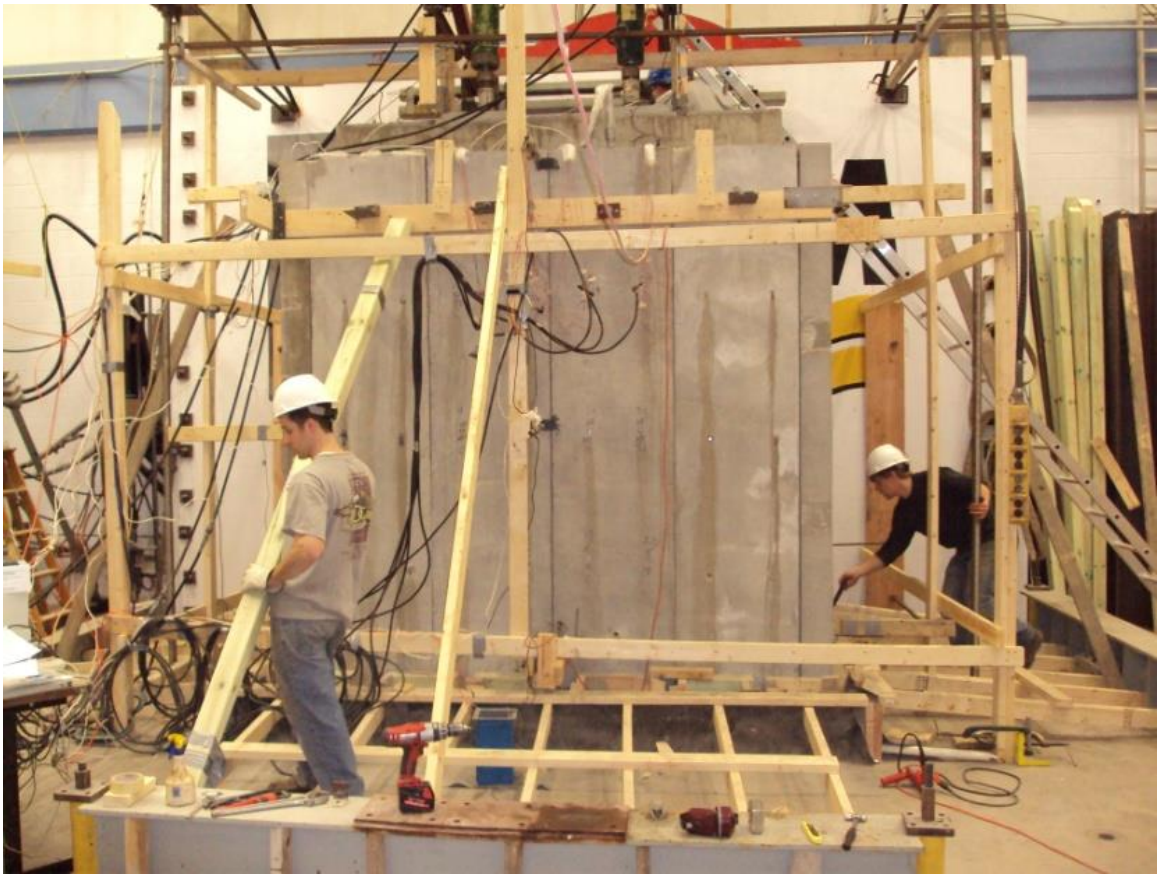

Figure 4.23: Removing lateral supports.

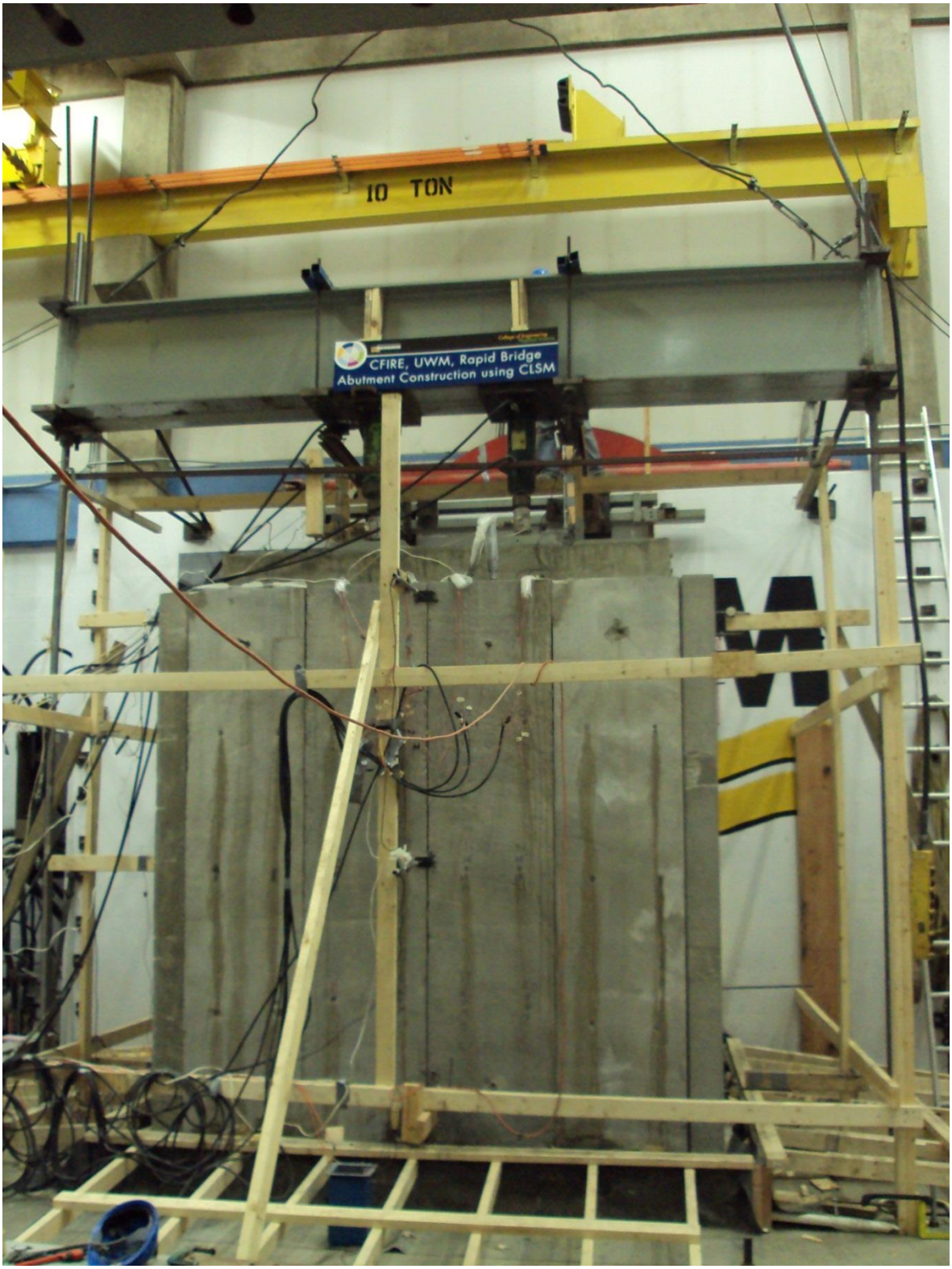

Figure 4.24: Large Scale CLSM Bridge Abutment.

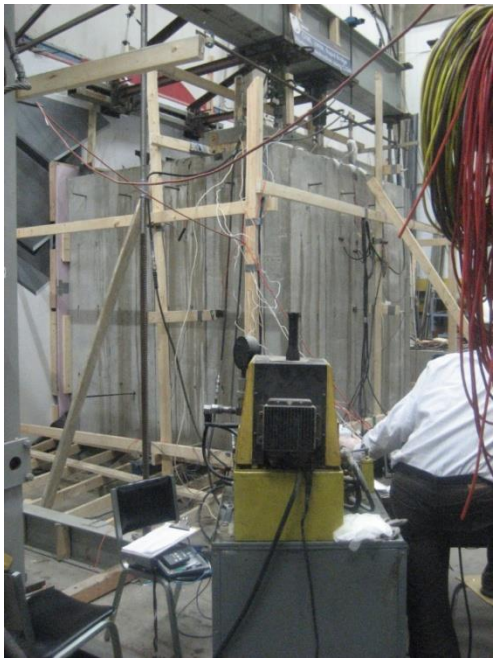

Figure 4.25: Loading the CLSM Abutment with electronic hydraulic pump.

4.2.3 Excavation

After completing the test, CLSM abutment must be removed from the laboratory. Initially the panels were detached from the backfill. This took a lot of effort because of the fact that the abutment itself did not damaged during loading and all panels were remained tight to the backfill. Then the backfill was easily excavated because of the low strength of the CLSM, see Figure 4.26.

Figure 4.26: (top) Detachment of the panels, (bottom) excavation of CLSM backfill.

4.3 Experimental Results

Up to 780 kN of vertical load was applied to the CLSM abutment without any failure or damage in the system. It was not possible to apply more load because of the capacity limit of the laboratory's rigid floor. This load applies a pressure of 535 kPa on the bridge sill. The corresponding pressure from the dead load of a single-span bridge of 24 m length and 11 m width on an 11 × 1.5 m bridge sill should be 93 kPa for a typical bridge. Therefore the applied pressure on the CLSM bridge sill was almost six times larger than this pressure, even though it was not a failure pressure. Figure 4.27 shows that the front face and wing walls did not suffer any noticeable deformations.

Figure 4.27: Final undamaged state of the abutment after loading.

4.3.1 Displacements

Settlements at the four corners of the bridge sill are shown in Figure 4.28. The observed small variation in settlements is possibly due to the initial gap(s) between the sill and the top surface of CLSM. Bridge load versus settlement response (average settlement of four LVDTs at corners of the bridge sill) is shown in Figure 4.29. The average final settlement of the bridge sill was about 6 mm. Since the specimen was constructed over a rigid foundation, settlement of the bridge sill represents the deformation of the CLSM abutment itself. Data from the LVDT on the leveling pad, as illustrated in Figure 4.30, shows that the underlying foundation experienced only negligible settlement, as small as 0.4 mm.

The maximum lateral displacement of the front facing panel occurred at the top of the panel and was about 3 mm. Lateral deflection of this point and the middle and bottom of the front face with gradually applied load is shown in Figure 4.31a. The lateral displacement at the middle and the bottom of the panel was considerably smaller as shown in the same figure. Also profile of lateral deflection of the front wall panel due to the maximum applied vertical load on bridge sill is illustrated in Figure 4.31b. Lateral displacements of the wing walls were negligible with the maximum value of 1 mm at the top.

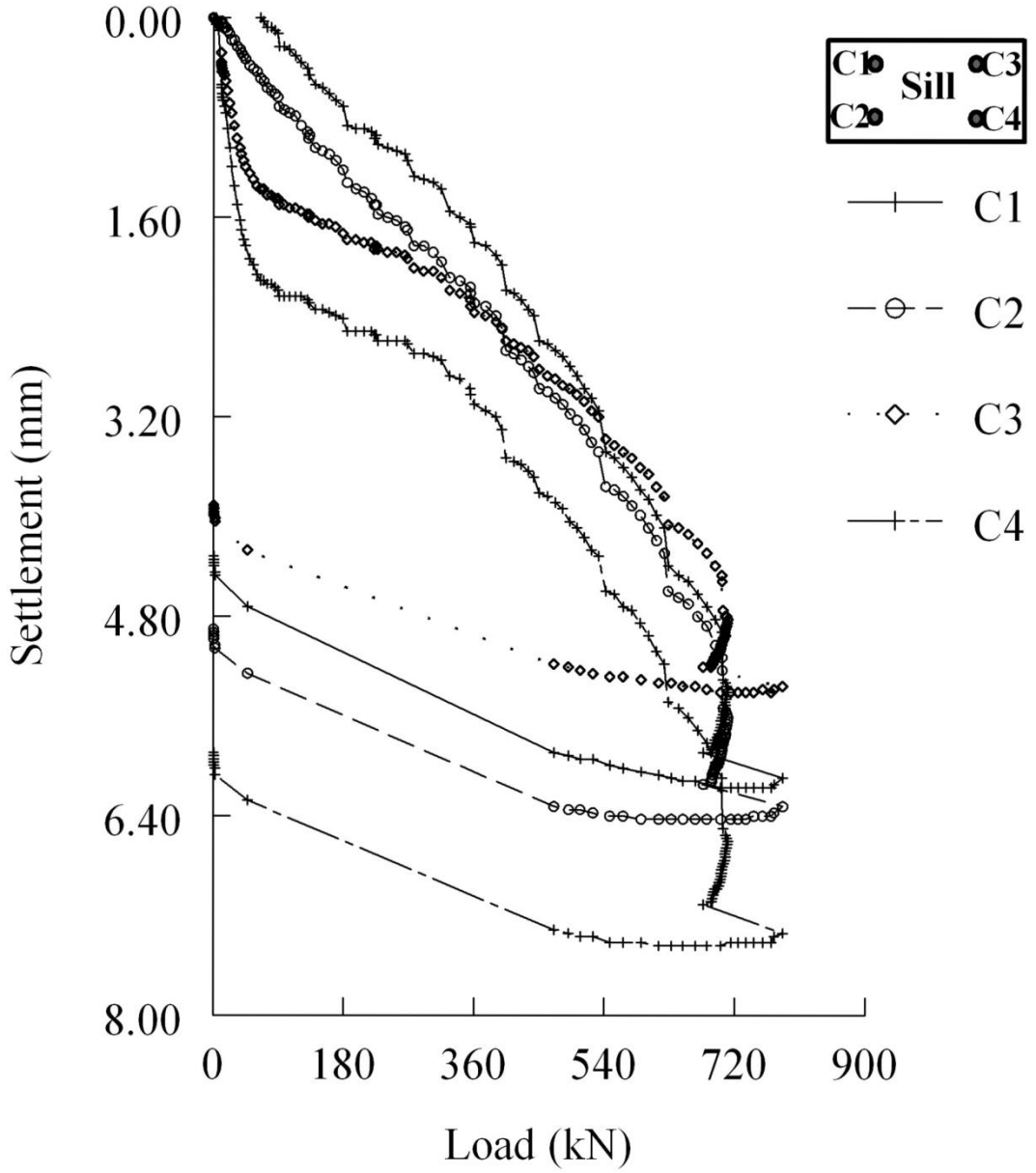

Figure 4.28: Settlement of the bridge sill at corners.

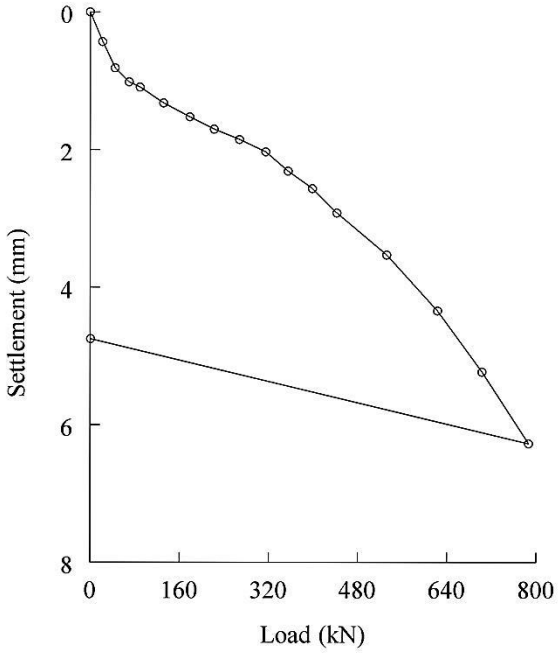

Figure 4.29: Average settlement of the bridge sill.

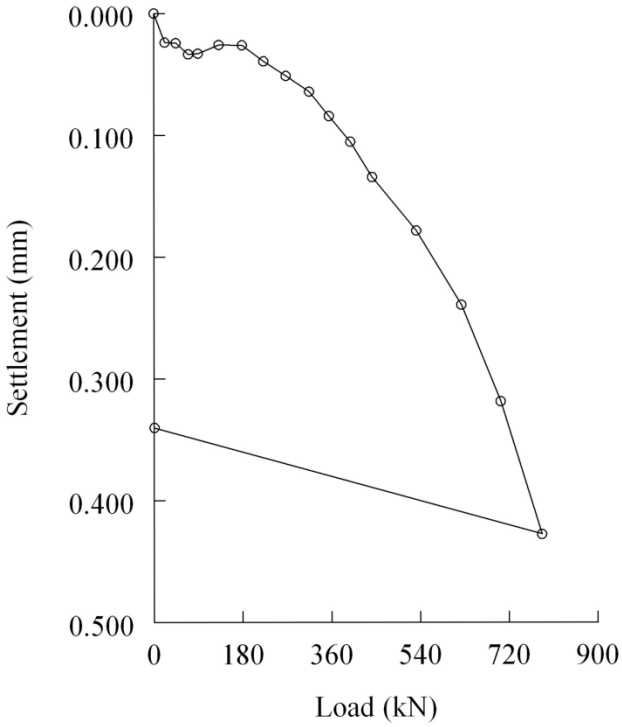

Figure 4.30: Settlement of the foundation soil.

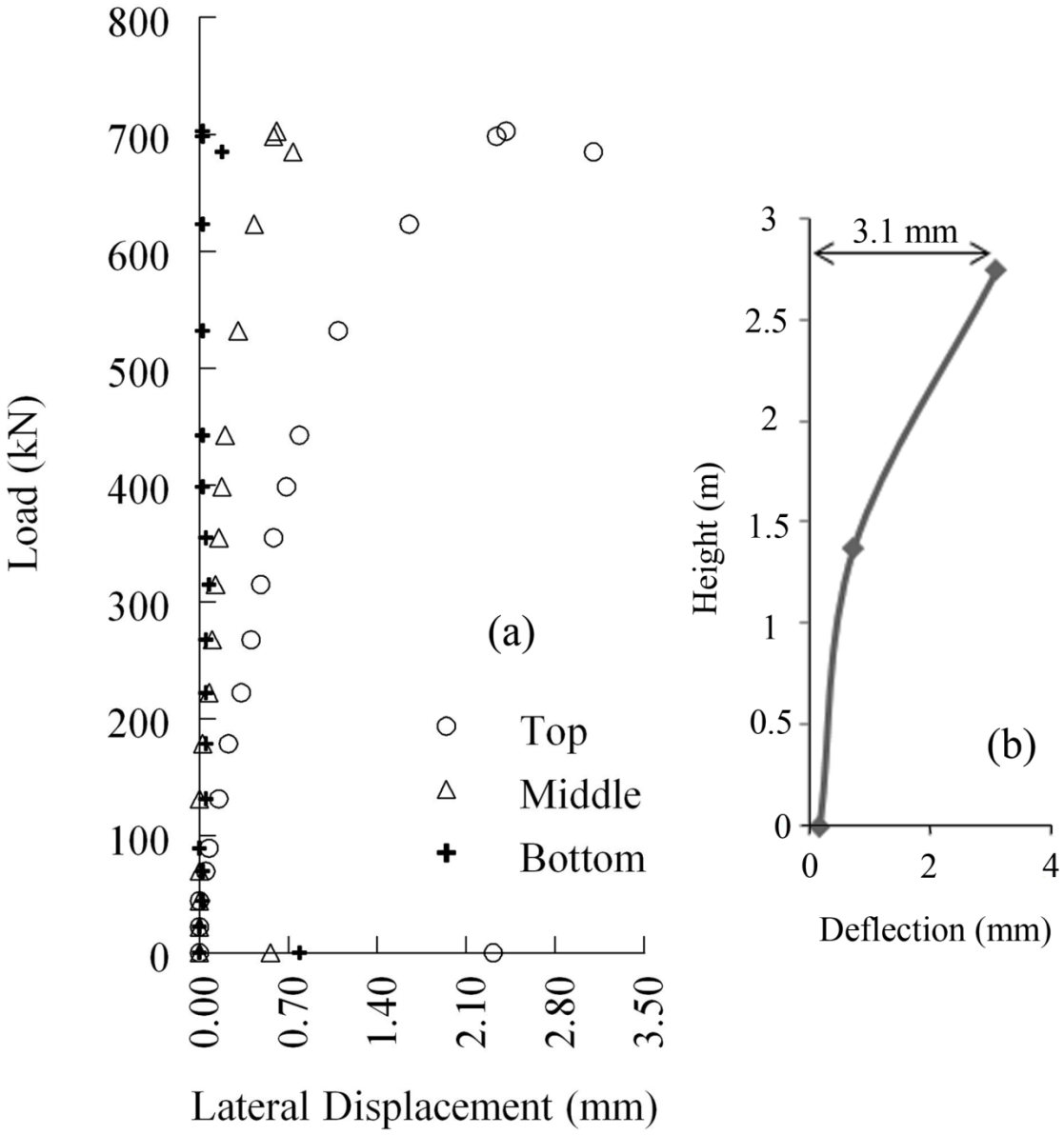

Figure 4.31: (a) Lateral deflection of the front facing wall, (b) deflection profile of the front panel.

4.4.3 Lateral Pressures

The lateral pressure of backfill against the front facing panel was monitored during and after the placement of the CLSM material as well as during the loading stage of the experiment. It is known that a freshly placed concrete behaves temporarily like a fluid, producing a hydrostatic pressure that acts laterally on a wall. For flowable fills, Schmitz et al. (2004) concluded that the lateral pressure on a wall after the curing stage is negligible. However, during the placement of CLSM, the structure must be designed to temporarily support the fluid pressures. The varying profile of the measured lateral pressure of the CLSM as a function of age against the abutment panels of the front face is shown in Figure 4.32 and compared with the hydrostatic pressure. As it can be seen, fresh flowable fill results in smaller lateral pressure on the abutment than that from normal fluid pressure. The maximum lateral pressure of about 24 kPa was measured at the bottom of the facing panels initially but it was gradually reduced to about 7 kPa as the CLSM material cured, but the pressure at the mid-height of the panels increased to 24 kPa as the material aged, see Figure 4.33. This higher lateral pressure at the mid-height areas of the abutment is due to the speed of hydration and the length of the drainage path. This was verified by the large volume of drained water observed at the base of the test abutment. Past studies have also shown that at the mid-height regions of CLSM abutments, water cannot dissipate or evaporate as fast as regions near the surface (Snethen et al. 1997).

Figure 4.34 shows the lateral pressure on front panels during the application of bridge loading. The figure shows that the lateral pressure is very small in general with the

maximum value of 30 kPa recorded near the middle of the panel. As illustrated in Figure 4.35, upon applying the bridge load, the lateral pressure at the top of the panel was unchanged in the beginning and then started to increase approaching about 10 kPa at 790 kN load. The pressure at the bottom of the panel remained unchanged. It is interesting to note the pressure elsewhere consistently decreased as the bridge load increased. This may be attributed to the lateral (outside) deflection of the facing panel.

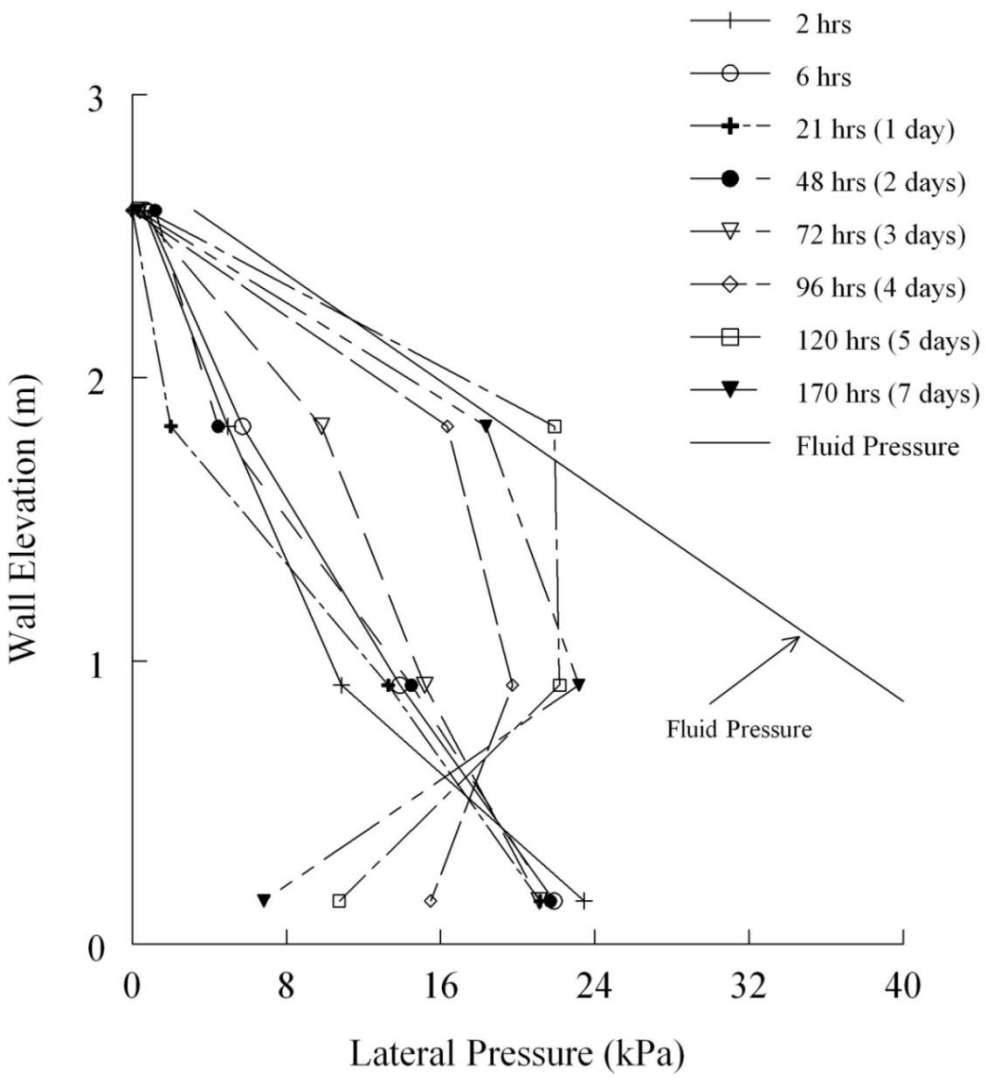

Figure 4.32: Lateral pressure profile against abutment with CLSM age.

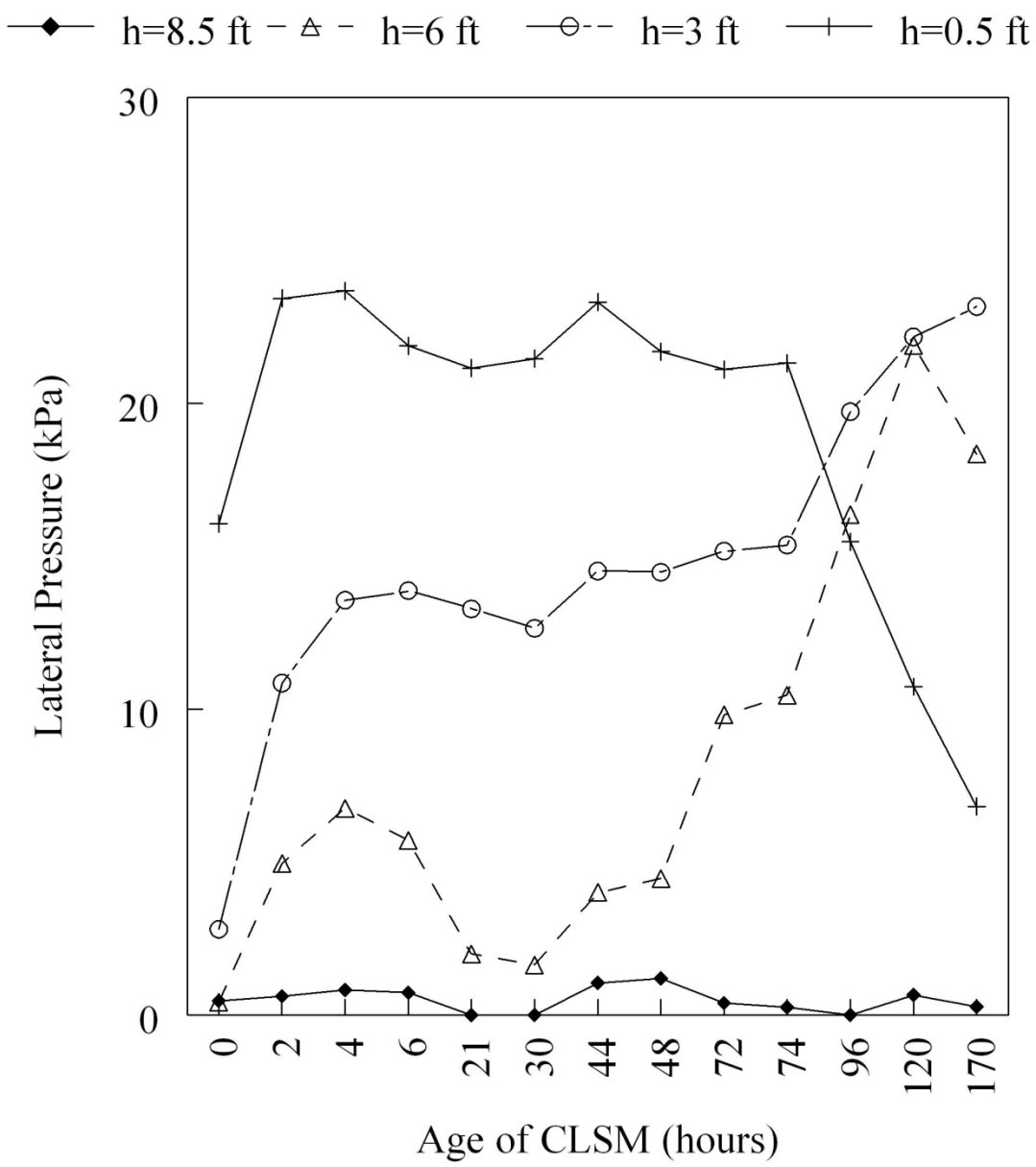

Figure 4.33: Development of lateral pressure at different heights with CLSM age.

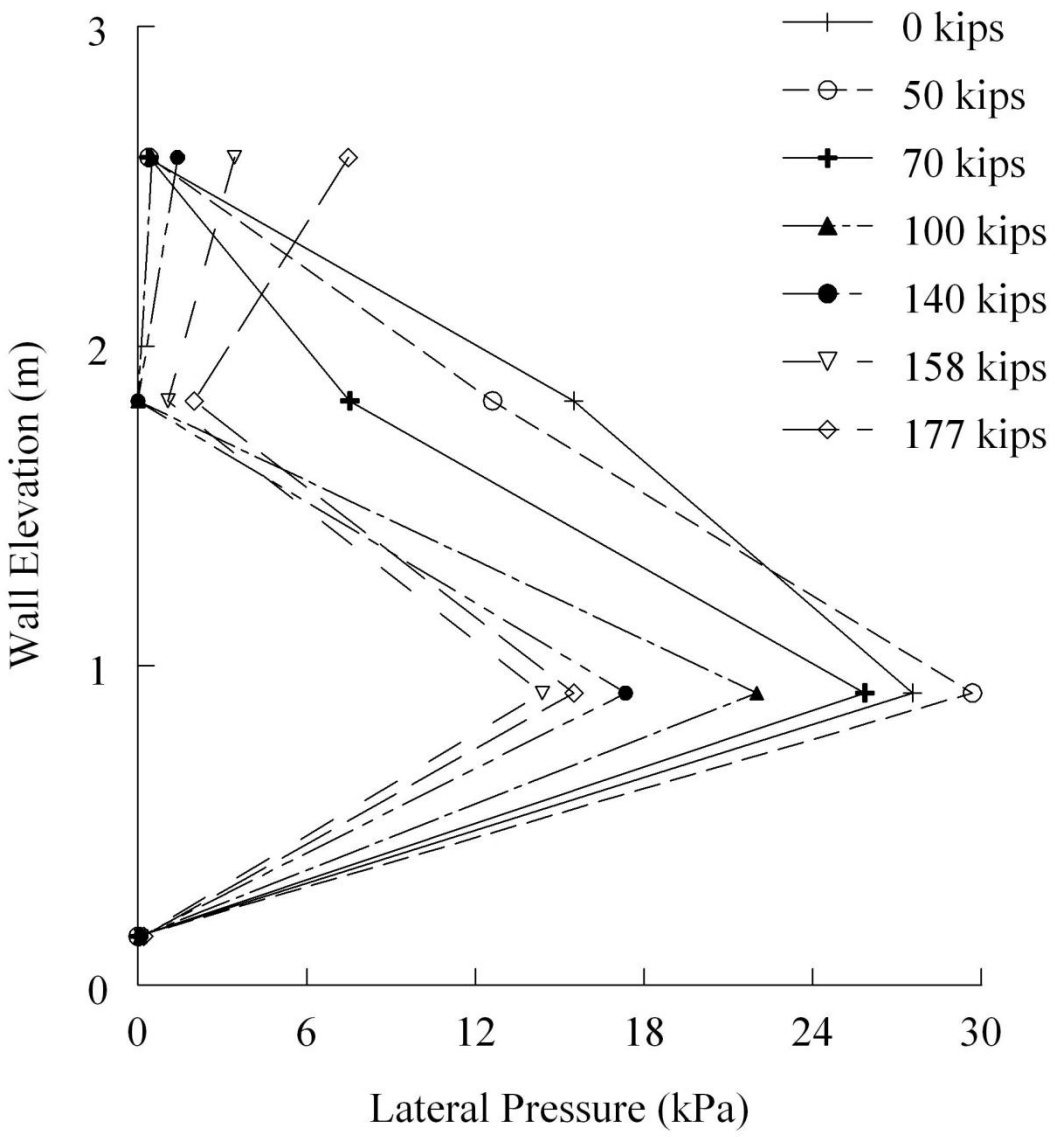

Figure 4.34: Lateral pressure on the front wall with applied load.

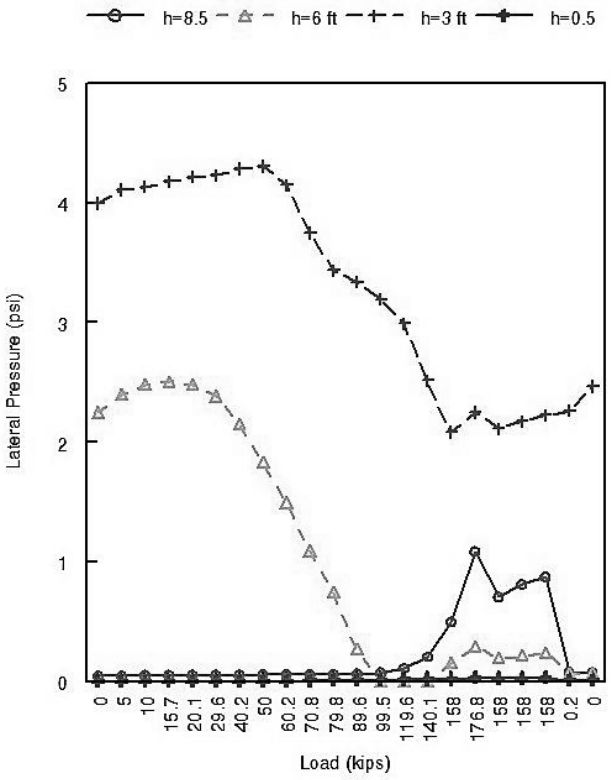

Figure 4.35: Development of lateral pressure at different heights with the applied bridge load (1 psi = 6.895 kPa, 1 kip = 4.448 kN)

4.4.4 Strain Gauges

Several strain gauges were used to measure the strains at the top and bottom sides of several steel anchors at their points of attachment with the facing panels (Figure 4.16b). Figure 4.36 shows location of steel anchors with strain gauges at the facing panels. The measured strains in the steel anchors installed at different heights of the facing panels are shown in Figures 4.37 and 4.38 as function of the applied bridge load. The measured strains indicated that steel anchors installed at the top of the panels experienced almost symmetrical strains at the top and bottom of cross section which

demonstrates bending strains rather than axial ones. From top to bottom of the panels this symmetrical pattern transforms to similar strains at the top and bottom of cross section which reveals more axial than bending strains. At the bottom it seems the axial strain prevails. With assumption of linear and elastic stress-strain relationship for steel anchors which means stress, σ, is proportional to strain, ϵ, $\sigma = E\epsilon$, cross sectional stresses at top and bottom of the anchors is determined and plotted in Figures 4.39 and 4.40. Young's modulus for steel is 207 GPa. The maximum calculated stress in rebars was about 110 MPa at the top of the panel which is considerably less than yield stress of steel rebar anchors.

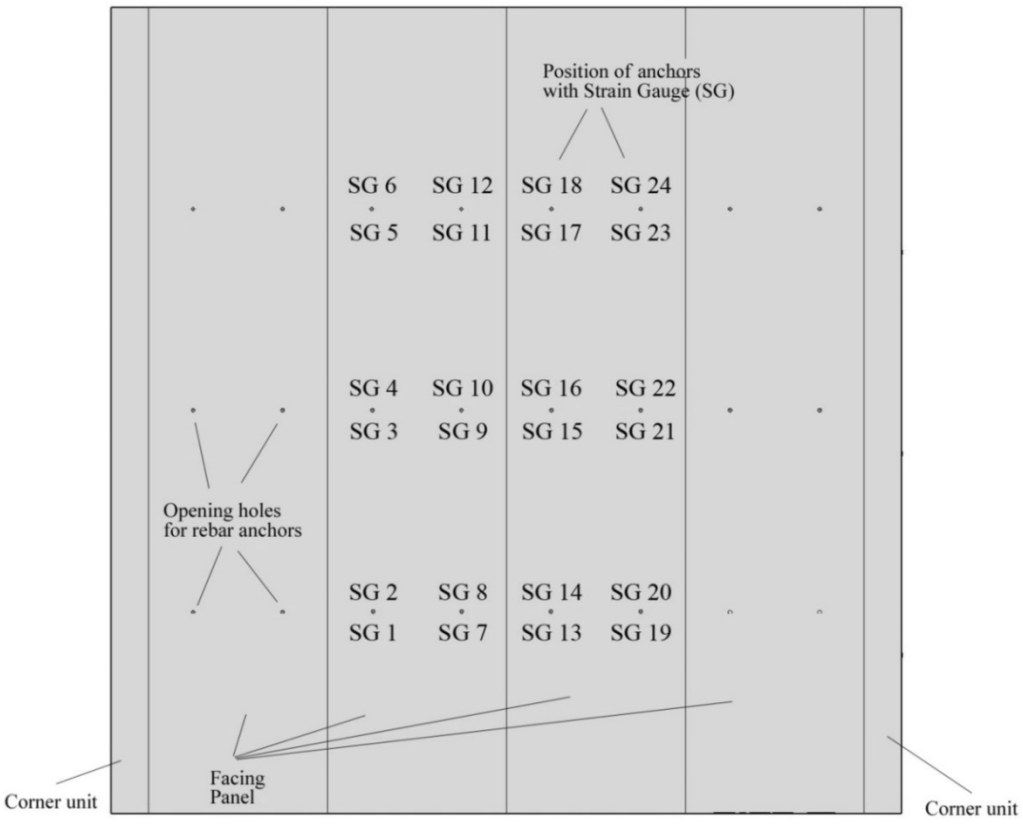

Figure 4.36: Position of steel anchors with the strain gauges at the facing panels.

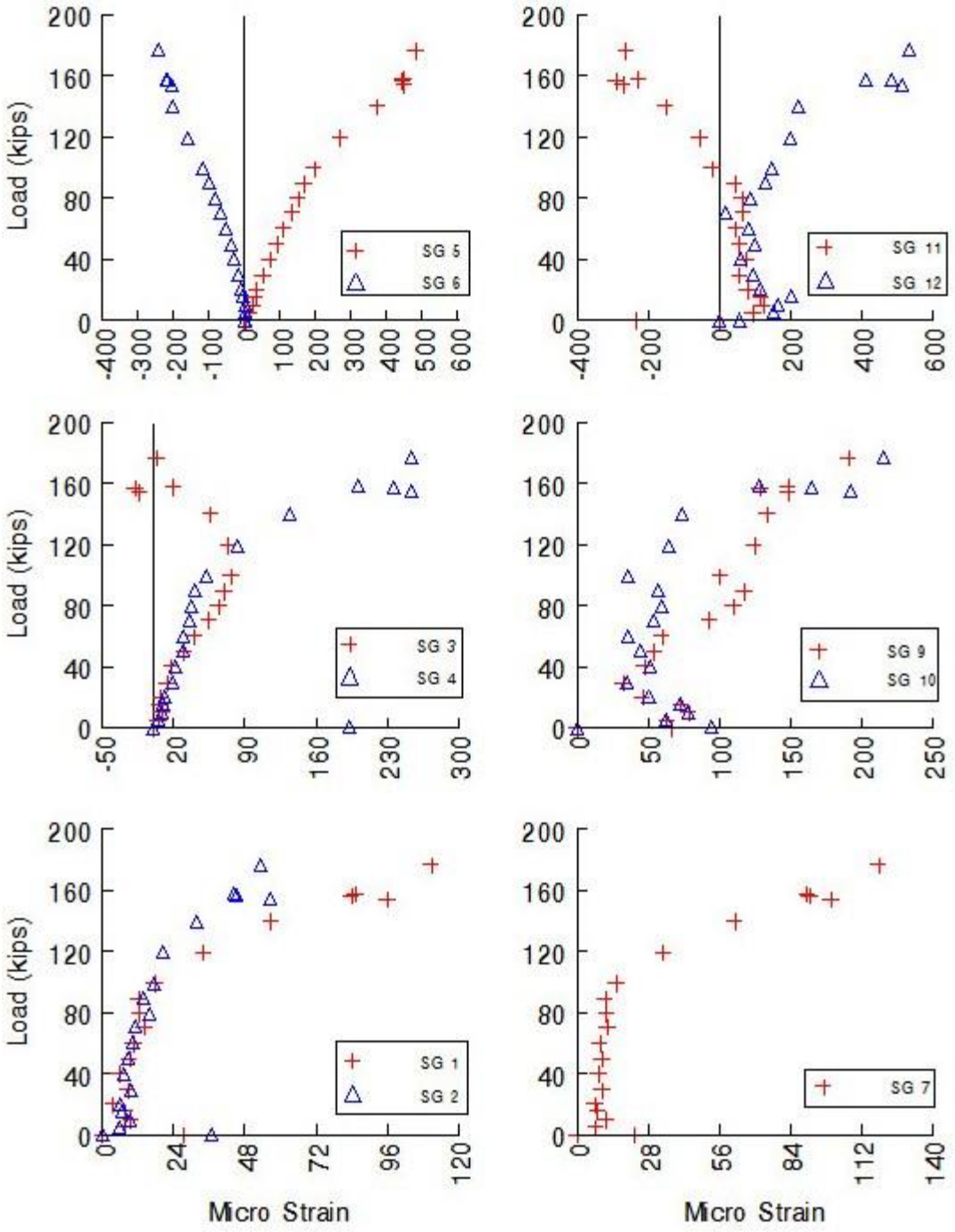

Figure 4.37: Strains at top, middle and bottom anchors of left middle panel of front face (1 kip = 4.448 kN).

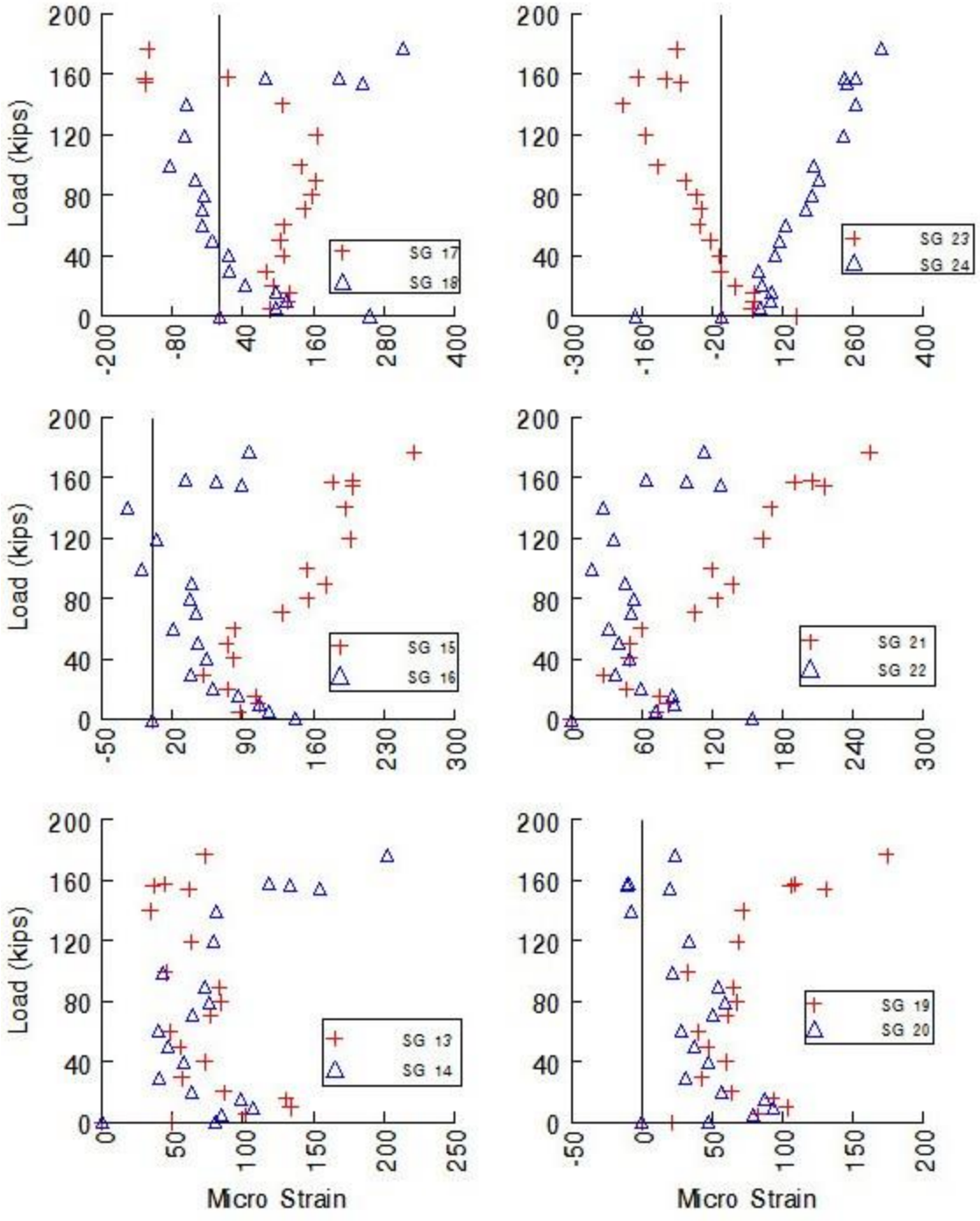

Figure 4.38: Strains at top, middle and bottom anchors of right middle panel of front face (1 kip = 4.448 kN).

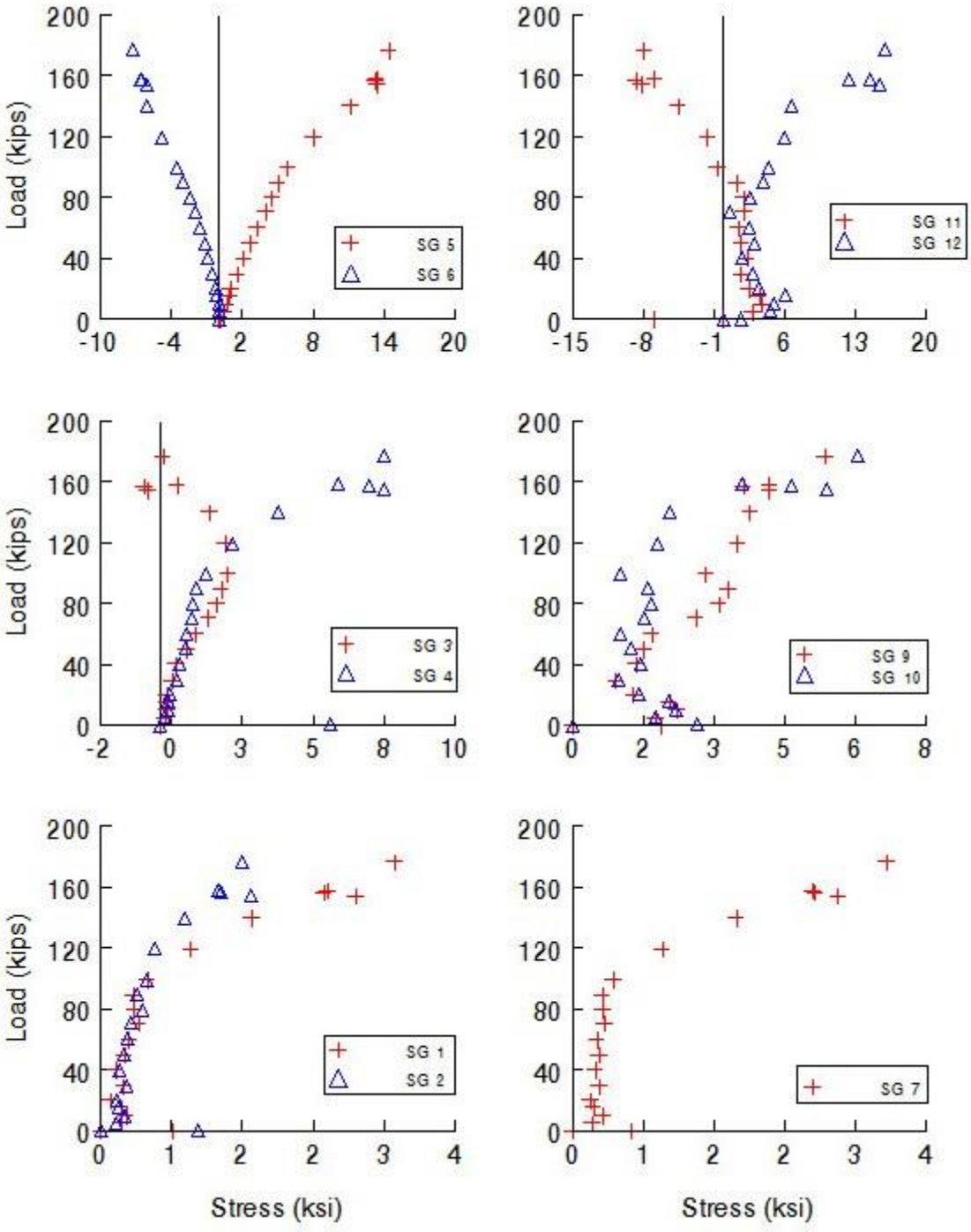

Figure 4.39: Stresses at top, middle and bottom anchors of left middle panel of front face (1 kip = 4.448 kN).

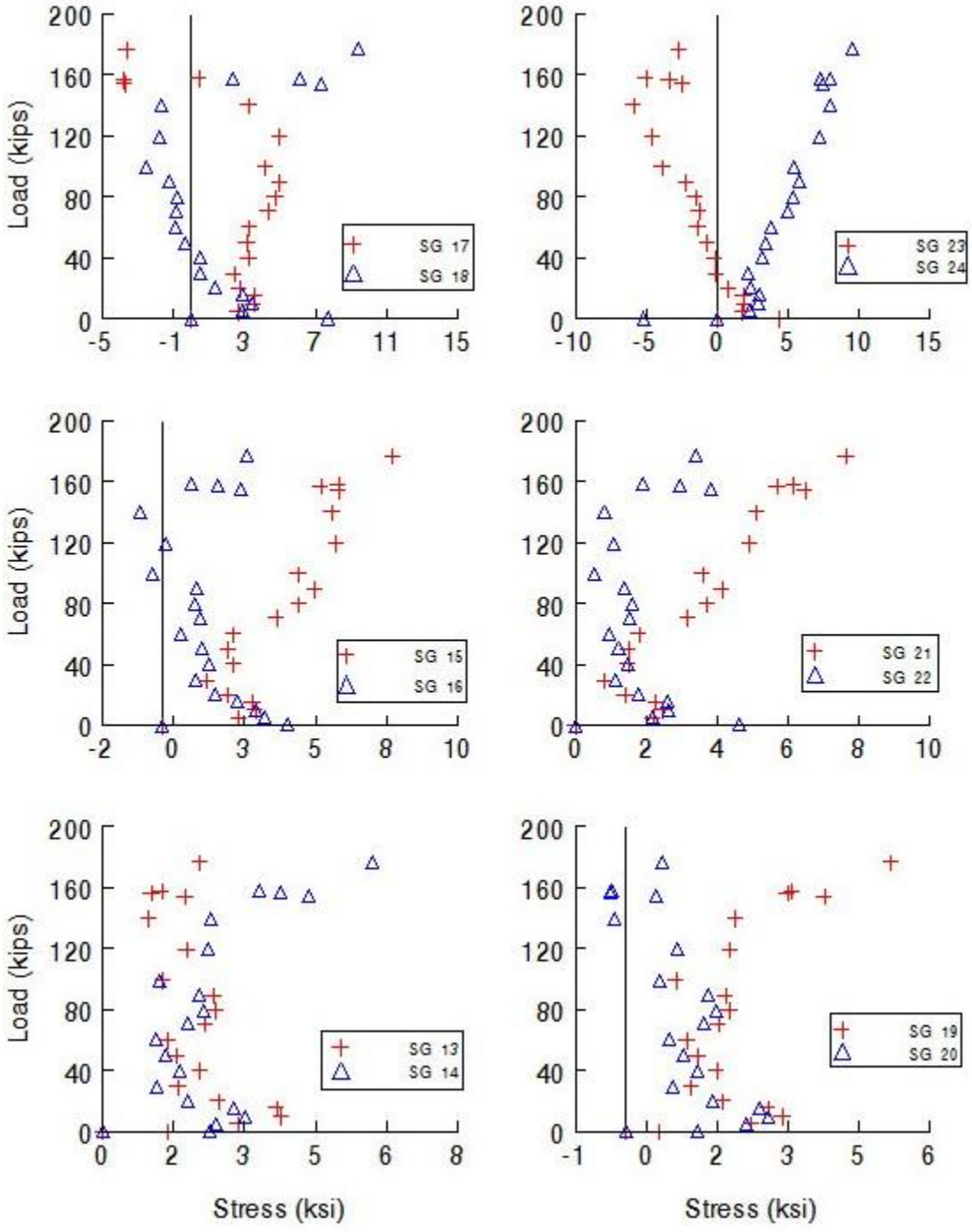

Figure 4.40: Stresses at top, middle and bottom anchors of right middle panel of front face (1 kip = 4.448 kN).

The anchors subjected to the simultaneous action of bending loads of the bridge sill and axial tension forces from facing panels. In order to compare the developed axial loads with the pullout resistance of the steel rebar in CLSM mass, the axial stress had to be isolated from the measured total stress. An example of the calculation to determine the axial stress for an anchor acted upon by combined bending and axial stress is shown in Figure 4.41. Development of axial tension forces (axial stress multiplied by the cross sectional area) in the anchors with the applied bridge load is shown in figure 4.42. The highest computed axial load in the anchors was about 5.3 kN.

In order to evaluate the bond strength of the CLSM and steel anchors, a full-scale pullout test (with the same rebar embedded in the CLSM abutment specimen, section 3.3.3) was performed. The ultimate pullout force was about 22 kN. Based on strain measurements of the anchors under the bridge load, the axial tensile forces were less than 30% of the ultimate pullout force.

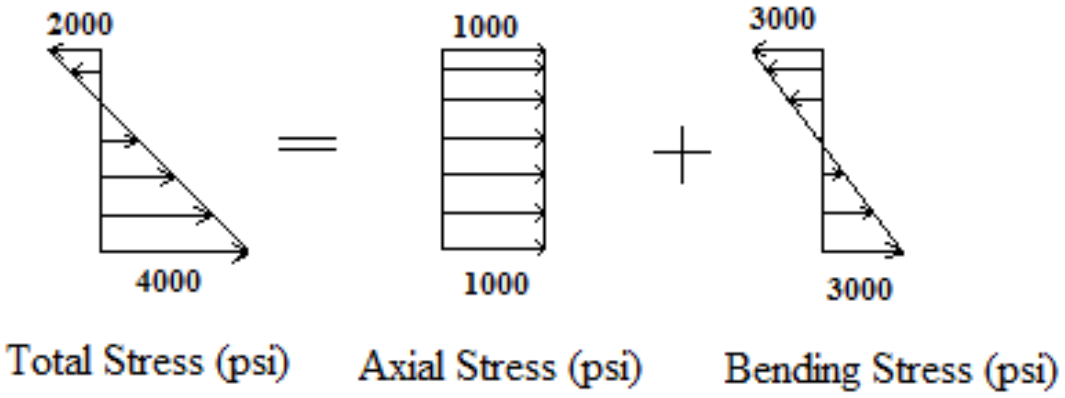

Figure 4.41: Combined bending and axial stresses for an anchor (1 psi = 6.895 kPa).

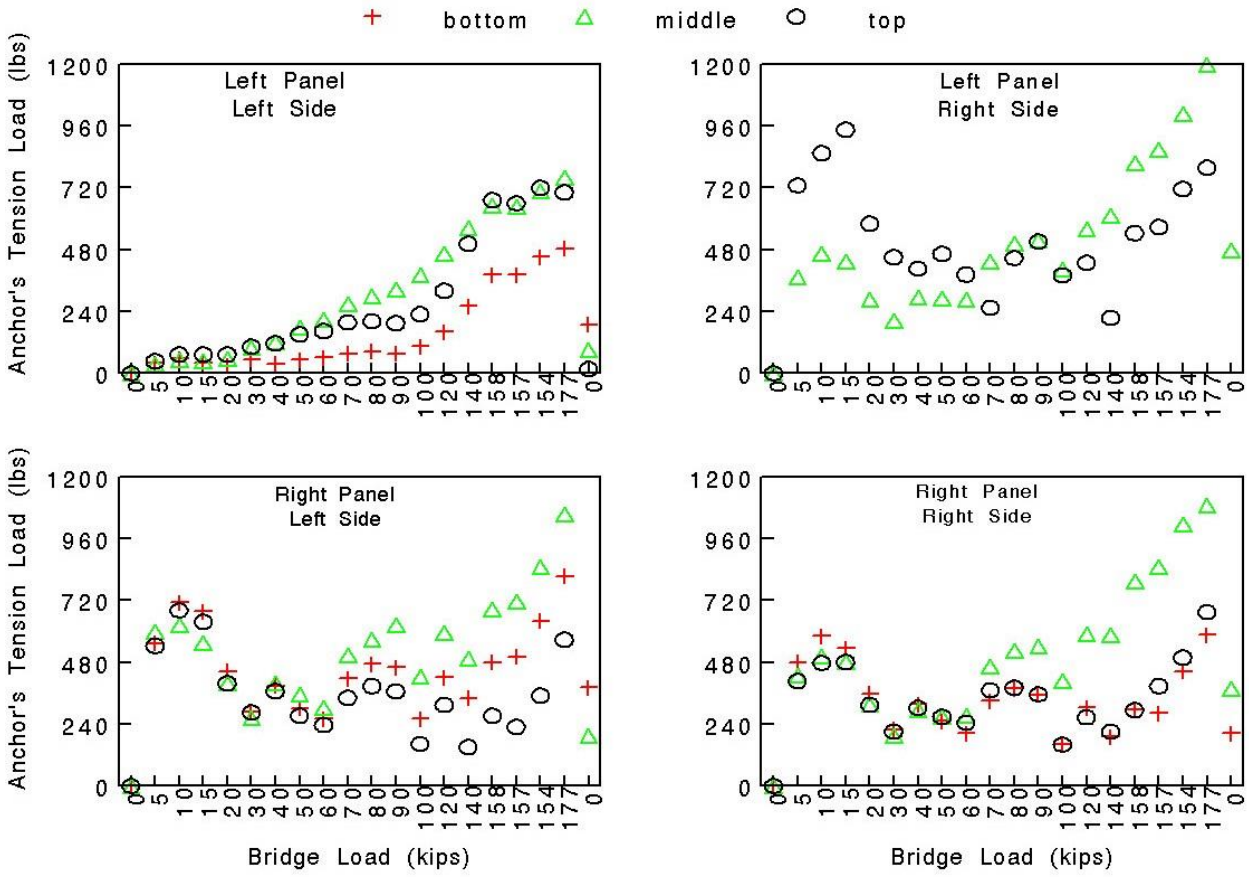

Figure 4.42: Development of axial tension forces in the anchors with the applied bridge load (1 lb = 0.004448 kN).

Chapter 5

Numerical Modeling of CLSM Bridge Abutment and Parametric Studies

In this chapter, in order to further study the performance and evaluate the effect of different material properties and geometrical parameters on the load carrying capacity and deformations, and also to provide a numerical tool for assessment of the safety and serviceability of the design, CLSM bridge abutment is simulated numerically with a three dimensional finite element model. Results of the numerical analysis are compared with the experimental results from the full scale laboratory test which was conducted to prove the constructability of the CLSM bridge abutments (chapter 4).

The plastic–damage material model for concrete, proposed by J. Lubliner et. al. (1988) and modified by Lee and Fenves (1998), was applied to model the CLSM mass. Plastic-damage model captures the material behavior using both classical theories of elasto-plasticity and continuum damage mechanics. Thus, this model is capable of modeling the failure and can serve as an appropriate material model for the present material.

5.1 Finite Element Modeling

Behavior of the CLSM is similar to that of other quasi-brittle materials such as concrete, rock and ceramics, and therefore, a material model developed for quasi-brittle materials is considered. Besides, the model input parameters must be obtainable from uniaxial test experiments. Based on these requirements, the Concrete Damaged Plasticity model proposed by Lubliner et al. and extended by Lee and Fenves has been chosen for the present study. The notion of concrete applies for a wide range of materials with quantitatively and qualitatively different properties for typical tests (compression and tension) (Jankowiak and Tomasz, 2005).

Modeling of the material behavior has been performed with the finite element software Abaqus v.6.12 where an implementation of the proposed plastic-damage model is available. In order to study the capability of the plastic-damage model to simulate the material behavior of CLSM, the uniaxial compression tests were initially simulated with finite element method and compared with the experimental results. Moreover, the capability of the model to predict the failure state is assessed. In the next step, with the verified model parameters, a CLSM bridge abutment was simulated to compare the results with the laboratory large scale CLSM bridge abutment test. Finally, the verified numerical simulation was used for a parametric study to support the design of the CLSM bridge abutments.

A brief review of the plastic-damage model, the material parameter determination process, finite element modeling and the simulation results for uniaxial compression test

on CLSM cylinders, and CLSM abutments test specimen are presented in the following sections.

5.1.1 Plastic-Damage Model

This section describes the plastic-damage model provided in finite element software Abaqus v6.12 for the analysis of quasi-brittle materials. In the Plastic-damage model proposed by Lublineret al. and extended by Lee and Fenves, stiffness degradation due to damage is embedded in the plasticity part of the model. An independent scalar (isotropic) damage variable *d* is used to describe the irreversible damage that occurs during the fracturing process. Quasi-brittle materials show different failure mechanisms; in compression the damage is associated with crushing while in tension it is associated with cracking. To account for the different degradation of the elastic stiffness in tension and compression, the damage parameter *d* is characterized by d_c for compressive and d_t for tensile damage.

The initial undamaged state and total loss in strength of the material under tension and compression are indicated by $d_t = d_c = 0$ and $d_t = d_c = 1$ respectively. Any intermediate value indicates a partially damaged state.

In Plastic-damage model, the constitutive equation for stress-strain relation is:

$$\sigma = (1 - d)\mathrm{D}_0^{el}\colon(\varepsilon - \varepsilon^{pl}) = D^{el}\colon(\varepsilon - \varepsilon^{pl})$$

Where σ is the stress tensor, ε is the strain tensor, D_0^{el} is initial undamaged elastic stiffness of the material, while $D^{el} = (1 - d)D_0^{el}$ is the degraded elastic stiffness, d is the scalar degradation variable and ε^{pl} is the plastic strain.

The effect of damage is embedded in the plasticity theory and all stress definitions (true stress) are reduced to the effective stress. This enables the decoupling of the constitutive relations for the elastic–plastic response from stiffness degradation (damage) response. Consequently, the numerical implementation of the model becomes much simpler. The effective stress is defined as;

$$\bar{\sigma} = \mathrm{D}_0^{el} : (\varepsilon - \varepsilon^{pl})$$

Therefore, the stress tensor is related to the effective stress through the scalar degradation relation:

$$\sigma = (1 - d)\bar{\sigma}$$

Damage states in tension and compression are assumed to be functions of two hardening variables, $\tilde{\varepsilon}_c^{pl}$ and $\tilde{\varepsilon}_t^{pl}$, which are referred to as tensile and compressive equivalent plastic strains, respectively. These variables control the evolution of the yield (or failure) surface and the degradation of the elastic stiffness.

For the plasticity part of the model, a non-associated plasticity scheme is used. The yield surface proposed by Lubliner et al. is based on modifications of the classical Mohr–Coulomb plasticity to reflect different strength evolution in tension and compression and is as follow. (In the following equations a line above the stress expressions indicates effective stress. All strain symbols with a tilde are equivalent strains. The Macauley brackets ⟨⟩ is defined by ⟨x⟩ = x if x> 0, otherwise ⟨x⟩= 0).

$$F = \frac{1}{1-\alpha}\left(\bar{q} - 3\alpha\bar{p} + \beta(\tilde{\varepsilon}^{pl})\langle\hat{\bar{\sigma}}_{max}\rangle - \gamma\langle-\hat{\bar{\sigma}}_{max}\rangle\right) - \bar{\sigma}_c\left(\tilde{\varepsilon}_c^{pl}\right)$$

With

$$\alpha = \frac{(\sigma_{b0}/\sigma_{c0}) - 1}{2(\sigma_{b0}/\sigma_{c0}) - 1}; 0 \leq \alpha \leq 0.5$$

$$\beta = \frac{\bar{\sigma}_c\left(\tilde{\varepsilon}_c^{pl}\right)}{\bar{\sigma}_t\left(\tilde{\varepsilon}_t^{pl}\right)}(1-\alpha) - (1+\alpha)$$

$$\gamma = \frac{3(1-K_c)}{2K_c - 1}$$

Here,

$\hat{\bar{\sigma}}_{max}$ Maximum principal effective stress,

$\bar{\sigma}_c$ Uniaxial effective compressive stress,

$\bar{\sigma}_t$ Uniaxial effective tensile stress,

$\bar{p}$ Effective hydrostatic pressure,

$\bar{q}$ Equivalent effective deviatoric stress,

$\tilde{\varepsilon}^{pl}$ Equivalent plastic strain.

σ_{b0}/σ_{c0} is the ratio of initial equibiaxial compressive yield stress to initial uniaxial compressive yield stress (the default value is 1.16); K_c is the ratio of the second stress invariant on the tensile meridian, J_2, to that on the compressive meridian in the form:

$$K_c = \frac{\left(\sqrt{J_2}\right)_{TM}}{\left(\sqrt{J_2}\right)_{CM}}$$

At a given value of the pressure invariant *p* such that the maximum principal stress is negative, $\hat{\sigma}_{max} < 0$ (see Figure 5.1); it must satisfy the condition $0.5 < K_c \leq 1$ (the default value is ⅔).

Typical yield surfaces are shown in Figure 5.1 on the deviatoric plane and in Figure 5.2 for plane stress conditions.

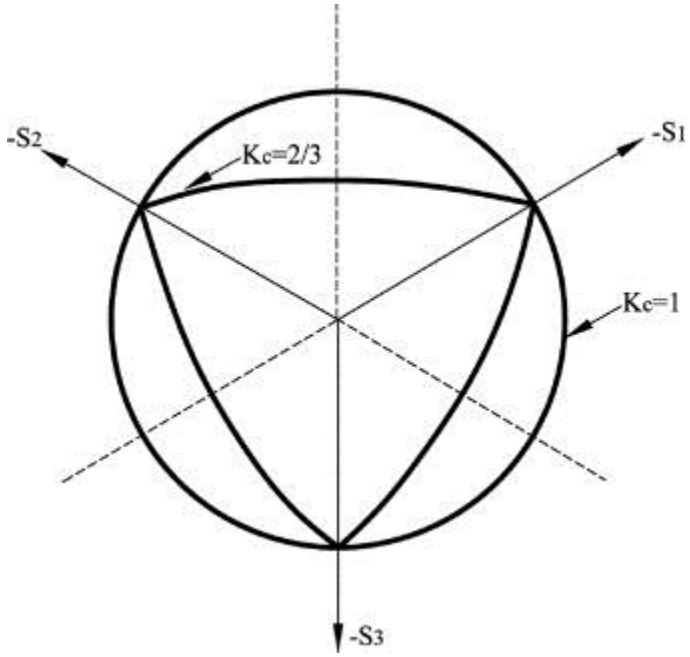

Figure 5.1: Yield surfaces in the deviatoric plane, corresponding to different values of K_c.

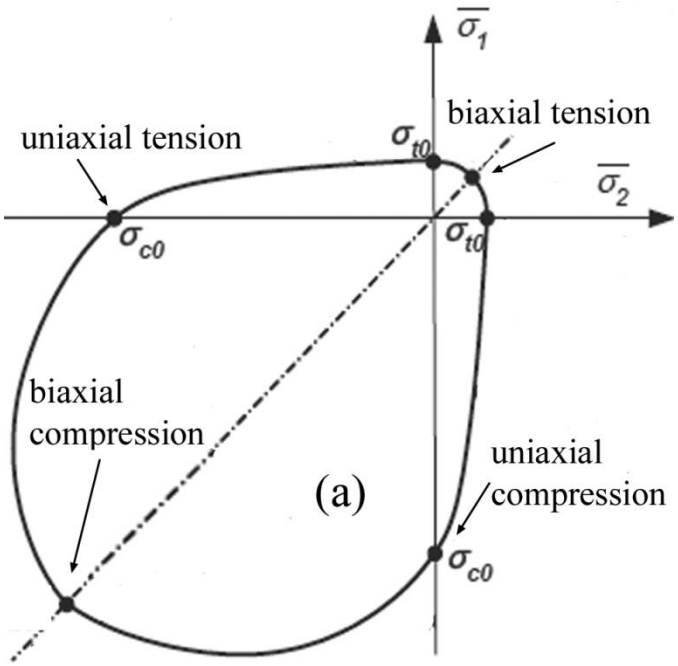

Figure 5.2: Yield surface in plane stress.

Assumption of the non-associated flow rule in the plastic damage model requires a separate flow potential to determine the direction of plastic flow. The flow potential *G* accepted for this model is the Drucker–Prager hyperbolic function:

$$G = \sqrt{(\epsilon\sigma_{t0}\tan\psi)^2 + \bar{q}^2} - \bar{p}\tan\psi$$

Where, ψ is the dilation angle measured in the *p*–*q* plane and controls the orientation of the flow potential function *G*, σ_{t0} is the uniaxial tensile stress at failure, taken from the user-specified tension stiffening data; and ϵ is an eccentricity of the flow potential, that defines the rate at which the function approaches the asymptote (the flow potential tends to a straight line as the eccentricity tends to zero), see Figure 5.3. Hydrostatic pressure stress $\bar{p}$ and the Mises equivalent effective stress $\bar{q}$ are defined as:

$$\bar{p} = -\frac{1}{3}\bar{\sigma} : I$$

$$\bar{q} = \sqrt{\frac{3}{2}(\bar{S}:\bar{S})}$$

Where *I* is the unit matrix and $\bar{S}$ is the effective stress deviator, defined as:

$$\bar{S} = \bar{\sigma} + \bar{p}I$$

When high confining stress is present, the flow potential function *G* approaches the linear Drucker-Prager flow potential asymptotically and intersects the hydrostatic pressure axis at 90°, Figure 5.3.

The default flow potential eccentricity is $\epsilon = 0.1$, which implies that the material has almost the same dilation angle over a wide range of confining pressure stress values. Increasing the value of ϵ provides more curvature to the flow potential, implying that the dilation angle increases more rapidly as the confining pressure decreases. Values of ϵ that

are significantly less than the default value may lead to convergence problems if the material is subjected to low confining pressures because of the very tight curvature of the flow potential locally where it intersects the *p*-axis.

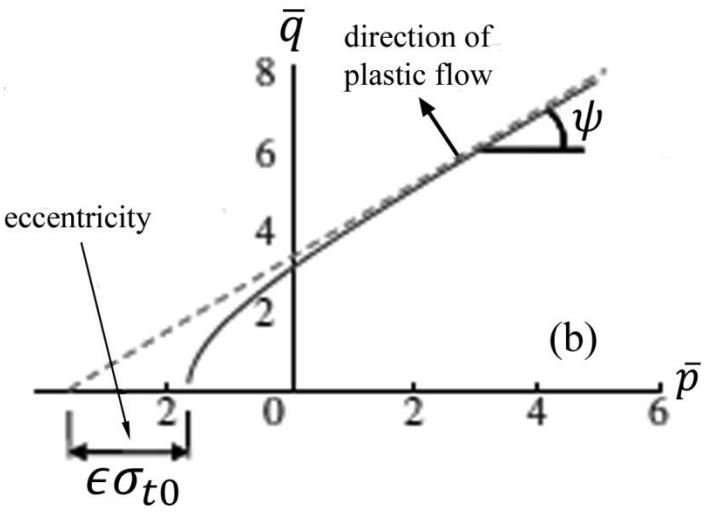

Figure 5.3: Illustration of flow potentials and dilation angle.

The details of the mathematical formulation of the model are given in the Abaqus theory and analysis manual. With these assumptions, this model is capable of reproducing both the softening branch of the brittle material under mono dimensional tensile test and the hardening effect of material under compression with the successive softening after achieving the compressive strength, as shown in Figure 5.4.

5.1.2 Identification of Material Parameters

Modeling of the material behavior of the CLSM mass has been performed using the finite element software Abaqus with its existing plastic damage material model. The

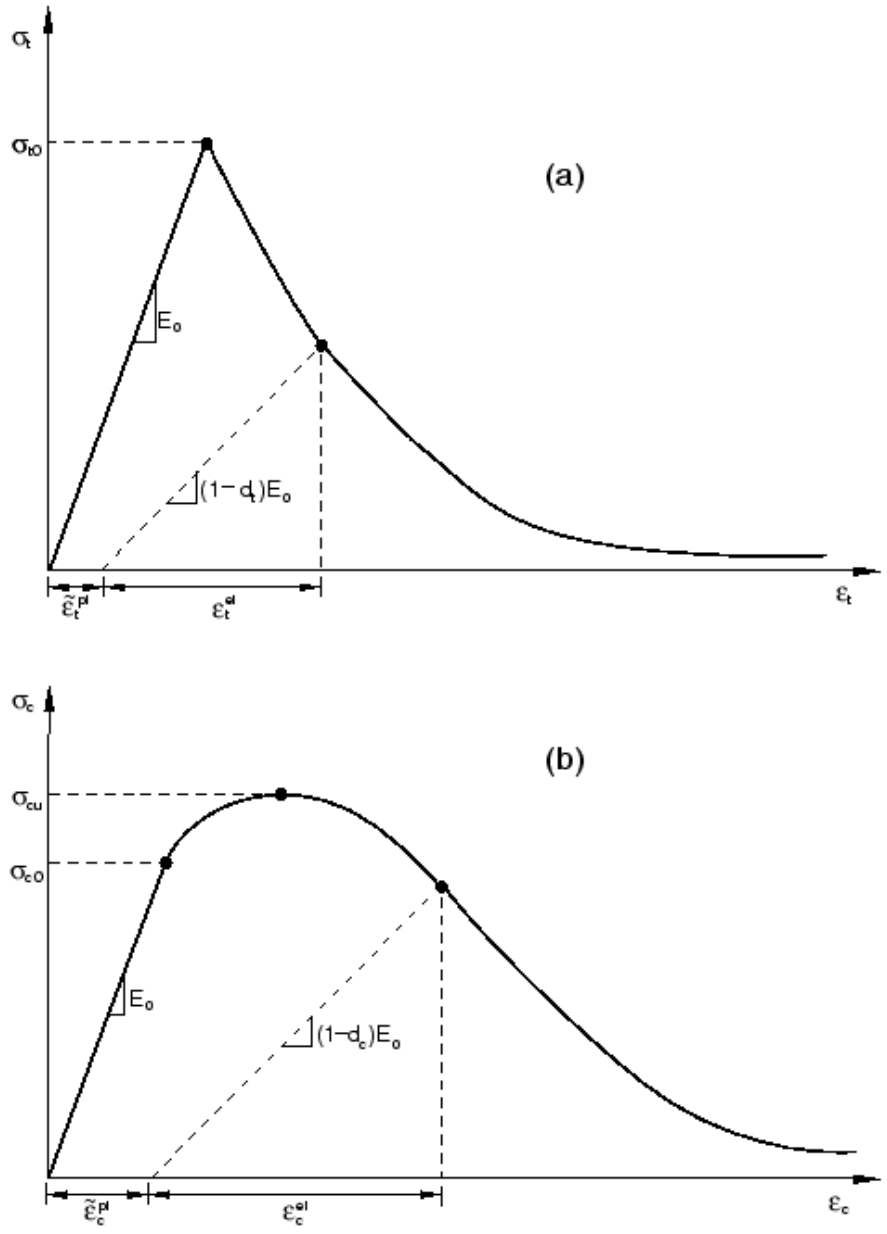

Figure 5.4: Illustration of the definition of (a) cracking and (b) crushing strain used for the definition of strain softening data in tension and compression, respectively.

Identification of constitutive parameters that describe the material properties is fundamental. The material parameters required for the model can be categorized into

three types, namely elasticity, plasticity and damage. In the elastic zone, from the experimental stress-strain curve for CLSM mixture M3 (chapter 3), Young's modulus of 22.6 MPa and yield stress of 134.3 kPa was determined and Poisson's ratio was assumed to be 0.19.

Generally four parameters are required to define the yield surface and flow potential function of the plasticity part; the dilation angle in degrees, ψ, the flow potential eccentricity, ϵ, the ratio of initial equibiaxial compressive yield stress to initial uniaxial compressive yield stress and σ_{b0}/σ_{c0}, the ratio of the second stress invariant on the tensile meridian to that on the compressive meridian, K_c. The aforementioned parameters were set to 35°, 0.1, 1.16, and 0.67, respectively, as recommended (Abaqus, 2012). It is not possible to obtain ψ directly from the results of the experiments and it was explored by applying inverse modeling by comparing the simulated and the experimentally measured stress-strain curves (Jankowiak and Tomasz, 2005).

For plasticity and damage, compressive and tensile behavior of the material must be specified by strain softening and damage evolution functions. The strain softening curve is provided in the material model in the form of yield stress as a function of inelastic strain. The inelastic strain is identified by subtracting the elastic strain corresponding to the undamaged material from total strain as given in:

$$\varepsilon^{in} = \varepsilon - \varepsilon^{el} \Rightarrow \varepsilon^{in} = \varepsilon - \frac{\sigma}{E}$$

Therefore, the inelastic strain which is denoted by cracking strain $\tilde{\varepsilon}_t^{in}$ in uniaxial tension and crushing strain $\tilde{\varepsilon}_c^{in}$ in uniaxial compression can be extracted based on the softening zone of a stress–strain curve obtained from experiments. Figure 5.4 shows which values

in the plastic damage model are interpreted as the cracking strain and the crushing strain. In uniaxial tensile loading, the stress-strain relation consists of a linear elastic response until the failure stress, σ_{t0}. The failure stress is actually the onset of micro-cracking in the material. Post-failure behavior is then represented by the formation of micro-cracks macroscopically with a softening stress-strain response, which induces strain localization. Under uniaxial compressive load, the stress-strain curve is linear until the initial yield, σ_{c0}, is reached. Plastic response of the material is considered by stress hardening followed by strain softening beyond the ultimate stress, σ_{cu} (Abaqus, 2012). Abaqus automatically calculates the plastic strain from the inelastic strain using the relationship:

$$\tilde{\varepsilon}^{pl} = \tilde{\varepsilon}^{in} - \frac{d}{(1-d)}\frac{\sigma}{E_0}$$

As shown in Figure 5.4, when the concrete specimen is unloaded from any point on the strain softening zone of the stress-strain curves, the unloading response is damaged (or degraded). The damage evolution curve is given as damage parameter *d* and the corresponding inelastic strain at certain points in the softening zone of experimental stress–strain curve. Definition of the damage variables in tension d_c and compression loading d_t are shown in Figure 5.4.The corresponding damage parameter *d* is determined from the varying slope (*E*) and the initial stiffness (E_0) as:

$$d = 1 - \frac{E}{E_0}$$

In this way, stress-strain behavior of the CLSM under uniaxial compression was defined by compressive stress and corresponding inelastic (or crushing strain) data. Compressive stress data as a tabular function of inelastic strain was obtained by selecting

several points from the softening zone of an experimental stress-strain curve. The selected points initiated by the yield strength and include stress-strain data beyond the ultimate compressive stress, into the strain softening zone. To avoid potential numerical problems that would arise once stress reached zero in a given element, a complete loss of strength in compression was not considered. An idealized stress-strain curve is provided in Figure 5.5. The last two points defining the idealized curve were selected to facilitate solution convergence.

Compressive damage response of the CLSM is provided to Abaqus v6.12 by tabular data which specifies the decimal percentage of stiffness degradation at corresponding values of inelastic strain. The compressive damage d_c can be computed from the degraded unloading stiffness E (d is replaced by d_c). Dashed lines in Figure 5.5 represent stiffness degradation (moduli E_1, E_2, and E_3) in terms of compressive damage (d_c).Values for the degraded elastic modulus were calculated as the slope of the line connecting points (0, σ_{ret}) and ($\varepsilon_{c,i}$,$\sigma_{c,i}$) where σ_{ret} is the value of tensile stress to ensure that negative plastic strain values will not evolve and ($\varepsilon_{c,i}$,$\sigma_{c,i}$) are the total strain and stress values for a given point on the idealized stress-strain curve.

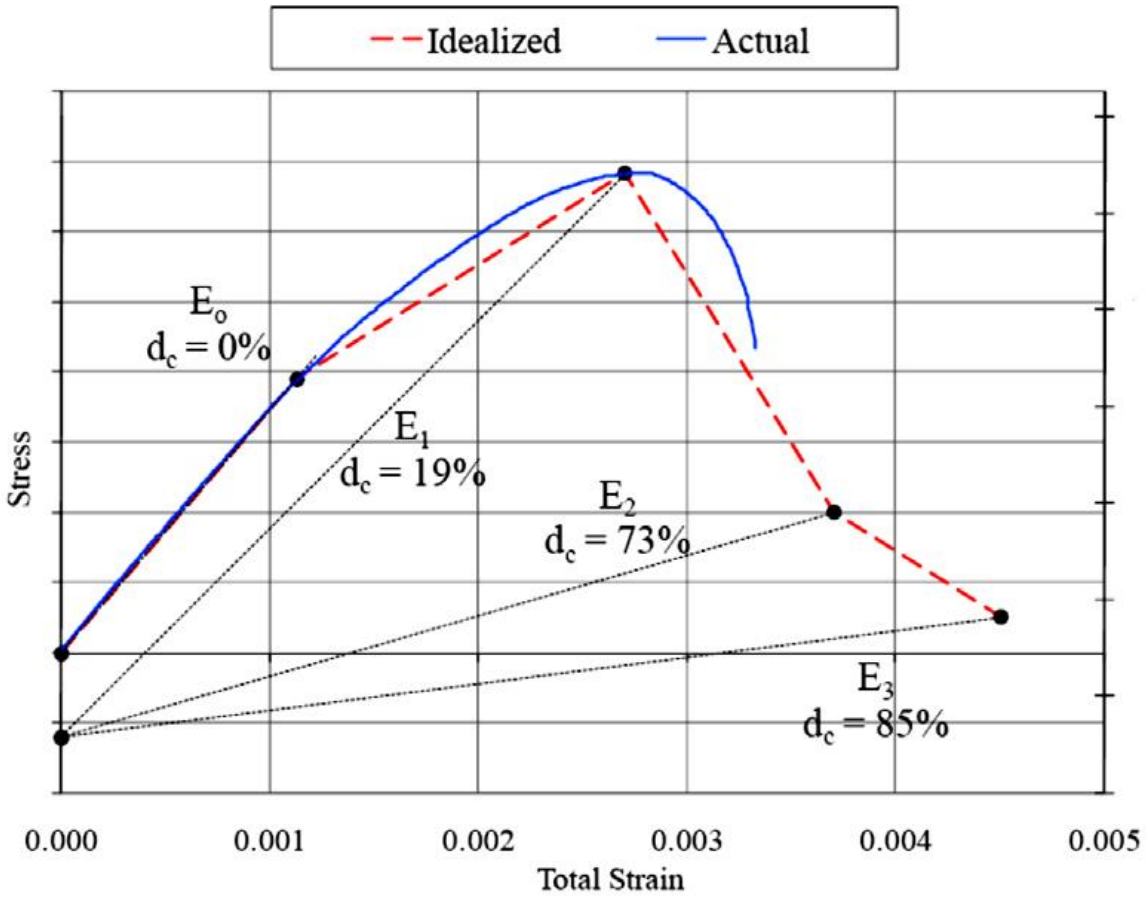

Figure 5.5: Idealized Compressive Stress-Strain Relationship of the CLSM.

Accordingly, compressive behavior of the CLSM is given by strain softening and damage evolution curves as illustrated in Figure 5.6 as a material input for the Plastic-Damage material model.

In this study, tensile damage is absent (d_t=0) and damage occurs due to compressive loading (crushing) and therefore only strain softening curve is presented to define the tensile behavior of the CLSM. This was estimated from uniaxial compressive yield strength ($\sigma_{t0} \approx 0.1\sigma_{c0}$). In general, the ratio of the direct tensile strength to compressive strength ranges from about 0.07 to 0.11 (Mindess et al., 2003). Material

parameters of Plastic-damage model for the 7-days cured CLSM mixture M3 is summarized in Table 5.1.

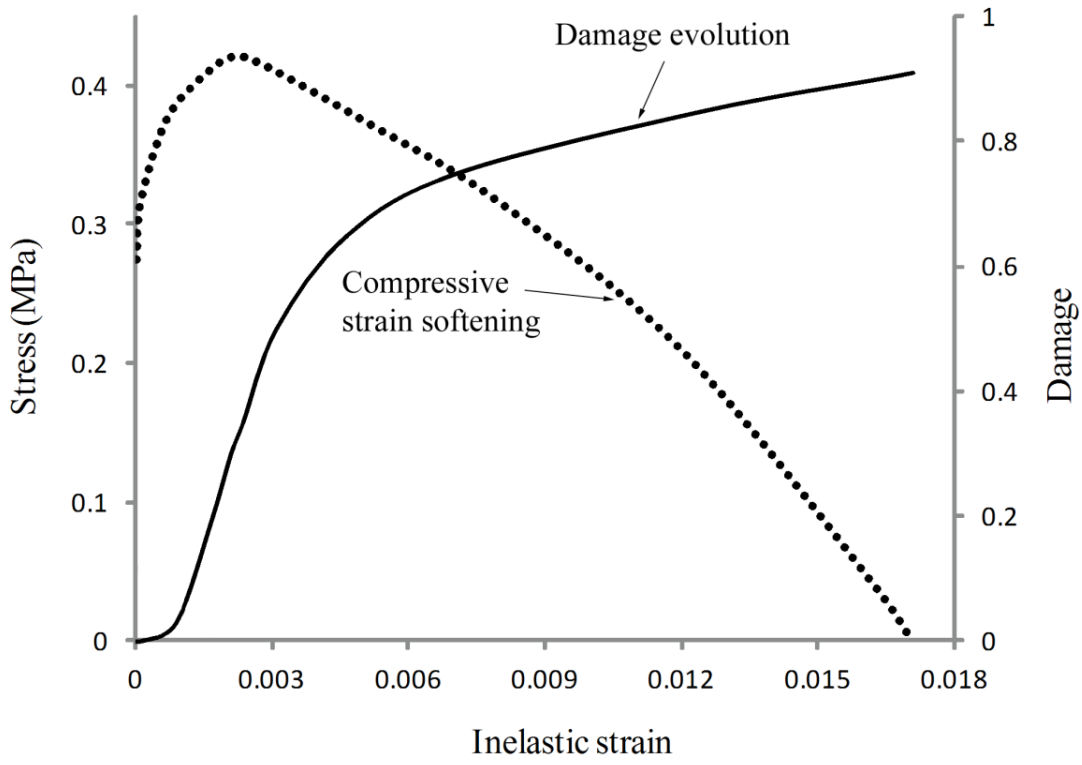

Figure 5.6: Material input curves, compressive strain softening and damage evolution curve.

Table 5.1: Material parameters of Plastic-Damage Model for 7-days cured CLSM mixture M3.

Elasticity		Plastic-Damage Model	
E [MPa]	22.57	dilation angle, ψ	35°
υ	0.19	eccentricity, ϵ	0.1
		σ_{b0}/σ_{c0}	1.16
		K_c	0.67
Compression Hardening		Compression Damage	
Stress [kPa]	Crushing Strain	Damage, d_c	Crushing Strain
134.31	0.00595	0	0.00595
155.47	0.00699	0	0.00699
185.89	0.00897	0	0.00897
204.17	0.0109	0.099494	0.0109
206.06	0.0114	0.130905	0.0114
205.85	0.011485	0.138025	0.011485
201.67	0.0119	0.18261	0.0119
181.49	0.0127	0.301814	0.0127
155.47	0.014	0.445489	0.014
102.27	0.0171	0.677447	0.0171
16.90	0.0171	0.894194	0.0171
1.35	0.01706	0.932936	0.01706
Tension Stiffening		Tension Damage	
Stress [kPa]	Cracking Strain	Damage, d_t	Cracking Strain
25.75	0	0	0
0.26	0.0017		

5.2 Finite Element Modeling of CLSM Cylinder Tests

Finite element analysis was performed to simulate the uniaxial compressive testing on CLSM cylinders to evaluate the capability of the Plastic-damage model to predict the stress-strain response and failure of a CLSM specimen. Similar to concrete, there are two main modes of failure commonly observed in the testing of CLSM cylinders, shear band failure and conical type shear failure. For this numerical analysis, a *3D* solid finite element model was employed to simulate a 206 kPa CLSM cylinder under uniaxial compressive loading.

The CLSM cylinders were modeled by 8-node linear brick with reduced integration, hourglass control elements (C3D8R). In order to simulate different modes of failure, different boundary conditions were applied to the cylinders. Figures 5.7 and 5.8 show the distribution of stiffness degradation (damage) variable *d* at maximum compressive stress and at failure. This distribution is similar to the modes of failure frequently observed in the testing of CLSM cylinders. Thus the contour plot of damage parameter is capable of visualizing failure of a CLSM mass.

As illustrated in Figure 5.7, a cylinder with fixed ends (laterally constrained ends) exhibits a symmetrical conical type shear failure mode at the center of the cylinder. To stimulate the unsymmetrical shear failure, one end were set free for lateral displacements, see Figure 5.8. Capped end conditions were also analyzed to determine the effect of frictional lateral end constraints on failure response of a CLSM cylinder. Two caps with solid elements were modeled to contact the two ends of the cylinder with friction coefficient of 0.3. As a result of the simulation, the CLSM cylinder fails with

unsymmetrical shear bands, see Figure 5.8c. It was observed that location of the shear band changes with the change of the friction between the pads and cylinder.

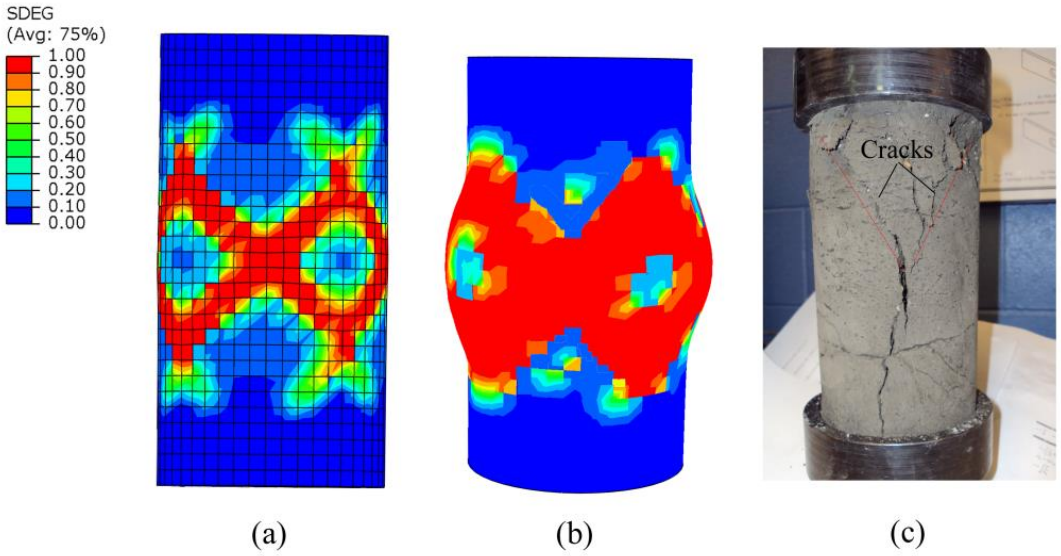

Figure 5.7: Conical damage (a) at compressive strength, (b) at failure with fixed end conditions, and (c) experimental conical failure.

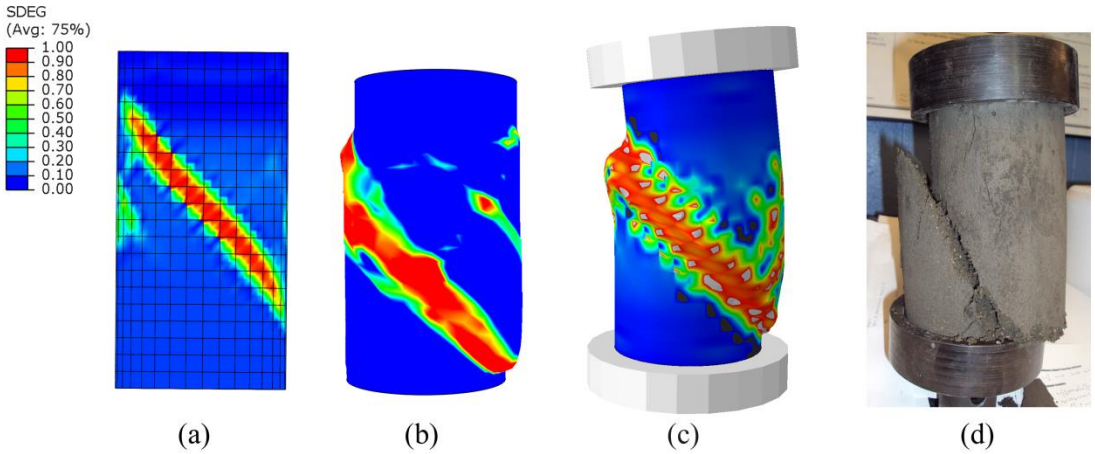

Figure 5.8: Shear damage (a) at compressive strength, (b) at failure with one unconstrained end, (c) at failure with capped end conditions, and (d) experimental shear failure.

The simulation results for the uniaxial compressive testing on CLSM cylinders and effect of mesh size on the stress-strain behavior are presented in Figure 5.9. The stress was computed as the summation of the nodal forces at one end of a cylinder divided by the cross-sectional area of the cylinder. Due to the fracture energy criterion of Hilleborg in the plastic-damage model, the effect of mesh size on the simulated stress-strain behavior is negligible (Abaqus, 2012). The stress–strain curves with different dilation angles have also been compared with the experimental results in the same Figure. The dilation angle of 35° shows quite good agreement with the experiment. It can be concluded that the plastic damage model with the identified model parameters is capable of simulating the stress-strain response and failure of a CLSM mass.

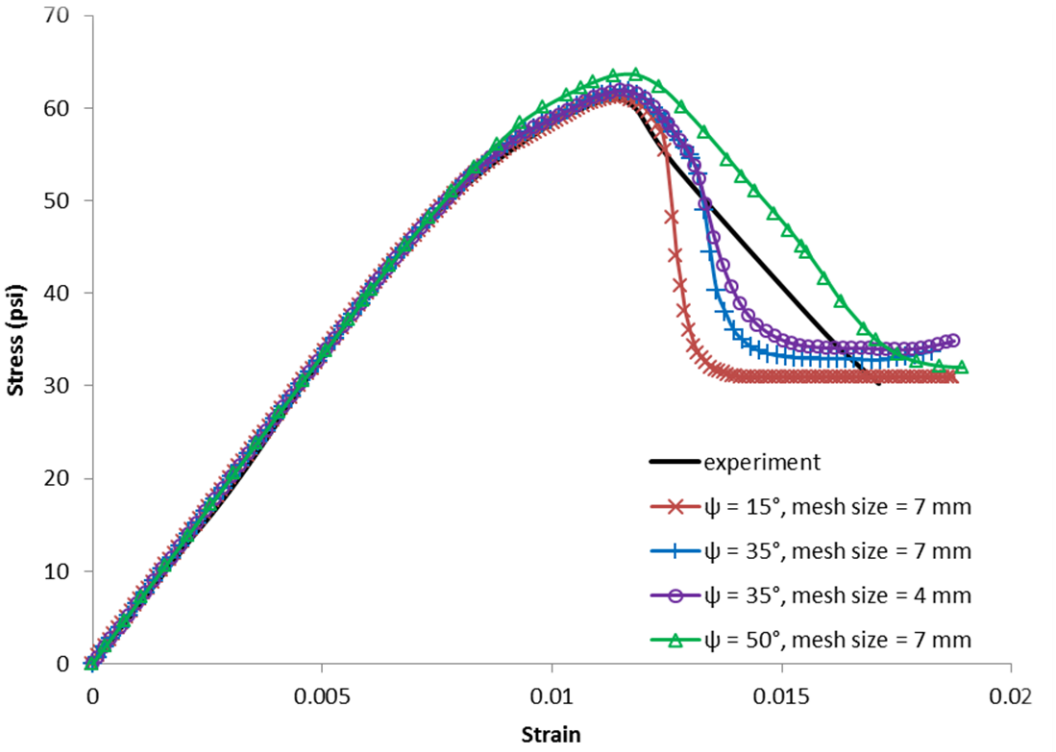

Figure 5.9: Comparison of dilation angle ψ and mesh size on numerical results.

5.3 Finite Element Modeling of the CLSM Bridge Abutment

A low-cost and accurate tool to design and analysis the behavior and performance of the CLSM abutments under different field conditions is finite element method. Based on the achievement in finite element modeling in the preceding section, further studies could extend the material model to the structural level. For structural analysis in this section, the CLSM bridge abutment was simulated with a *3D* finite element model to compare the performance with the experimental results of the laboratory large-scale CLSM bridge abutment specimen. The geometry and boundary conditions of the FE model illustrated in Figure 5.10 matched the conditions of the laboratory construction of the abutment presented in Figures 4.1 and 4.2, and for symmetry considerations, only half of the abutment is modeled. The finite element mesh depicted in Figure 5.10 consists of C3D8R solid elements for CLSM backfill, concrete panels and bridge sill. As the response of the CLSM backfill was of high interest in this study, a finer mesh was assigned to it. Although more computational time was needed for the finer mesh, the higher mesh density allowed for more accurate analysis of the strains, stresses, and deflections at the most relevant points.

Steel rebar anchors were modeled as 3-node quadratic beam elements (B32), assumed to be fully bonded to the surrounding material and embedded inside the elements of the concrete panels and CLSM backfill. The embedded region technique results in significant savings in the number of nodes needed to account for the effect of

bond-slip, particularly, in three dimensional finite element models. As in the experiment, for FE analysis a rigid foundation was considered.

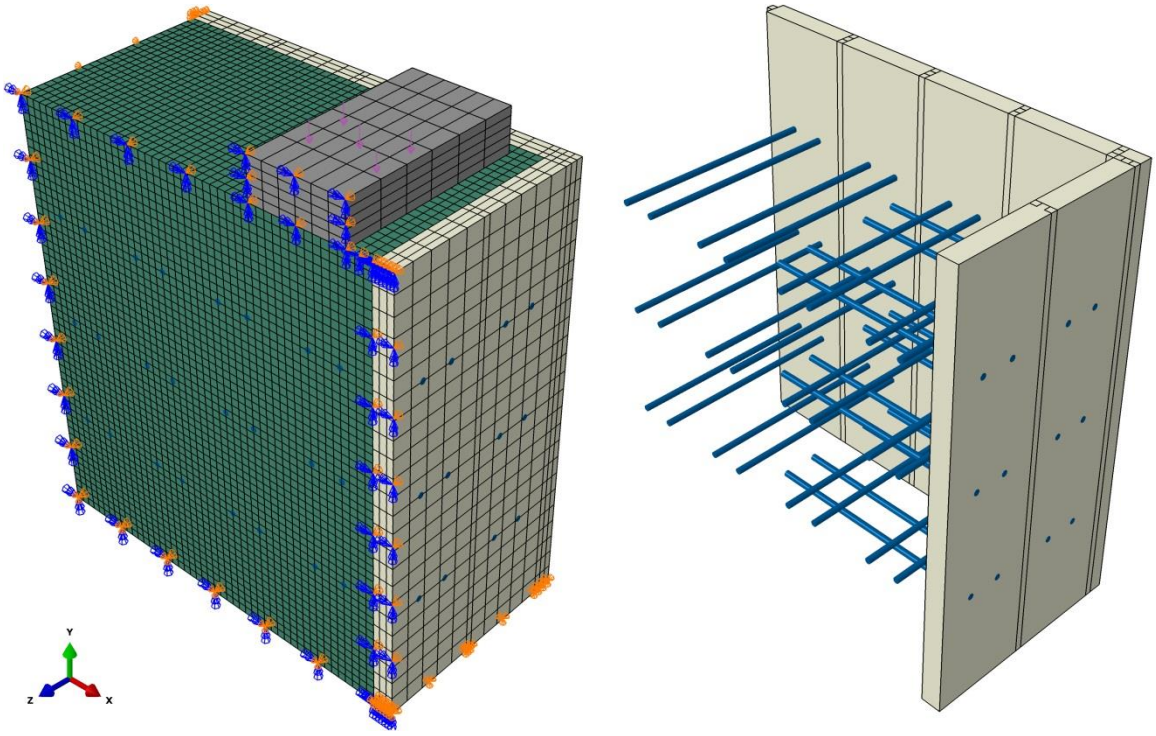

Figure 5.10: Finite element simulation of the CLSM abutment.

Plastic-damage model with the same material parameters used for FE modeling of CLSM cylinders is implemented here. The rebar cross-section is simultaneously subjected to normal and bending actions. For nonlinear response of the steel anchors, the linear elastic branch is defined by the Young's modulus E = 200 GPa and a Poisson's ratio of 0.3, whereas the nonlinear stage, assumed to be perfectly plastic, is only defined by the yield strength f_y = 345 MPa. Concrete behavior is assumed to be linearly elastic, with Young modulus E = 25 GPa and Poisson's ratio of 0.2.

Force is simulated by a prescribed displacement on the surface of the bridge sill sitting on the CLSM backfill. Between the rigid sill and the CLSM, where the load is applied, contact conditions are realized, rough friction as the tangential behavior and hard contact as the normal behavior which does not allow separation after the contact. Hence, the pressure loading is distributed in a way as in the experiment. Since the quasi-static explicit solver was used to model a static problem, the analysis time was carefully chosen to avoid dynamic effects.

5.4 Comparison of Numerical and Experimental Results

Performance of the CLSM bridge abutment based on the load bearing capacity, displacements and lateral pressures from finite element model were compared with those experimentally measured in the large-scale laboratory test to ensure proper order of magnitude of the studied effects. For the following investigation, settlement and lateral deformation of the panels, and axial stress acting on steel anchors were normalized by the height and yield stress (σ_{yield}), respectively.

In the FE analysis the gravity load was initially applied to the backfill in a smooth step to develop initial stresses in all CLSM elements. The lateral pressure of backfill against a facing panel at this step was compared and reasonably in agreement with the lateral pressure after the placement of the fresh CLSM, Figure 5.11. Higher lateral pressure at the mid-height areas of the abutment after 7 days setting time in the experiment is due to the speed of hydration and length of the drainage path which could not be considered in the numerical modeling. After curing and during the loading stage of

the experiment, lateral pressure decreased to negligible levels due to shrinkage and therefore was not compared with the numerical values.

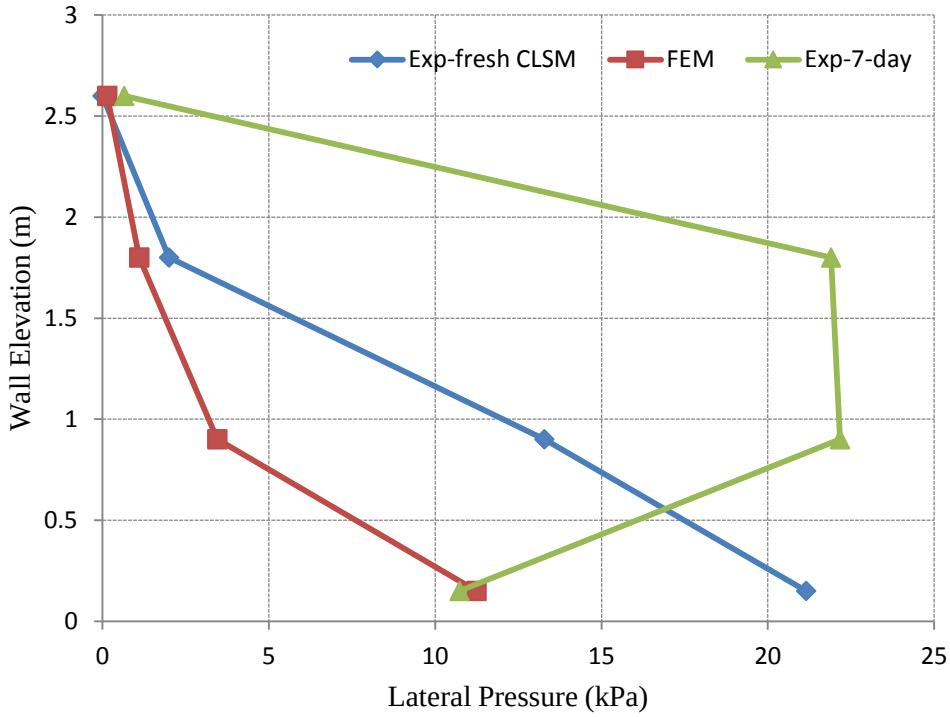

Figure 5.11: Lateral pressures on a facing wall, comparison of experimental results with finite element method.

As shown in Figure 5.12, the applied load versus settlement of the bridge sill in the experiment agreed well with the numerical results up to the load of 703 kN, equivalent to the pressure of 483 kPa on the bridge sill. Likewise, Figure 5.13 compares favorably the predicted maximum lateral deflection of a face panel (top of the panel) with the experimental data at different load levels. In the experimental testing, it was not possible to apply failure load because of the capacity limit of the laboratory's rigid floor. With the aid of the FEM simulation, the load bearing capacity of the abutment can also

be determined. Figure 5.14 predicts the bearing pressure capacity and values of settlement and maximum lateral deflection up to failure of the CLSM abutment. From this numerical results, the load bearing capacity of the CLSM bridge abutment (backfilled with the same mixture as in the experiment) is about 1637 kN which applies a pressure of 1175 kPa on the bridge sill. The allowable bearing pressure of a bridge sill over reinforced soil retaining walls has been limited to 200 kPa in the NHI, Preliminary design guidelines for reinforced soil bridge abutment provided by a National Highway Institute (NHI) reference manual entitled Mechanically Stabilized Earth Walls and Reinforced Soil Slopes Design and Construction Guidelines (Elias et al. 2001), and the formerly Demo 82 design guidelines (Elias and Christopher 1996) without any provisions (Wu et al, 2006). The bearing pressure capacity of the CLSM bridge abutment backfilled with a 206 kPa CLSM mixture is almost six times larger than this allowable pressure.

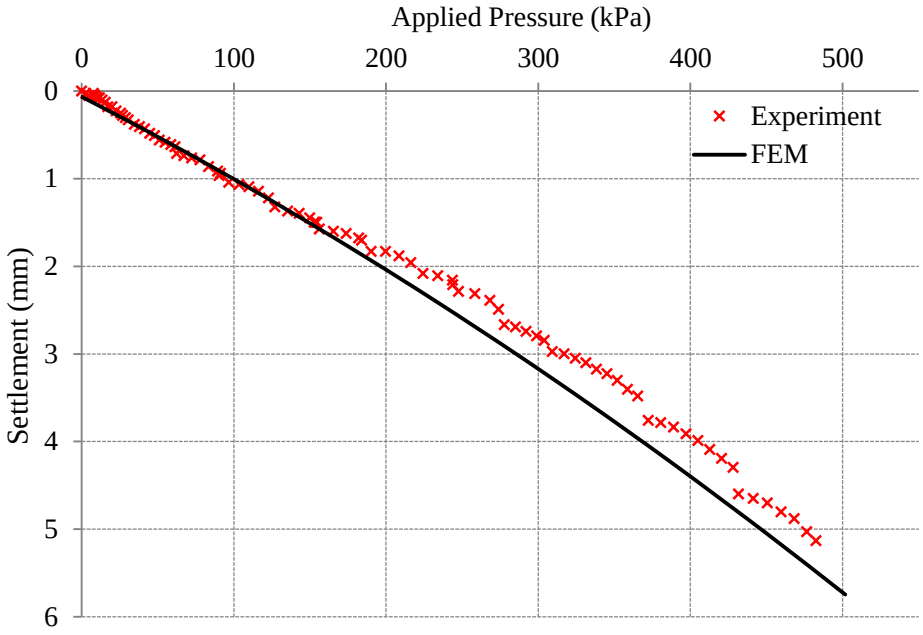

Figure 5.12: Bridge sill settlement, comparison of experimental results with finite element method.

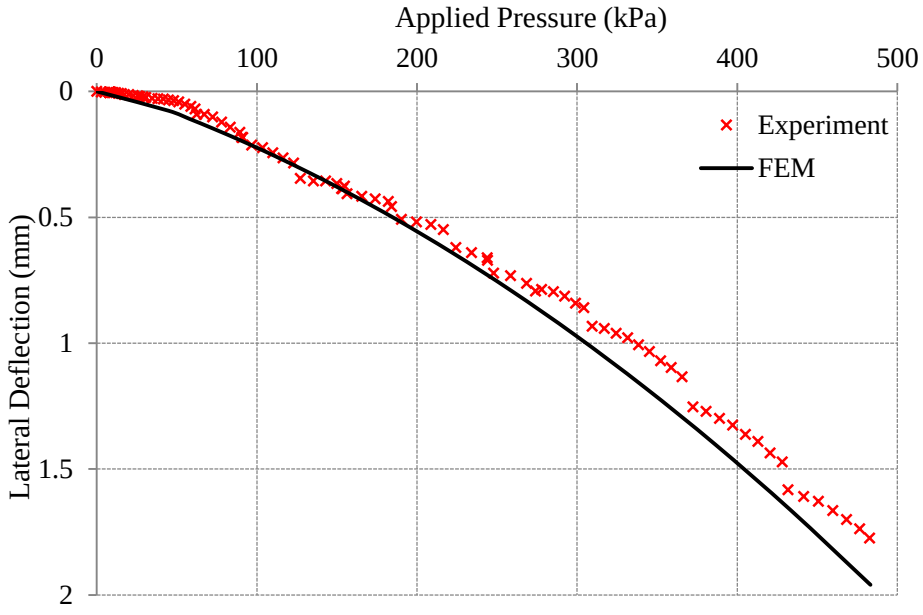

Figure 5.13 Maximum lateral deflection of a front panel, comparison of experimental results with finite element method.

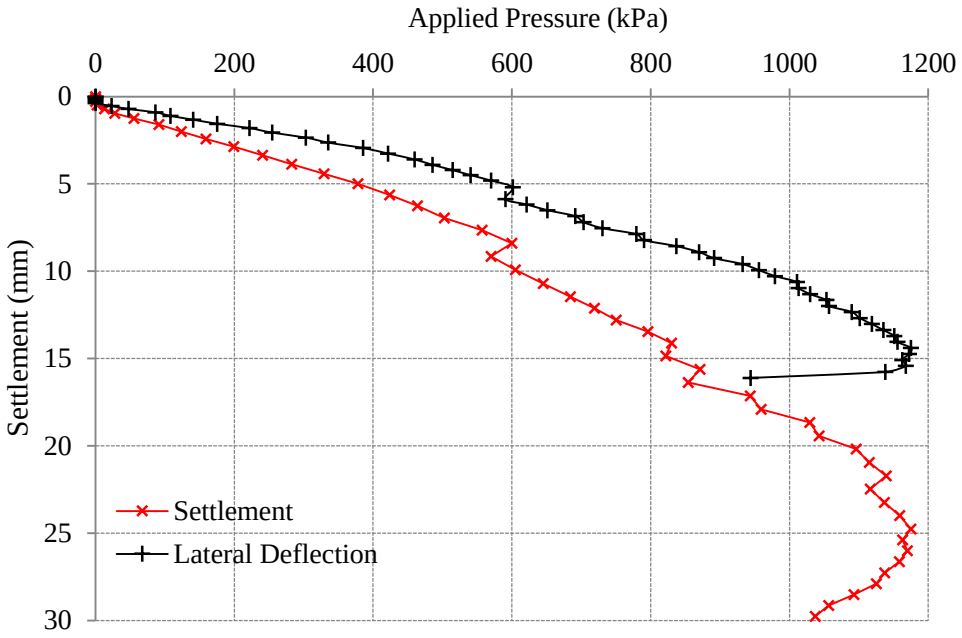

Figure 5.14: Prediction of the bearing pressure capacity, settlement and maximum lateral deflection.

Figure 5.15 illustrates four stages of the predicted damage propagation using the fine mesh with mesh size of 1 in. (2.54 cm), where the cracks are represented by red areas consisting of highly-damaged elements (with the damage index $d \geq 0.93$). At P = 570 kPa (48% of the peak pressure P = 1175 kPa), longitudinal cracks initiated at the back of the bridge sill from the surface to the depth of the CLSM mass (Figure 5.15a). More pressure caused more longitudinal cracks (Figure 5.15b). As the applied pressure approached the peak, a splitting-mode crack initiated below the sill and propagated in the diagonal direction (Figure 5.15c). Beyond the peak load, the splitting-mode crack propagated rapidly, leading to a drastic decline on the pressure-settlement curve (Figure 5.15d).

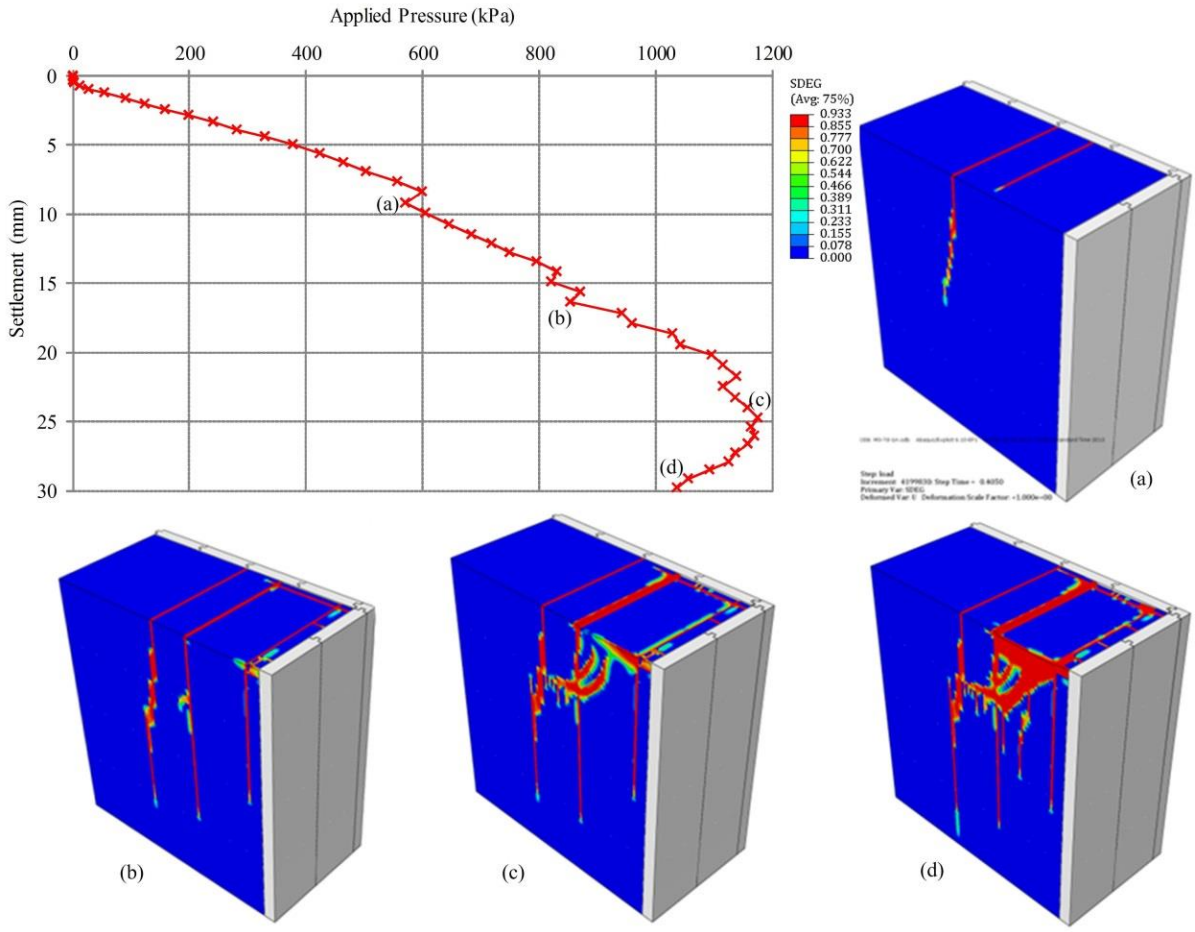

Figure 5.15: Predicted damage propagation.

Mesh-dependence of the results investigated using three mesh sizes for the CLSM backfill, 4, 2 and 1 in. (10.2, 5.1 and 2.54 cm). It can be seen in Figure 5.16 that all three meshes predicted similar curves. Mesh size of 2 in. predicted a peak bearing pressure slightly higher than mesh size of 1 in. The fine mesh case (mesh size of 1 in.) with 501588 solid elements and 525225 nodes in total, required approximately 10 days of runtime on a supercomputer with sixteen processors allocated for the job. Given the

similarity in results obtained from different meshes, mesh size of 2 in. was selected for the further analysis in order to reduce the computational time.

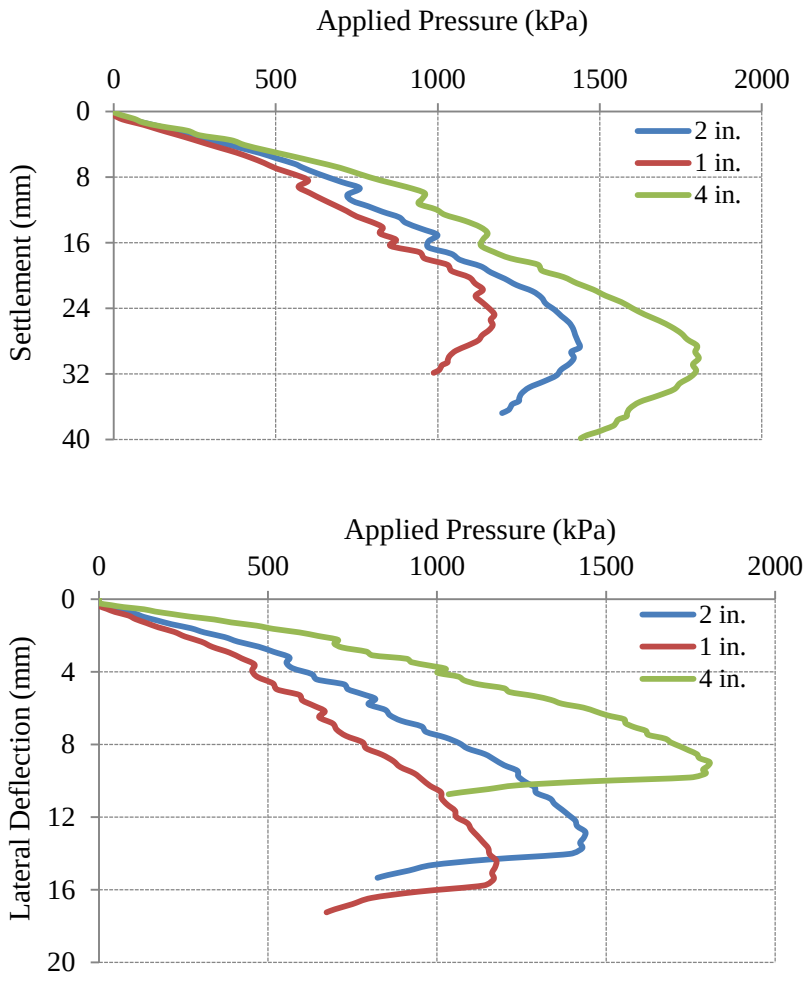

Figure 5.16: Effect of mesh size of finite element analysis on (top) settlement of the bridge sill, and (bottom) maximum lateral deflection.

Strain measurements were made with two strain gauges glued at opposite locations (top and bottom) on cross section of the rebars at their points of attachment with the facing panels. Figure 5.17 compares the measured and computed strain histories at

three locations, top, middle, and bottom of a facing panel. The strain history from FEM analysis shows the same pattern as the measured; steel anchors installed at higher elevations experienced both axial and bending loads while those at the lower elevation experienced mainly axial loads. Small difference in comparison of the strain magnitudes is because of the assumption that steel rebars are fully bonded to the CLSM mass. In the full-scale experimental pullout test, with the same rebar embedded in the CLSM abutment specimen, the ultimate pullout force was measured to be about 22 kN. Based on strain measurements, the axial tensile forces caused by the axial actions of the panels on the rebars were calculated and normalized by the ultimate pullout force. Comparison of the measured axial anchor load with the numerical results in Figure 5.18 shows a satisfactory agreement considering the bond assumption.

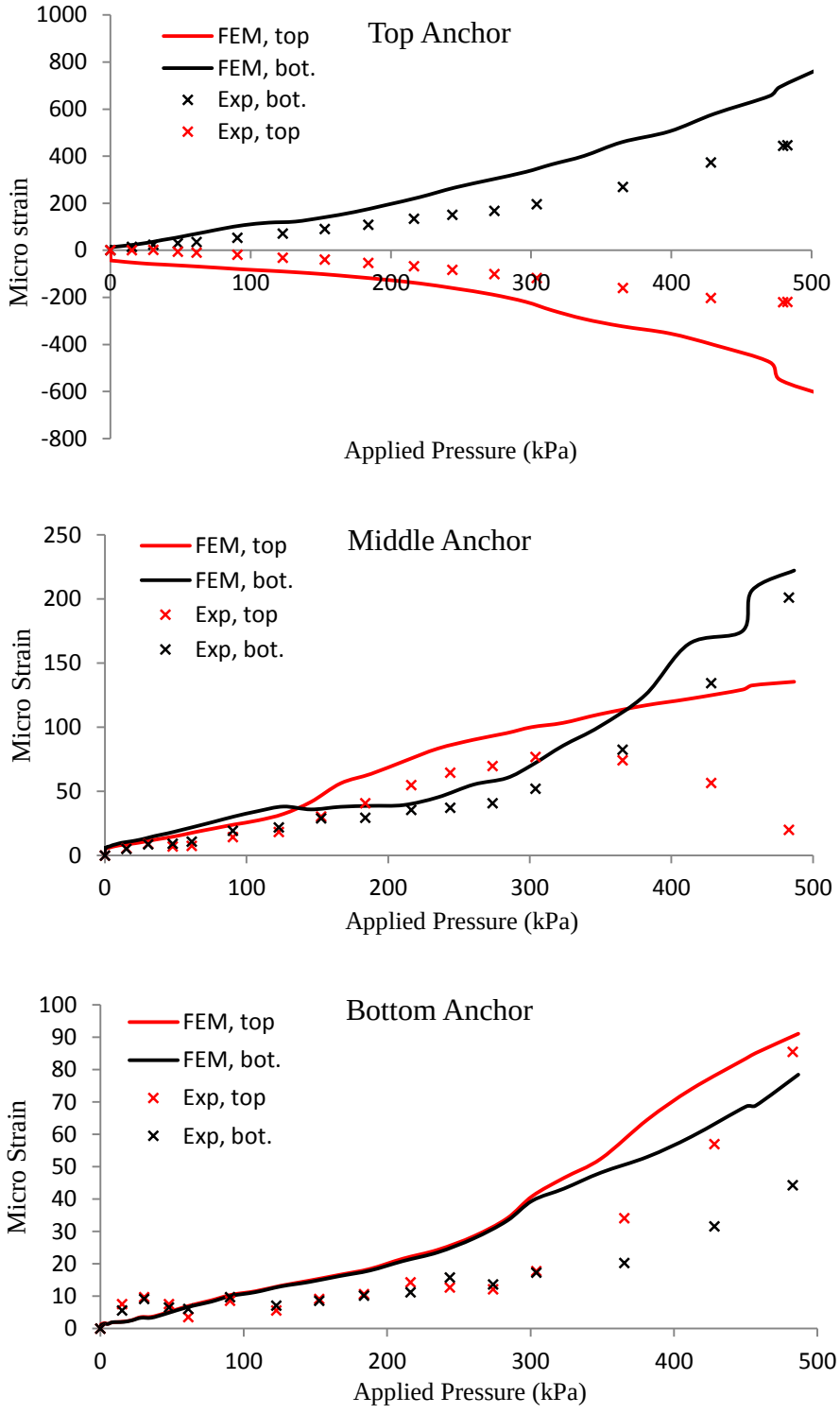

Figure 5.17: Comparison of the measured and computed strain histories at three locations, top, middle, and bottom of a facing panel.

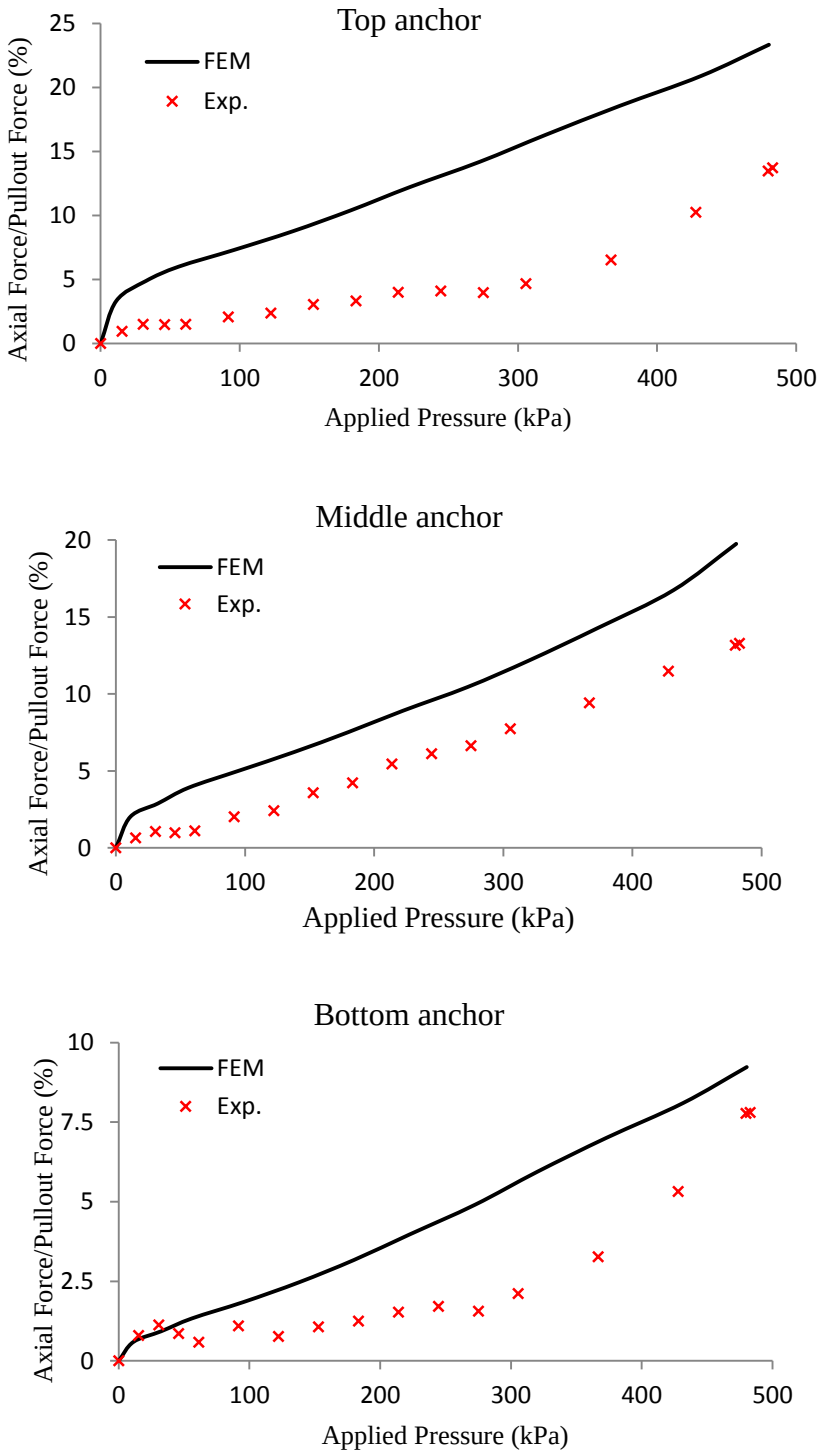

Figure 5.18: Comparison of the measured and computed axial anchor load at three locations, top, middle, and bottom of a facing panel.

5.5 Parametric Study

The quasi-static analysis method presented in this study is capable of predicting the failure, load bearing capacity, vertical and lateral displacement of the CLSM bridge abutment. It also can predict the developed axial load in the anchors with acceptable accuracy. The validated FE model was used for conducting a series of parametric studies to evaluate the influence of a number of material and geometrical parameters on the load bearing capacity and performance of the abutment based on the settlement of the bridge sill and lateral displacement of the facing panels. The axial anchor load was also controlled with respect to the bond and yield strength of steel rebars. The typical mesh (mesh size of 2 in.) and geometry in Figure 5.10 which was used for the FE modeling of CLSM bridge abutment, was considered as the base case in the parametric studies.

Since the construction duration of CLSM abutment is restricted by initial strength development of the CLSM, the influence of CLSM curing age and so influence of compressive strength of a CLSM mixture on load bearing capacity and performance of the abutment was studied. For this analysis, mixture M7 with compressive strengths of 0.08, 0.38, 0.85, and 1.03 MPa at 1day, 7 days, 28 days, 90 days, respectively, was implemented. Figure 5.19 shows that the pressure bearing capacity of the bridge abutment increases as the CLSM mixture cures and the ductility of the response decreases. As can been seen, strength development is considerable at 7 days and the abutment continues to gain more bearing capacity thereafter. In this case, bearing capacity of the abutment at 1 day is controlled with the bond failure of steel anchors (at 95% of the peak pressure) located at top of the facing panels.

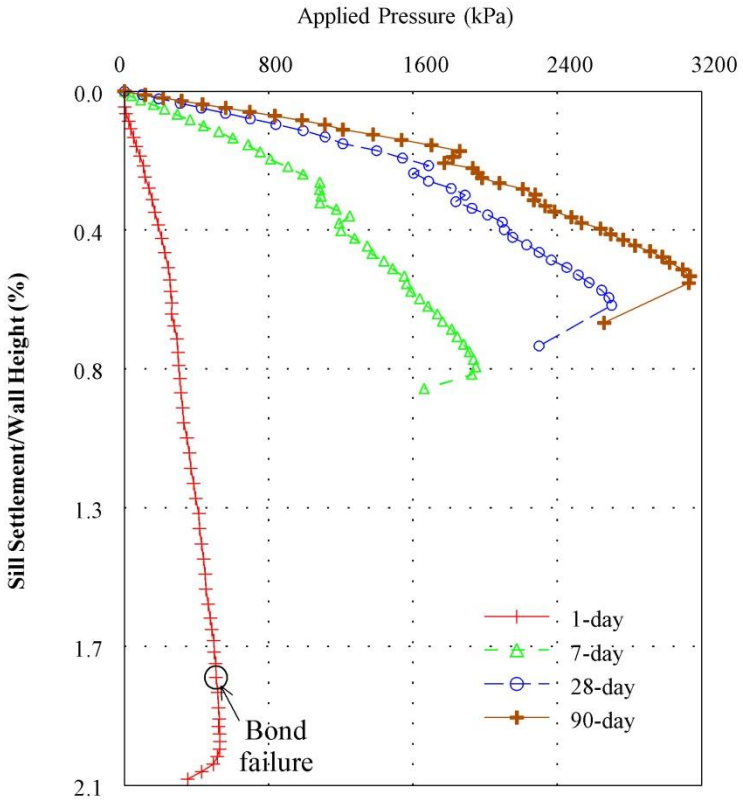

Figure 5.19: Performance of the bridge abutment with CLSM curing time.

The curing temperature is also an important factor that affects the strength gain of CLSM mixtures and so the load bearing capacity and performance of the CLSM bridge abutment. This influence was studied with a mixture (M7) cured for 7 days at 40°F, 73°F and 100°F that lead to compressive strengths of 0.24, 0.38, and 1.38 MPa, respectively. Figure 5.20 shows that bearing capacity of the CLSM abutment cured at a cold temperature of 40°F is about 30% less than if cured in the cool temperature of 73°F, while the abutment can gain almost twice strength at hot temperature of 100°F.

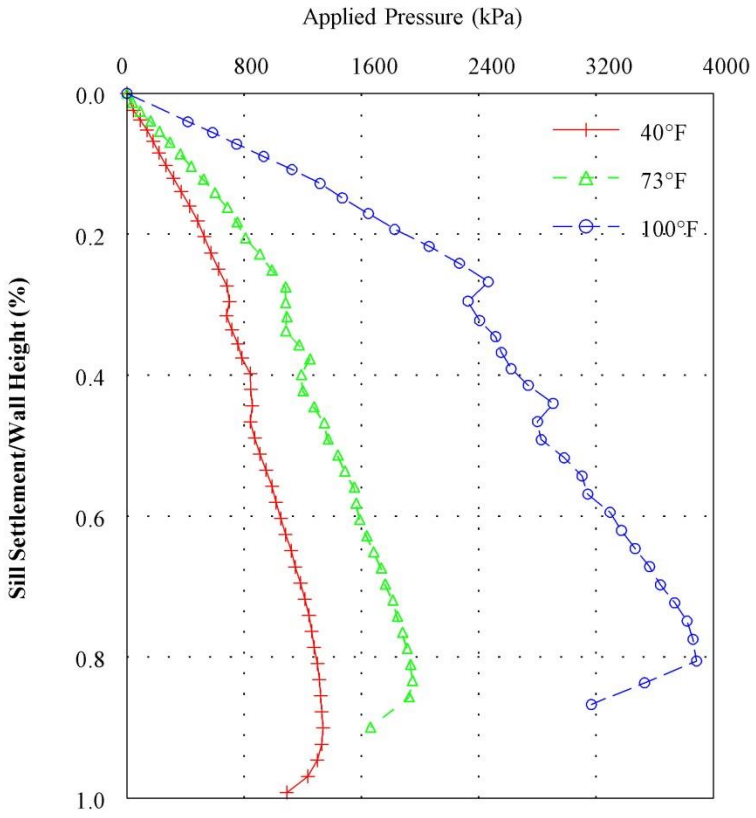

Figure 5.20: Performance of the bridge abutment with curing temperature.

In another analysis, early strength (1-day) and late strength (28-day) of six different CLSM mixtures (from table 3.4, mixtures M2, M4, M5, M7, M9, M10) was considered. The 28-day compressive strength of these mixtures was ranged from a low strength of 0.85 MPa to a relatively high strength of 8.2 MPa. Figure 5.21 show the early performance of the abutment (after 1 day) backfilled with different CLSM mixtures, and Figure 5.22 exhibit the late performance (after 28 days). It generally shows that with the increase in compressive strength, the maximum pressure taken by the abutment increases and displacements decrease.

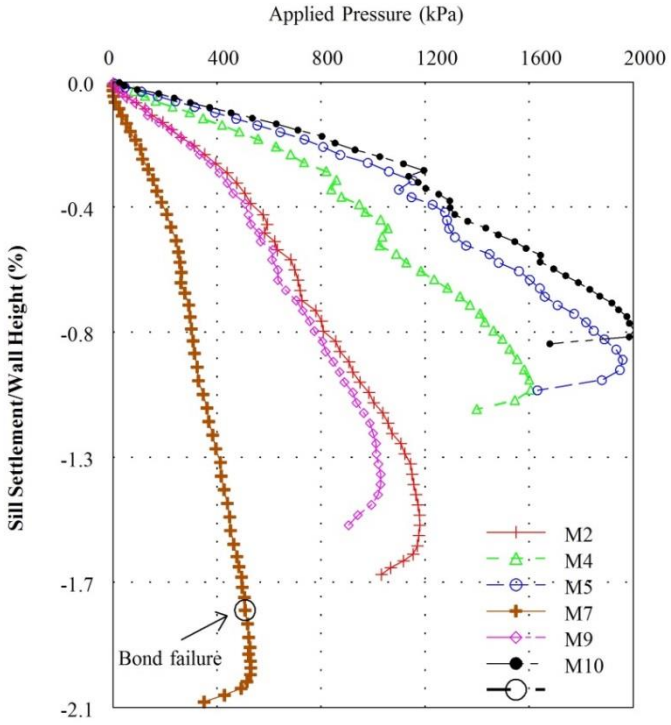

Figure 5.21: Early performance of the abutment with different CLSM mixtures.

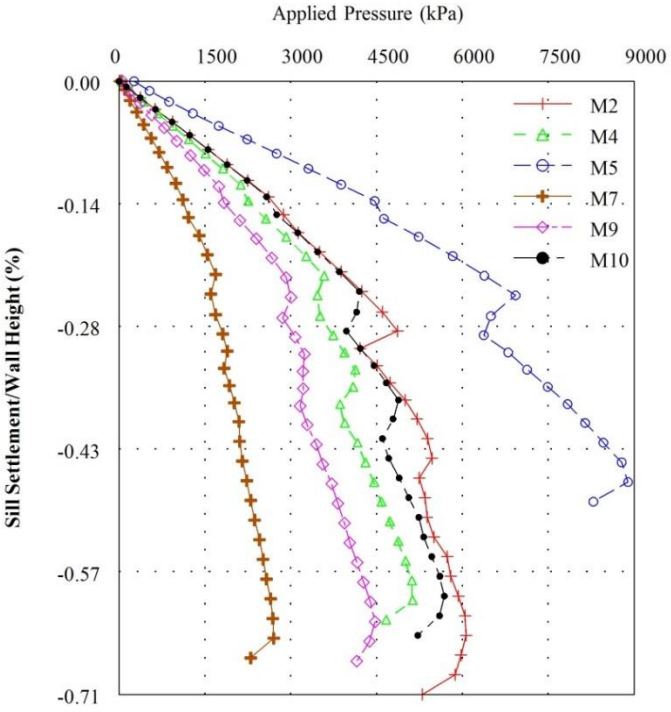

Figure 5.22: Late performance of the abutment with different CLSM mixtures.

Also comparison of the damage pattern of failure in Figure 5.23 indicate that when the abutment backfilled with a relatively low strength CLSM mixture, the splitting cracks are focused near the surface, below the bridge sill, however it spreads to the depth of the backfill when it becomes stronger. It can be seen that stronger backfill gets more intense damage to fail.

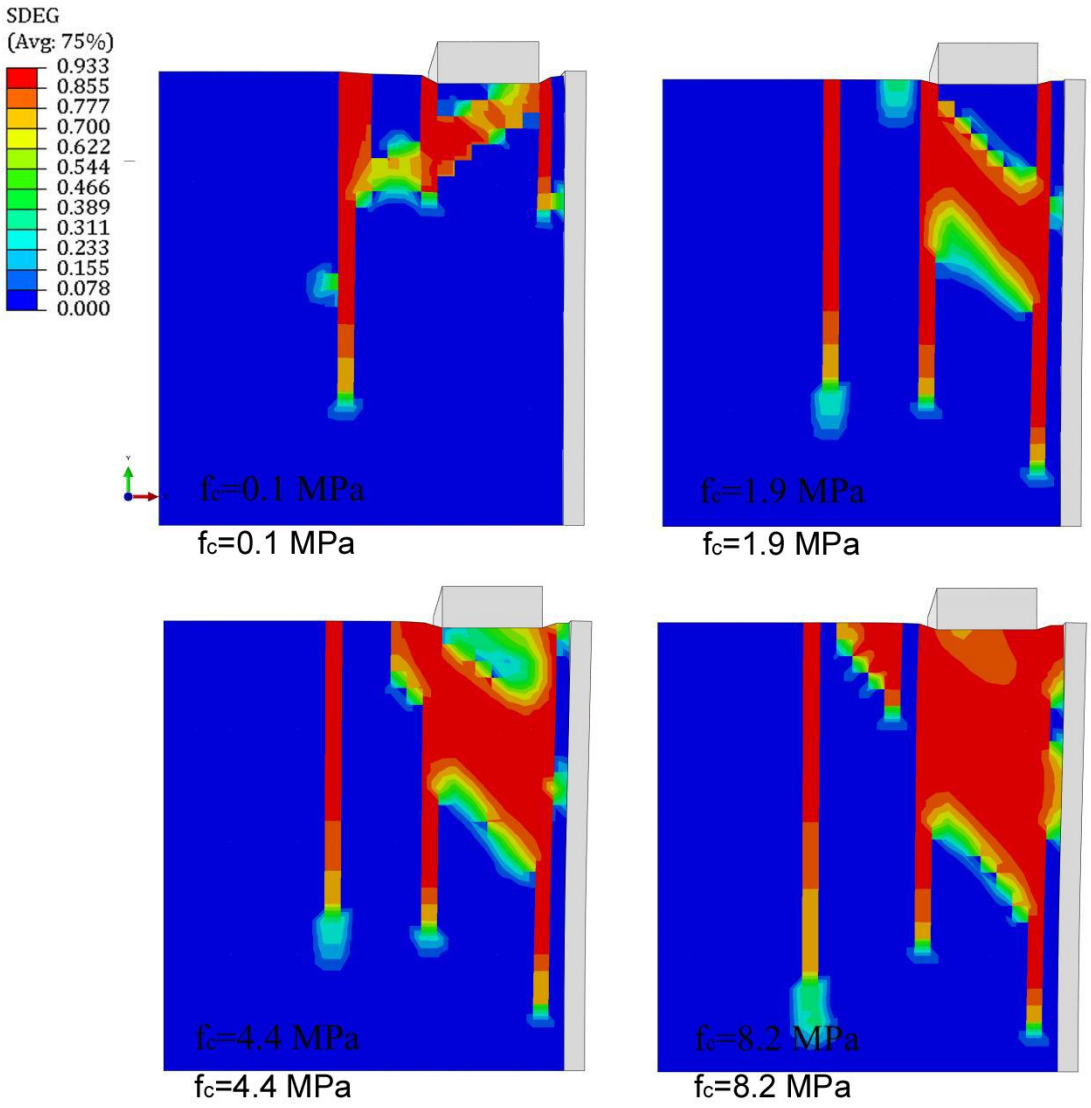

Figure 5.23: Comparison of the damage pattern of failure with different strengths of backfill.

The effect of CLSM strength on the abutment performance based on lateral deformation at the wall face, and mobilized load in the anchors is also investigated. These values were normalized by the height (Δ/H) for lateral deformation, and yield and bond strength for the anchors. Figure 5.24 illustrates that the largest lateral deformation of the concrete panels occurs at the top of the face wall. Figure 5.25 is the profile of lateral deformation of a face panel at failure for different CLSM mixtures. As it shows, as the mixture becomes stronger, a panel undergoes more deformation before failure. For the case of the strongest mixture, the backfill behaves with more rigidity and so less displacement (both lateral and vertical) is measured.

Figure 5.26 is a typical behavior of a CLSM abutment with respect to the lateral deformation. It shows that a facing panel deforms slightly as the load on bridge sill approaches the 70% of bearing capacity of a CLSM abutment, thereafter lateral deformations become more significant. 70% of the bearing capacity relates to the Figure 5.15b when a longitudinal crack develops close to the face.

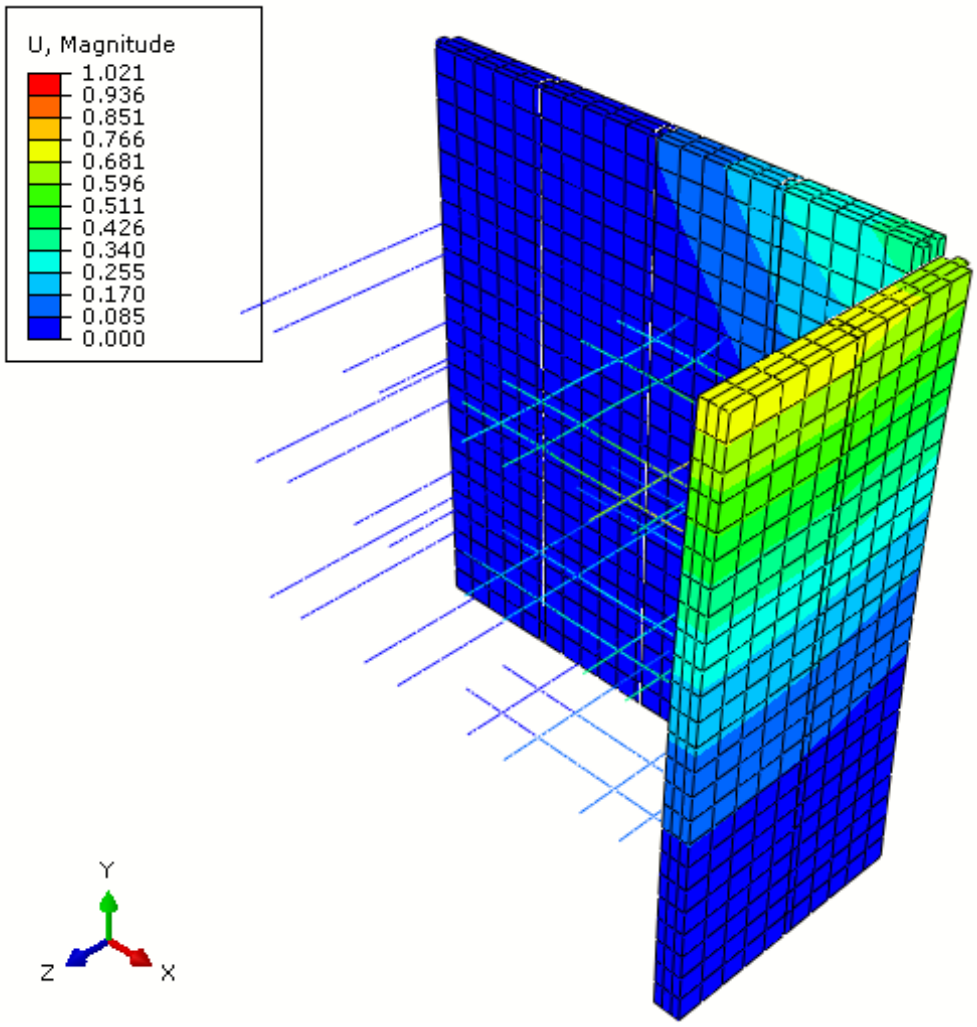

Figure 5.24: Lateral deformations of the concrete panels (unit is in inches).

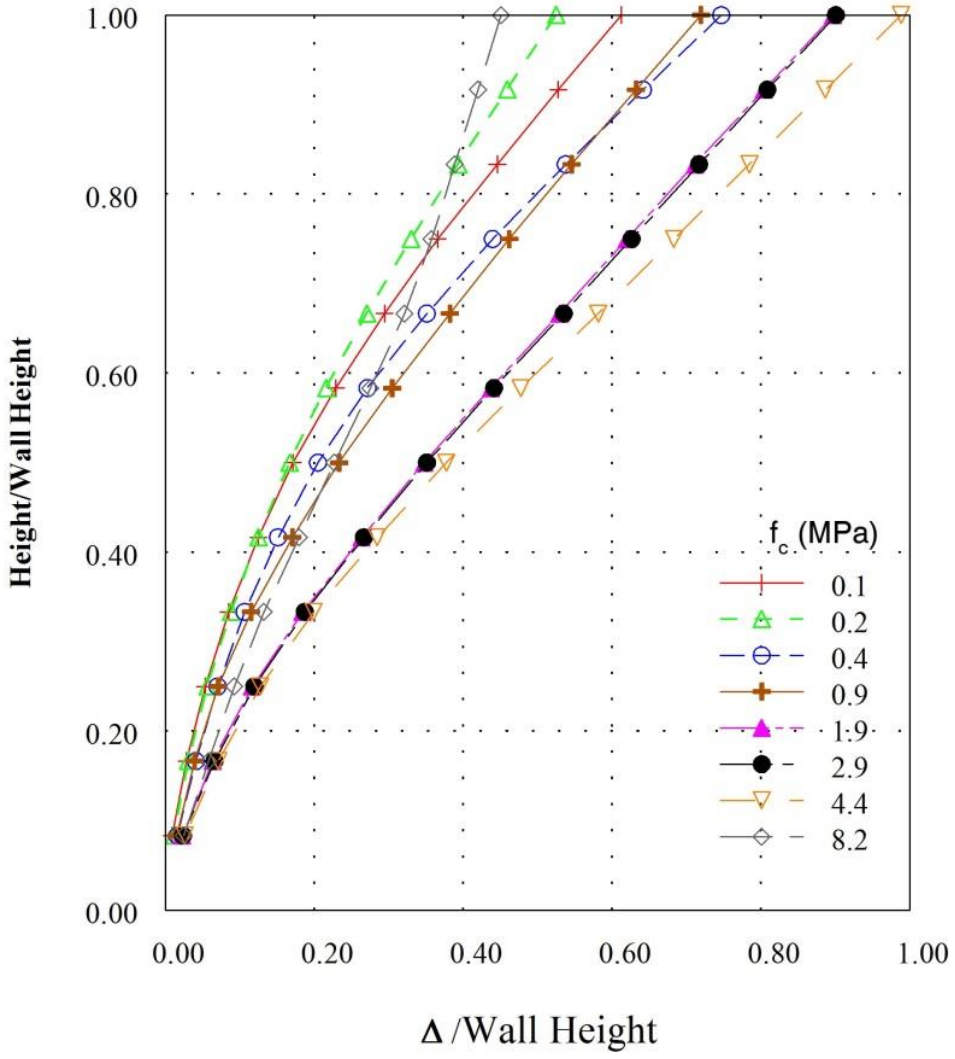

Figure 5.25: Profile of lateral deformation at the maximum applied pressure with different CLSM strengths.

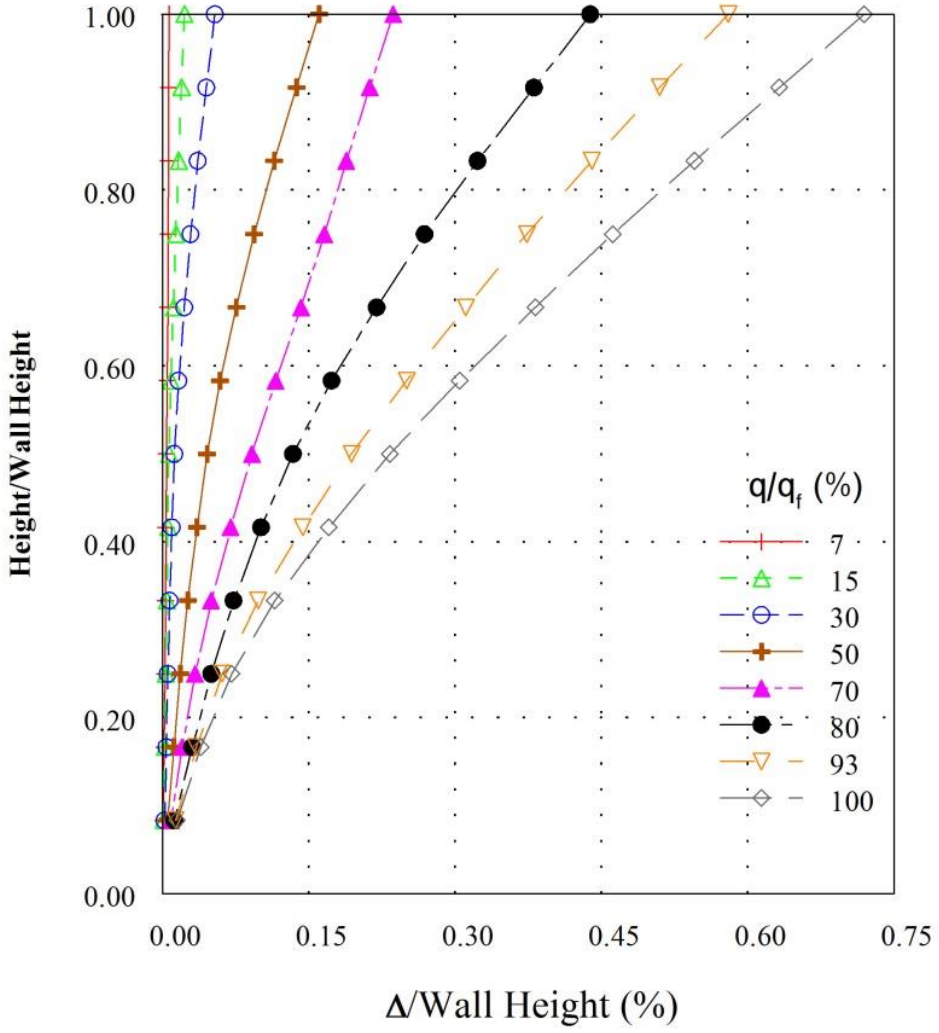

Figure 5.26: Profile of lateral deformation of a face panel as a function of the applied pressure.

Figure 5.27 is a typical behavior of a CLSM abutment based on mobilized load in the anchors. It shows that axial stress in the anchors increases as the pressure (q) on bridge sill approaches the bearing capacity of a CLSM abutment (q_f). Figure 5.28 shows mobilized axial stress in anchors located at top, middle and bottom of a face panel at a specific applied load (500 kPa) as a function of CLSM mixture strength. Typically, more stress is mobilized at the top anchor, and the stronger mixture transfer less load to the

anchors. It is seen that the middle anchor in case of the weakest mixture captures more load. The fact is 500 kPa is close to maximum applied pressure in this case and even though the splitting cracks are developed at top, the backfill shows more ductile response and anchors at lower levels take a little more load to fail. This ductility is not a typical response for stronger mixtures. Figure 5.29 shows mobilized axial stress in anchors at failure for mixtures with different compressive strengths. Typically, anchors embedded in a weaker CLSM mass are more susceptible to bond strength and in a stronger mass, the yield strength is controlling.

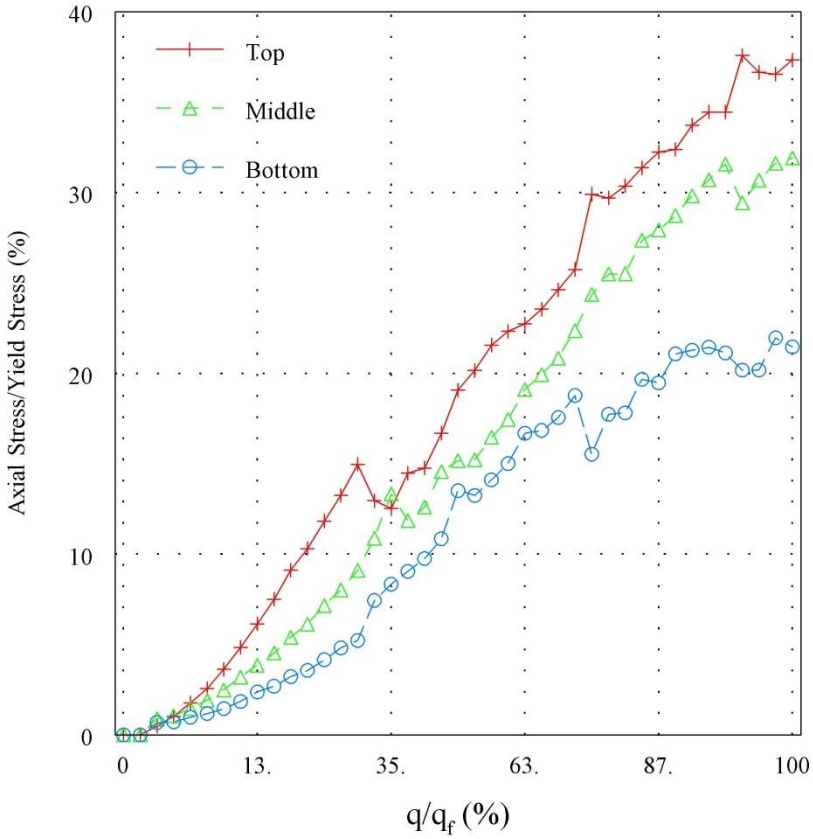

Figure 5.27: Development of axial stress in anchors as a function of applied pressure.

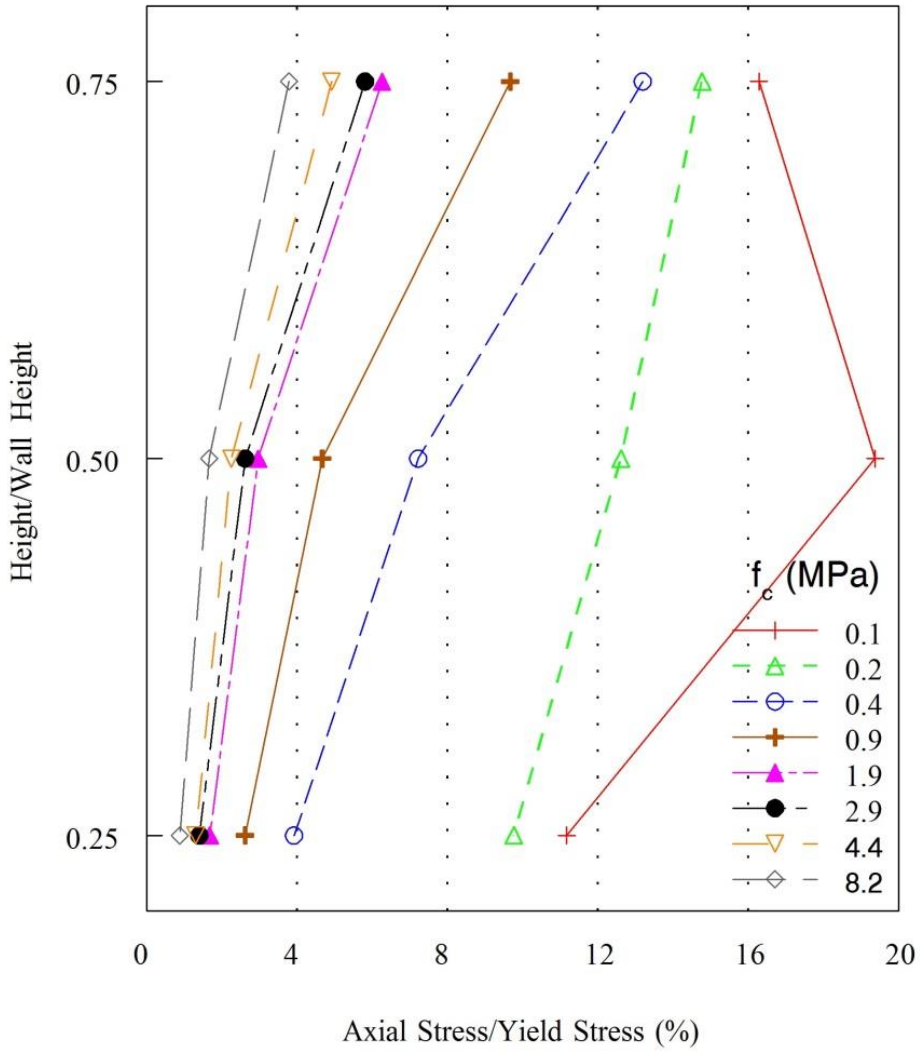

Figure 5.28: Effect of CLSM strength on mobilized axial stress in anchors (at 500 kPa).

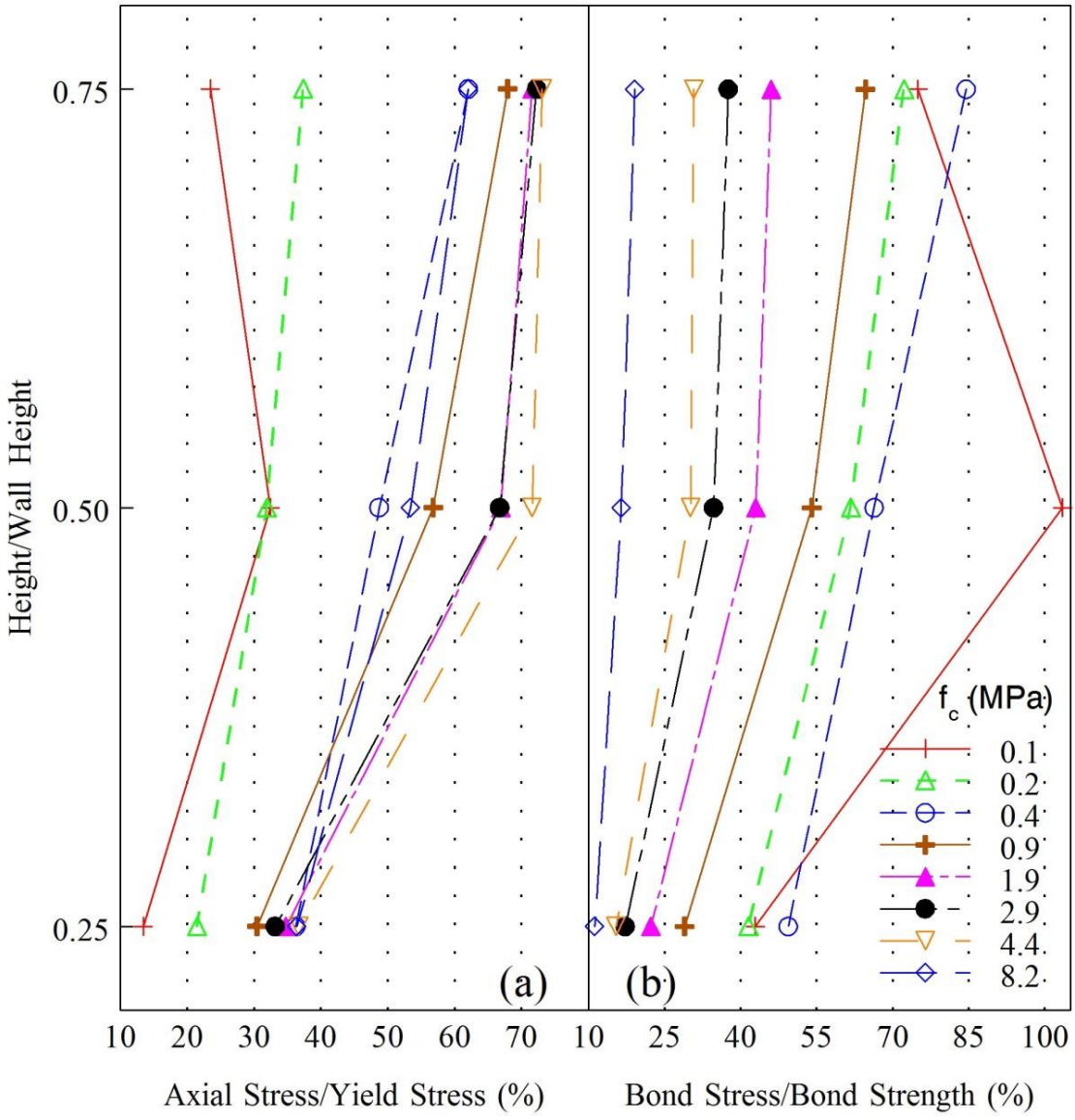

Figure 5.29: Effect of CLSM strength on mobilized axial stress in anchors (at failure).

Figure 5.30 illustrates plan of the developed axial stress in all anchors of the face and wing wall at failure. It can be seen that except the panel close to the face, less load is transmitted to the anchors of wing walls. This can be used to modify the design and implement less number of anchors for the wing walls.

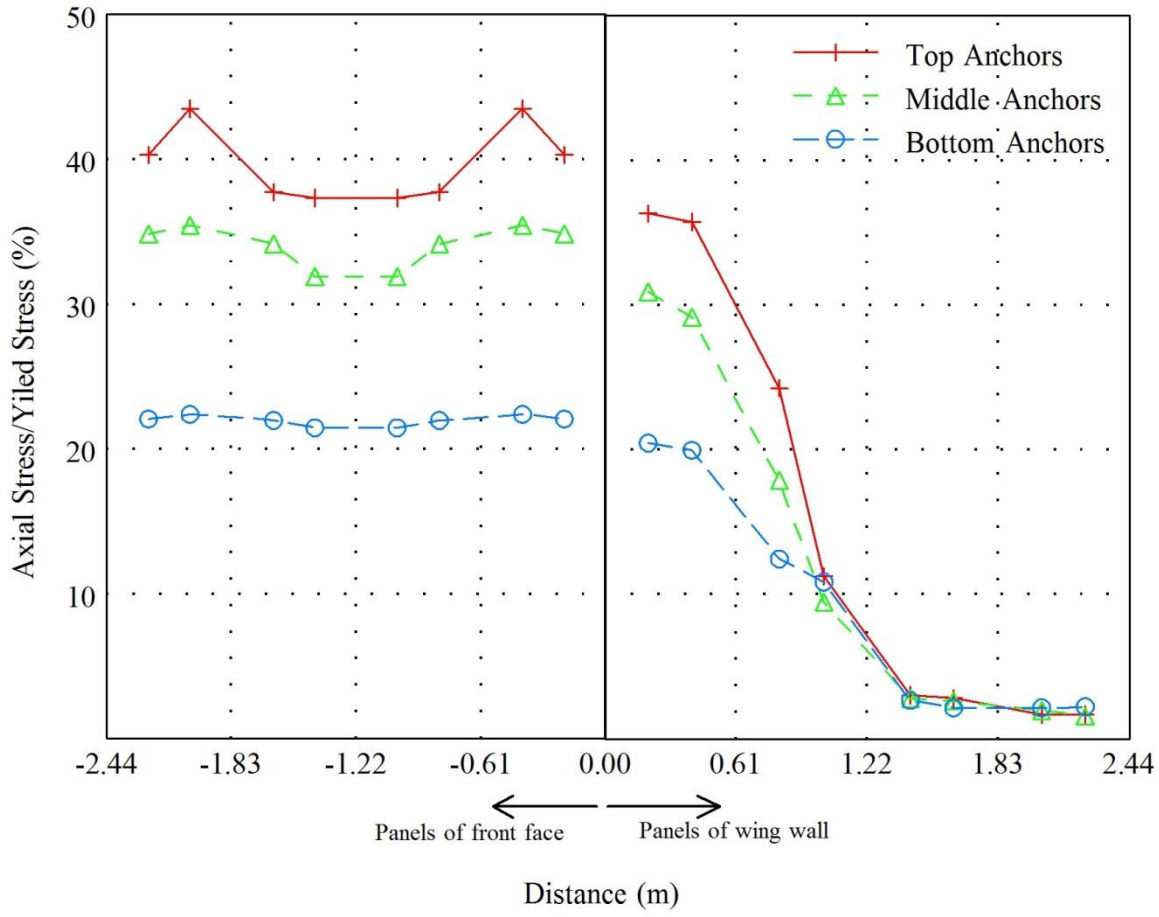

Figure 5.30: Plan of mobilized stress in all anchors of the face and wing wall (at failure).

The finite element model was used to examine the effect of some design modifications on performance of the CLSM bridge abutment. Four different cases were considered and compared with the base case (in Figure 5.10) as follow:

- Case 1: a backfill without the concrete panels and anchors
- Case 2: a backfill with the concrete panels and without the anchors
- Case 3: one column of steel rebars is used to anchor the panels at wing walls
- Case 4: vertical connection detail (groove and tongue) is eliminated between panels

The first two cases reveal the effect of concrete panels and anchors in the load bearing capacity and displacements of the CLSM abutment. Case 3 was considered since it was observed that the anchors used for wing walls are not taking considerable load. Case 4 was to examine the value of existence of the vertical connections between the panels. Figures 5.31 and 5.32 compare behavior of the abutment in these cases (with the same mixture, M3). Figure 5.31 shows that the abutment loses half of its load bearing capacity without the anchored panels to provide lateral support and confining pressure. This is also can be seen in Figure 5.32 when these two case show large lateral deformations. Performance of the abutment in case 3 reveals that one column of steel rebars (at top, middle and bottom of a panel) would be enough to anchor the panels of wing walls (in the base case two columns of anchors is used for all panels as in Figure 5.10). Also case 3 demonstrates that the vertical connection detail (groove and tongue connection) between panels does not have influence on performance of the abutment and it would be safe to be eliminated. These two modifications lead to faster and more economical construction design for CLSM bridge abutments. Figure 5.33 also shows the damage state of failure for the case 1 (without the anchors) and compares it with the base case. It demonstrates that the existence of anchors reduce the damage propagation.

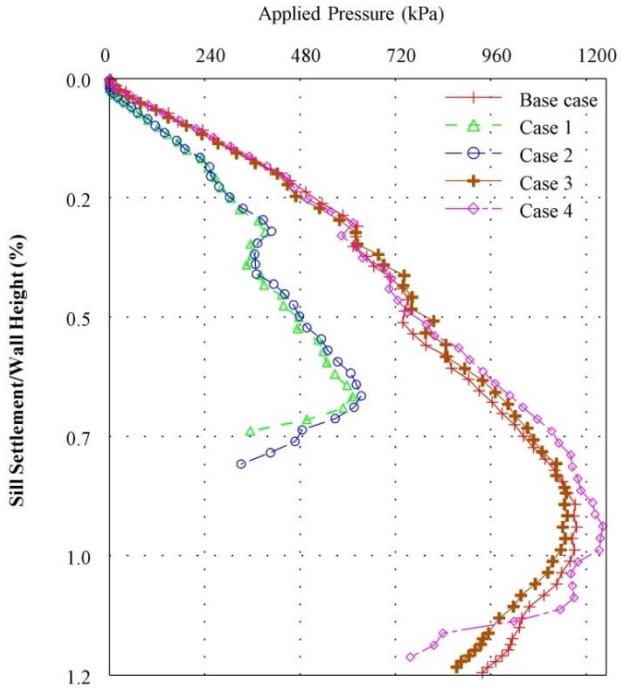

Figure 5.31: Effect of some design modifications on performance of the CLSM abutment.

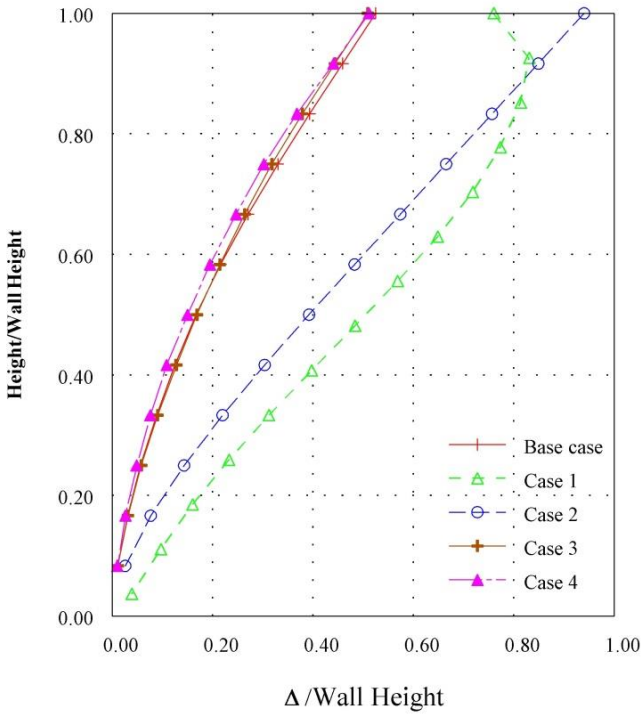

Figure 5.32: Effect of some design modifications on lateral deformation of the CLSM abutment.

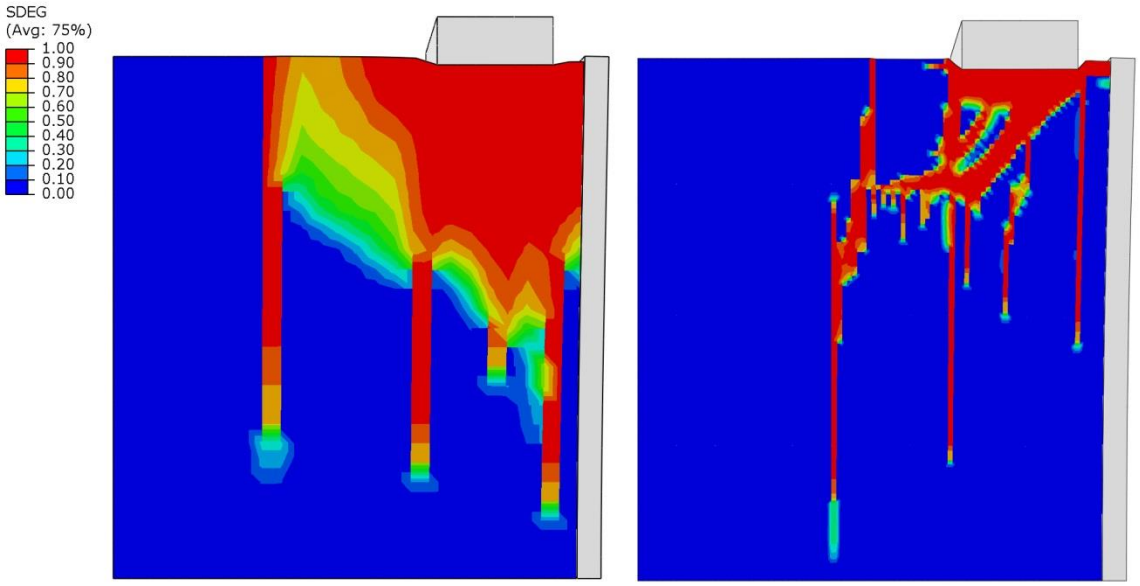

Figure 5.33: Effect of anchors on damage propagation, (left) without anchors, (right) with anchors.

Chapter 6

SUMMARY AND CONCLUSIONS

One of the major obstacles facing rapid bridge construction for typical span type bridges is the time required to construct bridge abutments and foundations. This can be remedied by using the controlled low strength materials (CLSM) bridge abutment. The CLSM bridge abutment is assumed to have full-height precast concrete panels that are attached to a CLSM backfill by steel anchors. The CLSM bridge abutment provides a load-bearing support for the bridge sill, thus eliminating the need for piling systems. CLSM is a self-compacting material; hence it reduces the amount of compacting operation needed for construction of the abutment. Therefore, CLSM bridge abutments can be constructed in a shorter time because they do not require heavy machinery for excavation, compaction, and piling equipment.

The main objective of this study was to examine the behavior of an instrumented laboratory large-scale CLSM bridge abutment with full-height precast concrete panels that was subjected to a monotonically increasing sill (foundation) pressure. Construction duration of a CLSM abutment is restricted by initial strength development of the CLSM. The CLSM abutment test specimen was built in seven days and in the field, depending on the project size, it is anticipated that several weeks or even months may be saved as compared with the construction of a conventional bridge abutment.

The following conclusions have been drawn from this study:

1- In order to design an optimum CLSM mixture for application in a bridge abutment, several different mixtures were tested for flowability, density, compressive strength, stress-strain relationship and bond strength. The main performance properties to select a suitable mixture were compressive strength to support the bridge loads and flowability to fill the entire abutment in one continuous pour by pumping. A total of 12 mixtures with different levels of cement content, fly ash dosage, and water to cementitious materials ratio and therefore different ranges of compressive strength and flowability were developed. It was confirmed that the curing temperature is an important factor that affecting the strength gain of CLSM mixtures. Higher curing temperatures promote an early strength gain in CLSM, but lower the rate of strength gain at later ages.

   CLSM has significantly lower strength than concrete; therefore, the bond strength to steel anchors becomes a critical issue in the design of CLSM bridge abutment for the internal stability. Bond performance was studied with the experimental pullout tests and modeled using FE numerical simulation. From the pullout tests it was concluded that a CLSM mixture with higher compressive strength results in higher CLSM - steel rebar bond strength. In fact, the average bond strength (in MPa) was consistent with the square root of compressive strength of a CLSM mixture. Numerical simulation of pullout tests indicated that the bond capacity decreases slightly with increasing bar size. Also because of a non-linear

distribution of the bond stress along the embedment length of the rebar, the average bond strength decreases with increase in embedment length.

2- Using the selected CLSM mixture, an instrumented, large-scale laboratory CLSM bridge abutment specimen with full-height concrete panels was constructed to test its performance due to the application of a gradually increasing bridge load. The test results show that the CLSM bridge abutment, with a relatively short cure time of 7 days, is capable of carrying bridge loads with a reasonably large safety margin, and with minimal deformations. The CLSM bridge abutment in this study resisted 780 kN of static load or sill pressure of 535 kPa without any failure and with minimal settlement and lateral deflections. This was several times larger than sill pressure of about 93 kPa for a typical bridge dead load and the corresponding sill settlement was about 6 mm (1/4 in.) which is about %0.2 of wall height. The measured lateral pressure against the abutment wall panels was very small in general, and was higher in the mid-height layers of the CLSM during the curing time due to the speed of hydration that could have taken place in such regions. After curing, the lateral pressure decreased to negligible levels due to shrinkage. Therefore, it is safe to design the concrete panels and the temporary lateral bracing to support fluid pressure of the fresh CLSM, even though, except the mid-height regions, the lateral pressures were smaller. Steel anchors experienced maximum values of combined axial and bending strains while those at the lower elevation experienced mainly axial strains. Based on strain measurements of the

anchors under the bridge load, the axial tensile forces were determined to be less than 30% of the ultimate pullout force.

3- A three dimensional FE model is implemented to analyze the performance of CLSM bridge abutments based on the bearing pressure capacity, displacements and the developed axial force in anchors, and to provide an assessment of safety of the design. The procedure utilized a plastic-damage model which captures the material behavior using both classical theory of elasto-plasticity and continuum damage mechanics, as provided in the FE software Abaqus.

The FE modeling of the compression tests demonstrated the capability of the material model for a realistic prediction of the failure patterns in the CLSM test cylinders and stress-strain response. The numerical results were coherent with the measurements obtained in a full scale laboratory test on a CLSM bridge abutment. The FE model showed that the CLSM abutment is capable of carrying typical bridge loads after one day with adequate margins and with small deformations. It also indicated that the lateral movement of the facing panels was negligible up to about 70% of the bearing capacity of the abutment when a longitudinal crack developed close to the face.

The validated numerical model was used to conduct a series of analytic parametric studies related to the effect of CLSM strength, curing age, environment temperature and some construction details on the load bearing capacity and performance of the abutment. It was predicted that the bearing

capacity of the bridge abutment increases as the CLSM mixture cures but the ductility of the response decreases. Also, it was confirmed that the curing temperature is an important factor that affecting the bearing capacity of the CLSM abutment. Higher curing temperatures promote the bearing capacity. Early (1 day) and late age (28 days) performance of the abutment backfilled with different CLSM mixtures is also considered to provide an initial guide for the selection of a mixture based on its compressive strength for the abutment. With the increase in compressive strength of a CLSM mixture, the maximum pressure taken by the abutment increases and the displacements decrease. For anchors, stronger mixtures transfer less load to the anchors and more stress is mobilized at the top anchor. Typically, anchors embedded in a weaker CLSM mass are more susceptible to failure due to bond strength and in a stronger mass, to the yield strength of the steel rebar. This study showed that the abutment loses half of its load bearing capacity without the anchored panels to provide lateral support and confining pressure. The FE model also can be used to modify the design details. For example, the number of anchors can be decreased for wing walls, and the vertical connection detail (groove and tongue connection) between panels may be safely eliminated.

The CLSM mixtures reported in this study can be used as an initial guide for the selection of raw materials and their proportions to use as a structural fill for the CLSM bridge abutment based on minimum strength requirements and flowability. However,

since requirements and locally available materials can vary considerably from project to project, adjustments can be made to achieve the desired properties. For example, sustainability or speedy construction might be emphasized by producing a CLSM using only by-product materials or using accelerating admixtures, respectively. Considering the test results, it can be concluded that excluding some modifications, the construction sequence of CLSM bridge abutment was successful and can be repeated for future works. Suggested modifications are as follows:

- Groove and tongue connection showed strong enough to keep the panels together. Nonetheless, in both fabrication and installation steps they were one of the major obstacles. There is a very high degree of precision required for the proper fit up between precast panels. To accommodate the fabrication and installation, simple to construct connections with enough strength must be considered. Shear keys, lateral post-tensioning, splice sleeve connections, welded connections, and bolted connections are alternatives connection methods currently used to attach precast concrete components. It has been noted through the literature that vertical connection detail can be eliminated between wall elements (except on walls more than 6 m high) because of minor load transfer at the vertical joints (Stamnas and Whittemore, 2005).
- The panels were overdesigned; as have been noted from the test results, they do not actually endure considerable structural loads in the system. Therefore it is recommended to design them with enough reinforcement to just tolerate the

lifting loads and the lateral pressures of fresh CLSM. This way lighter and more economical panels can be fabricated which makes the assembly even easier.

- It has to be expected that the designed mixture strength may vary when a large volume of CLSM has to be produced. The designed compression strength was 0.38 MPa after seven days for this study but the collected samples of the CLSM backfill had 0.2 MPa strength. Therefore a precise inspection is required for CLSM mixing process.
- Because construction duration of CLSM abutment is restricted by initial strength development of the CLSM, a mixture with high early strength can be designed. In order to achieve this, a suitable admixture might be utilized.

Recommendations for future research:

The research team suggests a full-scale field construction of a CLSM bridge system to demonstrate its feasibility as a rapid bridge construction method. In addition to showing the short- and long-term performance of the CLSM bridge abutment, the field work will also enable bridge engineers and geotechnical engineers to gain experience and become familiar with the proposed rapid construction method. The work will also improve current understanding of the behavior of CLSM bridge abutments carrying realistic bridge loads.

The CLSM bridge abutments, the concrete slab (deck), and the bridge girders can be instrumented, with strain gauges, pressure cells, displacement gauges, and surveying points to measure their behavior during construction and upon application of construction

and service loads. Measurements should continue for several years after completion of the construction to investigate the long-term behavior of the precast bridge elements and the CLSM abutments. Of particular interest are the vertical displacement of the bridge and the lateral displacement of the full-height facing panels. An extensive array of displacement gauges and surveying targets can be used to measure horizontal and vertical displacements of the bridge, the approach fill, and the abutment facing. A pavement profiler can be used to quantify approach settlements. Also, because of the three-dimensional nature of the proposed construction, the wing walls should be instrumented with surveying targets to measure their lateral displacements. Based on the results of the field testing and monitoring, an updated design guide can be developed.

REFRENCES

1- Abaqus Analysis User's Manual (2012). Dassault Systèmes, Version 6.12.

2- Adaska, W. S. (1997). "Controlled Low Strength Materials" *Concrete International*, Vol. 19, No. 4, pp. 41–43.

3- American Association of State Highway and Transportation Officials (AASHTO). (1995). "Standard Specifications for Transportation Materials and Methods of Sampling and Testing." Seventeenth Edition, Part 1 Specifications, Washington, D.C.

4- ACI 229R (1999). "Controlled Low-Strength Materials." *ACI Committee 229 (Reproved 2005).* American Concrete Institute (ACI), Farmington Hills, MI.

5- ACI 408.2R (1992). "State-of-the-Art Report on Bond under Cyclic Loads." *ACI Committee 408*. American Concrete Institute (ACI), Farmington Hills, MI.

6- ACI 408R (2003). "Bond and Development of Straight Reinforcing Bars in Tension." *ACI Committee 408*. American Concrete Institute (ACI), Farmington Hills, MI.

7- Bhat, S. T., and C. W. Lovell (1996). "Use of Coal Combustion Residues and Foundry Sands in Flowable Fill." Joint Highway Research Project, School of Civil Engineering, Purdue University, 222 p.

8- Brewer, W. E. (1990). "The Design and Construction of culverts using Controlled Low Strength Material – Controlled Density Fill (CLSM – CDF) Backfill." Structural Performance of Flexible Pipes. *Proceedings of the First National Conference on Flexible Pipes.* pp. 109-118.

9- Brewer, W.E. (1994). "Durability Factors Affecting CLSM." Controlled Low-Strength Materials, ACI SP 150, W.S. Adaska, ed., *American Concrete Institute*, Detroit, MI, 113 p.

10- CEB-FIP (2000). "Bond of reinforcement in concrete: state-of-art report," Fib Bulletin No. 10, Lausanne, Switzerland.

11- Cheng, H., Capers, H. (2009). "Overnight Delivery – New Jersey DOT Rapid Bridge Replacement." *Proc., 25th US-Japan Bridge Engineering Workshop*, Tsukuba, Japan, 163-172.

12- Darwin, D., and Graham, E. K., (1993). "Effect of Deformation Height and Spacing on Bond Strength of Reinforcing Bars." *ACI Structural Journal*, V. 90, No. 6, pp. 646-657.

13- Dockter, B.A. (1998). "Comparison of Dry Scrubber and Class C Fly Ash in Controlled Low-Strength Materials (CLSM) Applications." The Design and Application of Controlled Low-Strength Materials (Flowable Fill), *ASTM STP 1331*, A. K. Howard and J. L. Hitch, eds., American Society for Testing and Materials, West Conshohocken, PA.

14- Dolen, T. P., and Benavidez A. A. (1998). "Properties of Low-Strength Concrete for Meeks Cabin Dam Modification Project, Wyoming" in the Design and Application of Controlled Low-Strength Materials (Flowable Fill), *ASTM STP 1331*, A. K. Howard and J. L. Hitch (Eds.). American Society for Testing and Materials (ASTM), West Conshohocken, PA, pp. 213–230.

15- Elias, V., and Christopher, B. (1996). "Mechanically Stabilized Earth Walls and Reinforced Soil Slopes Design and Construction Guidelines." *FHWA Demonstration Project 82*, FHWA SA-96-071, 371 pp.

16- Elias, V., Christopher, B. R., and Berg, R. R. (2001). "Mechanically stabilized earth walls and reinforced soil slopes design and construction guidelines." *National Highway Institute Course No. 132042, FHWA NHI-00-043*, Federal Highway Administration, Washington, D.C.

17- Federal Highway Administration (FHWA) (1997). "User Guidelines for Waste and By-Product Materials in Pavement Construction." Report No. FHWA-RD-97-148.

18- Federal Highway Administration (FHWA) (2004). "National Bridge Inspection Standards (NBIS)." < http:// www.fhwa.dot.gov/bridge/nbis.htm>

19- Folliard, K. J., Du, L., Trejo, D., Halmen, C., Sabol, S., and Leshchinsky, D. (2006). "Corrosion Study and Implementation Plan for NCHRP Report 597 NCHRP". Web Document, Issue 116, 56p.

20- Folliard, K. J., Du, L., Trejo, D., Halmen, C., Sabol, S., and Leshchinsky, D. (2008). "Development of a Recommended Practice for Use of Controlled Low-Strength Material in Highway Construction." *NCHRP Report 597*, Transportation Research Board, Washington DC.

21- Folliard, K. J., Trejo, D., Sabol, S. A., and Du., L. (1999). "Controlled Low-Strength Material for Backfill, Utility Bedding, Void Fill, and Bridge Approaches." *NCHRP Phase I Interim Report*, Delaware Transportation Institute, University of Delaware, Newark.

22- Gress, D. (1996). "The Effect of Freeze-Thaw and Frost Heaving on Flowable Fill." UNH Civil Engineering No. 1096-1 for New Hampshire Department of Transportation, University of New Hampshire, 56 p.

23- Halmen, C, Trejo, D., Folliard, K.J., and Du, L. (2005). "Corrosion of Metallic Materials in Controlled Low-Strength Materials- Part 3." *American Concrete Institute (ACI) Materials Journal*, Volume 102, Issue 6, pp. 429-437.

24- Hill, J.C., and Sommers J. (1997) "Production and Marketing of Flowable Fill Utilizing Coal Combustion By-Products." *American Coal Ash Association Proceedings: 12th International Symposium on Coal Combustion By-Product (CCB), Management and Use*, Vol. 2, pp 38-1 through 38-13.

25- Hitch, J. L. (1998). "Test Methods for Controlled Low-Strength Material (CLSM): Past, Present, and Future." The Design and Application of Controlled Low-Strength Materials (Flowable Fill), *ASTM STP 1331*, A. K. Howard and J. L. Hitch, eds., American Society for Testing and Materials, West Conshohocken, PA.

26- Hoopes, R. J. (1998). "Engineering Properties of Air-Modified CLSM" in the Design and Application of Controlled Low-Strength Materials (Flowable Fill), *ASTM STP 1331*, A. K. Howard and J. L. Hitch (Eds.). American Society for Testing and Materials (ASTM), West Conshohocken, PA, pp. 87–101.

27- Horiguchi T., Okumura H., and Saeki N. (2001). "Optimization of CLSM Mix Proportions with Combination of Clinker Ash and Fly Ash." ACI Special publication SP-199. *American Concrete Institute*: Farmington Hills, pp. 307-325.

28- Howard, A. (1998). "Proposed Standard Practice for Installing Buried Pipe Using Flowable Fill." The Design and Application of Controlled Low-Strength Materials (Flowable fill), *ASTM STP 1331*, A. K. Howard and J. L. Hitch, Eds., American Society for Testing and Materials.

29- Howard, A. Hitch, J. (1998). "The Design and Application of Controlled Low-Strength Materials (Flowable fill)." *ASTM STP 1331*, American Society for Testing and Materials.

30- Janardhanam, R., Burns F., and Peindl R. D. (1992). "Mix Design for Flowable Fly-Ash Backfill Material." *Journal of Materials in Civil Engineering*, Vol. 4, No. 3, pp. 252–263.

31- Jankowiak, T. and Tomasz L. (2005). "Identification of parameters of concrete Damaged Plasticity constitutive model." *Foundations of civil and environmental engineering*, (6), pp. 53-69.

32- Javed, A., Lovencin, W., and Najafi, F.T. (2002) "Current Status of Accelerated Flowable Fill in the Pavement Section." *Proceedings, Canadian Society for Civil Engineering 20th Annual Conference*, Montreal, Quebec, Canada.

33- Kasemchaisiri, R. and Tangtermsirikul S. (2006). "A method to determine water retainability of porous fine aggregate for design and quality control of fresh concrete." *Construction and Building Materials*, 21 (6), pp.1322-133.

34- Khalfallah, S. and Ouchenane, M. (2007). "A Numerical Simulation of Bond for Pull-Out Tests: The Direct Problem." *Asian Journal of Civil Engineering (Building and Housing),* Vol. 8, No. 5, pp. 491-505.

35- Kennedy, D. O. and Linne, C. L. (1987). "Environmental and Economical Aspects of Sand Reclamation System." *EPRI*, Vol. 2, Palo Alato, CA.

36- Larralde, J., Silva-Rodrigues, R., Burdette, J., and Harris, B. (1994). "Bond Tests of Fiberglass- Reinforced Plastic Bars in Concrete." *ASCE J Test. Eval.*; 22(4), pp. 351-359.

37- Lee J. and Fenves G. (1998). "Plastic-Damage Model for Cyclic Loading of Concrete Structures." *Journal of Engineering Mechanics*, 124 (8), pp. 892–900.

38- Lovencin, W., Najafi, F.T., and Chaudhry, H. (2006). "Assessment of Flowable Fill Strength in Pavement Construction." *J. TRB 1979*, National Academies, NRC, Washington, DC, pp. 84-92.

39- Lubliner J., Oliver J., Oller S., and Oñate E. (1989). "A Plastic-Damage Model for Concrete." *International Journal of Solids and Structures*, 25 (3), pp. 299–329.

40- Lundgren, K. (1999). "Three-Dimensional Modelling of Bond in Reinforced Concrete." PhD Dissertation, Chalmers University of Technology, Göteborg, Sweden.

41- Magnusson, J. (1997). "Bond and Anchorage of Deformed Bars in High-Strength Concrete." Licentiate Thesis. Division of Concrete Structures, Chalmers University of Technology, Publication 97:1, Göteborg, Sweden.

42- Melton, J. S., Nourse, W. A., Gardner, K. H., and Seager, T. P. (2005). "A Rational Mix Design for Flowable Fill Containing Contaminated Sediment." *Third International Conference on Remediation of Contaminated Sediments*, New Orleans, LA.

43- Mindess, S., Young J.F., and Darwin D. (2003). "*Concrete"*, Pearson Education, Inc., Upper Saddle River, NJ.

44- Najafi, F.T., and Tia, M. (2004). "Use of Accelerated Flowable Fill in pavement Section." *Final Report, Volume 1,* Florida Department of Transportation, Tallahassee, 124 pp.

45- Naik, T. R., Kraus, R. N., Sturzl, R. F. and Ramme, B. W. (1998). "Design and Testing Controlled Low Strength Materials (CLSM) Using Coal Ash." Testing Soil Mixed with Waste or Recycled Materials, *ASTM STP 1275*, West Conshohocken, PA.

46- Nantung, T. E. (1993). "Design Criteria for Controlled Low Strength Materials." Ph.D. Dissertation, Purdue University, 345 p.

47- Newman, F.B., Rojas-Gonzalez, L.F., and Knott, D.L. (1993). "Implementation Plan for Design and Use of Flowable Backfills by PennDOT for Highway and Bridge Construction." *Report No. FHWA-PA-91-007+90-12*, FHWA, Washington, D.C. and Pennsylvania Department of Transportation, Harrisburg, 9 pp.

48- NRMCA (1989). "What, Why, and How? Flowable Fill Materials." Concrete in Practice No. 17, *National Ready Mixed Concrete Association*, Silver Spring, MD.

49- Pierce, C. E., Tripathi H., and Brown T. W. (2003). "Cement Kiln Dust in Controlled Low-Strength Materials." *ACI Materials Journal*, Vol. 100, No. 6, pp. 455–462.

50- Ramme, B.W. and Naik T.R. (1997). "Controlled Low Strength Materials (CLSM) State-of the- Art New Innovations." *Third CANMET/ACI International Symposium on Advances in Concrete Technology*, Auckland, New Zealand, pp 125-131.

51- Ramme, B.W., Naik, T.R., and Kolbeck, H.J. (1995). "Construction Experience with CLSM Fly Ash Slurry for Underground Facilities." *American Concrete Institute*, Special Publication 153, pp. 403-416.

52- Riggs, E. H., and Keck, R. H. (1998). "Specifications and Use of Controlled Low-Strength Material by State Transportation Agencies." The Design and Application of Controlled Low-Strength Materials (Flowable Fill), *ASTM STP 1331*, A. K. Howard and J. L. Hitch, eds., American Society for Testing and Materials, West Conshohocken, PA.

53- Schmitz, M.E., Parsons, R.L., Ramirez, G., Zhao, Y. (2004). "Use of Controlled Low-Strength Material as Abutment Backfill." *Report No. K-TRAN: KU-02-6*, Kansas Department of Transportation, Topeka, 76 pp.

54- Simmons A. R. (2002). Use of flowable fill as a backfill material around buried pipes, M.S. Thesis., West Virginia University, 2002, 160 pages.

55- Smith, A. (1991). "Controlled Low-Strength Material." Aberdeen's Concrete Construction, Vol. 36, No. 5, pp. 389–398.

56- Snethen, D.R. and Benson, J.M. (1998). "Construction of CLSM Approach Embankment to Minimize the Bump at the End of the Bridge." The Design and Application of Controlled Low-Strength Materials (Flowable Fill), *American Society of Testing Materials (ASTM), STP 1331*, pp. 165-179.

57- Snethen, D.R., Schwidder, A.J., Benson, J.M., and Koening, S.A. (1997). "Performance of Experimental Approach Embankments at Slat River Bridges on U.S. 177." *Final Report FHWA/OK-97(04)*, Oklahoma Department of Transportation, Oklahoma City, 240 pp.

58- Sobolev, K. (1999) "High performance cement: A solution for next millennium." *Materials Technology*, 14 (4), pp. 191-193.

59- Stamnas, P. E., and Whittemore, M. D. (2005). "All Precast Substructure Accelerates Construction of Prestressed Concrete Bridge in New Hampshire." *PCI Journal*, 50(3), pp. 26-39.

60- Straud, Troy F. (1989). "Corrosion Control Measures for Ductile Iron Pipe." *Proceedings of Corrosion 89*, New Orleans, LA, Paper 585, 38 pages.

61- Trejo, D., Folliard, K.J, and Du, L. (2004). "Sustainable Development Using Controlled Low-Strength Material." *Proceedings of International Workshop on Sustainable Development and Concrete Technology*, Beijing, China, 231-250.

62- U.S. Environmental Protection Agency (EPA). "Flowable Fill Content Mixtures and Specifications." http://www.epa.gov/osw/conserve/tools/cpg/products/flow-ast.htm

63- U.S. Environmental Protection Agency (EPA) (1998). "Back Document for Proposed CPG III and Draft RMAN III." *EPA Report EPA530-R-98-003*.

64- Wilson, J. (1999). "Flowable Fill as Backfill for Bridge Abutments." *Report No. WI-16-99*, Wisconsin Department of Transportation, Madison, 26 pp.

65- Wu, J. T. H., Lee, K. Z. Z., and Pham, T. (2006). "Allowable bearing pressures of bridge sills on GRS abutments with flexible facing." *Journal of Geotechnical and Geoenvironmental Engineering*, ASCE, 132(7), 830-841.

Vahid Alizadeh

PhD Candidate
Department of Civil Eng. & Mechanics
University of Wisconsin-Milwaukee
3200 N Cramer St. Milwaukee WI, 53211
E-mail: alizadeh@uwm.edu, vahid.alyzadeh@gmail.com
URL: www.uwm.edu/~alizadeh

ACADEMIC PREPARATION

Doctor of Philosophy in Civil Engineering, University of Wisconsin, Milwaukee, May 2014
Major: Geotechnical Engineering
Minors: Construction Materials, Mathematics & Computational Science
Dissertation: *A Rapid Construction Technique for Bridge Abutments Using Controlled Low Strength Materials (CLSM),* Advisor: Professor Sam Helwany

Master of Science in Civil Engineering, Shiraz University, Iran, May 2008
Major: Geotechnical Engineering
Thesis: *Estimating Lateral Deflection of Reinforced Soil Walls Due to Seismic Loads Using Neural Networks,* Advisor: Professor Arsalan Ghahramani

Bachelor of Science in Civil Engineering, Azad University, Iran, February 2005
Senior Project: *Application of Geosynthetics in Civil Engineering*

RESEARCH INTERESTS

- Sustainable Infrastructures (By-Products Utilization, Sustainable Geomaterials)
- Geotechnical Engineering (Geosynthetic Reinforced Soil Structures, Bridge Abutments, Soil Stabilization, shallow and deep foundations, slope stability, etc)
- Energy (Geothermal Energy Systems)
- Pavement Testing and Analysis

PUBLICATIONS

Vahid Alizadeh, Sam Helwany, Al. Ghorbanpoor, and Konstantin Sobolev. "Design and Application of Controlled Low Strength Materials as a Structural Fill." *Construction and Building Materials,* 53, 425-431, 2014.

Vahid Alizadeh, Sam Helwany, Al. Ghorbanpoor, and Michael Oliva. "A Rapid Construction Technique for Bridge Abutments Using Controlled Low Strength Materials (CLSM)." *ASCE Journal of Performance of Constructed Facilities*, 28 (1), 2014.

Sam Helwany, Jonathan Wu, and Vahid Alizadeh. "Seismic Behavior of Geosynthetic-Reinforced Soil Bridge Abutments-Experimental Study." *Transportation Infrastructure Geotechnology Journal* (accepted).

Sam Helwany, Jonathan Wu, and Vahid Alizadeh. "Seismic Behavior of Geosynthetic-Reinforced Soil Bridge Abutments- Analytical Study." *Transportation Infrastructure Geotechnology Journal* (accepted).

Vahid Alizadeh, and Mojtaba Jahanandish. "Construction of Road Embankment over a Highly Saline River, Designed to Lift Crystalline Salt from the River Bed." *4th National Congress in Civil Engineering*, Tehran University, May 1-3 2008, Tehran, Iran.

TEACHING EXPERIENCE

University of Wisconsin, Milwaukee
Department of Civil Engineering and Mechanics

Instructor (Spring 13), Strength of Materials (CIV ENG-303): Stress and strain, torsion, bending of beams, shearing stress in beams, combined stresses, principal stresses, defections of beams, statically indeterminate members and columns. Developed the syllabus, lecture notes, homework assignments, and examinations.

Laboratory Instructor (Spring 09, Fall 09, Fall 10). Soil Mechanics (CIV ENG-335), Instructed students through laboratory experiments including classification of soils, Atterberg limits, Proctor test, permeability tests, Consolidation test, direct shear test, triaxial test. Held office hours for students, graded lab reports, and guest lectured.

Teaching Assistant and Coordinator of Lab Sessions
CIV ENG-303: Strength of Materials (Fall 12, Spring 12)
CIV ENG-201: Statics (Fall 11)
CIV ENG-456: Foundation Engineering (Spring 10)